PAST, PRESENT AND FUTURE RAINFALL TRENDS IN QUEENSLAND

A dissertation submitted by

David Andrew Matthew Cottrill

BSc, MSc (Hons), Grad Dip Sci (Math), GDCL

For the award of

Doctor of Philosophy

Department of Biological and Physical Sciences

Faculty of Sciences

University of Southern Queensland

Australia

2009

Frontispiece: This thesis is dedicated to my two dogs Kelly (Australian terrier) and Snapper (Blue Heeler), who both passed away early in 2009 from untreatable cancer, both at the age of 15 years, soon after my initial PhD submission. Your friendship and loyalty will be forever remembered.

ABSTRACT

Queensland and much of eastern Australia have had significant rainfall declines since ~1951, causing economic hardship on rural and urban communities. However, no significant attempt has been made to identify and understand the physical causes of the rainfall declines over southeast Queensland (SE QLD) and whether they are likely to continue into the 21st century under higher levels of global warming.

In this research, climate observations, models and global climate data as well as palaeoclimate information are used to investigate past, present and future rainfall trends in SE QLD. Five global climate models (GCMs) from the Intergovernmental Panel on Climate Change Fourth Assessment Report (IPCC–AR4) show a significant decrease in rainfall will occur over the SE QLD region during the 21st century. Observations since ~1951 show the mean sea level pressure (MSLP) has been increasing over much of Queensland, indicating the subtropical ridge has been expanding. This study attributes the increase in the MSLP and some of the rainfall decline to changes in the subtropical ridge and the Southern Annular Mode (SAM). Projections show increases in the MSLP over the region are likely to continue during the 21st century associated with the positive polarity of SAM. Land cover changes over SE QLD were investigated using a regional climate model and show rainfall decreases with higher surface albedo values. Finally, a palaeoenvironmental record developed using lake sediments from Lake Broadwater in SE QLD, indicates a gradual rainfall decline has occurred during the last ~3.2 kyr B.P. Hence SE QLD has undergone a slow rainfall decline since the late Holocene and also since ~1951, with these conditions likely to continue and intensify during the 21st century.

ACKNOWLEDGEMENTS

A special thanks to the encouragement from my supervisors A/Prof Joachim Ribbe and Dr Martine Maron at the University of Southern Queensland (USQ) and to Dr Jerry Maroulis for reading the palaeoclimate section of my thesis. Thanks to Debbie White and Kris Lyon for their administrative support and to Peter Greenup, Colin Glasby, Richard Young and Jeffrey Chapman and others for computing assistance. I also acknowledge the support from USQ for the Postgraduate Research Scholarship over three years and the annual research fund allocation.

I would also like to thank Oliver Kinder for his assistance by providing the sampling equipment used at Lake Broadwater, Pat McConnell for laboratory inductions and Dr Andy Le Brocque for the use of the Ecology Research Lab for analysing and storing samples. Thanks to Condamine Drilling Pty Ltd in Toowoomba who gratefully provided the two lengths of PVC pipe used in the lake sampling.

A special thanks to the Australian Institute of Nuclear Science and Engineering (AINSE) for providing funding (AINGRA07103P) to support the analyses on the lake samples from Lake Broadwater and the attendance at the Winter School (2006). Thanks to Dr Dennis Mather and Dr Geraldine Jacobsen for the useful comments on the grant application, Atun Zawadzki (Laboratory Manager), Jennifer Harrison and other laboratory technicians for help on the preparation and ^{210}Pb dating on samples at Lucas Heights. Thanks to Henri Wong for the multi–element geochemistry and a special thanks to Rhiannon Still, who organised much of the paper work (security clearance), travel arrangements and other activities completed at AINSE.

I also acknowledge the assistance from Dr Wenju Cai and colleagues at the Commonwealth Scientific and Industrial Research Organisation (CSIRO) in Melbourne, Australia, the Program for Climate Model Diagnosis and Intercomparison (PCMDI) and the World Climate Research Program Coupled Modelled Intercomparison Project (WCRP CMIP3) multi–model data archive for providing the 20^{th} and 21^{st} century data from the Intergovernmental Panel on Climate Change (IPCC) Fourth Assessment Report (AR4) used in this analysis. I would like to thank Drs John McGregor, Marcus Thatcher and Kim Nguyen for the support and guidance for running the Conformal Cubic Atmospheric Model (CCAM) over the SE QLD region in Melbourne (Aspendale) at the CSIRO. A special thanks also to Dr Ramasamy Suppiah and Mark Collier for accommodation and their enthusiasm during my visits to Melbourne and the CSIRO.

Thanks to Peter DeVoil from the Department of Natural Resources and Water (DNRW) who provided some gridded monthly rainfall data from the Australian Bureau of Meteorology and to Drs Neil White and Jozef Syktus from the Queensland Climate Change Centre of Excellence for interesting discussions on various topics. Thanks to the Australian Research Council Network for Earth System Science (ARCNESS) for providing funds to attend the Climate Modelling Workshop in 2006.

A special thanks to my two dogs Kelly and Snapper (who both passed away in early 2009) and to various friends (including Carol Peak and Mark Missen) and housemates who maintained my persistence and enthusiasm during my university tenure at USQ.

CERTIFICATION OF DISSERTATION

I certify that the ideas, experimental work, results, analyses, software and conclusions reported in this dissertation are entirely my own effort, except where otherwise acknowledged. I also certify that the work is original and has not been previously submitted for any other award, except where otherwise acknowledged.

Signature of Candidate Date

ENDORSEMENT

Signature of Supervisor/s Date

Signature of Associate Supervisor/s Date

PUBLICATIONS, CONFERENCES AND AWARDS FROM THIS RESEARCH

Journal Articles

1. **Cottrill, D.A**. and Ribbe, J 2008. "Rainfall Projections over Northeast Australia from IPCC–AR4 Models," submitted to the International Journal of Climatology.

2. **Cottrill, D.A**.; Maron, M, Ribbe J. and Maroulis J. 2009. "A Holocene Palaeoenvironmental Record from Lake Broadwater, Southeast Queensland, Australia," in preparation to be submitted to the journal Holocene or similar.

Conference Presentations

1. **Cottrill, D.A**. and Ribbe, J. 2007. "Queensland Rainfall Variability in IPCC AR4 Model Runs," Australian Meteorological and Oceanographic Society, Adelaide, South Australia, 5–8 February, 2007

2. **Cottrill, D.A**. and Ribbe, J. 2007. "Queensland Rainfall Decline," Australian Meteorological and Oceanographic Society, Geelong, Victoria, 29 January 1–February, 2008.

3. **Cottrill, A.**, Ribbe, J and Maron, M. 2008. 4th AINSE Quaternary Dating Workshop, "A Detailed Proxy Rainfall Record from Lake Broadwater, Dalby, Southeast Queensland," 26–27 March, 2008. Poster Presentation.

4. **Cottrill, D.A**. and Ribbe, J. 2009. “Rainfall and MSLP Changes over Queensland and the Southern Hemisphere,” 9th International Conference on Southern Hemisphere Meteorology and Oceanography (ICSHMO), Melbourne, Australia, 9–13 February, 2009.

5. **Cottrill, A**., Ribbe, J. and Maron, M. 2009. “A Holocene Palaeoenvironmental Record from Lake Broadwater, Dalby, Southeast Queensland,” 9th International Conference on Southern Hemisphere Meteorology and Oceanography, Melbourne (ICSHMO), Australia, 9–13 February, 2009. Poster Presentation.

Awards and Grants

1. USQ Postgraduate Research Scholarship, 2006–2009.

2. Attendance at the Climate Modelling Workshop, 25 and 26 May 2006, School of Mathematics, UNSW. Travel support provided by Australian Research Council Network for Earth System Science (ARCNESS).

3. Attendance at the annual AINSE Winter School at ANSTO 1–5th July, 2006.

4. Attendance at the Earth System Science Winter School in Melbourne (Monash University) 10–4th July, 2006.

5. AINSE award number AINGRA07103P to Dr Martine Maron (Chief Investigator) for research on lake sediments from Lake Broadwater 2007/2008.

TABLE OF CONTENTS

LIST OF FIGURES

LIST OF TABLES

LIST OF MAPS

CHAPTER 1 : INTRODUCTION

1.1 INTRODUCTION

Rainfall over southeast Queensland (SE QLD) is an important factor for the management of the natural resources and the development of sustainable agriculture, industry and urbanisation in the region. Many years of below average rainfall, such as at Toowoomba during 1990–1995 (BoM 2004) and 2000–2009, have led to declining water supplies with increasing water restrictions in a region that has a rapidly growing population. A better understanding into the current rainfall trends and attribution of their causes in this region will greatly improve the management of this precious resource for coming decades.

Australia and much of Queensland have been in drought for many years and 2002 was one of the most severe and widespread droughts recorded in recent times (Nicholls 2004). Drought is the most costly economic climate factor in Australia (BoM 2004) and has been defined by the Australian Bureau of Meteorology as three or more months with rainfall below the 10^{th} percentile, producing serious or severe rainfall deficiencies (http://www.bom.gov.au/climate/glossary/drought.shtml). Nicholls (2004) argues that global warming associated with higher evaporation is acerbating drought conditions which are likely to intensify in the future. The high variability in Australian rainfall makes the detection of long–term trends in rainfall more difficult (Nicholls et al. 1997) and there is a large range of rainfall across Australia, with higher rainfall over coastal regions and lower rainfall over inland and southern regions (Figure 1.1). However, some decadal trends in annual rainfall have become more evident in the last ten years or so with New South Wales (NSW), Queensland, Victoria, Tasmania and southwestern Western Australia all showing a significant rainfall decline during the second half of the 20th century (Figure 1.2).

This rainfall decline was first identified by Allan and Haycock (1993) from southwestern Western Australia, which began in the late 1960s or early 1970s and in recent decades has developed to cover large areas in Queensland and eastern Australia. In contrast, northern Australia including most of the Northern Territory and much of central and northern Western Australia has received higher rainfall associated with the summer monsoon season (Figure 1.2). While some of the causes of the rainfall changes over southeast Australia have been recently described (Cai and Cowan 2008a; Rakich et al. 2008; Ummenhofer et al. 2009), they are yet to be reported for SE QLD.

The Australian continent extends over a wide latitude (~10ºS to 40ºS) and longitude (~113ºE to 153ºE) leading to a large and diverse range of influences on the weather and climate in this region. Its proximity to the equator means the trade winds, the austral summer monsoon, the Madden Julian Oscillation, tropical depressions, tropical cyclones and other tropical disturbances dominate much of the weather over northern Australia including much of Queensland (Colls and Whitaker 1993; Sturman and Tapper 2006). Further south, the subtropical ridge and the mid–latitude westerlies with the associated rain–bearing depressions dominate most of the weather variability, especially in austral winter (Hartmann 1994; Sturman and Tapper 2006). Seasonal east and west coast troughs and upper level disturbances also play a

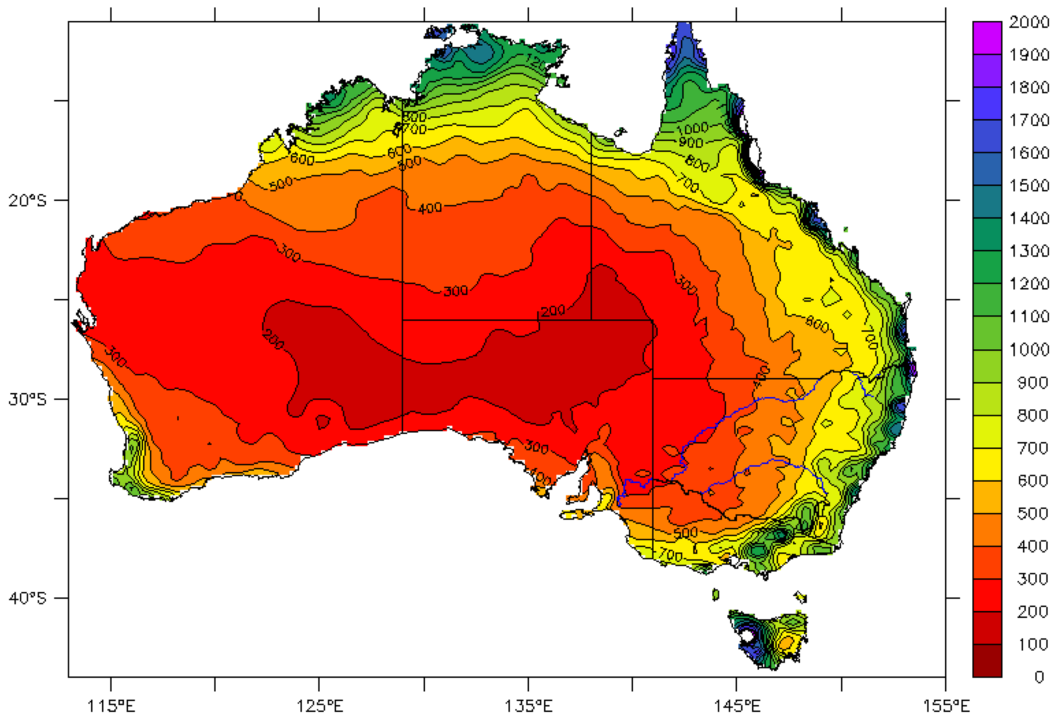

Figure 1.1 Australian climatological mean annual rainfall (mm) for 1961–1990. Contours are in 100 mm intervals, with regions in shades of red and orange showing lower rainfall and yellow, green and blue higher rainfall. Data from the Bureau of Meteorology.

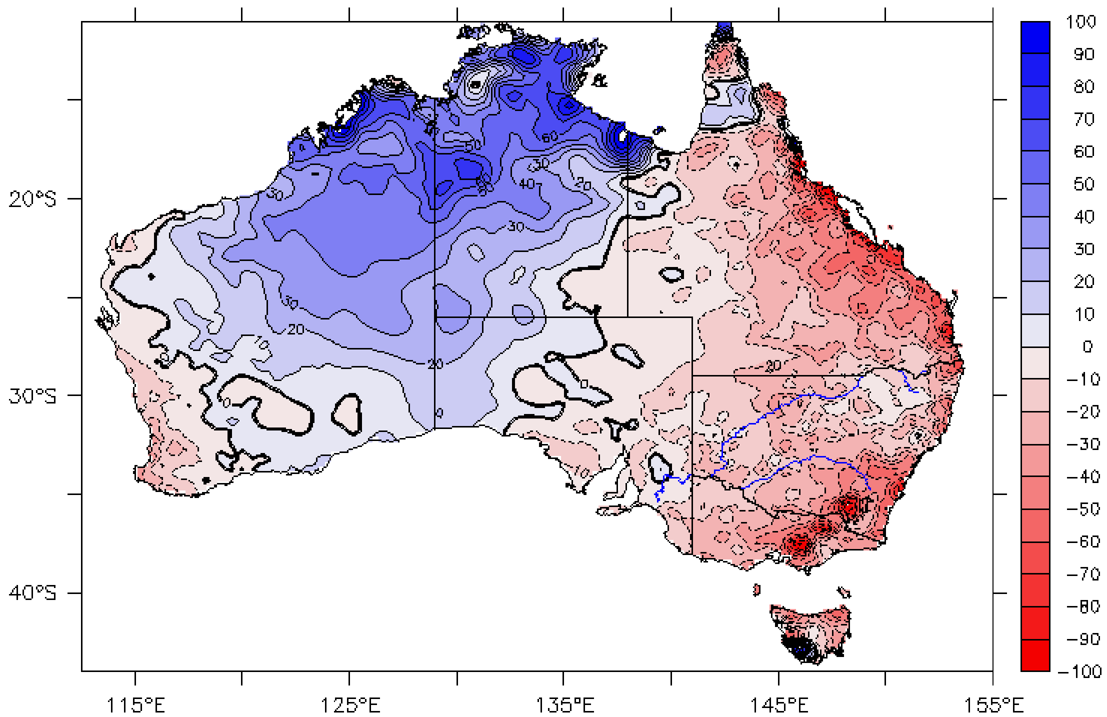

Figure 1.2 Australian decadal trends in annual rainfall (mm decade^{-1}) from 1951–2007. Contours are in 10 mm intervals, with regions in blue and red showing increasing and decreasing rainfall respectively. The thicker bold line delineates the zero rainfall change contour line. Data from the Bureau of Meteorology.

significant role in the weather over much of inland Australia. These influences provide a distinct contrast between the two regions, with northern Australia receiving a rainfall maximum in austral summer and southern Australia in austral winter. Spatial plots of the mean seasonal rainfall over Australia for the period 1961–1990 are shown in Figure 1.3 (a–d) and highlight the seasonal contrast in rainfall between northern and southern Australia, as well as the east and west coast. SE QLD is located between these two regions and therefore receives a combination of weather types, including onshore trade winds, east coast troughs and east coast lows. This

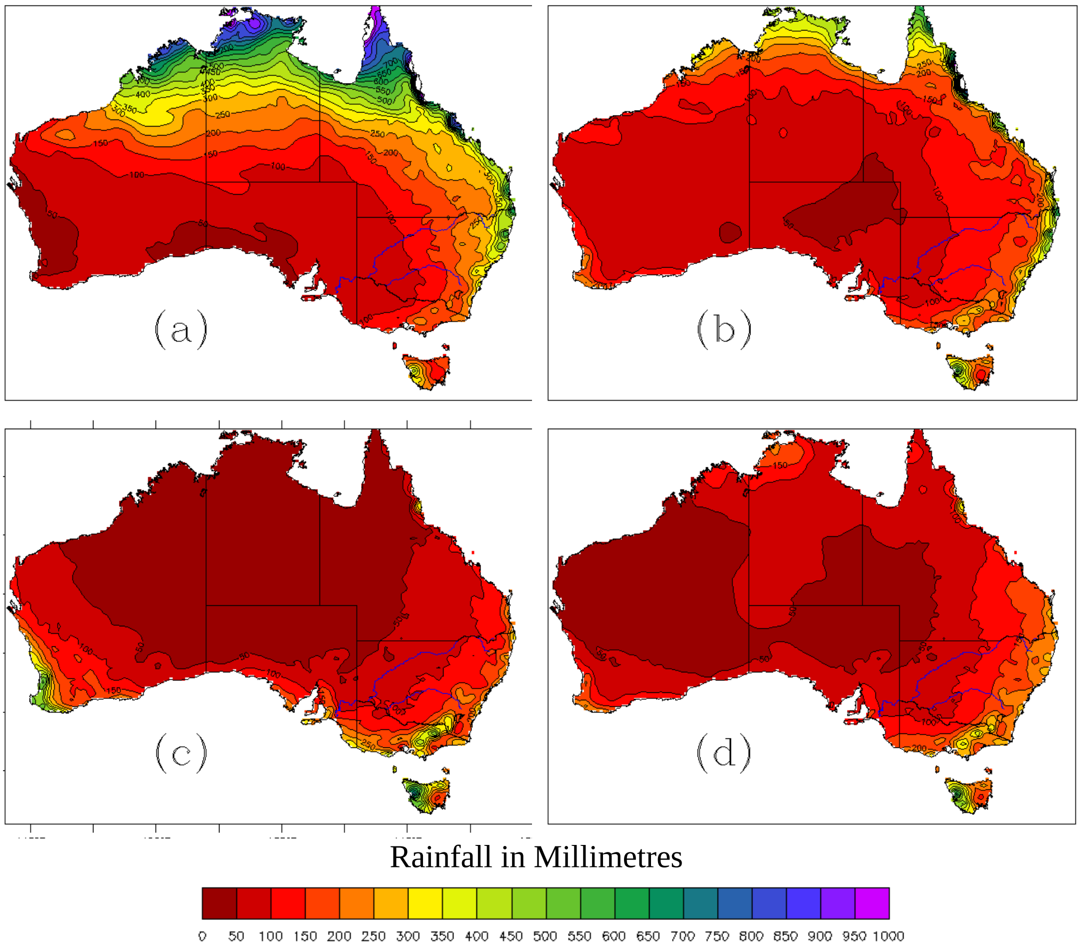

Figure 1.3 (a–d) Australian mean seasonal rainfall for 1961–1990. (a) DJF, (b) MAM, (c) JJA and (d) SON. Contours are in 50 mm intervals, with regions in shades of red and orange showing lower rainfall and yellow, green and blue, higher rainfall. Data from the Bureau of Meteorology.

produces a rainfall gradient with the highest rainfall along the coastal regions (and ranges), decreasing further inland. SE QLD receives most of its rainfall in the austral summer and autumn seasons, with much lower rainfall in austral winter and spring.

A number of remote climate drivers of Australian rainfall have been studied in detail including the El Niño–Southern Oscillation (ENSO) (Stone and Auliciems 1992; Stone et al. 1996; Murphy and Ribbe 2004), the Southern Annular Mode (SAM) (Cai and Cowan 2006; Hendon et al. 2007; Meneghini et al. 2007) and the Indian Ocean Dipole (IOD) (Ashok et al. 2003; England et al. 2006; Ummenhofer et al. 2009) and together (Shi 2008; Shi et al. 2008) they provide much of the rainfall variability experienced over the continent and Queensland.

1.2 AIM AND SCOPE OF RESEARCH

This study is motivated by the recent observations of declining rainfall in the SE QLD region. This leads to a number of questions, such as whether the rainfall declines will persist into the 21st century and what are some of the main climate drivers underlying this rainfall trend? To place the recent climate variability into a longer perspective, a detailed palaeoclimate record is required for the SE QLD region over the last few thousand years. To answer some of these questions, the following data sources will be utilised in this study:

(1) Recent climate observations of rainfall and mean sea level pressure from the Australian Bureau of Meteorology (station and gridded data);

(2) Global climate observations of mean sea level pressure from the National Centers of Environmental Prediction (NCEP) and the SAM index;
(3) Global climate model data of rainfall and mean sea level pressure from the Intergovernmental Panel on Climate Change's Fourth Assessment Report;
(4) Regional modelling using the conformal–cubic atmospheric model (CCAM) from the Commonwealth Scientific and Industrial Research Organisation and
(5) Palaeoclimatic information using lake sediments from a small lake in the upper reaches of the Murray-Darling Basin in SE QLD.

Firstly, a detailed analysis of the 20th century rainfall trends over northeast Australia (NEA) and Queensland is compared to rainfall from 21 global climate models (GCMs) from the Intergovernmental Panel on Climate Change's Fourth Assessment Report (IPCC–AR4) in a ranking analysis. This is followed by an analysis of the 21st century rainfall projections from a smaller group of models over the NEA region. To supplement this analysis, the mean sea level pressure (MSLP) trends from observations over the Queensland region are investigated and a correlation analysis between rainfall and the MSLP completed. The MSLP trends from observations are compared to the MSLP trends in the IPCC-AR4 models and the 21st century MSLP projections over the NEA region, discussed in association with the rainfall projections.

Secondly, an analysis into some of the characteristics associated with the rainfall decline over NEA and Queensland during the 20th century will be described using global observations from NCEP and GCMs from the IPCC-AR4. To identify regional climate driver(s), a more global perspective of the MSLP trends over

Australia and the Southern Hemisphere is undertaken to identify whether the MSLP trends in the NEA region are part of larger global MSLP trends and if they are likely to continue into the 21st century. A correlation analysis between the MSLP from the NEA region and the SAM index, as well as Norfolk Island is also completed. To identify local drivers of rainfall change, a study into the land cover changes (LCC) over SE QLD in a regional climate model (CCAM) from the Commonwealth Scientific and Industrial Research Organisation (CSIRO) is used to identify whether changes in the albedo or vegetation may have affected rainfall in this region.

Thirdly, the development of a palaeoenvironmental record (including a proxy rainfall record) from sediment samples from a small lake in SE QLD that extends over ~10,000 years will be established. This is developed by using techniques such as detailed stratigraphy, multi–element geochemistry, grain size analysis and carbon (^{14}C) dating on lake samples, with regolith mapping completed on the adjacent catchment. This will enable the dry conditions and the downward rainfall trend observed during the second half of the 20th century to be compared to the rainfall variability in the mid–late Holocene and identify major changes in rainfall that may have occurred during this time.

1.3 THESIS OUTLINE

- Chapter Two presents results from the analysis of rainfall data from observations and 21 IPCC–AR4 GCMs over Queensland and the NEA region, with an assessment of rainfall projections for the 21st century.

- Chapter Three provides results on the analysis of mean sea level pressure (MSLP) trends from observations and IPCC–AR4 GCMs over NEA and a correlation analysis between Queensland rainfall and the MSLP.
- Chapter Four describes the MSLP trends found in Chapter Three in context with the greater Australia region and the Southern Hemisphere, to identify important climate driver(s) of climate change in SE QLD, including a correlation analysis between the Queensland MSLP, the SAM index and the MSLP at Norfolk Island.
- Chapter Five utilises a regional climate model from the CSIRO to study the impacts of late 20th century land cover change and albedo to identify if they have contributed to the rainfall decline over SE QLD.
- Chapter Six presents a detailed palaeoenvironmental record developed using lake sediments from Lake Broadwater from inland SE QLD and compares these results to other proxy rainfall records from Queensland and eastern Australia.
- Chapter Seven discusses the main conclusions found by this research, including important local and remote climate drivers on the rainfall decline identified in this study for SE QLD and the overall implications for water resources in this region. Further avenues of climate research are proposed.

CHAPTER 2 : RAINFALL PROJECTIONS OVER THE QUEENSLAND REGION FROM IPCC–AR4 MODELS

2.1 INTRODUCTION

There have now been several detailed assessments of both 20^{th} century climate and 21^{st} climate change scenarios from the IPCC–AR4 using Global Climate Models (GCMs) over land in the Southern Hemisphere (Hope 2006; Vera et al. 2006; Pitman and Perkins 2008). In particular, the Commonwealth Scientific and Research Organisation (CSIRO) released a comprehensive review of climate change in Australia and for 21^{st} century projections for rainfall, temperature and other climate elements, as well as the potential impacts, using six emission scenarios and many of the Intergovernmental Panel on Climate Change’s Fourth Assessment Report) (IPCC–AR4) models (CSIRO and Meteorology 2007). However, few studies have compared 20^{th} century modelled rainfall to observations to identify the GCMs which best simulate annual, seasonal and monthly rainfall on a regional basis.

GCMs are the only tools that account for the complex set of processes which determine future climate change at global and regional scales (Trenberth 1992; Murphy et al. 2007). Coupled GCMs are the most complete representation of the climate system and are constructed by discretizing and solving equations which represent the basic laws that govern the behaviour of the atmosphere, ocean and land surface. These three dimensional models of the general circulation of the atmosphere and ocean have become known generally as GCMs (McGuffie and Henderson-Sellers 2005). They have typically a resolution of ~2–4° with about 30 and 20 distinct layers represented in the atmosphere and ocean respectively. Each layer can exchange heat, momentum and other factors horizontally and vertically in time steps of minutes (McGuffie and Henderson-Sellers 2005). The most comprehensive set of multi–model and multi–scenario simulations have been coordinated by the Intergovernmental Panel on Climate Change in its latest report (Zhang and Walsh 2006). The different emission scenarios are images of how the future may unfold and assist in climate change analysis, climate modelling and the assessment of impacts, adaption and mitigation (IPCC 2000). A brief summary of the four groups from the different emission scenarios and those used in this study for future projections are shown in Table 2.1.

Table 2.1 Summary of the Four Main Groups from the Special Report on Emission Scenarios (SRES).

Scenario Family	**Global Surface Warming by 2100 in °C**	**Comments**
A1	Range ~1.4–6.4 Average ~3.0	A future world of very rapid economic growth, global population that peaks mid–century and declines thereafter due to new and efficient technologies (A1B, A1T and A1Fl).
- A1B*	2.8	A variation of the A1 scenario but with an emphasis on new technologies evenly spread across all energy sectors.
A2*	3.6	A very heterogeneous world with continuously increasing global population and regionally oriented economic growth that is more fragmented and slower than in other storylines.
B1	1.8	A convergent world with the same global population as A1 but with rapid changes toward a service and information economy, with reductions in material intensity, and the introduction of clean and resource–efficient technologies.
B2	Range ~1.4–3.8 Average 2.4	A world with the emphasis is on local solutions to economic, social and environmental sustainability, with continuously increasing population (lower than A2) and intermediate economic development.

Notes. **1**. The asterisk (*) denotes the scenario used in this study.
2. Source: IPCC (2000). Summarised from Figure 1.

The projection of rainfall trends for the 21st century from all the IPCC–AR4 GCMs from the multi–model A1B climate change scenario showed less that less than 66% of models agree on the sign of the change over the NEA region (IPCC 2007). In contrast, high–resolution climate change projections completed by the CSIRO on the Fitzroy basin, about 400 kilometres north of Brisbane, showed relatively small changes in rainfall (up to 1 mm day^{-1}) for the 21st century using A2 projections, with the austral autumn and spring showing a decrease in rainfall and an increase in austral summer, relative to the base period 1961–1990 (McGregor et al. 2006). The aim of this research is to investigate whether the current downward rainfall trends over the NEA region will persist into the 21st century. The IPCC–AR4 used an area averaged ensemble mean of 21 models to describe rainfall changes expected in the Australian region in its latest report (Christensen et al. 2007), whereas this study uses five models that are best able to simulate 20th century rainfall climatology over NEA. A recent technical report from the CSIRO and the Bureau of Meteorology (BoM) (CSIRO and Meteorology 2007) and by Suppiah et al (2007) indicates lower rainfall projections over parts of Australia for the 21st century from a number of models and emission scenarios. A recent study by Pitman and Perkins (2008) shows small increases in mean rainfall by 2050 for all seasons except austral winter over the Queensland region. This chapter will compare rainfall projections developed in this chapter to the results found by these other studies.

Mean austral summer rainfall across Queensland varies from 250 mm or less in the far southwest region of the state, to more than about 750 mm along the entire length of the Queensland east coast (Lough 1991). Rainfall is dominated by the proximity of the Australian monsoon in the austral summer and autumn, which provides most of the rainfall over northern Queensland and over 80% of the annual rainfall to northern Australia (Lough 1993; Cai et al. 2001; Sturman and Tapper 2006). Other processes such as the El Niño–Southern Oscillation (ENSO) (Stone and Auliciems 1992; Nicholls et al. 1996; Trenberth and Caron 2000; Rakich et al. 2008), the location and strength of the subtropical ridge (Stone 1989; Nowak and Leighton 1997; Ansell et al. 2000; Murphy and Ribbe 2004; Drosdowsky 2005; Larsen 2008) and the Southern Annular Mode (SAM) (Shi et al. 2008) are important factors influencing rainfall over Queensland and NEA.

Although the high variability in Australian rainfall makes detection of long–term rainfall trends more difficult (Nicholls et al. 1997), declining rainfall over NEA has become stronger during the last ten years or so. Negative annual decadal rainfall trends (up to 200 mm decade^{-1}) have occurred along the Queensland coast since ~1951, and over half of Queensland is now affected by decreasing rainfall of 20 mm decade^{-1} or greater (Figure 2.1a). The phrase "annual decadal rainfall trends" explicitly means "the decadal trend in annual rainfall" and is used throughout this thesis. The largest rainfall declines have occurred around Mackay, Bowen and Ingham and along the coastal region to Brisbane and into NSW. In contrast, earlier annual decadal rainfall trends from 1901–1950 show weak to moderate rainfall increases over Queensland in austral spring and summer, and decreases in rainfall over SE QLD in austral autumn and winter (not shown). If the annual decadal rainfall trend from 1951–2007 is compared to the climatological mean rainfall for 1961–1990 base period, over half of inland Queensland as well as coastal areas, have had a significant rainfall decline of 20% or higher, with some areas north of Mackay, over a 50% decline (Figure 2.1b).

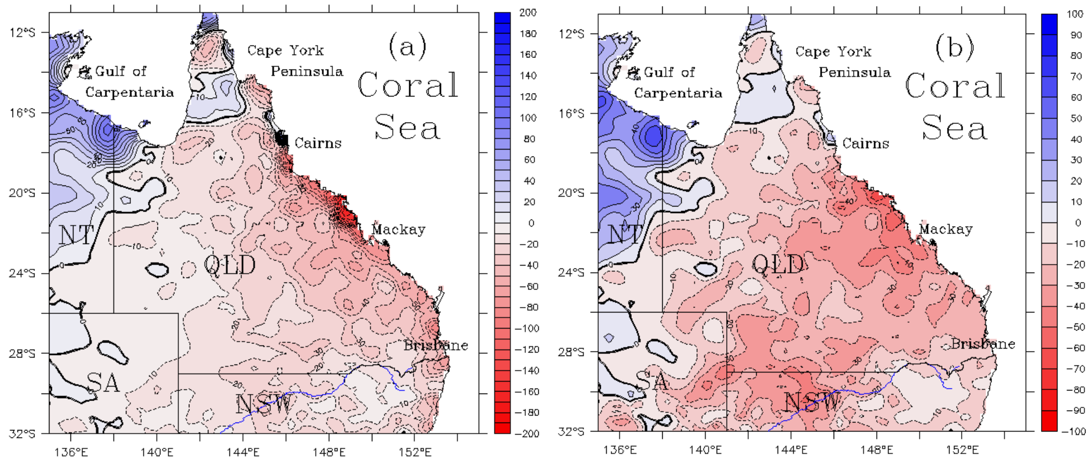

Figure 2.1 (a–b) Queensland annual decadal rainfall trends (mm decade^{-1}) from 1951–2007 (a), and the annual decadal rainfall trend (1951–2007) as a percentage of the annual mean (1961–1990) in percent (b). Data from the Bureau of Meteorology.

The decreasing rainfall in Queensland and eastern Australia has only recently been described (Hennessy et al. 1999; Murphy and Ribbe 2004; Smith 2004; Nicholls 2006; Alexander et al. 2007; CSIRO and Meteorology 2007; Gallant et al. 2007; Rakich et al. 2008) and less research has been completed compared to the decline in austral winter rainfall in southwest Western Australia since the mid–1960s (Allan and Haylock 1993; Hennessy et al. 1999; Ansell et al. 2000; Smith et al. 2000; Pittock 2003; Pitman et al. 2004; Smith 2004; Li, Y. et al. 2005; Ryan and Hope 2005; England et al. 2006; Hope et al. 2006; Timbal et al. 2006). Drought conditions have continued over much of eastern Australia since 2001 (Cai and Cowan 2008b; Rakich et al. 2008), including the severe drought of 2002 (Nicholls 2004). This is causing severe water deficits in the SE QLD region with unprecedented water restrictions, although useful rains have occurred in some areas during the 2007/2008 La Niña and early 2009. Queensland is an important agricultural producer in Australia (NLWRA 2001) with large numbers of cattle and sheep on extensive grazing lands (Hall et al. 1998). It also has a fast growing population in the southeast corner of the state and hence changes in rainfall and climate change during the 21st century, will have large impacts on these activities (Pittock 2003; McKeon et al. 2004).

In this thesis, data from 21 GCMs and the IPCC–AR4 has been used for rainfall analyses for the 20th century (1901–2000). Zonal and meridional sections of rainfall over NEA provide an overview of regional differences between modelled rainfall and BoM observations. The root mean square error (RMSE) has been calculated for each model to identify the lowest RMSE values and produce a model ranking. RMSE is a measure of the ability of the GCMs to reproduce regional characteristics of the present day climate (Salzmanna et al. 2007). As this skill improves, so potentially does the ability for forecasting future climate (Shukla et al. 2006; Whetton et al. 2007). Modelled rainfall data are compared to the observational record, with particular emphasis upon each model's ability to represent 20th century pattern of annual, seasonal and monthly climate variability. Five models with the best final ranking are selected to analyse the decadal rainfall trends across the NEA region for both the 20th and 21st centuries. Data and methodology are described in section 2.2. Results with zonal and meridional averaged sections, RMSE values and model ranking are shown in section 2.3, time series of annual rainfall in section 2.4 and decadal rainfall trends and projections are presented in section 2.5. Finally, a summary of the rainfall changes by 2031–2050 and 2081–2100 over the Queensland region are shown in section 2.6. A discussion follows on these results in section 2.7.

2.2 DATA AND METHODOLOGY

2.2.1 IPCC–AR4 Data

Rainfall simulations from 21 GCMs use the “climate of the 20th century experiment” (representing historical greenhouse gas concentrations during the 20th century) for rainfall analysis (1901–2000) and climate projections the higher emission climate scenarios A2 (~850 ppm CO_2 equivalent concentration by 2100) or A1B (~720 ppm CO_2) for the 21st century (IPCC 2007). Monthly rainfall data for these models is available from "the World Climate Research Programme's (WCRP's) Coupled Model Intercomparison Project phase 3 (CMIP3) multi–model dataset" or http://www-pcmdi.llnl.gov/ipcc/info_for_analysts.php website and links therein. In this study, the higher emission scenario is selected because increasing atmospheric CO_2 levels are likely to be closer to the highest projected estimates in the current climate models (Shukla et al. 2006) and have been used in other recent analysis (Charles et al. 2007). The GCMs used in this analysis are summarised in Table 2.2. A total of 69 simulations from 21 models for the 20th century climate and five models with eleven simulations for the 21st century projections are used for the rainfall analyses.

2.2.2 Rainfall Data from the Australian Bureau of Meteorology

Rainfall observations were obtained from the Australian Bureau of Meteorology National Climate Centre and consists of monthly gridded rainfall at 0.25º by 0.25º spacing from 1890–2007 over Australia (Jones and Beard 1998). BoM observations are used to compare rainfall simulations from the 21 IPCC–AR4 GCMs in annual

Table 2.2 Summary of the 21 IPCC–AR4 GCMs used for the 20th century Rainfall Analyses over NEA

Modelling Centre	Model Name	Number of Runs	Number Of Grid Points	Atmosphere Resolution (lat x long)
1.CCCma, Canada	**CGCM3.1-T47**	5	23	3.75º x 3.75º
2. CCCma, Canada	**CGCM3.1-T63**	1	43	2.8125º x 2.8125º
3. CNRM, France	**CNRM-CM3**	1	39	2.8125º x 2.8125º
4. CSIRO, Australia	**CSIRO-MK3.0**	3	85	1.875º x 1.875º
5. GFDL(CM2.0), USA	**GFDL-CM2.0**	3	51	2.0º x 2.5º
6. GFDL(CM2.1), USA	**GFDL-CM2.1**	3	50	2.0º x 2.5º
7. GISS, USA	**GISS-AOM**	2	27	3º x 4º
8. GISS1 (Model E-R)	**GISS-ER**	9	14	~3.913º x 5º
9. GISS3 (Model E-H)	**GISS-EH**	5	14	~3.913º x 5º
10. IAP, China	**IAP-FGOALS1.0**	3	39	3.0º x 2.8125º
11. INM, Russia	**INM-CM3.0**	1	17	4º x 5º
12. IPSL, France	**IPSL-CM4**	1	33	2.5º x 3.75º
13. CCSR/NIES/FRCGC (hires) Japan	**MIROC3.2 (hir)**	1	222	1.125º x 1.125º
14.CCSR/NIES/FRCGC(med/res) Japan	**MIROC3.2 (med)**	3	39	2.8125º x 2.8125º
15.MIUB Germany/Korea	**MIUB-ECHO-G**	5	23	3.75º x 3.75º
16. MPI, Germany	**MPI-ECHAM5**	3	85	1.875º x 1.875
17. MRI, Japan	**MRI-CGCM2.3.2a**	4	39	2.8125º x 2.8125º
18. NCAR (CCSM3), USA	**NCAR-CCSM3.0**	8	139	1.40625º x 1.40625º
19. NCAR (PCM1), USA	**NCAR-PCM1**	4	39	2.8125º x 2.8125º
20. UKMO (HadCM3), UK	**UKMO-HadCM3**	2	35	~2.466º x 3.75º
21. UKMO (HadGEM1), UK	**UKMO-HadGEM1**	2	127	~1.241º x 1.875º
	Average		**56**	

and seasonal zonal (10ºS–32ºS) and meridional (135ºE–155ºE) cross sections and monthly climatology, to compare and contrast coastal and inland regions as well as tropical and subtropical regions from over the NEA region. Observed rainfall discussed in this chapter refers to rainfall data obtained from the BoM.

2.2.3 RMSE Analysis

The RMSE has been used recently in a number of studies to assess model performance (Moise et al. 2005; Whetton et al. 2005; Gnanadesikan and Stouffer 2006; Salzmanna et al. 2007; Sloyan and Kamenkovich 2007; Smith et al. 2007; Suppiah et al. 2007). RMSE values are calculated for annual, seasonal and monthly rainfall over NEA (10ºS–32ºS and 135ºE–155ºE) for the period 1901–2000. This region has been selected and includes northern New South Wales, the far eastern Northern Territory and the Cape York Peninsula, so that the coarser resolution grid models can be included in the analysis and are not lost through edge effects. The larger region is also more likely to identify rainfall trends than smaller regions due to a larger number of grid points. The RMSE were calculated by taking the differences between the model and observations, squaring the difference and taking the square root. Hence an RMSE of 0.0 would indicate a perfect match between observed and simulated magnitudes (Suppiah et al. 2007) and large RMSE values a greater discrepancy between model and observations. Rainfall data has been converted to the same grid size represented in each of the 21 IPCC–AR4 models, similar to other recent studies (Dai 2006; Douville et al. 2006; Vera et al. 2006). Only the grid points from each model over land were used for RMSE and statistical calculations. Horizontal resolution of the IPCC–AR4 GCMs varies from 1.125º–5º (Table 2.2). The averaged RMSE value has been calculated from a different number of points for each model which varies from as few as 14 points (coarse resolution models) to 222 points (high resolution models) over NEA. The benefits of completing the analysis in this way by maintaining the original GCM grid, allows the spatial patterns from the RMSE analysis from each model to be compared and contrasted, as well as the relationship to the regional orography to be assessed.

The RMSE values for the annual, seasonal and monthly climatology are ranked from 1 (lowest RMSE) to 21 (highest RMSE) and a final ranking obtained by averaging the three ranks for each climatology. This identifies the 'best' performing models over NEA, which are used to produce decadal rainfall trends in section 2.5. Five models are arbitrarily selected for the 21st century projections, primarily because there was no significant 'break' in the top thirteen models (final rank versus averaged RMSE value). Five models also provide a range of rainfall responses with a mean temperature centred on about 3.5ºC by 2100 (CSIRO and Meteorology 2007) and allows a multi–model ensemble mean of the decadal rainfall trends to be calculated for the 20th and 21st centuries. An annual rainfall time series of the five models and BoM observations are discussed for the 20th century (1901–2000). Finally, seasonal and annual standardised decadal rainfall trends from the five models and BoM observations for the period 1951–2000 are discussed, along with rainfall projections for 2001–2050 and 2051–2100, plus the multi–model ensemble mean over the NEA region (10ºS–32ºS and 135ºE–158ºE).

Seasonal climatology and rainfall trends are represented for austral summer in December–January–February (DJF), austral autumn in March–April–May (MAM), austral winter in June–July–August (JJA) and austral spring in September–October–November (SON).

2.3 RESULTS OF THE RMSE ANALYSIS

2.3.1 Annual Climatology

Observed annual zonally averaged rainfall ranges from about 400 mm at 32ºS to over 1500 mm at 10ºS (Figure 2.2a). Most of the models simulate the change from lower rainfall in the mid–latitudes to higher rainfall associated with the Australian monsoon at 10ºS. Some models like the IPSL-CM4 and GISS-AOM models show a rainfall minimum at 23ºS. Eleven models simulate higher rainfall than the observed rainfall, with GISS-EH model simulating much higher rainfall. Five models simulate lower rainfall, with the IPSL-CM4 model simulating much lower rainfall than the observed rainfall across the region. A number of the models (IPSL-CM4, MRI-CGCM2.3.2a and GISS-AOM) with a lower resolution may not well represent the coastal ranges along the Queensland coast, especially the Cairns area where mountains are over 1500 m in height.

The observed annual meridionally averaged rainfall varies from about 400 mm at 135ºE rising to over 1000 mm east of about 152.5ºE by the coast (Figure 2.2b). Fourteen models simulate higher rainfall (three models lower rainfall) west of about

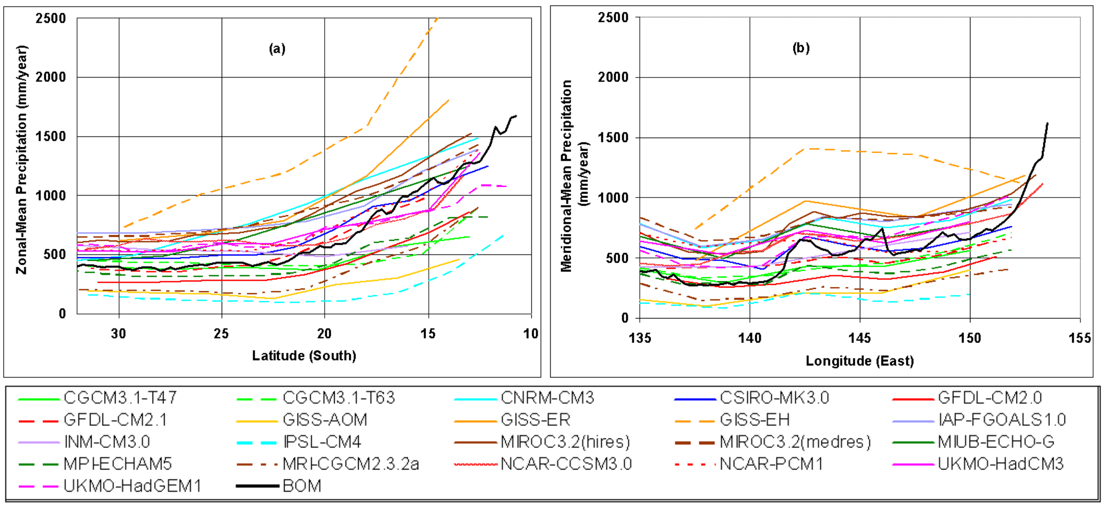

Figure 2.2 (a–b) Zonally (a) and meridionally (b) averaged annual rainfall (mm year $^{-1}$) over NEA and the period 1901–2000.

142ºE and about ten models higher or lower rainfall east of 142ºE. The GISS-EH model simulates much higher rainfall than observed rainfall and the IPSL-CM4 model lower rainfall than observed rainfall, similar to their latitudinal distribution.

The spatial distributions of the annual averaged RMSE values (mm year^{-1}) from the 20th century for NEA are shown in Figure 2.3. A number of the models show the highest RMSE values occur along the coastal regions of Queensland (including CGCM3.1-T47, GFDL-CM2.0, GISS-ER, GISS-EH, GISS-AOM, IPSL-CM4, MPI-ECHAM5 and MRI-CGCM2.3.2a, with lower RMSE values over inland regions. In contrast, the IAP-FGOALS1.0 and MIROC3.2(med) models show higher RMSE values over inland NEA. The NCAR-CCSM3.0 model shows a zone of higher RMSE values over the southwest portion of Queensland. Twelve of the models fail

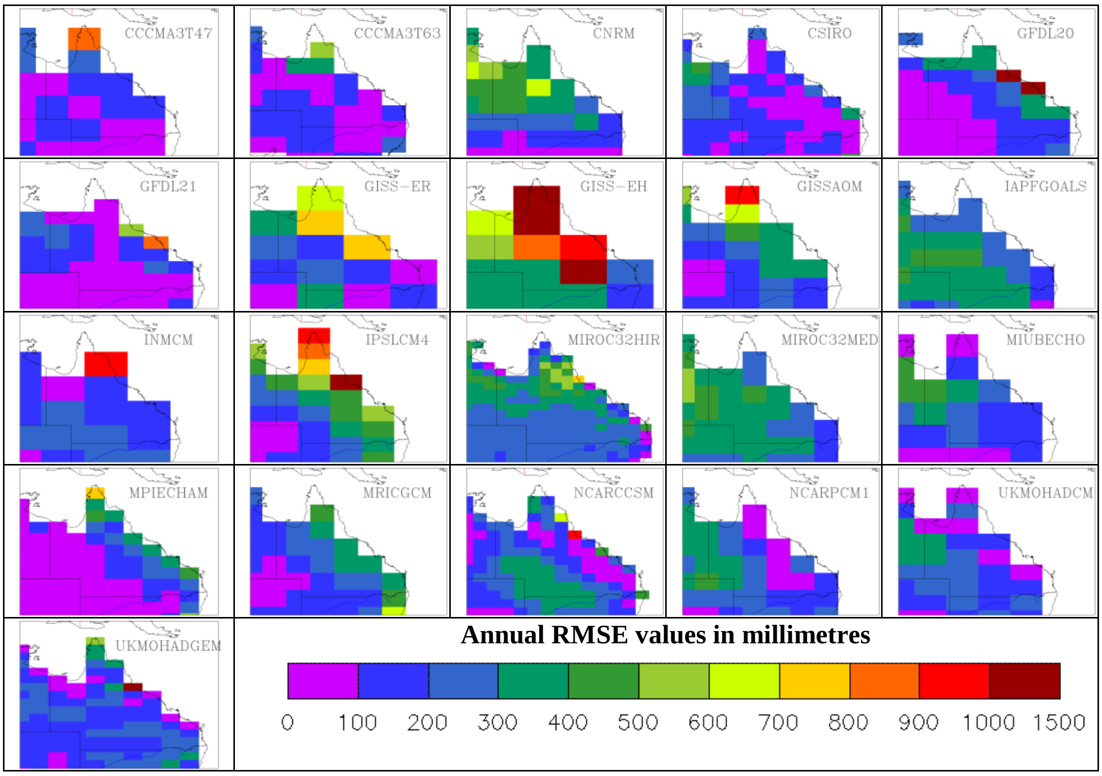

Figure 2.3 Annual RMSE values (mm year $^{-1}$) for IPCC–AR4 GCMs over NEA and the period 1901–2000.

in simulating the higher rainfall over the Cape York Peninsula. A summary of the area averaged annual RMSE values are shown in Table 2.3, which also shows seasonal and monthly values discussed in the following sections 2.3.2 and 2.3.3.

Table 2.3 Summary of the Average Annual (mm year^{-1}), Seasonal (mm season^{-1}) and Monthly (mm month^{-1}) RMSE values, Ranking and Final Rank from the 21 IPCC–AR4 models.

Model	Annual RMSE		Seasonal RMSE Value						Monthly RMSE		Final
Name	Value	Ranking	DJF	MAM	JJA	SON	Average	Ranking	Value	Ranking	Rank
1. CGCM3.1-T47	143.1	**4**	105.4	24.61	30.61	28.97	47.4	**5=**	17.3	6	**5**
2. CGCM3.1-T63	121.6	**3**	80.99	32.71	29.35	24.19	41.8	**3**	15.7	**3**	**3**
3. CNRM-CM3	280.7	15	157.2	94.18	18.53	41.65	77.9	16	27.0	16	16
4. CSIRO-MK3.0	146.6	**5**	95.47	42.79	24.96	18.46	45.4	**4**	16.9	**4**	**4**
5. GFDL-CM2.0	173.5	6	93.72	59.67	14.90	21.36	47.4	**5=**	17.0	**5**	6
6. GFDL-CM2.1	115.5	**1**	77.32	31.34	15.43	19.82	36.0	**2**	13.6	**2**	**2**
7. GISS-AOM	267.1	14	149.7	63.57	17.08	40.69	67.8	14	22.9	13	14
8. GISS-ER	288.8	17	177.9	60.09	26.91	78.1	85.8	19	29.2	19	19
9. GISS-EH	645.1	21	286.7	160.7	63.25	147.4	164.5	21	55.3	21	21
10.IAPFGOALS1.0	305.3	18	114.2	43.99	59.48	103.9	80.4	17	28.2	17=	17
11. INM-CM3.0	225.6	13	86.19	58.43	36.93	58.08	59.9	11	21.2	11	12
12. IPSL-CM4	361.0	20	203.4	85.93	21.01	55.55	91.5	20	30.7	20	20
13.MIROC3.2 hires	281.1	16	117.1	59.98	32.50	81.68	72.8	15	24.6	15	15
14.MIROC3.2med	325.1	19	119.5	63.16	39.33	112.1	83.5	18	28.2	17=	18
15. MIUB-ECHO-G	195.8	9	137.0	22.93	13.52	66.21	59.9	12	21.8	12	11
16. MPI-ECHAM5	115.7	**2**	53.79	22.63	16.91	28.04	30.3	**1**	11.0	**1**	**1**
17.MRICGCM2.3.2a	210.2	11	101.0	48.26	25.16	38.65	53.3	8	18.1	8	9
18.NCARCCSM3.0	205.0	10	121.7	35.45	24.48	55.75	59.4	10	21.0	10	10
19. NCAR-PCM1	222.1	12	136.6	46.32	25.6	32.8	60.3	13	23.0	14	13
20.UKMOHadCM3	182.6	7	112.2	26.99	21.79	57.5	54.6	9	19.8	9	8
21.UKMOHadGEM	188.8	8	87.04	53.16	26.97	35.94	50.8	7	17.6	7	7
Average	**238.1**		**124.5**	**54.1**	**27.8**	**54.6**	**65.3**		**22.8**		

Notes 1: The five models with the lowest RMSE values and ranking for the annual, seasonal and monthly intervals are highlighted in bold.
2. The overall final rank of each model is listed in the last column on the right.

The models with the lowest averaged annual RMSE values are the GFDL-CM2.1 (116 mm $year^{-1}$), MPI-ECHAM5 (116 mm $year^{-1}$), CGCM3.1-T63 (122 mm $year^{-1}$), CGCM3.1-T47 (143 mm $year^{-1}$) and CSIRO-MK3.0 (147 mm $year^{-1}$) models (rank highlighted in Table 2.3) and the highest averaged annual RMSE values are the IPSL-CM4 (361 mm $year^{-1}$) and GISS-EH (645 mm $year^{-1}$) models. The models with the lowest annual RMSE values generally show higher annual RMSE values along the Queensland coast and lower annual RMSE values over inland areas.

The higher resolution models like NCAR-CCSM3.0 and MIROC3.2(hires) have annual RMSE values of 205 and 281 mm $year^{-1}$ with a ranking of 10 and 16 respectively, indicating these higher resolution models have not produced lower annual RMSE values as would be generally expected. While it is generally assumed higher resolution models perform better than lower resolution models, they may not capture important features (such as large mountain ranges or sea surface temperature gradients) in an accurate representation and therefore may have been better not to have captured them at all.

2.3.2 Seasonal Climatology

In DJF (Figure 2.4a), the observed zonally averaged rainfall ranges from around 100 mm in the south (~30ºS) to over 600 mm (~16ºS), associated with the Australian monsoon. Twelve models simulate higher rainfall south of about 18ºS and most models lower rainfall north of 15ºS than observed rainfall. The IPSL-CM4 and GISS-AOM models simulate lower rainfall from 10–32ºS, whereas the GISS-EH model simulates much higher rainfall than observations. In MAM (Figure 2.4b),

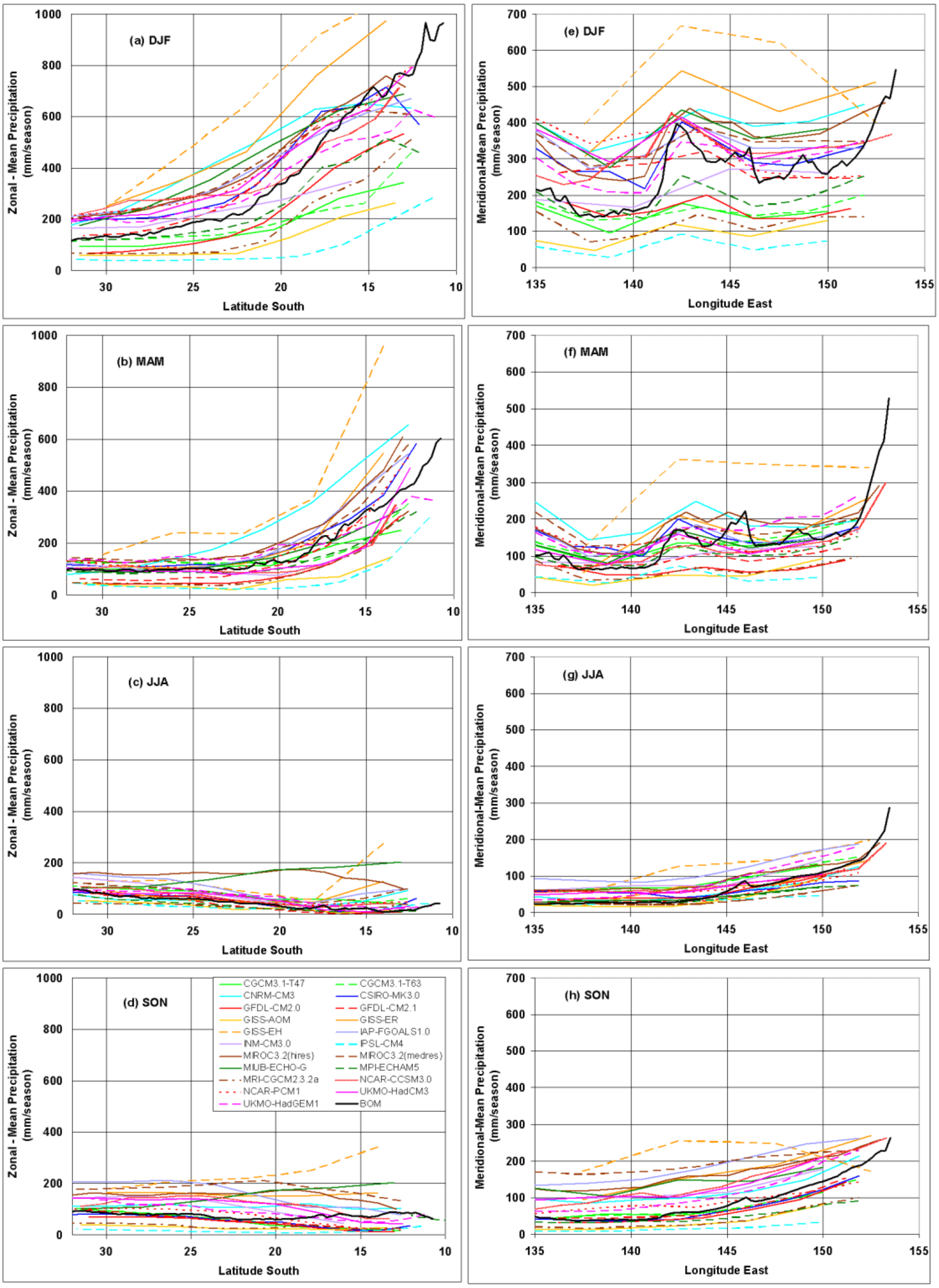

Figure 2.4 (a–h) Seasonal zonally (left) and meridionally (right) averaged rainfall (mm season^{-1}) over NEA and the period 1901–2000. (a,e) DJF, (b,f) MAM, (c,g) JJA and (d,h) SON. Legend applies to all plots.

observed rainfall is lower over the whole region, with about 100 mm south of about 20ºS rising to 600 mm at 12ºS. Nineteen models simulate rainfall close to the observed rainfall between 20º–32ºS. The IPSL-CM4 and GISS-AOM models simulate slightly lower rainfall and the CNRM-CM3 and GISS-EH models higher rainfall than observed rainfall. Rainfall associated with the monsoon trough is still well simulated north of about 15ºS in all models. In JJA (Figure 2.4c), observed rainfall is highest in the south at 32ºS (~100 mm) and decreases northward to very low levels (<50 mm) at 12ºS. Eleven models generally simulate slightly higher rainfall than observed rainfall across the entire latitudinal range. In SON (Figure 2.4d), observed rainfall is slightly higher than JJA across the region. Simulated rainfall is higher in twelve of the models than the observed rainfall, except in the IPSL-CM4, GISS-AOM and MRI-CGCM2.3.2a models, which are lower.

In DJF (Figure 2.4e), observed meridionally averaged rainfall varies from about 200 mm, west of about 141ºE, to about 400 mm at 142.5ºE (associated with higher rainfall over Cape York Peninsula) and over 400 mm east of 152.5ºE (associated with higher coastal rainfall). The austral summer has the greatest range of simulated rainfall in the GCMs from over 600 mm simulated by GISS-EH model, to under 100 mm in the IPSL-CM4 and GISS-AOM models. In MAM (Figure 2.4f), observed rainfall decreases across the region especially over Cape York Peninsula, while the coastal rainfall in the east is maintained. The GISS-EH model produces the highest simulated rainfall over most of the region and IPSL-CM4 and GISS-AOM models the lowest. In JJA (Figure 2.4g), the lowest observed rainfall occurs with less than 50 mm west of about 145ºE, and up to 200 mm or more about the east coast (~154ºE). Eleven of the models simulate higher rainfall west of about 145ºE and closer to observed rainfall further east. The GISS-EH model simulates higher rainfall across most of the region. In SON (Figure 2.4h), higher observed rainfall occurs than for

JJA, with eleven models simulating higher rainfall over all longitudes. The GISS-EH model produces the highest simulated rainfall and IPSL-CM4 and GISS-AOM models the lowest.

The models with the lowest seasonal RMSE values (averaged over all seasons) are the MPI-ECHAM5 (30 mm season^{-1}), GFDL-CM2.1 (36 mm season^{-1}), CGCM3.1-T63 (42 mm season^{-1}), CSIRO-MK3.0 (45 mm season^{-1}), CGCM3-T47 (47 mm season^{-1}) and GFDL-CM2.0 (47 mm season^{-1}) models. A summary of the seasonal and season averaged RMSE rainfall values and ranking are shown in Table 2.3 and the top five ranked models are highlighted. The models with the highest RMSE values are IPSL-CM4 (92 mm season^{-1}) and GISS-EH (165 mm season^{-1}) models. The seasonal RMSE for all the 21 IPCC–AR4 models is highest in DJF (averaging 125 mm season^{-1}), followed by SON (55 mm season^{-1}), MAM (54 mm season^{-1}) and JJA (28 mm season^{-1}). The results from the seasonal climatology are similar to the annual climatology (section 2.3.1), with the top five ranked models shown in the annual climatology also identified by the seasonal climatology, although with a slightly different order of ranking.

2.3.3 Monthly Climatology

The monthly climatology from the 21 IPCC–AR4 models over NEA are shown in Figure 2.5. Area–averaged rainfall from the BoM observations ranges from as high as 100 mm in January to as low as 13 mm in August. Simulated rainfall from many of the GCMs is similar to the observed low–rainfall period from about April to August (~25 mm month^{-1}), except for the GISS-EH model, which shows

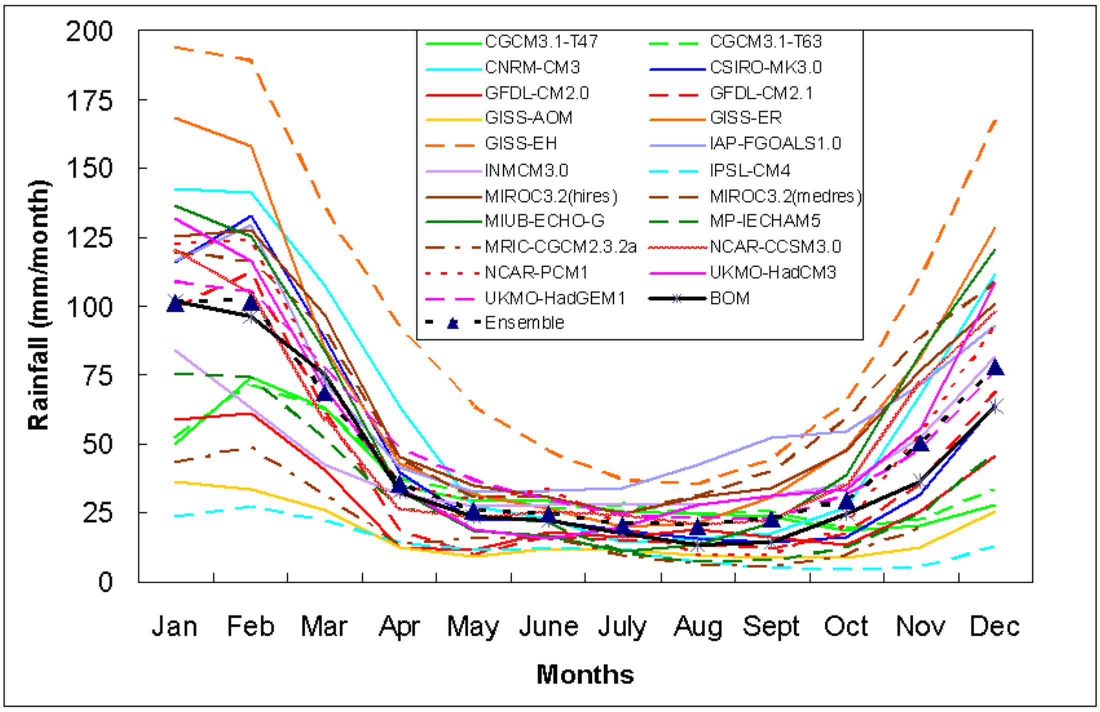

Figure 2.5 Monthly climatology for rainfall (mm month^{-1}) over NEA and the period 1901–2000.

considerably higher rainfall. During the higher–rainfall period from September to March, the simulated rainfall varies much more between models. It ranges from as low as 25 mm month^{-1} in the IPSL-CM4 model to as high as ~200 mm month^{-1} in the GISS-EH model. The IPSL-CM4 and GISS-EH models simulate much lower and higher rainfall respectively for all months compared to observations. Eleven models show a rainfall maximum in January and ten models in February, compared to January from observations. A rainfall minimum occurs for most of the models in August–September, similar to observations. An ensemble of all the models shows an overestimate (underestimate–negative) for DJF of +6.5 mm month^{-1}, MAM of -0.5 mm month^{-1}, JJA of +4 mm month^{-1}and SON of +9 mm month^{-1}.

A summary of the averaged monthly RMSE values are shown in Table 2.3. The average monthly RMSE value for each model is calculated and averaged for each of the 12 months to calculate a ranking number. The individual monthly RMSE values for the 21 IPCC–AR4 GCMs are shown in Appendix One. The top five models (lowest averaged monthly RMSE) for the monthly climatology are the MPI-ECHAM5 (11 mm month^{-1}), GFDL-CM2.1 (14 mm month^{-1}), CGCM3.1-T63 (16 mm month^{-1}), CSIRO-MK3.0 (17 mm month^{-1}) and GFDL-CM2.0 (17 mm month^{-1}) models (rank highlighted in Table 2.3). The model with the highest averaged monthly RMSE is the GISS-EH model (55 mm month^{-1}). The ranking results are very similar to the annual and seasonal RMSE analysis, with the top five models consistently selected by each analysis.

2.3.4 Model Ranking

To identify the five IPCC–AR4 models which simulate 20th century rainfall closest to the observed rainfall climatology for NEA, the three rankings for annual, seasonal and monthly RMSE are summed and the overall final ranking for all the models determined. The final rankings are shown in the final column in Table 2.3.

The two models with the lowest RMSE values are MPI-ECHAM5 and GFDL-CM2.1 with a final ranking of one and two respectively. They consistently score low ranks in each of the three climatologies. They are followed by CGCM3.1-T63, CSIRO-MK3.0 and CGCM3.1-T47 models (final ranks of 3 to 5 respectively). The two models with highest RMSE values are the IPSL-CM4 and GISS-EH models (highest sum of ranks with a final rank of 20 and 21 respectively). Although there are two different methods that can be used to rank the models in the seasonal and monthly climatologies, including using the average RMSE value for each period (month or season) and calculating the rank (Table 2.3) or ranking each season or month individually and calculating the final rank from their sum (not shown), it makes little difference to the final rank for most of the models over NEA. In the following sections 2.4 and 2.5, the five models with lowest RMSE are used for further 20th and 21st century analysis.

2.4 TIME SERIES OF ANNUAL RAINFALL

Five plots showing the area averaged annual rainfall over NEA from BoM observations and the five models with the lowest final rank for the period 1901–2000 are shown in Figure 2.6 (a–e). Observed annual rainfall (in black) shows a range of annual rainfall variability, with the highest yearly rainfall recorded in 1950 (~972 mm) and the lowest annual rainfall in 1902 (~255 mm). The observed mean annual rainfall for the 20th century is about 523 mm with a standard deviation (SD) of 125 mm. Trend analysis of observed mean annual rainfall shows an increase from 475 mm to 527 mm from 1901–1950 and 518 mm to 573 mm from 1951–2000. The increase in rainfall from 1951–2000 is due to the higher rainfall over northern and eastern parts of the Northern Territory and adjacent areas by the Queensland border (Figure 1.2 and 2.1a).

The GFDL-CM2, CGCM3.1-T63 and MPI-ECHAM5 models have a similar standard deviation and a lower mean annual rainfall (than BoM observations) of 477 mm (SD=99 mm), 435 mm (SD=87 mm) and 382 mm (SD=75 mm) respectively (Figures 2.6a–c). The CSIRO-MK3.0 model (Figure 2.6d) shows a similar amplitude in the rainfall variability compared to observations, with a slightly higher mean annual

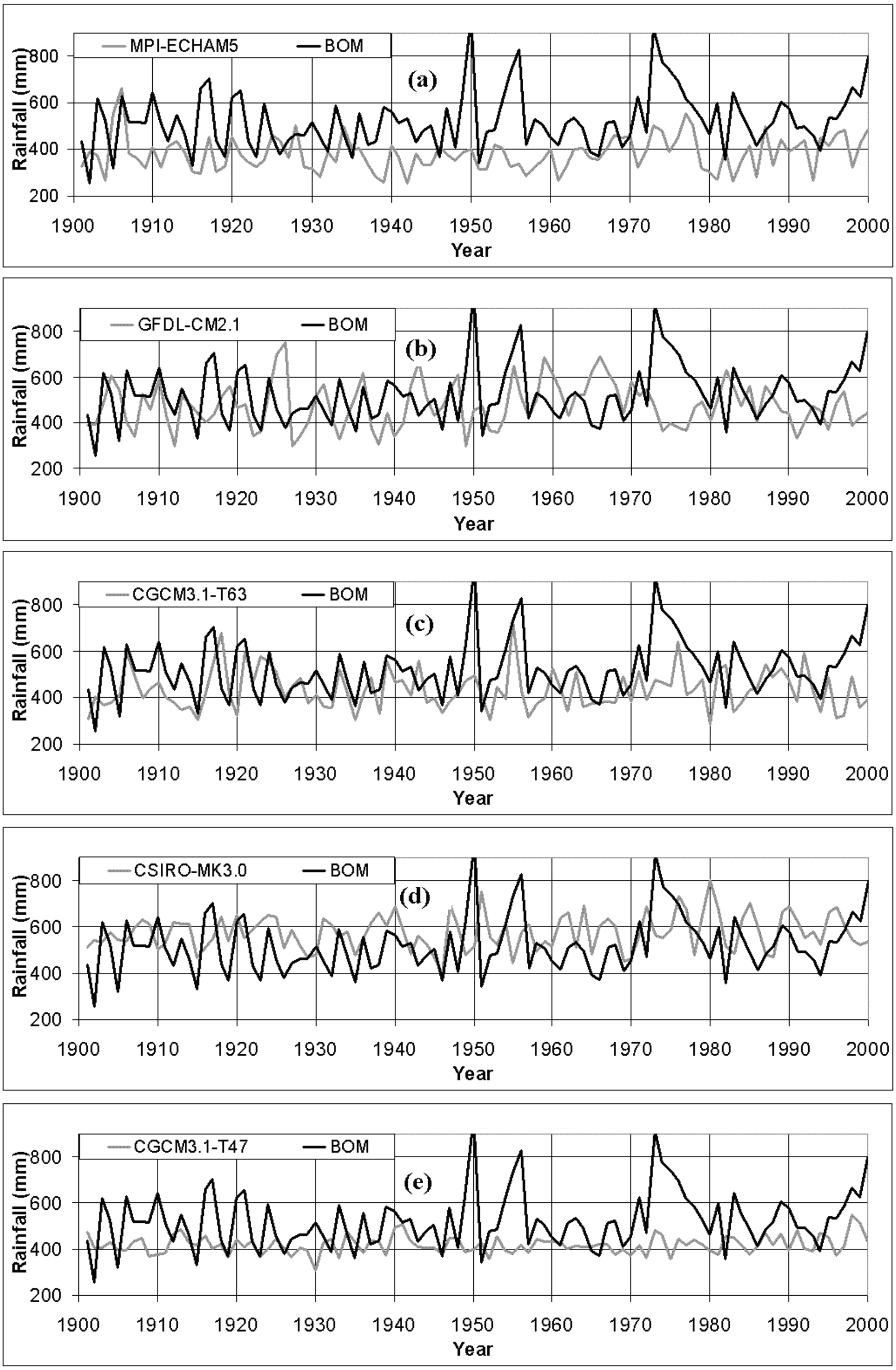

Figure 2.6 (a–e) Time series of the mean annual rainfall (mm) from five IPCC–AR4 models (grey) and BoM observations (black) over NEA and the period 1901–2000.

rainfall of 577 mm and lower SD of 78 mm. The CGCM3.1-T47 model (Figure 2.6e) shows mean annual rainfall of 419 mm and a lower amplitude in the rainfall variability, with a SD of 40 mm.

Decadal rainfall trends for the period 1901–1950 (details not shown) show a small increase in GFDL-CM2.1 and CGCM3.1-T63 models and a decrease in the MPI-ECHAM5 and CSIRO-MK3.0 models. No significant decadal rainfall trends occur in the CGCM3.1-T47 model. However, for the period 1951–2000, four models (MPI-ECHAM5, CSIRO-MK3.0, CGCM3.1-T63 and CGCM3.1-T47) show an increase in rainfall and the GFDL-CM2.1 model a decrease in rainfall, which overall is similar to observations for the whole region. Hence the models compare well to the BoM observations, indicating that they can capture some of the regional rainfall characteristics.

The correlation values between rainfall from the five GCMs and the BoM observations for the three time intervals 1901–2000, 1901–1951 and 1951–2000 are shown in Table 2.4. For the 1901–2000 period, the MPI-ECHAM5 and CGCM3.1-T63 models show a significant positive correlation (at the level of significance of 10%) of 0.187 and 0.279 respectively. The correlation values for the other three models are low and therefore indicate there is no significant correlation between rainfall from the GCMs and the BoM observations at this level of significance (10%). For the 1901–1951 period, only the CGCM3.1-T63 model shows a significant correlation of 0.320 to the BoM rainfall at the level of significance (10%). For the 1951–2000 period, three models MPI-ECHAM5, CGCM3.1-T63 and the GFDL-

Table 2.4 Summary of the Correlation Values of Annual Rainfall from BoM Observations and the five GCMs over NEA (1901–2000).

Model	MPI-ECHAM5	GFDL-CM2.1	CGCM3.1-T63	CSIRO-MK3.0	CGCM3.1-T47	Critical Values for Pearson r
Period						
1901–2000	**0.187**	-0.125	**0.279**	-0.003	0.093	0.164
1901–1951	0.089	-0.066	**0.320**	0.020	-0.043	0.231
1951–2000	**0.259**	**-0.243**	**0.254**	-0.070	0.200	0.231

Notes 1. Critical values for Pearson r and two tailed level of significance at 10%.
2. Values in bold are above the level of significance.

CM2.1 show a significant correlation to the BoM rainfall (above a value of 0.231 at a level of significance of 10%), although the GFDL-CM2.1 correlation is negative.

2.5 DECADAL RAINFALL TRENDS

2.5.1 Introduction

Decadal rainfall trends scaled by variability are presented from the five models with lowest RMSE. Instead of using non–standardised decadal rainfall trends, this study uses the rainfall trend divided by the standard deviation (standardised decadal rainfall trends), which highlights regions where rainfall trends are large compared to variability. A comparison between the non–standardised and standardised decadal rainfall trends from the BoM observations for 1951–2000 is provided (Figure 2.7–top two rows). Standardised decadal rainfall trends for the three periods 1951–2000, 2001–2050 and 2051–2100 from the five models are shown in Figures 2.7, 2.8 and 2.9 respectively. Finally, ensemble means of the standardised decadal rainfall trends for the A2 scenario (four models) for the three periods are shown in Figures 2.10 and 2.11. This analysis will provide information on the long–term rainfall trends over the

NEA region and identify the major differences between the 20th and 21st century simulations. As mentioned previously, the rainfall analysis for 1901–1950 is not completed due to the observed decadal rainfall trends from the BoM being much smaller than for 1951–2000. The two terms ‘annual decadal rainfall trends’ and ‘seasonal decadal rainfall trends’ refer directly to the ‘decadal trends in annual rainfall’ and the ‘decadal trends in seasonal rainfall’ respectively in this chapter.

For 21st century rainfall projections, the MPI-ECHAM5, CGCM3.1-T47, CSIRO-MK3 and GFDL-CM2.1 models use the A2 climate scenario. The CGCM3.1-T63 model uses the next highest emission scenario –A1B. All non–standardised seasonal decadal rainfall trends range in value between -100 to +100 mm decade^{-1} for the 20th century, but non–standardised annual decadal rainfall trends are larger and range from -225 to +150 mm decade^{-1} in the 2001–2050 and 2051–2100 periods (not shown).

2.5.2 Period 1951–2000

Seasonal and annual non–standardised and standardized decadal rainfall trends from the BoM observations for 1951–2000 are shown in Figure 2.7 (top two rows respectively). Non–standardised decadal rainfall trends (Figure 2.7 top row) in DJF, shows the largest decrease in rainfall (up to 100 mm decade^{-1}) occurs along and inland of the east coast of Queensland and the largest increase in rainfall (up to 100 mm decade^{-1}) over the Cape York Peninsula and the region bordering the Gulf of Carpentaria. DJF is the most important rainfall season in terms of the amount of rainfall for the NEA region. During MAM, decreasing rainfall (up to 100 mm decade^{-1}) covers most of NEA and is highest along the east coast. In JJA, decreasing rainfall covers much of NEA with values up to 25 mm decade^{-1}, highest over SE QLD. During SON, most of NEA shows an increase in rainfall (up to 20–25 mm

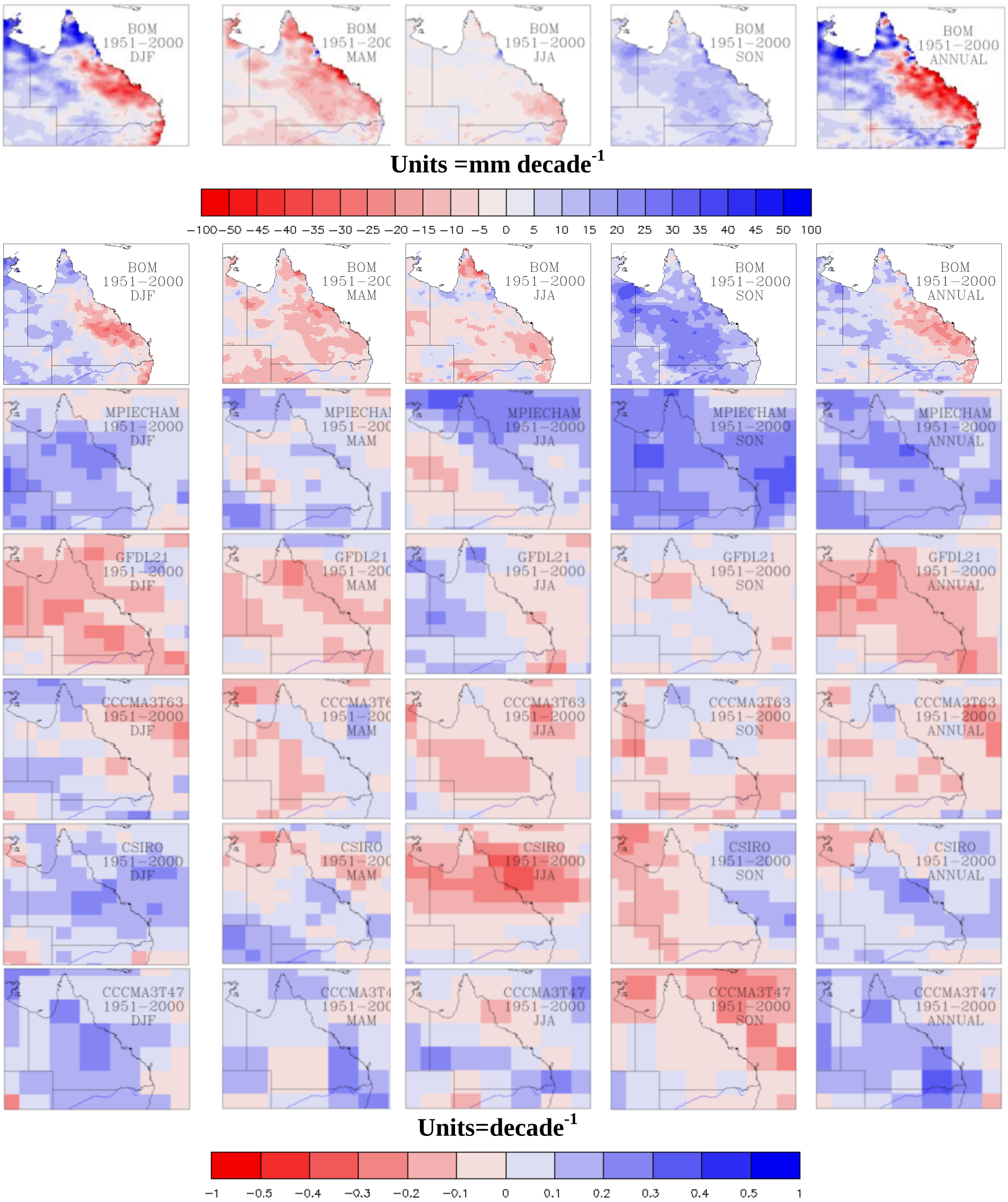

Figure 2.7 Non–standardised (mm decade^{-1}) and standardised (decade^{-1}) seasonal and annual decadal rainfall trends from BoM observations (top two rows) and standardised seasonal and annual decadal rainfall trends (decade^{-1}) from five IPCC–AR4 models (bottom rows) for NEA and the period 1951–2000. Regions shaded in red show decreasing rainfall and blue increasing rainfall. The GCMs are listed by rank from 1 (MPI-ECHAM5) to 5 (CCCMA3.1-T47).

decade^{-1}). The non–standardised annual decadal rainfall trends (Figure 2.7 top row–far right) show decreasing rainfall (up to 100 mm decade^{-1}) along the east coast region of Queensland, south of about Cairns and increasing annual decadal rainfall (up to 100 mm decade^{-1}) over parts of the Cape York Peninsula and the coastal region of the Gulf of Carpentaria. The inland region of western, southwestern Queensland and the adjacent border shows increasing rainfall of up to 20–25 mm decade^{-1}.

In the seasonal standardised decadal rainfall trends from the BoM observations (Figure 2.7-second row), most of the coastal rainfall trends are subdued for DJF due to the higher rainfall variability. Inland regions show only small changes compared to the non–standardised decadal rainfall trends. In MAM, the decadal rainfall trends change little between standardised and non–standardised values, although the coastal values are subdued a little. In JJA, a stronger decreasing rainfall response occurs, and in SON, a stronger increasing rainfall response is produced over inland areas than shown in the non–standardised decadal rainfall trends. The standardised annual decadal rainfall trends show subdued coastal rainfall trends and only small changes inland.

Standardised decadal rainfall trends from five GCMs for 1951–2000 are shown in Figure 2.7 (bottom five rows). In DJF, the MPI-ECHAM5, CSIRO-MK3 and CGCM3.1-T47 models simulate increasing rainfall over most of NEA. The GFDL-CM2.1 model shows decreasing rainfall and the CGCM3.1-T63 model, increases and decreases in rainfall or ‘mixed signals’ over most of NEA. In MAM, the MPI-ECHAM5 model shows increasing rainfall over much of NEA, the GFDL-CM2.1

model decreasing rainfall (especially along the east coast), the CGCM3.1-T63 model increasing rainfall along the east coast and decreasing rainfall inland and the CSIRO-MK3 and CGCM3.1-T47 models, 'mixed signals'. In JJA, the models CGCM3.1-T63 and CSIRO-MK3 show decreasing rainfall, the MPI-ECHAM5 and GFDL-CM2.1 models mostly small increasing and decreasing rainfall parallel to the east coast respectively, and the CGCM3.1-T47 model 'mixed signals' over NEA. During SON, the MPI-ECHAM5 model shows increasing rainfall over all of the NEA region, the CSIRO-MK3 and CGCM3.1-T47 models decreasing rainfall over most of NEA and the other two models 'mixed signals'. Standardised annual decadal rainfall trends show moderate increases in rainfall in the MPI-ECHAM5 model, smaller rainfall increases in the CSIRO-MK3 and CGCM3.1-T47 models, moderate decreases in rainfall in the GFDL-CM2.1 model and small decreases in rainfall in the CGCM3.1-T63 model.

In summary, the models show considerable variation between each other in the seasonal and annual decadal rainfall trends and only two models (GFDL-CM2.1 and CGCM3.1-T63) simulate the rainfall decline over the coastal region of eastern Queensland similar to the BoM observations.

2.5.3 Period 2001–2050

Standardised seasonal and annual decadal rainfall trends from the five GCMs for 2001–2050 are shown in Figure 2.8. The following descriptions are from the models with the A2 scenario. In DJF, the two models (MPI-ECHAM5 and CGCM3.1-T47) generally show decreasing rainfall over NEA. The GFDL-CM2.1 model shows

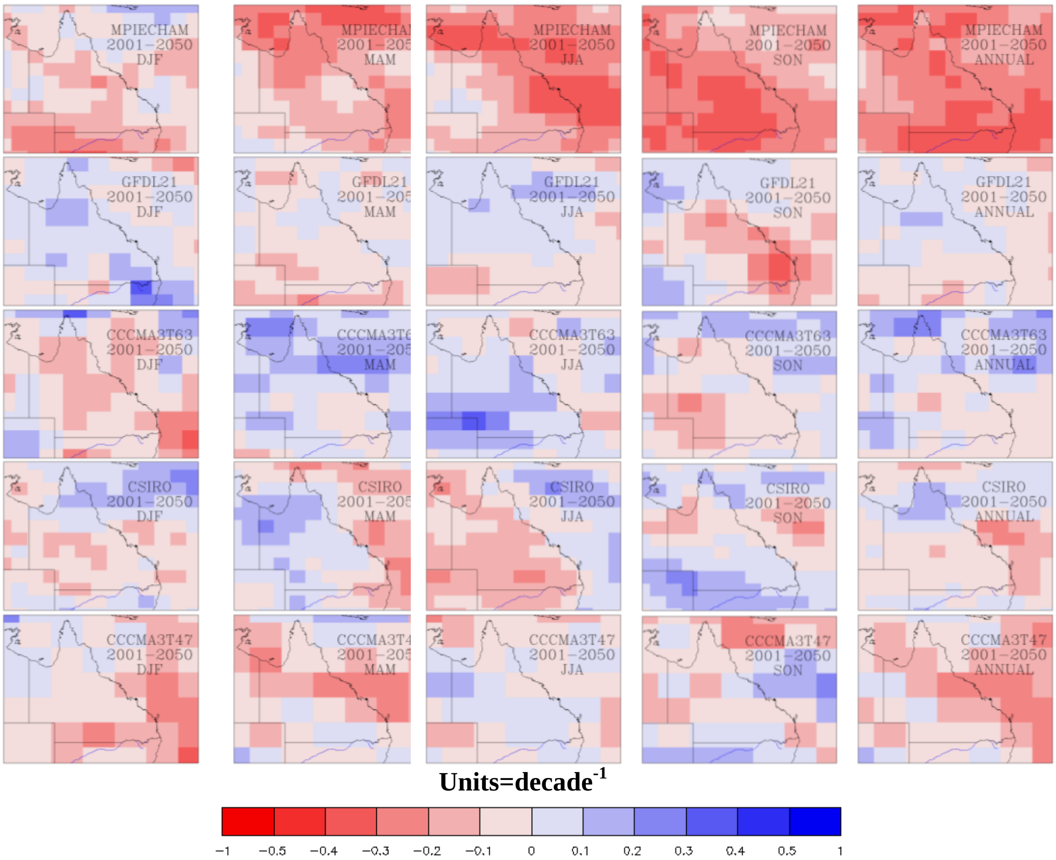

Figure 2.8 Standardised seasonal and annual decadal rainfall trends (decade^{-1}) from five IPCC–AR4 models over the NEA region and the period 2001–2050. Colour shading as in Figure 2.7.

increasing rainfall (especially over east coastal regions) and the CSIRO-MK3 model decreasing rainfall over central and southern Queensland, with increasing rainfall over the Cape York Peninsula region. In MAM, three models (MPI-ECHAM5, GFDL-CM2.1 and CGCM3.1-T47) mostly show decreasing rainfall over NEA and the CSIRO-MK3 model shows increasing rainfall (particularly over the base of the Gulf of Carpentaria). In JJA, the MPI-ECHAM5 and CSIRO-MK3 models show decreasing rainfall over most of NEA and 'mixed signals' in the GFDL-CM2.1 and CGCM3.1-T47 models. In SON, the MPI-ECHAM5 model shows decreasing rainfall over the entire NEA region, decreasing rainfall in GFDL-CM2.1 model and 'mixed signals' in the CSIRO-MK3 and CGCM3.1-T47 models.

Standardised annual decadal rainfall trends in the MPI-ECHAM5 and CGCM3.1-T47 models show mostly decreasing rainfall over the NEA region. The GFDL-CM2.1 and CSIRO-MK3 models show decreasing rainfall over central and southern Queensland and increasing rainfall over northern parts of NEA.

For the A1B scenario (CGCM3.1-T63 model), DJF shows decreasing rainfall, MAM shows increasing rainfall over northern parts of NEA, JJA shows increasing rainfall and SON decreasing rainfall over most of NEA. The standardised annual decadal rainfall trend shows decreasing rainfall over central and southern Queensland and increasing rainfall over northern parts of NEA.

In summary, most models now show a distinct change to lower rainfall over much of southern and central Queensland and the neighbouring Coral Sea and a few models, small increases in rainfall over far northern regions, such as Cape York Peninsula.

2.5.4 Period 2051–2100

Standardised seasonal and annual decadal rainfall trends from the five GCMs for 2051–2100 are shown in Figure 2.9. Using models from the A2 scenario, the seasons show the following. In DJF, the CSIRO-MK3 model shows decreasing rainfall over nearly all the NEA region and the MPI-ECHAM5 and GFDL-CM2.1 models, decreasing rainfall over most of NEA (except the base of the Gulf of Carpentaria). The CGCM3.1-T47 model shows increasing rainfall over most of NEA. In MAM, the MPI-ECHAM5 and CSIRO-MK3 models show decreasing rainfall over most of NEA. The GFDL-CM2.1 and CGCM3.1-T47 models generally show decreases in

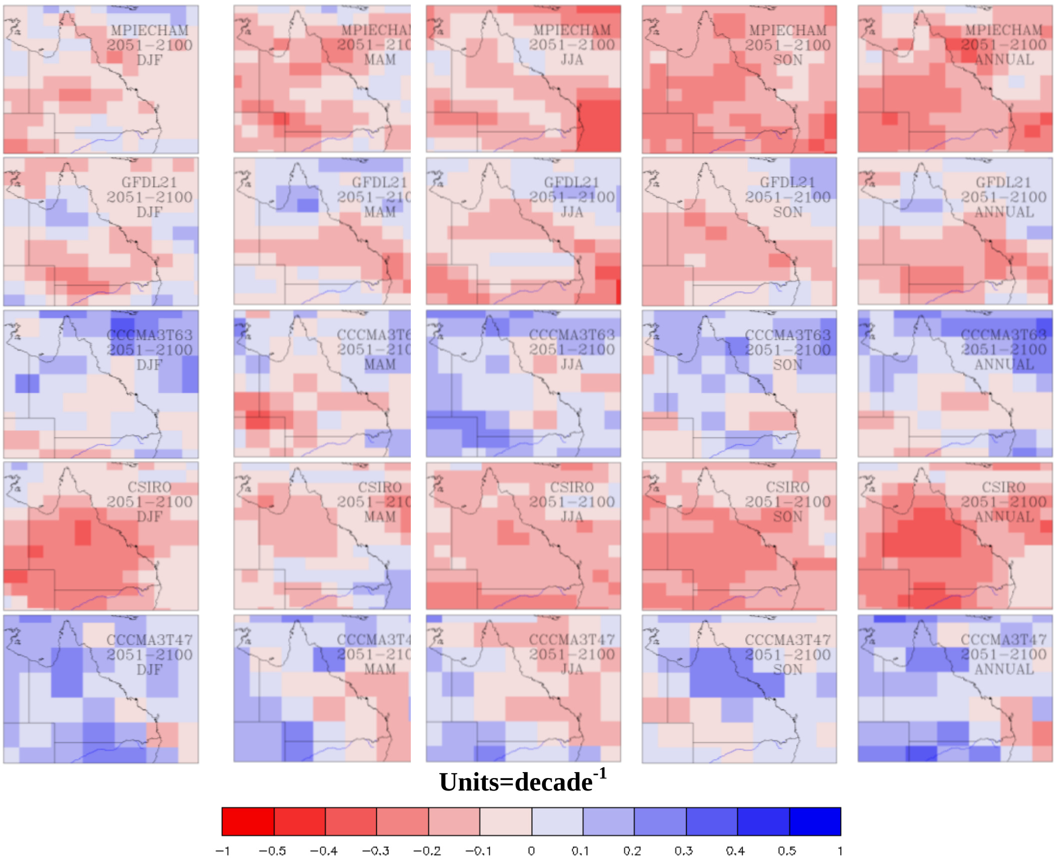

Figure 2.9 Standardised seasonal and annual decadal rainfall trends (decade^{-1}) from five IPCC–AR4 models over the NEA region and the period 2051–2100. Colour shading as in Figure 2.7.

rainfall over southern parts of Queensland with increasing rainfall over northern and western parts of NEA. In JJA, the MPI-ECHAM5, GFDL-CM2.1 and CSIRO-MK3 models show decreases in rainfall and CGCM3.1-T47 ‘mixed signals’ with decreasing rainfall over SE QLD. In SON, the MPI-ECHAM5 and CSIRO-MK3 models show decreases in rainfall over the entire NEA region and GFDL-CM2.1 decreases in rainfall over NEA. The CGCM3.1-T47 model show ‘mixed signals’.

Standardised annual decadal rainfall trends show decreases in rainfall in the MPI-ECHAM5 and CSIRO-MK3 models over nearly all the NEA region and decreases in rainfall in the GFDL-CM2.1 model (except over Cape York Peninsula). In contrast, the CGCM3.1-T47 model shows increases in rainfall over most of NEA.

The A1B scenario model (CGCM3.1-T63), in DJF shows 'mixed signals' in the decadal rainfall trends, MAM and JJA show decreasing and increasing rainfall respectively over most of NEA and SON shows 'mixed signals.' The standardised annual decadal rainfall trend shows decreasing rainfall over central and southern Queensland and increasing rainfall over northern parts of NEA, similar to 2001–2050.

In summary, the decreasing rainfall shown in 2001–2050 continues over much of NEA, with decreasing rainfall over central and southern areas of Queensland and some increases in rainfall in some of the models over northern regions of NEA.

2.5.5 Ensemble Means

Multi–model ensemble means (3.75º by 3.75º) of standardised seasonal and annual decadal rainfall trends from the four models (using the A2 scenario) are shown in Figure 2.10 for 1951–2000 and Figure 2.11 for the periods 2001–2050 and 2051–2100. BoM observations from 1951–2000 are shown (left column–Figure 2.10) for comparison. Grey shading represents all four models have the same sign of the rainfall trend over the region. For 1951–2000 (Figure 2.10–right column), DJF shows small increases in rainfall over most of NEA. This indicates that the ensemble does not pick up the decrease in rainfall along the Queensland coast shown in observations but does agree on some of the increasing rainfall further inland. Weak decreases and increases in rainfall in MAM and JJA are not particularly consistent with the BoM observations. However, weak increases in rainfall in SON over much of NEA are similar to the BoM observations.

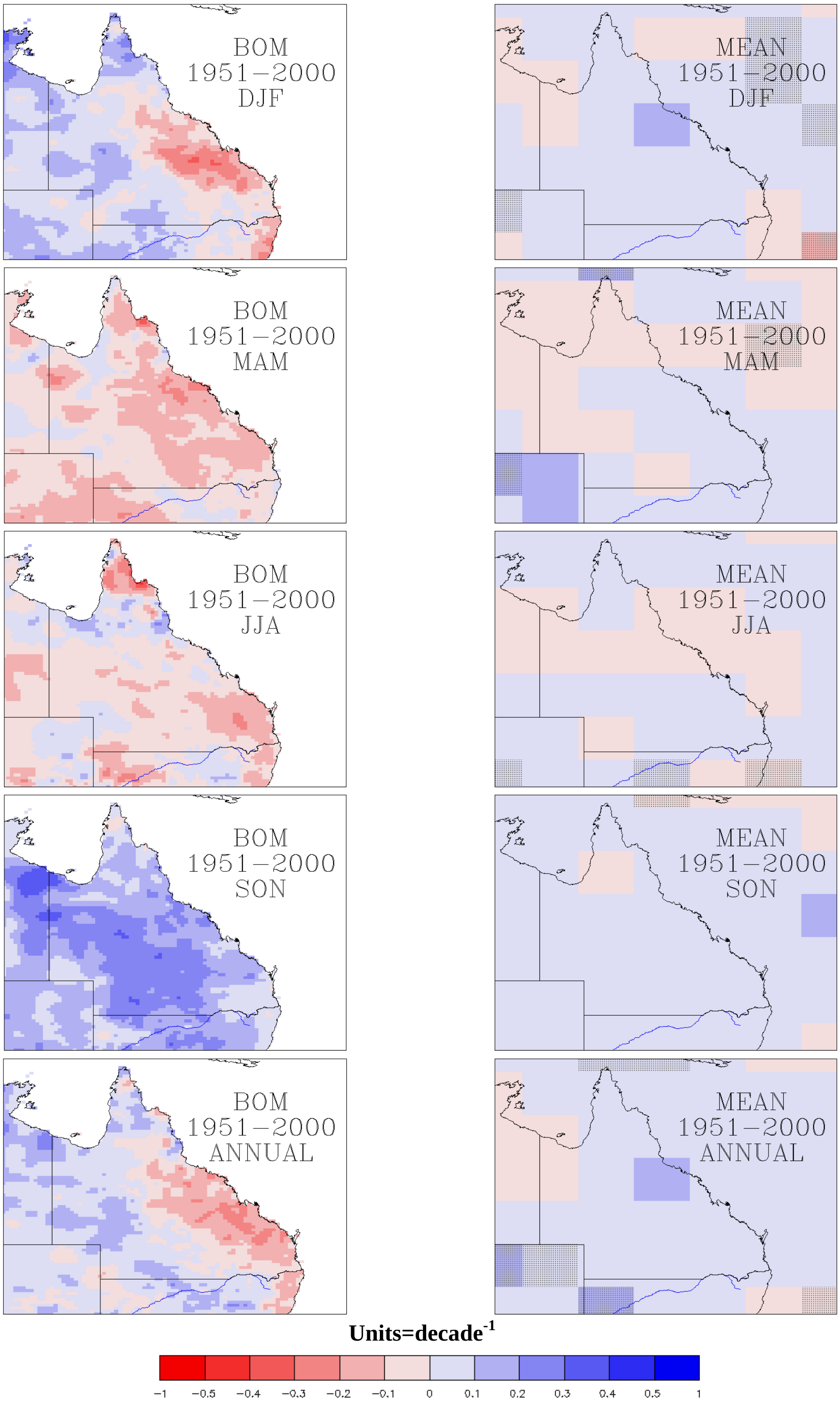

Figure 2.10 Standardised seasonal and annual decadal rainfall trends (decade^{-1}) from BoM observations (left column) and multi–model ensemble mean (right column) over the NEA region and 1951–2000. Colour shading as in Figure 2.7 and grey hatching indicates all models agree on the sign of the rainfall trend.

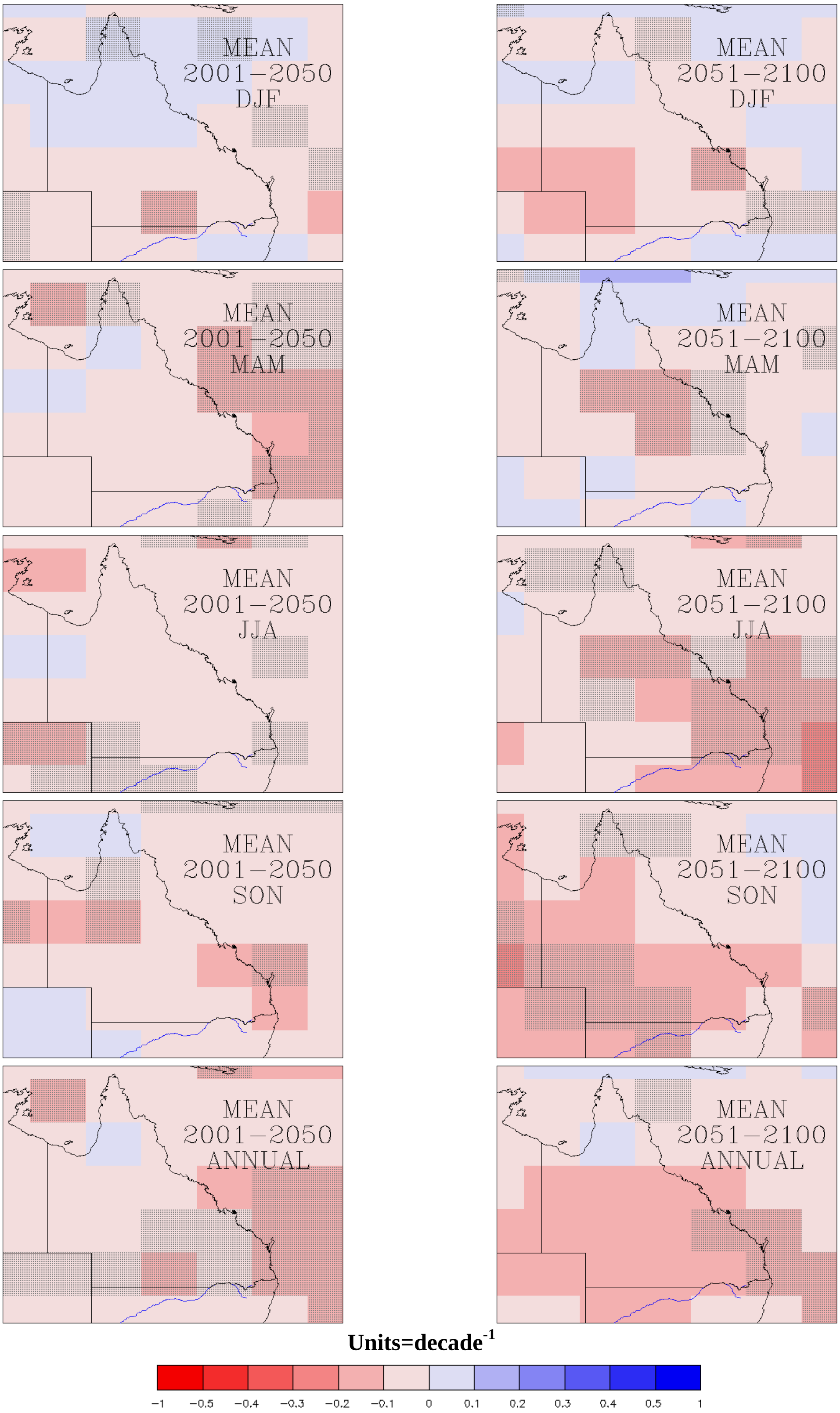

Figure 2.11 Standardised seasonal and annual decadal rainfall trends (decade^{-1}) from the multi–model ensemble mean over the NEA region and the periods 2001–2050 (left column) and 2051–2100 (right column). Colour shading as in Figure 2.7 and grey hatching indicates all models agree on the sign of the rainfall trend.

The annual decadal rainfall trend in the multi–model ensemble for 1951–2000 shows weak increases over most of NEA and does not produce the decreasing rainfall shown by observations along the Queensland coast. Few regions have grey shading and indicate the models do not agree on the rainfall trends very well.

For 2001–2050 (Figure 2.11–left column), the seasonal decadal rainfall trends become more aligned to decreasing rainfall over NEA, similar to BoM observations (1951–2000). All seasons now show most of central and southern Queensland and the Coral Sea have decreasing rainfall, with large areas of grey shading in the annual decadal rainfall trend, indicating all models agree on this rainfall decline.

For 2051–2100 (Figure 2.11–right column), all seasons now show stronger rainfall decreases compared to the 2001–2050 over NEA (except parts of the Cape York Peninsula in DJF and MAM). All seasons except DJF have larger regions shaded in grey over NEA (especially central and southern Queensland), where all models agree on the decreasing rainfall response. The annual decadal rainfall plot shows decreasing rainfall, significantly stronger over most of NEA than for 2001–2050, although with less grey shading.

2.5.6 Summary

Three models simulate increasing annual decadal rainfall and two models decreasing annual decadal rainfall over NEA for 1951–2000. The GFDL-CM2.1 model generally has the correct sign, strength and the closest geographical distribution of the decreasing rainfall located along the east coast of Queensland for DJF, MAM and

JJA, compared to BoM observations. The multi–model ensemble mean shows similar rainfall trends to observations in SON only, with MAM and JJA ‘mixed signals’ in the rainfall trends. The annual decadal rainfall trends in the multi–model ensemble mean did not show the higher rainfall in the west and lower rainfall in the east shown by the BoM observations.

Rainfall projections for 2001–2050, using standardised seasonal decadal rainfall trends show a significant change from the seasonal decadal rainfall trends in 1951–2000, with two models MPI-ECHAM5 and CGCM3.1-T47 changing sign from increasing to decreasing rainfall. Five models now show decreasing annual rainfall over southern Queensland. The MPI-ECHAM5 model has the strongest decrease in rainfall in all seasons across all of NEA. Twelve of the season plots show decreasing rainfall, four increasing rainfall and four ‘mixed signals’ over NEA. The multi–model ensemble mean of the seasonal decadal rainfall trend (2001–2050) shows a distinct change from the 1951–2000 rainfall trends, with decreasing rainfall in all seasons over central and southern Queensland.

The rainfall projections for 2051–2100, using standardised seasonal decadal rainfall trends, are similar to 2001–2050, except the GFDL-CM2.1 and CSIRO-MK3 models now have stronger decreasing rainfall over most of NEA in seven out of the eight plots. The CGCM3.1-T47 model has changed sign from decreasing rainfall in 2001–2050, to increasing rainfall in 2051–2100 in DJF and MAM. Twelve of the season plots show distinct decreasing rainfall, three increasing rainfall and five ‘mixed signals’ over NEA. The multi–model ensemble mean of annual decadal rainfall trend shows a stronger decreasing rainfall response over central and southern Queensland than in 2001–2050. However, it should be noted that the decrease in rainfall shown for 2051–2100 is on top of the decrease in rainfall that has already occurred in the 2001–2050 period and therefore points to considerable lower rainfall climatology (by 10–15%) by 2100, compared to the 20th century, over much of central and southern Queensland.

2.6 RAINFALL CHANGES OVER QUEENSLAND BY 2031–2050 AND 2081–2100

As described in section 2.5, widespread rainfall declines are expected over much of coastal, southern and central Queensland during the 21st century. To provide further information on these rainfall changes, the difference between the mean annual rainfall in the 1961–1990 climatology calculated from the multi–model ensemble mean (using the four models in section 2.5.5) and the mean annual rainfall from the two periods 2031–2050 and 2081–2100, also using the multi–model ensemble mean, are shown in Figures 2.12 and 2.13 respectively. The rainfall changes are presented in millimetres and also as a percentage of the 1961–1990 model climatology. Although the analysis could have used the difference between the BoM rainfall observations from the 1961–1990 climatology (Figure 1.1) and the mean annual rainfall from the two periods 2031–2050 and 2081–2100 from the multi–model ensemble mean, the results would have been affected by the higher and lower rainfall represented in the models over the inland and coastal regions respectively (discussed in section 2.3.1) and this would have led to significantly different 21st century rainfall trends. These differences in the rainfall between the coastal and inland regions also occurs in the four models selected for the A2 analysis (Figure 2.2 (a–b)), with the GFDL-CM2.1, MPI-ECHAM5, CSIRO-MK3 and CGCM3.1-T47 ranked one, two, four and five respectively in the annual 20th century climatology (Table 2.2). Hence, the rainfall changes shown in Figures 2.12 and 2.13 are the rainfall changes between the 20th and 21st century simulations and not between the 20th century BoM observations and the 21st century IPCC–AR4 models projections.

In Figure 2.12 (a–b), the mean rainfall change between the 1961–1990 model climatology and the rainfall projections for 2031–2050, show the east coast from Brisbane north to Cairns, and inland to the Northern Territory border has a small rainfall decline between 10 to 30 mm (2–6%), with locally higher rainfall declines in the Brisbane and Mackay regions (30–60 mm). The percentage of the rainfall decline is higher over some of the inland regions due to the lower annual rainfall away from the coastal regions. Over the Cape York Peninsula region, a small increase in rainfall between 20 to 70 mm (2–6%) occurs, presumably due to the closer proximity to the austral summer monsoon. The increase in rainfall over the Cape York Peninsula region was noted in some models from section 2.5.3. Since the models underestimated the coastal rainfall for the 20th century over the Queensland region, it is likely the actual rainfall declines maybe higher than the values stated here.

In Figure 2.13 (a–b), the mean rainfall change between the 1961–1990 model climatology and the rainfall projections for 2081–2100, show the east coast from Brisbane north to Cairns and most of inland Queensland have larger rainfall declines, compared to the rainfall projections for 2031–2050. Rainfall declines between 30 to 50 mm (6–12%) occur over most of the state, with the highest percentage rainfall

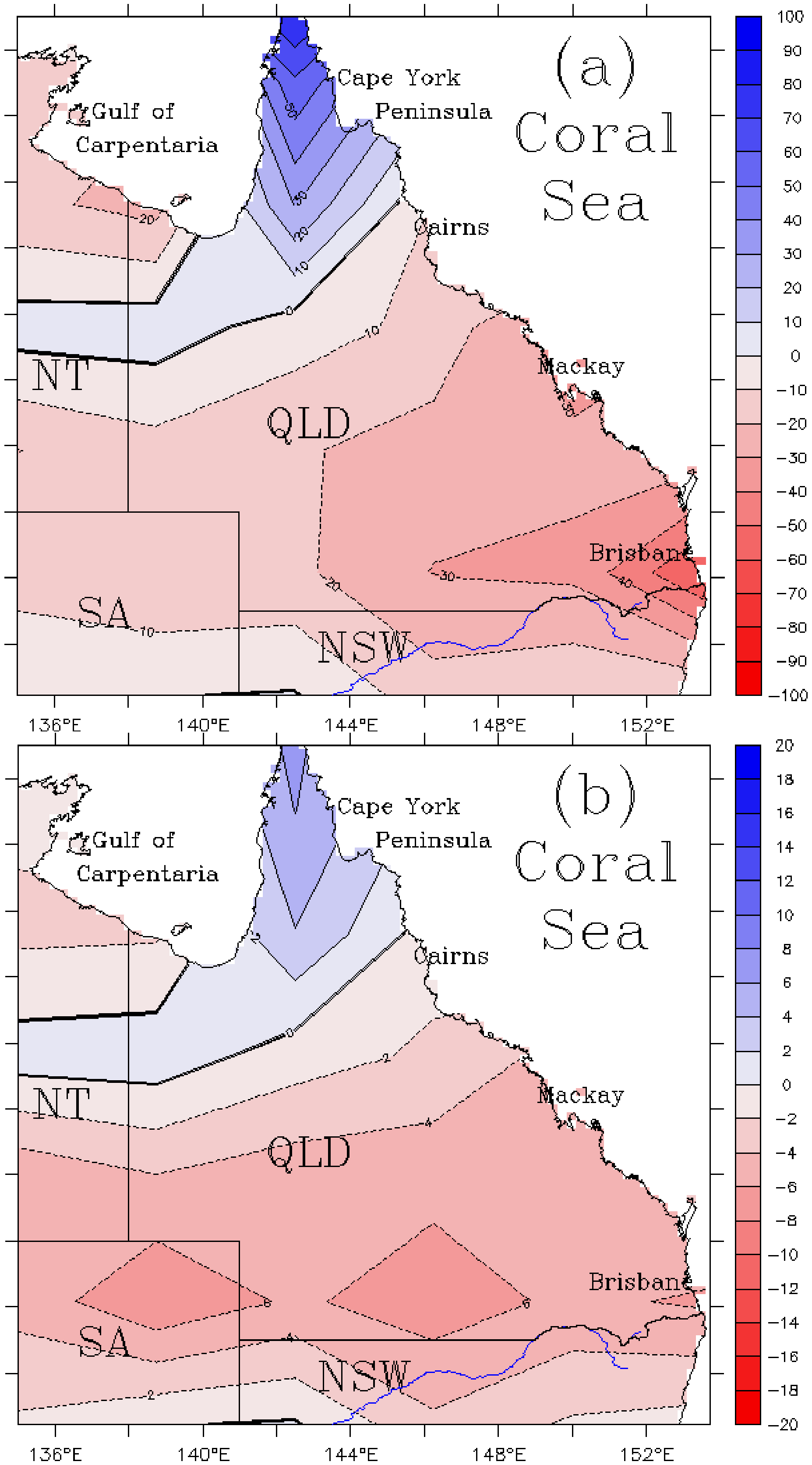

Figure 2.12 (a–b) Annual rainfall change in millimetres (a) and by percentage of rainfall (b) for 2031–2050 compared to the multi–model ensemble mean for 1961–1990 annual climatology. Regions in red and blue indicate a rainfall a decline or increase respectively. Solid black line denotes no change.

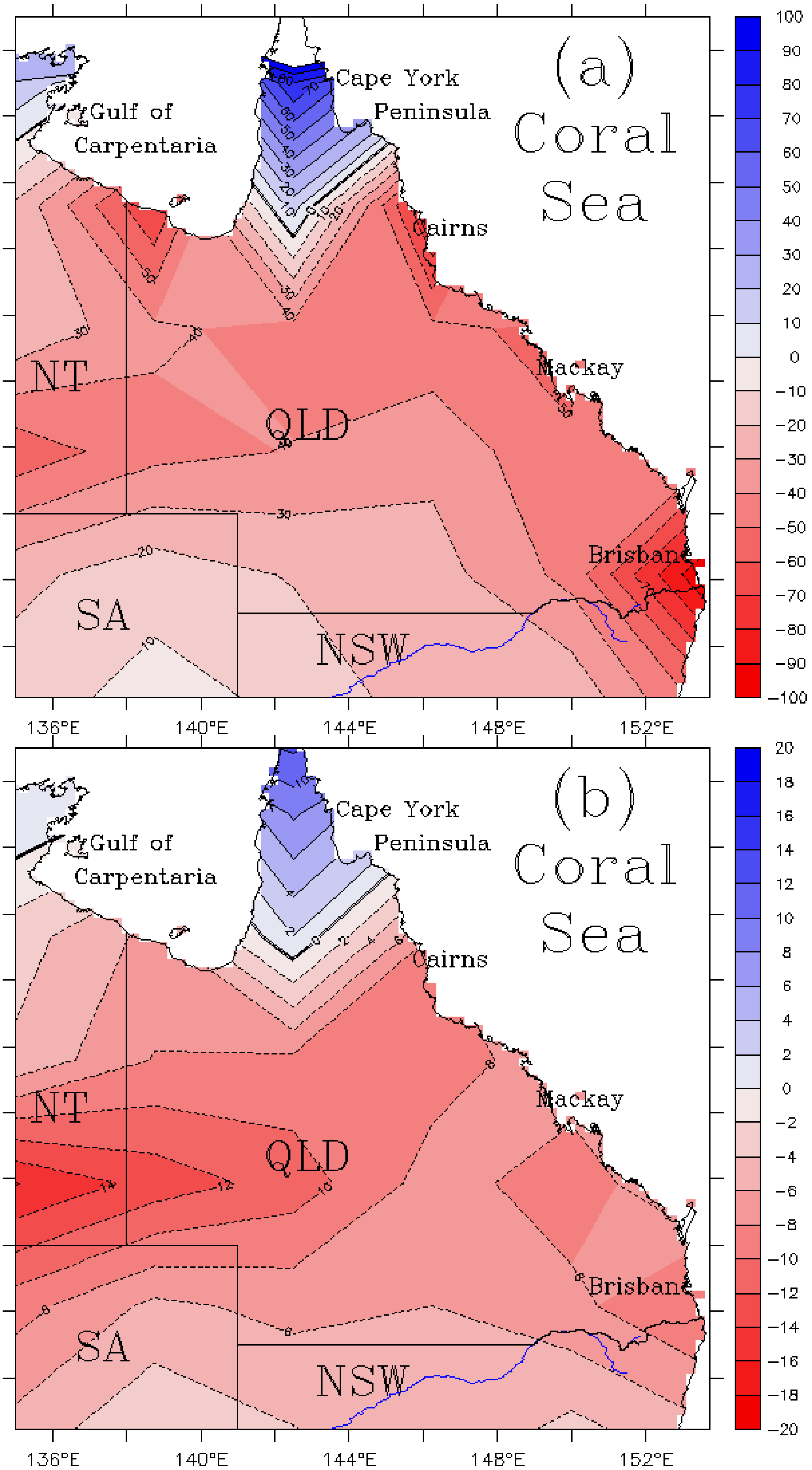

Figure 2.13 (a–b) Annual rainfall change in millimetres (a) and by percentage of rainfall (b) for 2081–2100 compared to the multi–model ensemble mean for 1961–1990 annual climatology. Regions in red and blue indicate a rainfall a decline or increase respectively. Solid black line denotes no change.

declines over western border regions and the coastal area from Brisbane north to Cairns. The highest decline in rainfall in millimetres occurs in the Brisbane region (70–90 mm) and the area from Cairns to Mackay (50–60 mm). Over the northern regions of the Cape York Peninsula, a rainfall increase from 40–100 mm (4–10%) or higher is simulated from the multi–model ensemble. Some of the colour shading and contouring in Figure 2.13 does not match in several places, such as in the Mt Isa region and just north of Mackay in Figure 2.13a and in the Brisbane region in Figure 2.13b. The contour values are correct.

In summary, rainfall projections from the multi–model ensembles for the 21st century show rainfall declines over much of Queensland during the first half of the century, increasing during the second half of the 21st century. In 2031–2050, rainfall declines by 2–6% cover much of coastal and southern and central Queensland, with a small increase in rainfall by 2–6% over the Cape York Peninsula region. By 2081–2100, the rainfall declines have intensified over much of the Queensland region, with rainfall declines now stronger between 6–12%. In contrast, the rainfall increases are now stronger over the Cape York Peninsula at 4–10%. The rainfall declines may actually be larger along the coastal regions due to the lower simulated rainfall in the models identified from the 20th century simulations, most likely due to the poor representation of regional orography and the coastal ranges in the models.

2.7 DISCUSSION

An analysis of the 20th century rainfall simulations (1901–2000) from 21 IPCC–AR4 models shows that many of the models simulate higher rainfall in the JJA and SON over NEA and lower rainfall in DJF over coastal regions and the tropics. These results are similar to the study conducted by Moise et al (2005). In general, the GCMs produce broad seasonal rainfall patterns similar to observations, which is consistent with global studies (Sun et al. 2006). Some of the models like GISS-EH and IPSL-CM4 consistently simulate higher and lower rainfall respectively over the NEA in all months and seasons. Most of the models are able to reproduce rainfall associated with the Australian monsoon trough during DJF and MAM. In JJA, most models simulate higher rainfall over southern NEA and less rainfall over northern Australia than in BoM observations. Models with a resolution between 1º–2º consistently simulate rainfall with values closer to the observed rainfall than models with lower resolution (>2º). Models with a resolution between 2º–4º have similar RMSE values, but the GCMs with a resolution of 4º or greater, consistently simulate higher or lower rainfall than observed rainfall and have the highest RMSE, possibly due to poor representation of the orography in the models.

In the latest report from the IPCC–AR4 on regional climate projections using the SRESA1B climate change scenario and mean annual precipitation, the changes in rainfall from 1980–1999 to 2080–2099 show rainfall decreases of 0–15% over most of the east coast of Queensland, south of Cairns in JJA, with a small increase in rainfall in DJF and a small annual decrease (Christensen et al. 2007). This is similar to the analysis completed here (except for DJF), although the A2 climate change response with higher greenhouse gas forcing will be slightly stronger. Increases in 21st century rainfall in DJF over southern Queensland have also been described in other studies (Moise et al. 2005; Suppiah et al. 2007). More recently, Pitman and Perkins (2008) describe rainfall projections (using only models with a skill score of

0.8 or higher calculated by measuring the overlap from two probability density functions) under the A2 scenario, showing widespread increasing mean rainfall in all seasons except winter by 2050 for NEA. However by 2100, decreasing rainfall becomes established in winter and spring but summer and annual trends still exhibit a small increase in rainfall. An interpretation of Australian rainfall projections by Shi et al (2008) shows rainfall is expected to increase by 0–10% by 2055–2085 over SE QLD. However, this projection was based on results from one model and combined results from three global warming scenarios. Clearly the results of this study are different and show lower rainfall in the 21st century projections by 4–6% by 2031–2050 and 6–12% by 2081–2100, with declines in all seasons by 2100 over much of Queensland, consistent with the current rainfall trends.

This study provides more robust rainfall projections over the Queensland region than other studies for several reasons. This study over the NEA region is much smaller in area and shows some similarities between the 20th century multi–model ensemble and observed rainfall trends. Also, the decadal rainfall trends include all years of rainfall variability during the 20th and 21st centuries and not the difference between one or more decades from different centuries in other studies. These rainfall projections contain a blend of results from over land and the Coral Sea, providing more certainty in the sign of the rainfall trend for the region. The rainfall projections from the Fitzroy Basin study (McGregor et al. 2006) are similar in magnitude and sign to the five models used here, but that analysis was much smaller in area. In this analysis, the five models with the lowest RMSE values show a distinct alignment toward a drier 21st century, irrespective of the season over central and southern Queensland. More importantly, whether four or six models are selected with lowest

RMSE values for the 21st century projections, the ensembles show similar 21st century rainfall trends to the five models used here. A recent study by Alexander and Arblaster (2009) used a bootstrapping technique to compare observed and model extremes over Australia for the 20th century in relation to future projections. They concluded that not one model was able to produce all the climate indices and only the multi–model ensemble was skilful in modelling trend patterns. This is similar to the study completed here except the RMSE analysis was used. It is likely that in the multi–model ensembles, some signal loss may have occurred due to the lower resolution, especially where there is substantial disagreement between members, such as in the 1951–2000 period. However, in the 21st projections, signal loss is less likely to be an issue as the rainfall trends become more aligned over the central and southern Queensland.

The convergence of the models toward less rainfall over most of NEA provides substantial evidence that further decreases in rainfall are likely during the coming decades. If the two models CGCM3.1-T63 and CGCM3.1-T47 are removed from the group of five as they do not have stratospheric ozone (Flato et al. 2000 in Cai and Cowan (2007)) and show unrealistic 20th century global warming (Douville et al. 2006; Brand et al. 2008), the decreasing rainfall response becomes much stronger over southern Queensland. The importance of ozone in model simulations should not be underestimated (Brand et al. 2008). Depletion of stratospheric ozone over the high latitudes of the Southern Hemisphere and the South Pole was first reported in the 1980s and is primarily caused by the production of anthropogenic chlorofluorocarbons (CFCs) (Skinner et al. 1999; Solomon 1999; Ahrens 2003).

Ozone is also an important factor in the strength and trend of the SAM (Marshall 2003).

The GFDL-CM2.1, CSIRO-MK3 and MPI-ECHAM5 models also show similar interdecadal variability with relatively good spectral peak of ENSO (Lin 2007). The MPI-ECHAM5, GFDL-CM2.1 and CSIRO-MK3 were the second, sixth and seventh ranked models respectively for rainfall over most regions of Australia (Perkins et al. 2007). This study shows the higher emission scenario A2 produces a stronger drying response in the second half of the 21st century, which is consistent with the recent report by CSIRO (2007) and by Pitman and Perkins (2008). The stronger response in the second half of the 21st century occurs when most of the global temperature rise will occur due to global warming under the A2 scenario (Christensen et al. 2007; CSIRO and Meteorology 2007).

The position, intensity and duration of the Australian monsoon trough during the austral summer and autumn seasons are the dominant controlling factors for much of the rainfall over tropical Australia (Suppiah and Hennessy 1996; Cook and Heerdegen 2001; Sturman and Tapper 2006). The GCMs used in this study are able to simulate the spatial, monthly and seasonal rainfall well in terms of the austral summer and autumn seasons over Queensland, indicating that they are able to simulate many of the features associated with the Australian monsoon. The understanding of the monsoon trough dynamics and tropical circulation (Douville et al. 2006) in the Australian region is of critical importance to determine the sign and intensity of future changes of rainfall over tropical NEA. Changes in the monsoon circulation may cause abrupt changes in the rainfall patterns (Narisma et al. 2007).

The ability of GCMs to simulate the Australian monsoon during the 20th century, will improve future 21st century simulations under a changing climate of rising greenhouse gases (Stainforth et al. 2005), increasing global temperatures (Smith et al. 2007) and an amplifying hydrological cycle (Wetherald and Manabe 2002; Brutsaert 2006; Oki and Kanae 2006; Wentz et al. 2007; Williams et al. 2007). In the austral winter and spring seasons, the GCMs generally produce lower rainfall over the entire NEA region similar to observations, showing the GCMs are able to simulate important synoptic features, such as the subtropical ridge (discussed further in Chapters Three and Four).

A number of factors have been suggested to account for the rainfall declines along the eastern seaboard of Australia (including southern Queensland) during the second half of the 20th century. Natural variability and factors such as atmospheric circulation changes such as the poleward shift in the westerly jet (Thompson and Solomon 2002; Archer and Caldeira 2008), the latitude and strength of the subtropical ridge (Nowak and Leighton 1997; Ansell et al. 2000; Murphy and Ribbe 2004), changes in the Walker (Tanaka et al. 2004; Vecchi et al. 2006; Power and Smith 2007) and Hadley (Clement 2006; Douville et al. 2006; Kobayashi and Maeda 2006; Lu et al. 2007) circulations, ENSO (Stone et al. 1996; Lavery et al. 1997; Cai et al. 2001; Suppiah 2004; Verdon et al. 2004), sea surface temperatures (Lough 1992; Drosdowsky 2002; Li, F. et al. 2005; Verdon and Franks 2005; England et al. 2006), the number of tropical cyclones in the Coral Sea (Evans and Allan 1992; Shaun and Jonathan 2007; Kuleshov et al. 2008) and the development of cloud bands (Wright 1997) may have all play a role.

However, anthropogenic factors including increasing atmospheric CO_2 and greenhouse gases (Cai 2004; Cai et al. 2005), aerosol concentrations (Cai et al. 2007; Rotstayn et al. 2008), ozone depletion (Cai 2006; Crook et al. 2008), the upward trend in SAM (Marshall 2003; Hendon et al. 2007; Meneghini et al. 2007) and land cover changes (Narisma et al. 2003; Siriwardena et al. 2005; Narisma and Pitman 2006) will become increasingly important on the changing rainfall patterns for this region and elsewhere. Anthropogenic forcing has altered global rainfall patterns (Zhang et al. 2007) and been proposed to account for about 50% in the reduction of rainfall in southwestern Western Australia (Cai and Cowan 2006). Significant anthropogenic temperature changes in Australia (Karoly and Braganza 2005) have already impacted on inflows into the Murray–Darling Basin (Cai and Cowan 2008b). Changes in the precipitation characteristics may explain some of the decreases in rainfall over NEA in 21st century projections. This includes decreases in the frequency, intensity and mean precipitation in the dry regions of the subtropics and Australia (Sun et al. 2007; Pitman and Perkins 2008). Changes in atmospheric circulation associated with enhanced oceanic rainfall around the equator and a corresponding drying in the subtropics (enhanced Hadley circulation) are seen in most GCMs for 21st century projections (Douville et al. 2006; Sun et al. 2007; Seidel et al. 2008).

This study shows the rainfall declines are likely to continue over southern and SE QLD well into the 21st century. More than one factor may have accounted for the rainfall decline during the 20th century and rising greenhouse concentrations in the atmosphere during the 21st century are likely to exacerbate this rainfall decline. Some of the contributing factors to the rainfall decline are investigated in the following three chapters.

In the next chapter, this study will explore the changes in mean sea level pressure (MSLP) and the subtropical ridge from BoM observations during the 20th century and investigate possible links to the decreases in rainfall over the NEA region. Such links have been very recently described by Nicholls (2009), where declines in rainfall over southern Australia south of 30ºS, have been directly correlated to an increase in MSLP over the region and changes in the SAM. The five IPCC–AR4 models selected in this chapter are also analysed for MSLP trends during the 20th and 21st centuries.

CHAPTER 3 : MEAN SEA LEVEL PRESSURE TRENDS OVER THE QUEENSLAND REGION

3.1 INTRODUCTION

The Queensland and NEA region is located in a unique position where austral winter and summer rainfalls are important for agriculture and other industries. Southern Queensland and much of the NEA region is strongly influenced by the location and strength of the subtropical ridge in all seasons (Murphy and Ribbe 2004; Drosdowsky 2005). The annual seasonal cycle of the MSLP over Queensland is dominated by higher MSLP in the austral winter associated with the subtropical ridge and lower MSLP in the austral summer associated with intrusion of the Australian monsoon trough over northern and central regions (Sturman and Tapper 2006). Other factors such as the ENSO (Rakich et al. 2008) and SAM (Cai and Cowan 2006; Shi 2008) provide regional climate variability on interannual and decadal time scales. Further factors were discussed in Chapter Two. Recently, Nicholls (2009) has described increases in MSLP over southern Australia between March and August are correlated to the trend in the SAM. This chapter investigates the MSLP changes over the NEA region and whether they are consistent with changes over the southern Australian region since ~1950.

As shown in Chapters One (Figure 2.1a) and Two (Figure 2.7), the rainfall declines have occurred on time scales of 50 years or longer and includes the austral summer and autumn over most of NEA, and to a lesser extent, the austral winter over southern and SE QLD. To account for this long–term rainfall decline, observations of seasonal and annual MSLP from the BoM are used to investigate whether the rainfall changes have also been accompanied by changes in MSLP. Rainfall projections discussed in Chapter Two also show central and southern Queensland will continue to have further rainfall declines over the region. This chapter will also investigate the MSLP trends in the 21st century projections.

Data and methodology are described in section 3.2. Results from BoM observations and the trends in seasonal and annual MSLP are shown in section 3.3, a time series of the MSLP changes in section 3.4 and the correlation between rainfall and MSLP from BoM observations in section 3.5. Finally, the five IPCC–AR4 models selected in Chapter Two are used to determine the decadal MSLP trends for both the 20th and 21st centuries over the NEA region in section 3.6. A discussion on the results is provided in section 3.7.

3.2 DATA AND METHODOLOGY

3.2.1 Mean Sea Level Pressure Data from the Bureau of Meteorology

Monthly MSLP data were obtained from the BoM from 39 stations over Queensland and nearby areas in NSW and from Norfolk, Lord Howe and Willis Islands, to identify the long–term MSLP trends over the NEA region and Queensland during the 20th and start of the 21st century. Although a larger number of stations with monthly MSLP data are available, many records are incomplete, too short or are located too close to other stations to be of benefit in this study. From 39 stations, several stations from the same location or town were amalgamated into one set of observations to form a continuous time series. Several stations could not be used due to the short period of observations (< ~15 years) and a number of stations had short periods of unreliable or erroneous data removed from the analysis. This resulted in a total of 25 stations of high quality MSLP data from the BoM over ~50 years, many which begin in the 1950s. Station names, identification numbers, the period of observations and percentage of months with observations available are shown in Table 3.1.

To calculate the seasonal MSLP (in hPa) at each station, the monthly MSLP values were firstly combined by averaging the three months for each season. The austral summer consists of December with January and February of the following year. The austral autumn, winter and spring consist of the months MAM, JJA and SON respectively. The annual MSLP is calculated by averaging the MSLP value from the 12 calendar months. This means there maybe small differences between the average of the four seasons and the annual MSLP from each station. The change in the seasonal and annual MSLP at each station for both the 9am and 3pm record was calculated using linear regression analysis on the entire time series in Excel. The absolute value of the MSLP change was determined by calculating the difference between the last and first MSLP value in the time series from the linear regression equation. The changes in MSLP from 9am and 3 pm were used to compare readings and both values used to calculate an overall mean MSLP change (shown in the 'Average' column in Table 3.2) in the seasonal and annual MSLP at each station. It is this 'Average' value of the change in MSLP that is used to determine the mean MSLP change and MSLP trends at each station. The results from this analysis are shown in section 3.3 (sections 3.3.1 to 3.3.3).

Table 3.1 Summary of the BoM stations used for the MSLP analysis over the NEA region from 1950–2008.

Number	Station Name	Station ID	Period	Percent Of Obs	Comments
Queensland					
1	Charleville	44021	Jul 1951-Oct 2007	98	Used
2	Roma Post Office	43030	Jan 1957-Jul 1992	98	Used
3	Roma Airport	43091	Jul 1992-Oct 2007	98	Used
4	Toowoomba	41103	Jan 1957-Jul 1998	98	Used
5	Toowoomba Airport	41529	Jun 1996- Oct 2007	97	Used
6	Brisbane Aero	40233	Jul 1951-Feb 2000	99	Used
7	Brisbane Aero	40842	Feb 2000 -Oct 2007	99	Used
8	Longreach Aero	36031	Mar 1966-Oct 2007	92	Used
9	Rockhampton	39083	Apr 1939-Oct 2007	98	Used
10	Mount Isa Aero	29127	Dec 1966-Oct 2007	95	Used
11	Townsville Aero	32040	Jan 1951-Oct 2007	99	Used
12	Mackay M.O.	33119	Sep 1959- Oct 2007	97	Used
13	Weipa Aero	27045	Nov 1992-Oct 2007	98	Used
14	Weipa Eastern Ave	27042	Jan 1959-Dec 1993	80	Used
15	Cairns Aero	31011	May1941-Oct 2007	97	Used
16	Clermont	35019	Jan 1970-Nov 2008	97	Used
17	Hughenden Airport	30022	Mar 2001-Nov-2008	96	Used
18	Hughenden Post Of	30024	Jan 1965-Feb 2001	93	Used
19	Birdsville Airport	38026	Jul 2000-Nov 2008	96	Used
20	Birdsville Police St	38002	Jan 1965-Apr 2001	96	Used
21	Thargomindah P.O.	45017	Dec 1965-Jul 1999	92	Used
22	Thargomindah Airp.	45025	Aug 1999-Nov 2008	96	Used
New South Wales					
23	Bourke P.O.	48013	Mar 1892-Nov 1994	95	Used
24	Bourke Airport AWS	48245	Dec 1998-Oct 2007	96	Used
25	Bourke Airport	48239	Nov 1994-Dec1998	95	Used
26	Moree Aero	53115	May 1995-Oct 2007	99	Used
27	Moree Comparison	53048	Mar 1964-Mat 1995	98	Used
28	Coffs Harbour	59040	Aug 1951-Oct 2007	98	Used
Islands					
29	Lord Howe Island	200440	Jul 1951-Nov 1988	98	Used
30	Lord Howe Island A.	200839	Nov 1988-Oct 2007	99	Used
31	Norfolk Island Aero	200288	Jul 1951-Oct 2007	98	Used
32	Marion Reef	200704	Jan 1992-Oct 2007	70	Not Used
33	Cato Island	200601	Dec 1992-Oct 2007	72	Not Used
34	Willis Island	200283	Nov 1921-Oct 2007	78	Not Used
100 Year Records					
35	Georgetown P.O.	30018	Jan 1894-Oct 2007	96	Used
36	Gaynah P.O.	39039	Feb 1889-Oct 2007	93	Used
37	Burketown P.O	29004	Nov 1890-Oct 2007	90	Used
38	Bundaberg P.O	39015	Feb 1894-Jun 1990	89	Used
39	Boulia Airport	38003	Jan1888-Oct2007	90	Used

Most of the stations have reliable MSLP data from the 1950s and 1960s, and five stations (numbers 35–39 in Table 3.1) have records dating back to the 1880s and 1890s. Five stations are selected from across the NEA region to provide a comparison of the annual MSLP changes during the last 50 years or so in time series plots. A six year moving average is shown for each station in the time series to show the large year to year variability, but still preserve the longer interdecadal and decadal MSLP trends. It was not used to calculate any of the absolute MSLP trends. The location of each station over NEA and Queensland is shown in Figure 3.1.

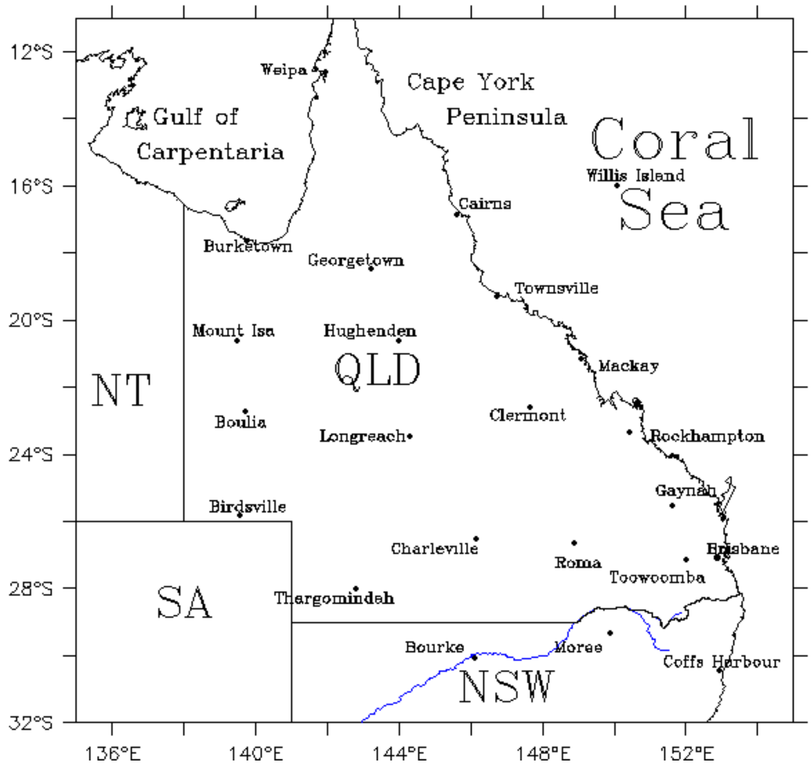

Figure 3.1 Location map of the BoM stations used for the MSLP analysis over the NEA region. Norfolk and Lord Howe Islands are located further to the east in the Tasman Sea and are not shown.

Decadal trends of the seasonal and annual MSLP are calculated for each station by dividing the total MSLP change by the number of years of each record and the result multiplied by ten (section 3.3.4). This provides an estimate of the average decadal change at each station. However, its does make the assumption of a constant rate of MSLP change for each decade. This data is displayed graphically as contoured seasonal and annual decadal MSLP trends. Although many of the time series from the stations used have different lengths, this has been taken into account by calculating the MSLP trend over a ten year interval (hPa decade^{-1}) and thereby reducing possible errors. The start and end date of each time series does not affect the value of the decadal MSLP trend.

A time series of the annual MSLP has been produced for the period ~1950–2008 for each station so the interdecadal variability, long–term MSLP trends and similarities (and differences) between stations could be assessed (section 3.4). A multi–station ensemble mean of all the stations is shown to demonstrate the overall MSLP trend for the entire NEA region. A six year moving average is shown for each station in this time series.

To identify significant relationships between the changes in MSLP and rainfall, a correlation analysis has been completed on the seasonal and annual values from the BoM observations. The correlation between the MSLP and rainfall has been calculated from 25 stations from 1950–2008, with rainfall data obtained from the same stations as the MSLP. Station rainfall data was downloaded from the BoM website (http:// www.bom.gov.au/climate/data/weather-data.shtml). The correlation was calculated using monthly values and the following formula:

$$Correl(X,Y) = \frac{\sum (x-\bar{x})(y-\bar{y})}{\sqrt{\sum (x-\bar{x})^2 \sum (y-\bar{y})^2}}$$

X–bar and y–bar are the sample means for the two variables. If r is the sample correlation coefficient and r^2 the square of the correlation, then r^2 is the sample coefficient of determination, which is the proportion of variability explained by the linear bivariate association between the two variables (Dowdy et al. 2004). Results are shown in section 3.5.

3.2.2 IPCC–AR4 Data

In Chapter Two, five models were identified with the lowest RMSE from the 20th century rainfall analysis over NEA. These are the MPI-ECHAM5, GFDL-CM2.1 CGCM3.1-T63, CSIRO-MK3 and CGCM3.1-T47 models (see Tables 2.2 and 2.3). The five GCMs for the 20th century used the "climate of the 20th century experiment" for MSLP analysis, and the 21st century climate projections the higher emission climate scenarios A2 or A1B (IPCC 2007). Monthly MSLP data for these models is available from http://www-pcmdi.llnl.gov/ipcc/info_for_analysts.php website and links therein. The five models are used to calculate the MSLP trends over Queensland and the NEA region and compared to the BoM MSLP trends for the period 1951–2000. The MSLP trends for the 21st century projections for the two periods 2001–2050 and 2051–2100 are also shown. The MPI-ECHAM5, CGCM3.1-T47, CSIRO-MK3 and GFDL-CM2.1 models use the A2 climate scenario and the CGCM3.1-T63 model uses the next highest emission scenario – A1B. A multi–model ensemble is computed from the four models with the A2 emission scenario.

Although an analysis could have been completed on the 21 IPCC–AR4 models to identify the five models with the lowest RMSE using MSLP, similar to the methodology used in Chapter Two with rainfall, there currently is no available gridded dataset of MSLP observations from the BoM. This means that the National Centers of Environmental Prediction (NCEP) reanalysis data would have had to be used, but it is limited in its resolution and accuracy (Marshall 2003). This alternative method may have selected different GCMs than those used in Chapter Two and therefore prevented a direct comparison made between the results from the rainfall analysis and the MSLP trends from the same models. In Chapter Four, the MSLP from NCEP data is used in conjunction with the five GCMs to identify Australia wide and global MSLP trends and how they relate to the rainfall decline and MSLP changes over the NEA region.

3.3 MEAN SEA LEVEL PRESSURE TRENDS FROM BOM OBSERVATIONS

3.3.1 Regional MSLP Trends

Absolute seasonal and annual MSLP trends calculated from the 25 stations from the NEA region are summarized in Table 3.2. This data shows the MSLP has been increasing over most of the NEA region from ~1950–2008. Averaged across all stations, the MSLP increase is highest in the JJA (1.60 hPa), followed by increases in MAM (1.46 hPa), DJF (0.98 hPa) and SON (0.74 hPa). The annual MSLP increase for the NEA region is ~1.22 hPa from all stations. Although not all of the stations have complete records since the early 1950s, the overall MSLP trend across the region is the same with increasing annual MSLP at nearly all locations. Five stations with records starting from 1880s and covering the first half of the 20th century do not show any significant changes in the MSLP up to ~1950 (not shown). Therefore all the analysis on the MSLP changes conducted in this study has been from ~1950 onwards, which is the period noted in Chapter Two, when the rainfall declines began.

Table 3.2 Summary of the Absolute Seasonal and Annual MSLP changes (hPa) from BoM observations over the NEA region from ~1950–2008.

			Season												
	Location		**DJF (Summer)**			**MAM (Autumn)**			**JJA (Winter)**			**SON (Spring)**			**Annual**
		Period	**9am**	**3pm**	**Average**	**9am**	**3pm**	**Average**	**9am**	**3pm**	**Average**	**9am**	**3pm**	**Average**	**MSLP Trend**
1	Charleville	1951-2007	0.95	0.65	**0.80**	1.77	1.24	**1.51**	1.79	1.47	**1.63**	0.78	0.50	**0.64**	**1.13**
2	Roma*	1957-2007	1.20	0.96	**1.08**	1.54	1.24	**1.39**	2.10	1.61	**1.86**	1.12	1.01	**1.07**	**1.44**
3	Toowoomba*	1974-2007	2.08	0.46	**1.27**	2.52	0.97	**1.75**	3.24	1.75	**2.50**	2.45	0.56	**1.51**	**1.91**
4	Brisbane Aero*	1952-2007	1.33	1.10	**1.22**	2.18	1.87	**2.03**	2.40	2.06	**2.23**	1.19	0.85	**1.02**	**1.66**
5	Longreach	1970-2007	1.46	0.87	**1.17**	1.07	0.36	**0.72**	1.32	0.7	**1.01**	1.06	0.54	**0.80**	**1.04**
6	Rockhampton	1950-2007	1.55	0.93	**1.24**	2.02	1.55	**1.79**	1.82	1.52	**1.67**	1.01	0.66	**0.84**	**1.41**
7	Mount Isa	1967-2007	0.73	0.61	**0.67**	0.28	-0.03	**0.13**	0.39	-0.02	**0.19**	-0.19	-0.49	**-0.34**	**0.17**
8	Townsville	1952-2007	1.10	0.86	**0.98**	1.54	1.26	**1.40**	1.34	1.11	**1.23**	0.86	0.57	**0.72**	**1.19**
9	Mackay PO	1960-2007	0.96	0.64	**0.80**	1.36	1.08	**1.22**	1.39	1.20	**1.30**	1.12	0.85	**0.99**	**1.04**
10	Weipa*	1959-2007	1.40	0.54	**0.97**	1.63	1.26	**1.45**	1.44	1.04	**1.24**	1.55	1.05	**1.30**	**1.25**
11	Cairns	1950-2007	1.13	0.68	**0.91**	1.32	0.95	**1.14**	1.18	0.69	**0.94**	0.67	0.01	**0.34**	**0.83**
12	Bourke*	1950-2007	0.90	0.92	**0.91**	2.71	1.91	**2.31**	2.95	2.06	**2.51**	1.11	0.57	**0.84**	**1.75**
13	Moree*	1965-2007	0.90	1.20	**1.05**	0.65	0.99	**0.82**	1.44	1.09	**1.27**	0.38	0.32	**0.35**	**1.09**
14	Coffs Harbour	1952-2007	0.96	1.24	**1.10**	2.35	2.34	**2.35**	2.30	2.17	**2.24**	1.02	1.11	**1.07**	**1.75**
15	Lord Howe Island*	1955-2007	1.64	1.89	**1.77**	2.78	2.82	**2.80**	3.14	3.06	**3.10**	1.83	1.87	**1.85**	**2.45**
16	Norfolk Island	1955-2007	1.88	1.74	**1.81**	3.12	2.78	**2.95**	3.36	2.97	**3.17**	2.12	1.83	**1.98**	**2.47**
17	Willis Island	1952-2007	1.33	0.99	**1.16**	1.38	1.21	**1.30**	1.03	0.90	**0.97**	0.86	0.73	**0.80**	**0.96**
18	Georgetown	1950-2007	1.64	-0.29	**0.68**	2.92	1.23	**2.08**	2.83	1.86	**2.35**	1.90	0.00	**0.95**	**1.39**
19	Gaynah PO	1950-2007	1.28	1.36	**1.32**	1.80	1.65	**1.73**	1.94	1.85	**1.90**	0.77	0.82	**0.80**	**1.51**
20	Burketown	1950-2007	1.87	1.90	**1.89**	1.88	1.55	**1.72**	2.17	2.13	**2.15**	1.37	1.22	**1.30**	**1.77**
21	Boulia	1950-2007	1.06	0.68	**0.87**	1.44	1.04	**1.24**	1.25	0.79	**1.02**	0.61	0.24	**0.43**	**0.96**
22	Clermont	1970-2008	1.38	0.50	**0.94**	1.68	0.66	**1.17**	1.91	1.30	**1.6**	1.52	0.55	**1.04**	**1.25**
23	Hughenden*	1965-2008	0.43	0.36	**0.40**	0.27	-0.07	**0.10**	0.31	0.10	**0.21**	-0.33	-0.58	**-0.46**	**-0.01**
24	Birdsville*	1957-2008	0.13	0.03	**0.08**	1.11	0.55	**0.83**	1.07	0.62	**0.85**	-0.61	-1.24	**-0.93**	**0.13**
25	Thargomindah*	1957-2008	-0.37	-0.77	**-0.57**	0.82	0.10	**0.46**	1.20	0.49	**0.85**	0.01	-0.61	**-0.30**	**-0.04**
	Overall Average		1.16	0.80	**0.98**	1.69	1.22	**1.46**	1.81	1.38	**1.60**	0.97	0.52	**0.74**	**1.22**

Notes 1. Asterisk(*) indicates combined records from two or more stations from the same location.

2. **Average** values of the 9am and 3pm reading and **Overall Average** values are rounded to 2 decimal places.

3. The average value for the MSLP changes corresponds to the time interval shown.

4. The Annual MSLP trend is calculated from the 12 calendar months (average of the 9am and 3pm readings).

3.3.2 Annual MSLP Trends

Five stations were selected from across Queensland and the NEA region to show the regional similarities (and differences) in the annual MSLP trends during the second half of the 20th century. These stations are Mount Isa, Cairns, Mackay, Brisbane Airport and Norfolk Island (Figures 3.2 (a–e) respectively). Graphs in each figure show both the 9am and 3pm average annual MSLP values, with a six year moving average line calculated for each. The patterns of both trends lines from 9am and 3pm for each station are very similar. The Mount Isa time series (Figure 3.2a) covers the period from 1967–2007 and shows the MSLP varies by up to ~2.5 hPa year^{-1}. There is only a very small increase in the MSLP by 0.17 hPa over the 41 years (Table 3.2). The difference between the 9am and 3pm values is ~3.5 hPa. The time series from Cairns (Figure 3.2b) covers the period from 1950–2007 and shows the MSLP varies between ~1–2 hPa year^{-1}. The difference between the 9am and 3pm values is ~2.50–3.0 hPa and the MSLP has increased by 0.83 hPa over the 58 years. The time series from Mackay (Figure 3.2c) for the period 1960–2007, shows the MSLP varies between ~1–2 hPa year^{-1}, with the difference between the 9am and 3pm MSLP values of ~2.50–3.0 hPa. The MSLP has increased by about 1.04 hPa over the 58 years. The time series from Brisbane Airport (Figure 3.2d) for the period 1952–2007, shows the MSLP varies ~1–2 hPa year^{-1}, which is similar to the Cairns and Mackay stations. The difference between the 9am and 3pm values is about 2.50–3.0 hPa and the MSLP has increased by 1.66 hPa over the 56 years. The time series from Norfolk Island (Figure 3.2e) for the interval 1955–2007 shows the MSLP varies ~0.5–1.5 hPa year^{-1}. The difference between the 9am and 3pm values is ~1.0 hPa, and is the lowest of the five stations. The MSLP has increased by ~2.5 hPa over the 53 years.

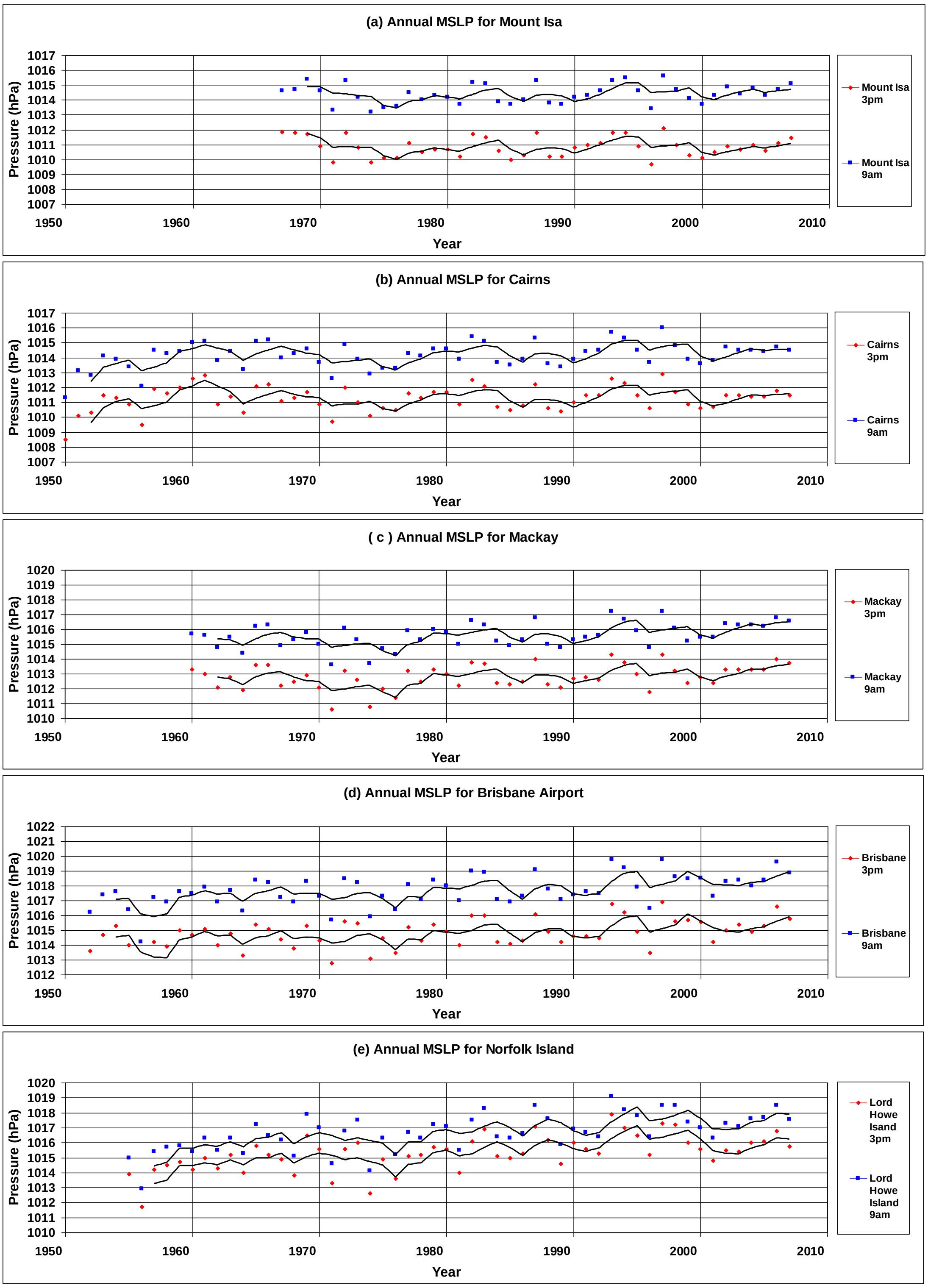

Figure 3.2 (a–e) Time series of the MSLP (hPa) from (a) Mount Isa, (b) Cairns, (c) Mackay, (d) Brisbane Airport and (e) Norfolk Island. Solid black line is a six year moving average. The solid black line represents a six year moving average in the time series and highlights the interannual and decadal MSLP variability and was not used to calculate absolute or decadal MSLP trends.

The two stations with the largest increase in the annual MSLP are from Lord Howe and Norfolk Islands off the east coast of eastern Australia (Table 3.2). These stations show an increase of 2.45 hPa and 2.47 hPa respectively over 53 years. On the Australian mainland, Toowoomba and Burketown have had the largest increase in annual MSLP with 1.91 hPa from 1974–2007 and 1.77 hPa from 1950–2007 respectively. Other stations with a large increase (>1.50 hPa) in the annual MSLP are Brisbane Aero, Bourke, Coffs Harbour and Gaynah P.O. Other stations which show an increase in annual MSLP (>1.30 hPa) include Roma, Rockhampton and Georgetown. The smallest changes in the annual MSLP occur at Hughenden (-0.01 hPa) and the far western region of Queensland at Thargomindah (-0.04 hPa), Birdsville (0.13 hPa) and Mount Isa (0.17 hPa) stations.

In summary, with the exception of very small or slightly negative MSLP trends at a few stations, the annual MSLP has increased over nearly all of Queensland on averaged by ~1.22 hPa over the last ~40–50 years, higher along eastern coastal regions and in the Tasman and Coral Sea (Table 3.2). This indicates that decadal and multi–decadal MSLP trends have been important aspects of climate and climate change in this region.

3.3.3 Seasonal MSLP Trends

The Lord Howe and Norfolk Island stations have had the largest increases in MSLP in nearly all seasons (except DJF) from 1955–2007 (Table 3.2). The MSLP has increased by over 3.1 hPa in JJA, followed by MAM (~2.85 hPa), SON (~1.9 hPa) and DJF (~1.8 hPa) over 53 years. On mainland Australia, Toowoomba and Bourke have had the largest increase in the seasonal MSLP during JJA, with a 2.50 hPa and 2.51 hPa respectively. Other stations with a large increase in the MSLP (>2.20 hPa) in JJA are Georgetown, Coffs Harbour and Brisbane Aero. In SON, stations with a large increase in MSLP (>1.30 hPa) are Toowoomba, Weipa and Burketown. In contrast, a small decrease in MSLP (<1.0 hPa) occurs at Birdsville, Hughenden, Thargomindah and Mount Isa, with decreases up to -0.93 hPa. In DJF, the largest increase in the MSLP is at Burketown, with a rise of 1.89 hPa from 1950–2007. Other stations with an increase in MSLP (>1.20 hPa) in DJF are Gaynah, Toowoomba, Rockhampton and Brisbane Aero. In MAM, a large increase in the MSLP (>2.00 hPa) occurs at Coffs Harbour, Bourke, Georgetown and Brisbane Aero.

The seasonal MSLP trends show the 9am record has a larger value than the 3pm record and this is consistent across all seasons from most stations (Table 3.2). The average difference from all stations in the change in the MSLP between the 9am and 3pm reading is 0.43 hPa (DJF), 0.50 hPa (MAM), 0.43 hPa (JJA) and 0.46 hPa (SON). The stations which have the largest difference in MSLP values between the 9am and 3pm reading are Toowoomba and Georgetown with 1.89 hPa and 1.93 hPa respectively. The reason for the MSLP difference at these two stations is unclear. A number of stations have very small differences between the two readings including Gaynah (0.09 hPa) and Lowe Howe Island, Coffs Harbour and Burketown with a difference of ~0.10–0.14 hPa. It is likely the coastal stations have lower differences between the two readings due to the smaller range of daytime temperatures.

Although not shown here, the highest average MSLP occurs in austral winter and the lowest MSLP values in austral summer with austral autumn and spring having intermediate average MSLP values.

3.3.4 Decadal Trends in MSLP

A summary of the seasonal and annual decadal MSLP trends are shown in Table 3.3. In DJF, the decadal MSLP trends are mostly upward with the largest (>0.30 hPa decade^{-1}) at Toowoomba (0.37 hPa decade^{-1}), Norfolk Island (0.34 hPa decade^{-1}), Lord Howe Island (0.33 hPa decade^{-1}), Burketown (0.33 hPa decade^{-1}) and Longreach (0.31 hPa decade^{-1}). The lowest increases in the DJF decadal MSLP are at Birdsville (0.02 hPa decade^{-1}), Hughenden (0.09 hPa decade^{-1}) and Georgetown (0.12 hPa decade^{-1}) and a small decrease at Thargomindah (-0.11 hPa decade^{-1}). The average DJF decadal increase in MSLP over the entire region is ~0.19 hPa decade^{-1}. In MAM, the decadal MSLP trend is upward at all stations and largest (>0.5 hPa decade^{-1}) at three stations –Norfolk Island (0.56 hPa decade^{-1}), Lord Howe Island (0.53 hPa decade^{-1}) and Toowoomba (0.51 hPa decade^{-1}). The smallest increases in MSLP occur at Hughenden (0.02 hPa decade^{-1}), Mount Isa (0.03 hPa decade^{-1}) and Thargomindah (0.09 hPa decade^{-1}). The average MAM decadal increase in MSLP over the entire region is ~0.28 hPa decade^{-1}. In JJA, the decadal MSLP trend is also upward at all stations and shows the largest increases have occurred at the same three stations as in MAM –Toowoomba (0.74 hPa decade^{-1}), Norfolk Island (0.60 hPa decade^{-1}) and Lord Howe Island (0.59 hPa decade^{-1}). The smallest increases in MSLP have occurred at Mount Isa (0.05 hPa decade^{-1}), Hughenden (0.05 hPa decade^{-1}) and 0.16 hPa decade^{-1} shared by Cairns, Birdsville and Thargomindah. The

Table 3.3 Summary of the Seasonal and Annual Decadal MSLP trends (hPa decade^{-1}) from BoM observations over the NEA region from 1950–2008.

				Season									
	Location			**DJF (Summer)**		**MAM (Autumn)**		**JJA (Winter)**		**SON (Spring)**		**Annual**	
		Period	**Years**	**Average**	**Decadal**	**Average**	**Decadal**	**MSLP Trend**	**Decadal**	**Average**	**Decadal**	**MSLP Trend**	**Decadal**
1	Charleville	1951-2007	57	0.80	0.14	1.51	0.27	1.63	0.29	0.64	0.11	1.13	0.20
2	Roma	1957-2007	51	1.08	0.21	1.39	0.27	1.86	0.37	1.07	0.21	1.44	0.28
3	Toowoomba	1974-2007	34	1.27	0.37	1.75	0.51	2.50	0.74	1.51	0.44	1.91	0.56
4	Brisbane Aero	1952-2007	56	1.22	0.22	2.03	0.36	2.23	0.40	1.02	0.18	1.66	0.30
5	Longreach	1970-2007	38	1.17	0.31	0.72	0.19	1.01	0.27	0.80	0.21	1.04	0.27
6	Rockhampton	1950-2007	58	1.24	0.21	1.79	0.31	1.67	0.29	0.84	0.14	1.41	0.24
7	Mount Isa	1967-2007	41	0.67	0.16	0.13	0.03	0.19	0.05	-0.34	-0.08	0.17	0.04
8	Townsville	1952-2007	56	0.98	0.18	1.40	0.25	1.23	0.22	0.72	0.12	1.19	0.21
9	Mackay PO	1960-2007	48	0.80	0.17	1.22	0.25	1.30	0.27	0.99	0.21	1.04	0.22
10	Weipa	1959-2007	49	0.97	0.20	1.45	0.30	1.24	0.25	1.30	0.27	1.25	0.26
11	Cairns	1950-2007	58	0.91	0.16	1.14	0.20	0.94	0.16	0.34	0.06	0.83	0.14
12	Bourke	1950-2007	58	0.91	0.16	2.31	0.40	2.51	0.43	0.84	0.15	1.75	0.30
13	Moree	1965-2007	43	1.05	0.24	0.82	0.19	1.27	0.30	0.35	0.08	1.09	0.25
14	Coffs Harbour	1952-2007	56	1.10	0.20	2.35	0.42	2.24	0.40	1.07	0.19	1.75	0.31
15	Lord Howe Island	1955-2007	53	1.77	0.33	2.80	0.53	3.10	0.59	1.85	0.35	2.45	0.46
16	Norfolk Island	1955-2007	53	1.81	0.34	2.95	0.56	3.17	0.60	1.98	0.37	2.47	0.47
17	Willis Island	1952-2007	56	1.16	0.21	1.30	0.23	0.97	0.17	0.80	0.14	0.96	0.17
18	Georgetown	1950-2007	58	0.68	0.12	2.08	0.36	2.35	0.41	0.95	0.16	1.39	0.24
19	Gaynah PO	1950-2007	58	1.32	0.23	1.73	0.30	1.90	0.17	0.80	0.14	1.51	0.26
20	Burketown	1950-2007	58	1.89	0.33	1.72	0.30	2.15	0.37	1.30	0.22	1.77	0.31
21	Boulia	1950-2007	58	0.87	0.15	1.24	0.21	1.02	0.18	0.43	0.07	0.96	0.17
22	Clermont	1970-2008	39	0.94	0.24	1.17	0.30	1.6	0.41	1.04	0.27	1.25	0.32
23	Hughenden	1965-2008	44	0.40	0.09	0.10	0.02	0.21	0.05	-0.46	-0.11	-0.01	0.00
24	Birdsville	1957-2008	52	0.08	0.02	0.83	0.16	0.85	0.16	-0.93	-0.18	0.13	0.03
25	Thargomindah	1957-2008	52	-0.57	-0.11	0.46	0.09	0.85	0.16	-0.30	-0.06	-0.04	-0.01
	Overall Average			**0.98**	0.19	**1.46**	0.28	**1.60**	0.31	**0.74**	0.15	1.22	0.24

Notes **1**. The 'Average' values for the seasonal MSLP trends and the MSLP trend for the annual values are from Table 3.2.

2. Decadal values calculated by total trend divided by years.

3. Small differences in the totals of seasonal and annual decadal trends due to rounding of figures.

4. Significant MSLP trends which are discussed in the text are highlighted in red (increasing MSLP) and blue (decreasing MSLP).

average JJA decadal increase in MSLP over the entire region is ~0.31 hPa decade^{-1}. In SON, the decadal MSLP trend is upward at most stations and is largest at Toowoomba (0.44 hPa decade^{-1}), Norfolk Island (0.37 hPa decade^{-1}) and Lord Howe Island (0.35 hPa decade^{-1}). The smallest increase in the decadal MSLP is at Moree (0.08 hPa decade^{-1}) and Boulia (0.07 hPa decade^{-1}) and several stations show a small decrease including Birdsville (-0.18 hPa decade^{-1}), Hughenden (-0.11 hPa decade^{-1}), Mount Isa (-0.08 hPa decade^{-1}) and Thargomindah (-0.06 hPa decade^{-1}). The average SON decadal increase in the MSLP over the entire region is ~0.15 hPa decade^{-1}.

The annual decadal MSLP trend is upward at all stations except at Thargomindah, with the largest increases over coastal and eastern regions of Queensland and NSW. This includes Toowoomba (0.56 hPa decade^{-1}), Clermont (0.32 hPa decade^{-1}) and Coffs Harbour (0.31 hPa decade^{-1}). Norfolk and Lord Howe Islands have also had large increases in MSLP of 0.47 and 0.46 hPa decade^{-1} respectively. The smallest change in the annual decadal MSLP has occurred at Hughenden (no change), Thargomindah (-0.01 hPa decade^{-1}), Birdsville (0.03 hPa decade^{-1}) and Mount Isa (0.04 hPa decade^{-1}). The average annual decadal MSLP trend is upward over the entire region, with a value of ~0.24 hPa decade^{-1}.

Contoured maps of the NEA region for the seasonal and annual decadal MSLP trends are shown in Figure 3.3 (a–e). In DJF (Figure 3.3a), the upward trend in decadal MSLP is strongest over SE QLD and the north Tasman Sea. A small area with a downward trend in decadal MSLP occurs over the far southwestern Queensland around Thargomindah. In MAM and JJA (Figures 3.3b and 3.3c respectively), the upward trend in the decadal MSLP is strongest over SE QLD (Toowoomba and

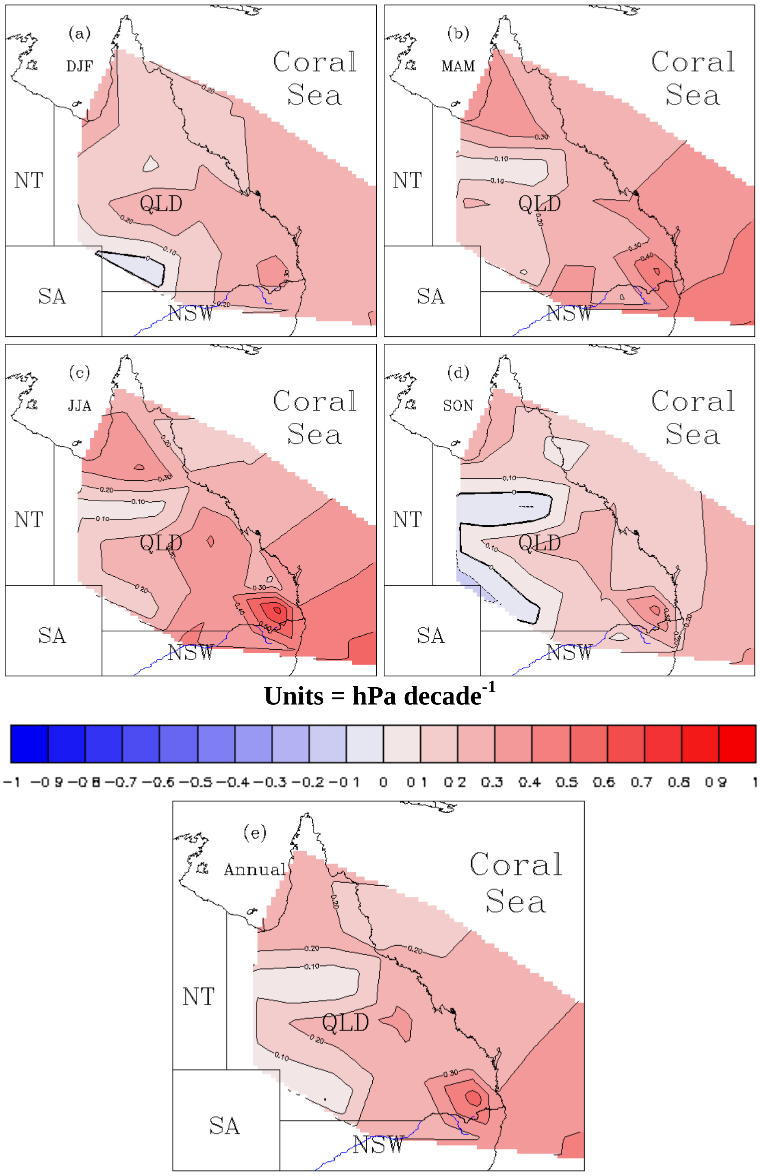

Figure 3.3 (a–e) Contoured seasonal and annual decadal MSLP trends (hPa decade^{-1}) from BoM observations over the NEA region for the period 1951–2008. (a) DJF, (b) MAM, (c) JJA, (d) SON and (e) Annual. Regions shaded in red show increasing MSLP and blue decreasing MSLP. Bold contour line is zero MSLP change.

coastal areas south of Rockhampton), with the entire state is covered by increasing MSLP (although lower in the Mount Isa–Hughenden area). In SON (Figure 3.3d), the upward trend in decadal MSLP is lower over much of the state, with the largest increases over SE QLD and western areas of Cape York Peninsula. A small downward trend in the decadal MSLP occurs over the southwest (Birdsville) and western–central parts of Queensland (Mount Isa to Hughenden).

The annual decadal MSLP trend (Figure 3.3e) shows nearly the entire region is covered by small to moderate upward trend in the decadal MSLP, strongest over SE QLD and the Tasman Sea.

3.3.5 Summary

In summary, there has been a clear trend of increasing MSLP over much of NEA and the Queensland region during the second half of the 20th century and the start of the 21st century. The strongest increases in MSLP have occurred over southern and coastal parts of Queensland and adjacent NSW, and further to the east at Lord Howe and Norfolk Islands, especially in MAM and JJA. This is also the region with some of the largest rainfall declines (Chapter Two). It is interesting that the upward trend in the MSLP shown for SON occurs over a large area of eastern Australia with trends of increasing rainfall (Figures 3.3d and 2.7 (top row) respectively).

3.4. TIME SERIES OF THE MSLP TRENDS

A time series of the annual MSLP trends over the NEA region from the 25 stations for the period ~1950–2008 are shown in Figures 3.4 and 3.5 for drought and flood years respectively. All years with El Niños and major Australian drought events described by BoM (2004) and from the Natural Resources and Mines (Queensland State Government) poster titled " Australia's Variable Rainfall" from 1890 to 2004, are marked on the time series (Figure 3.4). To compliment Figure 3.4, a further graphic (Figure 3.5) shows all La Niña years, major floods in SE QLD and years

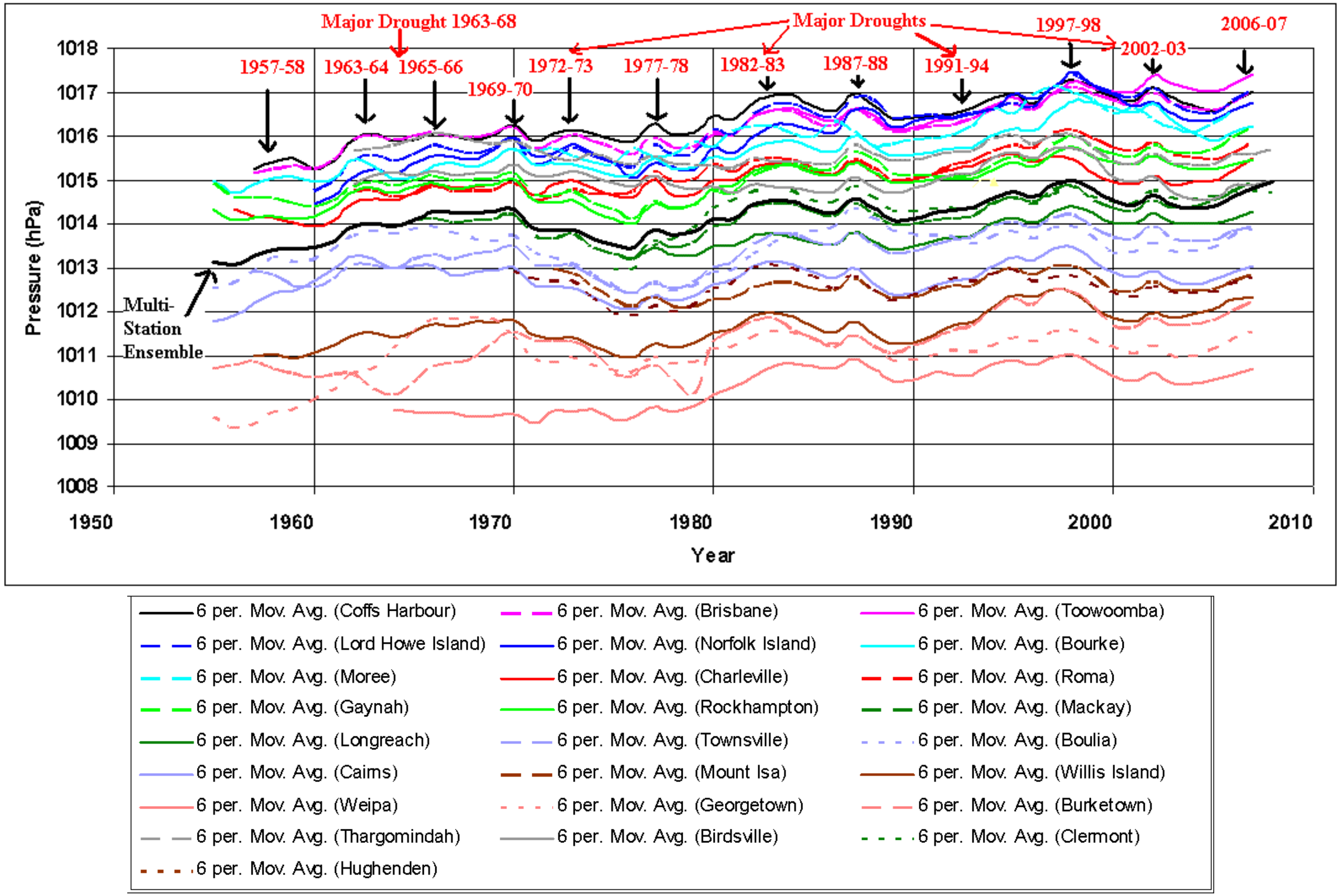

Figure 3.4 Annual BoM MSLP trends (hPa) using a six year moving average from 1950–2008. The multi–station ensemble MSLP line is arrowed. El Niño years (red) and major drought years (arrowed) are shown. Data from BoM (2004) and the Natural Resources and Mines "Australia's Variable Rainfall" (1890–2004) poster.

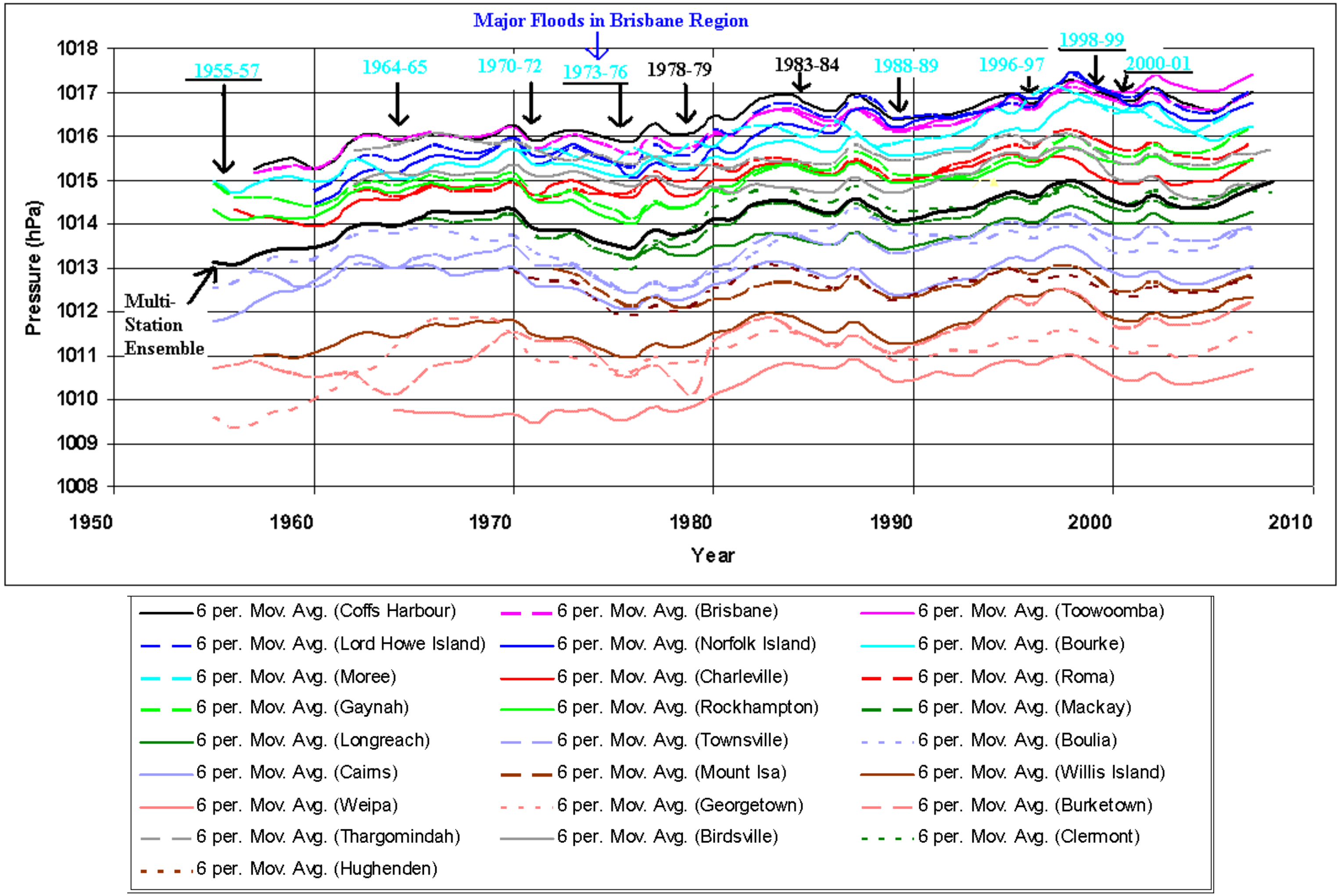

Figure 3.5 Annual BoM MSLP trends (hPa) using a six year moving average from ~1955–2008. The multi–station ensemble MSLP line is arrowed. La Niña years (blue), flood years (black) or both (underlined) are shown. Data source as in Figure 3.4.

with well above rainfall over the Queensland region (>80% rainfall percentile). A six year moving average is selected to show the MSLP changes, as it tends to smooth out the large ranges in year to year variability in the MSLP, but still preserves the decadal and interdecadal changes. A multi–station ensemble is shown (solid black line) calculated from all stations across the NEA region.

During 1950–2008, the average increase of MSLP across all stations has been ~0.24 hPa decade^{-1} from the mid–1950s (Table 3.3). However, each decade shows some variability, with the MSLP oscillating up and down over a period of several years or longer and each decade showing different overall MSLP changes. Most stations show an increase of ~0.5–1.0 hPa in MSLP during the period 1958–1962 and this increase slows for the rest of the 1960s. The 1970–1980 decade shows little change from the start to the end of the decade. However, the MSLP decreases ~1.0 hPa in the middle of the decade (1973–1976) at ~14 stations, forming a distinct 'trough', which corresponds to a number of very wet years over Australia and Queensland with 1974 known as the 'Big Wet' (BoM 2004). At the other stations, the MSLP remains fairly static over the decade. From ~1979–1983, there is another abrupt increase in MSLP of ~1.0 hPa over the region, which corresponds to a number of dry years including the 1982–1983 drought. A peak in the MSLP occurs in 1982–1983 and also at ~1987 represent warm ENSO years. From 1988–1989, the MSLP falls sharply by ~0.5–0.75 hPa over the region, forming another 'trough', and then slowly rises ~1.0 hPa over about 10 years to form another peak in ~1997. From ~1998–2001, the MSLP decreases ~0.5–0.75 hPa forming another small 'trough' (~2001), and increases again to form a small peak at ~2002–2003, representing another major Australian drought episode (BoM 2004). A small decrease in the MSLP from 2003 is followed by a small increase in the MSLP from ~2005–2008, to reach the same peak recorded in the MSLP in 1998.

The multi–station ensemble mean (solid black line in Figures 3.4 and 3.5) shows many of the features already described above. The multi-station ensemble mean shows a steady increase in the MSLP during the mid 1950s to ~1970, followed by a decrease during the mid–1970s. A slow increase in the MSLP returns in ~1977–1978 until ~1988, when a small decrease in the MSLP occurs for a few years. Increasing MSLP continues until ~1998 and this is followed by another small decrease in the MSLP during the early 2000s. A small rise in the MSLP starts at ~2005, reaching the maximum MSLP attained during the peak in 1997–1998, in 2007–2008. The multi–station ensemble mean shows the average MSLP has increased by ~2 hPa from the mid 1950s to 2008. This is higher than the average annual MSLP trend noted in Table 3.3 of 1.22 hPa, which was derived from all the stations, because many stations have a shorter period of observations than the multi–station ensemble mean, which spans from 1950–2008.

The lowest MSLP (1010–1012 hPa) occurs at the northern stations in Queensland (Weipa, Burketown, Georgetown and Willis Island) reflects the closer proximity to the equator and the austral summer and autumn Australian monsoon trough (lower MSLP), whereas the highest MSLP (1015–1017 hPa) occurs at stations at a higher latitude, such as Coffs Harbour, Toowoomba, Brisbane, Norfolk Island and Lord Howe Island, which are closer to the axis of the mid–latitude subtropical ridge.

The year to year changes in MSLP between stations shows a remarkably similar upward and downward trends, irrespective of the location of each station such as inland, coastal or from an island. The rise and fall of the MSLP from year to year is almost simultaneous across most stations. The changes in MSLP and the ‘mirror’ like patterns indicate the changes are regional in nature and not caused by small regional variations and poor quality data. The year to year changes in MSLP closely follow the ENSO cycle with generally higher MSLP in El Niño years and lower MSLP in La Niña years. However, this is not always the case with 2007–2008 having had a higher MSLP in a La Niña year. The overall upward trend in the MSLP is investigated further in Chapter Four.

In summary, the time series across the entire time interval (1950–2008) shows each successive major peak or ‘trough’ is followed by a slightly higher MSLP, indicating an underlying and persistent increase in the MSLP across the region. The average increase in the MSLP across the region since ~1950 is ~2 hPa. The MSLP changes began at about the same time that the rainfall decline began over much of eastern Australia and much of SE QLD. The next section will discuss these relationships.

3.5 CORRELATION BETWEEN MEAN SEA LEVEL PRESSURE AND RAINFALL

A summary of the seasonal and annual correlations between MSLP and rainfall from BoM observations over the NEA region are shown in Table 3.4. In DJF, the locations with the highest negative correlation are Gaynah (-0.50), Cairns (-0.49), Willis Island

Table 3.4 Summary of the Seasonal and Annual Correlation between MSLP and Rainfall from BoM observations over NEA from ~1950–2008.

	Location	Period	Years	Level of Significance at 5% Level	DJF (Summer)	MAM (Autumn)	JJA (Winter)	SON (Spring)	Annual
1	Charleville	1951-2007	51	0.27	-0.07	-0.44	-0.23	-0.07	-0.22
2	Roma	1957-2007	49	0.27	-0.07	-0.28	-0.45	-0.23	-0.18
3	Toowoomba	1974-2007	34	0.35	-0.12	-0.36	-0.24	-0.24	-0.65
4	Brisbane Aero	1952-2007	50	0.27	-0.35	-0.13	0.01	0.06	-0.36
5	Longreach	1970-2007	38	0.33	-0.07	-0.29	-0.43	-0.29	-0.29
6	Rockhampton	1950-2007	51	0.27	-0.36	-0.45	-0.27	-0.22	-0.56
7	Mount Isa	1967-2007	40	0.30	-0.24	-0.21	-0.51	-0.42	-0.18
8	Townsville	1952-2007	51	0.27	-0.23	-0.54	-0.25	-0.36	-0.31
9	Mackay PO	1960-2007	46	0.29	-.0.43	-0.49	-0.13	-0.41	-0.41
10	Weipa	1959-2007	37	0.33	-0.32	-0.46	0.14	-0.50	-0.11
11	Cairns	1950-2007	51	0.27	-0.49	-0.42	0.29	-0.43	-0.31
12	Bourke	1950-2007	49	0.27	0.23	-0.33	-0.17	-0.16	-0.21
13	Moree	1965-2007	43	0.30	-0.05	-0.10	-0.14	0.06	-0.03
14	Coffs Harbour	1952-2007	51	0.27	-0.25	-0.19	0.11	0.33	-0.13
15	Lord Howe Island	1955-2007	49	0.27	-0.38	-0.44	-0.51	-0.46	-0.45
16	Norfolk Island	1955-2007	50	0.27	-0.35	-0.50	-0.33	-0.42	-0.32
17	Willis island	1952-2007	48	0.29	-0.49	-0.39	-0.20	-0.43	-0.30
18	Georgetown	1950-2007	48	0.29	-0.38	-0.30	-0.20	-0.31	-0.29
19	Gaynah PO	1950-2007	50	0.27	-0.50	-0.37	-0.22	-0.01	-0.43
20	Burketown	1950-2007	39	0.33	-0.28	-0.32	0.04	-0.06	-0.24
21	Boulia	1950-2007	43	0.30	-0.30	-0.50	-0.34	-0.43	-0.54
22	Clermont	1970-2008	38	0.33	-0.37	-0.26	-0.22	-0.28	-0.31
23	Hughenden	1965-2008	41	0.30	-0.29	0.01	-0.17	-0.39	-0.37
24	Birdsville	1957-2008	51	0.27	-0.14	-0.36	-0.25	-0.38	-0.22
25	Thargomindah	1957-2008	50	0.27	0.05	-0.15	0.31	-0.24	-0.27
	Overall Average				**-0.23**	**-0.33**	**-0.17**	**-0.25**	**-0.29**
	Average R^2 value				**0.15**	**0.17**	**0.16**	**0.16**	**0.17**

Notes: **1**.Overall Average values (second lowest row) are rounded to three significant figures.

2. The ‘Years’ column stands for the number of exact years used in calculating the correlation value.

3. Significant correlation values which are discussed in the text are highlighted in red (negative) or blue (positive).

4. The level of significance (p=0.05) is for a two–tailed test

5. R^2 is calculated only from stations with correlation values which exceed the statistically significant 5% level.

(-0.49) and Mackay (-0.43). Thirteen stations have lower negative correlations between -0.20 and -0.40. A total of eleven stations have correlation values which are statistically significant above the 5% level of significance. This indicates rainfall decreases as the MSLP increases across these stations. At Bourke in northern New South Wales, rainfall increases with increasing MSLP (r=0.23). In MAM, the highest negative correlation values occur at Townsville (-0.54), Norfolk Island (-0.50), Boulia (-0.50) and Mackay (-0.49). Sixteen other stations have negative correlations between -0.20 and -0.46. A total of sixteen stations have correlations which are statistically significant above the 5% level of significance and this is the highest number of stations for all seasons. The negative correlations indicate rainfall decreases as the MSLP increases. In JJA, four stations have negative correlations between -0.4 and -0.6 including Lord Howe Island (-0.51), Mount Isa (-0.51), Roma (-0.45) and Longreach (-0.43). Eleven stations have negative correlations between -0.2 and -0.4. A total of eight stations have correlation values which are statistically significant above the 5% level of significance. This means rainfall decreases as the MSLP increases, similar to the austral summer and autumn seasons. In contrast, rainfall at Cairns and Thargomindah increases with increasing MSLP (r=0.29 and r=0.31 respectively) and this is statistically significant at the 5% level. In SON, the highest negative correlations occur at Weipa (-0.50), Lord Howe Island (-0.46), Willis Island (-0.43) and Boulia (-0.43), indicating rainfall decreases with increasing MSLP. Fourteen stations have negative correlations between -0.2 and -0.4 and a total of thirteen stations have correlation values which are statistically significant above the 5% level of significance. Interestingly, at Coffs Harbour, the rainfall increases with increasing MSLP (r=0.33) in SON.

The annual negative correlation is highest at Toowoomba (r=-0.65) and r^2 indicates 42% of the rainfall variance can be explained by the increase in MSLP. The other largest negative correlations are at Rockhampton (-0.56), Boulia (-0.54) and Lord Howe Island (-0.45). Sixteen stations have negative correlations between -0.2 and -0.4 and twelve stations have correlation values which are statistically significant above the 5% level of significance. MAM has the highest average negative correlation across all stations with -0.33, followed by SON (-0.25), DJF (-0.23) and JJA (-0.17). A total of four stations (Cairns, Lord Howe Island, Norfolk Island and Boulia) have correlation values which are statistically significant above the 5% level of significance in every season. The largest rainfall decreases have occurred in the austral summer and autumn and eleven stations have values which are statistically significant above the 5% level of significance for both seasons. These are located along or close to the east coast of Queensland or from the islands. Boulia is an exception, which is located well inland. The average annual correlation across the NEA region from the 25 stations is -0.29 and is similar in magnitude with the values from each season, indicating there is good agreement between decreasing rainfall and increasing MSLP trends at many of the stations across the region.

Contoured maps of the seasonal and annual spatial correlation between the MSLP and rainfall over the NEA region are shown in Figure 3.6 (a–e). In DJF, the negative correlation is largest over eastern and northern coastal Queensland with values above -0.3. A small region over the southwest border of Queensland with NSW shows a positive correlation centred at Bourke. In MAM, the negative correlation covers the entire NEA region, with the highest values along east coastal regions. The negative correlation is strongest at Townsville. In JJA, the negative correlation covers most of

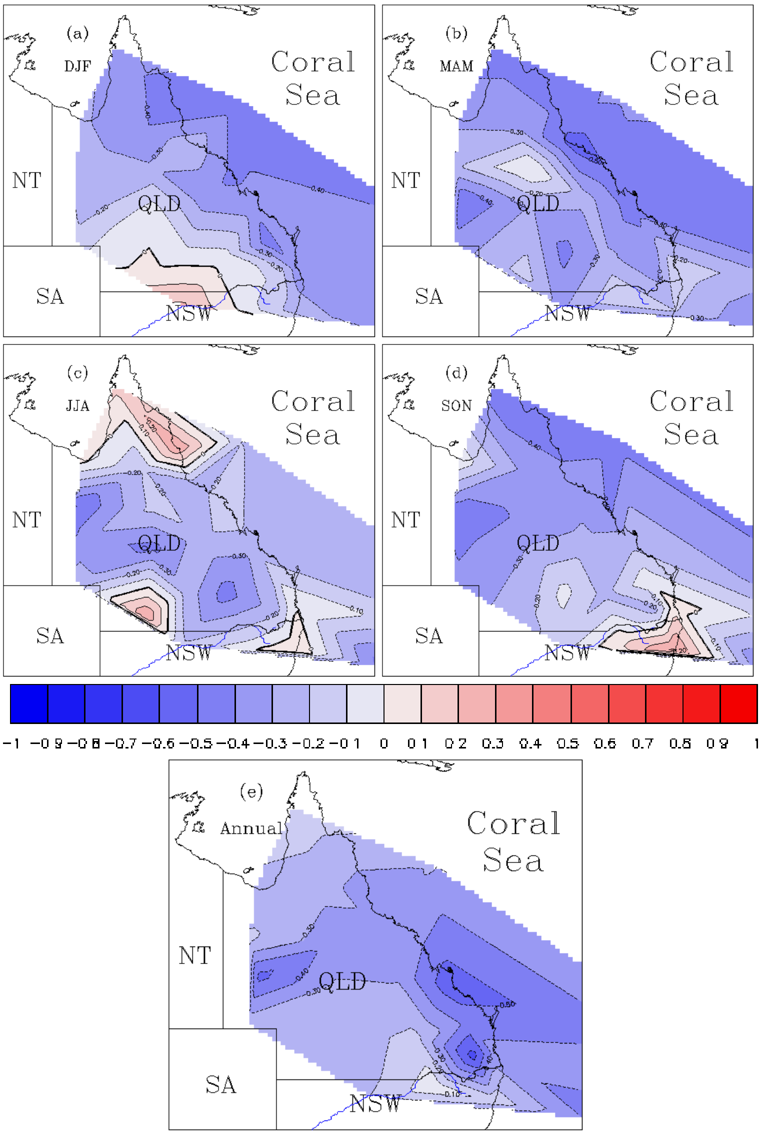

Figure 3.6 (a–e) Contoured seasonal and annual spatial correlation of MSLP (hPa) and rainfall (mm) from BoM observations over the NEA region for the period 1951–2008. (a) DJF, (b) MAM, (c) JJA, (d) SON and (e) Annual. Regions shaded in red show positive correlation and blue negative correlation. Bold contour line is zero correlation.

the region except for small positive correlation over the southwest of Queensland (Thargomindah) and the Cape York Peninsula (Cairns northward). The highest positive correlation is at Cairns. In SON, the negative correlation covers nearly all of Queensland except the far corner of SE QLD, where the highest positive correlation occurs at Coffs Harbour in NSW. The annual correlation shows the entire NEA region is covered by negative values, with the largest values over central coastal Queensland, SE QLD and the region around Boulia.

If the absolute values from the correlation analysis (Table 3.4) are averaged for each season and the r^2 value calculated (for values which are statistically significant at the 5% level), the following r^2 values are reported: DJF=0.15; MAM=0.17, JJA=0.16 and SON=0.16. The annual r^2 value for the thirteen stations which exceed the statistically significant level of 5% is 0.17. This indicates the MSLP can account for about 15-17% of the variance in rainfall at about half the stations in Table 3.4 and this is very evenly spread across all seasons. However, values for individual stations are generally higher along the east coast, in SE QLD and the Tasman Sea. In the SE QLD region, three stations (Brisbane, Toowoomba and Gaynah) have an average r^2 value of 0.23, and hence 23% of the rainfall variance can be explained by the increase in MSLP. Although this is lower than some of the total rainfall reductions (percent) described in Chapters One and Two, it does indicate changes in the MSLP are very likely to be playing an active role in the rainfall decline. It may also indicate the changes in MSLP and rainfall are not linear and further small increases in the MSLP may actually lead to larger rainfall declines (or increases such as at Cairns). It may also show other factors may be also playing a role in the rainfall decline.

In summary, this analysis indicates there is a significant relationship between increasing MSLP and decreasing rainfall over most of eastern and coastal Queensland, in the austral summer, autumn and spring and to a lesser degree in austral winter. Toowoomba and Rockhampton have the highest and most negative annual correlation and have experienced some of the highest rainfall decreases in the Queensland region (Figure 1.2).

3.6 DECADAL MEAN SEA LEVEL PRESSURE TRENDS FROM IPCC–AR4 MODELS OVER THE QUEENSLAND REGION

3.6.1 Period 1951–2000

Seasonal and annual decadal MSLP trends from observations and five IPCC–AR4 models over the NEA region for 1951–2000 are shown in Figure 3.7. BoM observations from the decadal MSLP trends (top row) discussed in section 3.3.4, are shown for comparison. In DJF, the MPI-ECHAM5 and CGCM3.1-T47 models show a small increase in the MSLP over all of Queensland (similar to observations) and the CSIRO-MK3 model a small decrease in MSLP. The GFDL-CM2.1 and CGCM3.1-T63 models show small increases in the MSLP over the Coral Sea and small decreases in the MSLP over inland regions. In MAM, the CSIRO-MK3 model shows a small increase in MSLP over all of Queensland (similar to observations) and the MPI-ECHAM5, CGCM3.1-T63 and GFDL-CM2.1 models, generally a small decrease in the MSLP. The CGCM3.1-T47 model shows ‘mixed’ results in the MSLP trends, with small increases and decreases in MSLP over different regions. In JJA, the MPI-ECHAM5 model shows a small increase in the MSLP over most of Queensland and the GFDL-CM2.1 model a small decrease. The CGCM3.1-T63 and CGCM3.1-T47 models show a small decrease in the MSLP over the entire NEA region and the CSIRO-MK3 model ‘mixed’ results. In SON, the MPI-ECHAM5 and CGCM3.1-T47 models show a small increase in the MSLP and the CGCM3.1-T63

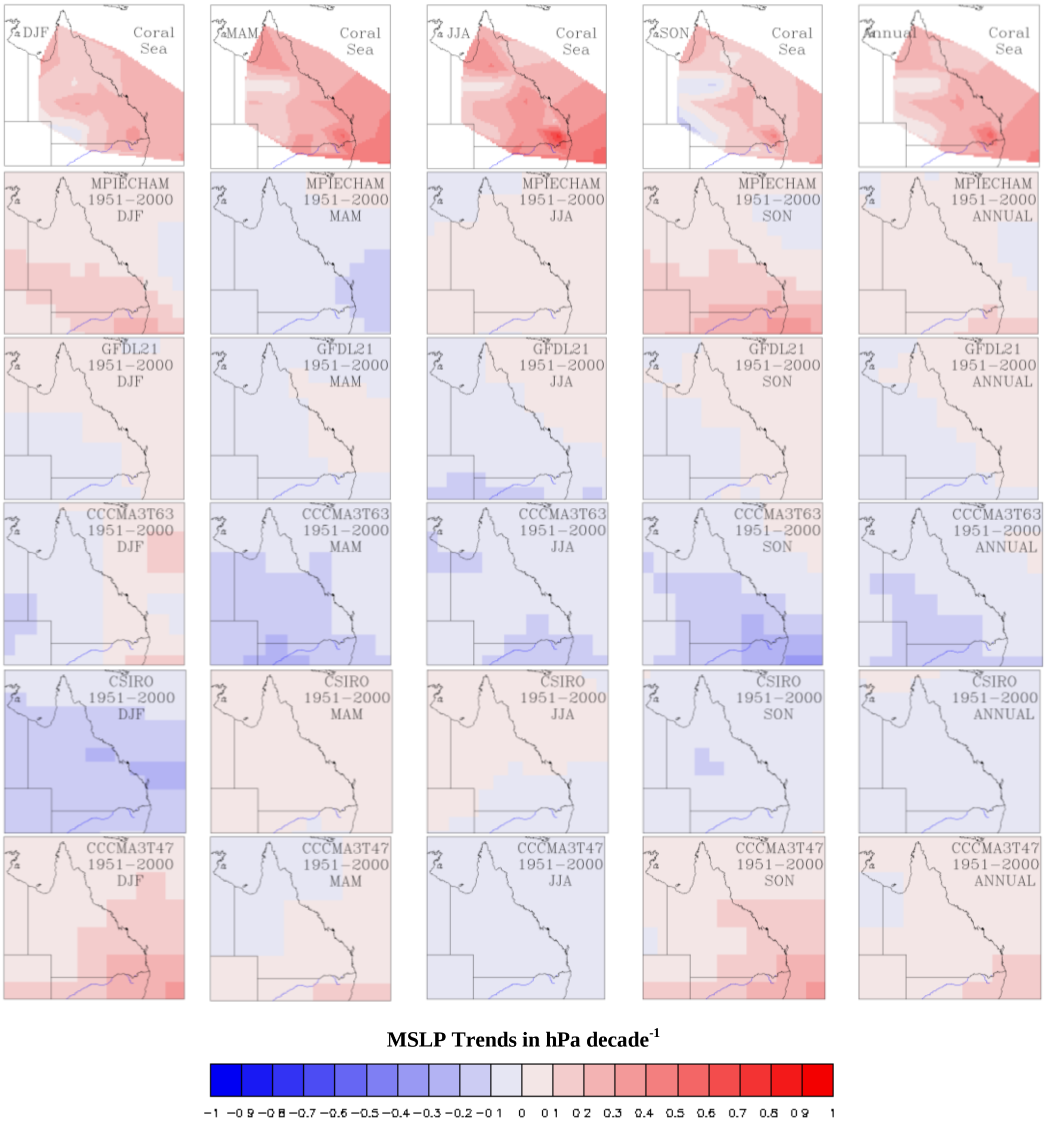

Figure 3.7 Seasonal and annual decadal MSLP trends (hPa decade^{-1}) for the NEA region and the period 1951–2000. BoM observations are shown in the top row and five IPCC–AR4 models below. Regions shaded in red show increasing MSLP and blue decreasing MSLP.

and CSIRO-MK3 a small decrease. The GFDL-CM2.1 model shows increases in the MSLP over the Coral Sea and coastal areas and decreases over inland regions, similar to the other seasons.

The annual MSLP plot shows a small upward trend over most of Queensland in the MPI-ECHAM5 and CGCM3.1-T47 models (similar to BoM observations) and the

CGCM3.1-T63 and CSIRO-MK3 models, a small decrease in the MSLP. The GFDL-CM2.1 model shows 'mixed' results, with small increases in MSLP over the Coral Sea and decreases over inland Queensland.

In summary, only two models (MPI-ECHAM5 and CGCM3.1-T47) show the upward trend in the annual MSLP similar to the BoM observations over the Queensland region, whereas the GFDL-CM2.1 model shows the closest 20th century rainfall trends to the BoM observations (section 2.5.3). This is consistent with the lack of coherent rainfall amongst the models seen in Chapter Two (section 2.5.2) for the 1951–2000 period.

3.6.2 Period 2001–2050

Seasonal and annual decadal MSLP trends from the five IPCC–AR4 models over the NEA region for 2001–2050 are shown in Figure 3.8. In DJF, the GFDL-CM2.1 and CGCM3.1-T47 models show small increases in MSLP over Queensland and the Coral Sea and the CSIRO-MK3 model, mostly small decreases. The CGCM3.1-T63 and MPI-ECHAM5 models show increases in the MSLP over the Coral Sea and coastal Queensland and decreases over inland regions. In MAM, the GFDL-CM2.1 model shows increasing MSLP over the entire region, with the strongest increases over the east coast and the Coral Sea. In contrast, the CGCM3.1-T63 and CGCM3.1-T47 models shows decreasing MSLP over nearly the entire NEA region. The MPI-ECHAM5 and CSIRO-MK3 models show increases in the MSLP over the Coral Sea and coastal regions and decreases over the southwest inland region. In JJA, the GFDL-CM2.1 model shows increasing MSLP over the entire NEA region, similar to

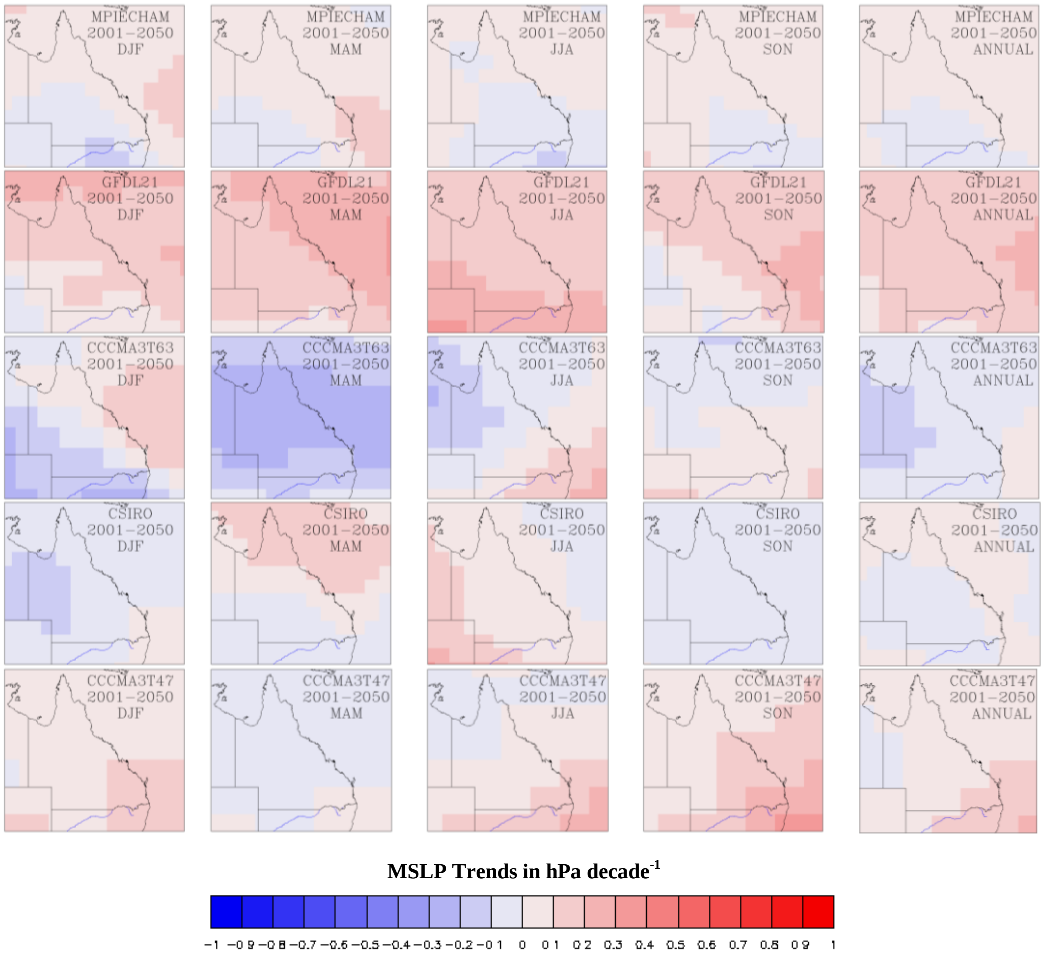

Figure 3.8 Seasonal and annual decadal MSLP trends (hPa decade^{-1}) from five IPCC–AR4 models over the NEA region and the period 2001–2050. Colour shading as in Figure 3.7.

MAM, with the largest increases over southern regions. The CSIRO-MK3 model shows small increases in MSLP over all of Queensland. The MPI-ECHAM5, CGCM3.1-T63 and CGCM3.1-T47 models show 'mixed' results, with the last two models showing small increases in MSLP over southern and southeast regions of NEA. In SON, the CGCM3.1-T47 and GFDL-CM2.1 models show increases in MSLP over the entire NEA region, strongest over SE QLD. In the MPI-ECHAM5 model, small increases in MSLP cover much of NEA, except over SE QLD. The CSIRO-MK3 model shows small decreases in MSLP over the entire NEA region.

The upward trend in the annual decadal MSLP is strongest in the GFDL-CM2.1 model, with increases in MSLP over the entire NEA region, highest over the Coral Sea. The CGCM3.1-T47 model shows increases in MSLP over most of Queensland and the Coral Sea. In contrast, the CGCM3.1-T63 model shows decreases in MSLP over all of NEA. The CSIRO-MK3 and MPI-ECHAM5 models show 'mixed' results, with small decreases in MSLP over southern inland areas and small increases in MSLP over northern regions and the Coral Sea.

In summary, three models show upwards trends in the annual MSLP and two decreasing annual MSLP over the Queensland region with more seasons showing increases in MSLP, compared to 1951–2000. Two of the models which show increasing MSLP are the same models (MPI-ECHAM5 and CGCM3.1-T47) which showed the rainfall declines discussed in section 2.5.3.

3.6.3 Period 2051–2100

Seasonal and annual decadal MSLP trends from the five IPCC–AR4 models for 2051–2100 are shown in Figure 3.9. In DJF, the CSIRO-MK3 model shows small to moderate increases in MSLP over the entire NEA region, whereas in contrast, the CGCM3.1-T63 model shows small to moderate decreases. The GFDL-CM2.1 and CGCM3.1-T47 models show small decreases in MSLP over the Queensland region. The MPI-ECHAM5 model shows 'mixed' results with small decreases over inland regions and small increases over the Coral Sea. In MAM, the CGCM3.1-T63 and CGCM3.1-T47 models show small decreases over the entire NEA region. The MPI-ECHAM5, GFDL-CM2.1 and CSIRO-MK3 models show small decreases in MSLP

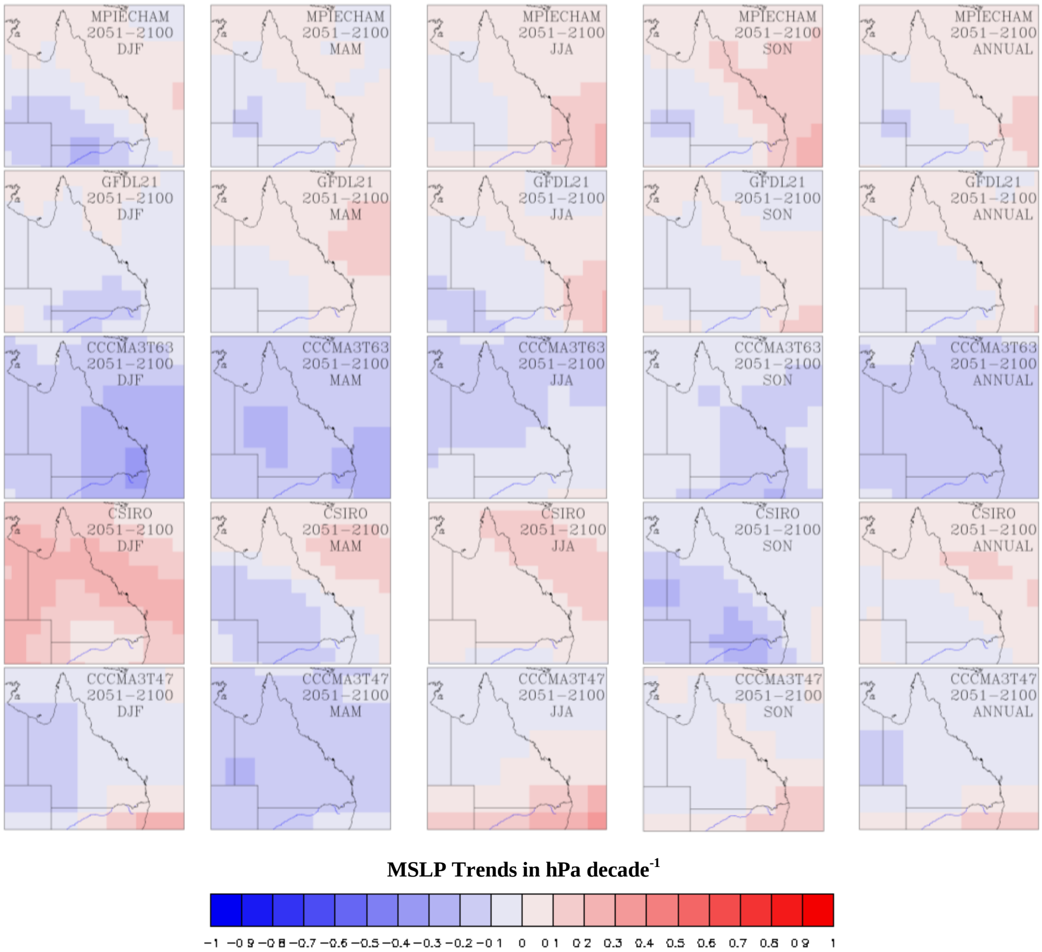

Figure 3.9 Seasonal and annual decadal MSLP trends (hPa decade^{-1}) from five IPCC–AR4 models over the NEA region and the period 2051–2100. Colour shading as in Figure 3.7.

over inland areas and small increases over eastern coastal areas and the Coral Sea. In JJA, the MPI-ECHAM5 and GFDL-CM2.1 models show similar changes to MAM. The CSIRO-MK3 model shows increasing MSLP over most of the NEA region, in contrast to the CGCM3.1-T63 model, which shows small MSLP decreases. The CGCM3.1-T47 model shows small decreases in MSLP across northern and northwestern regions of Queensland and small increases across the southern and southeastern regions. In SON, the CGCM3.1-T63 and CSIRO-MK3 models show small decreases in MSLP over most of the NEA region. The MPI-ECHAM5 and GFDL-CM2.1 show similar changes to JJA, with small MSLP decreases over inland areas and small MSLP increases over coastal regions and the Coral Sea. The CGCM3.1-T47 model shows 'mixed' results in the MSLP changes.

The CGCM3.1-T63 model shows downward trends in the annual decadal MSLP over the entire NEA region. The MPI-ECHAM5, GFDL-CM2.1 and CSIRO-MK3 models show a decrease in MSLP over inland regions and increases over coastal parts and the Coral Sea. The CGCM3.1-T47 model shows a small decrease in MSLP over most of the NEA region, except far SE QLD.

In summary, three models show upward trends in the annual MSLP over the Coral Sea and coastal Queensland and all models decreases in the annual MSLP over the inland regions of NEA. The three models (MPI-ECHAM5, GFDL-CM2.1 and CSIRO-MK3), which show increases in MSLP over the Coral Sea and coastal Queensland, are the same three models in section 2.5.4 that show the strongest rainfall declines.

3.6.4 Ensemble Means

Multi–model ensemble means of the seasonal and annual decadal MSLP trends over the NEA region for the periods 1951–2000, 2001–2050 and 2051–2100 are shown in Figure 3.10. The four models used are the MPI-ECHAM5, GFDL-CM2.1, CGCM3.1-T47 and CSIRO-MK3 models from the A2 scenario. The CGCM3.1-T63 model was not used in the ensemble as it is from the A1B scenario. The MSLP trends from BoM observations are shown in the top row for comparison. Grey shading indicates all four models agree on the sign of the MSLP trend over the region.

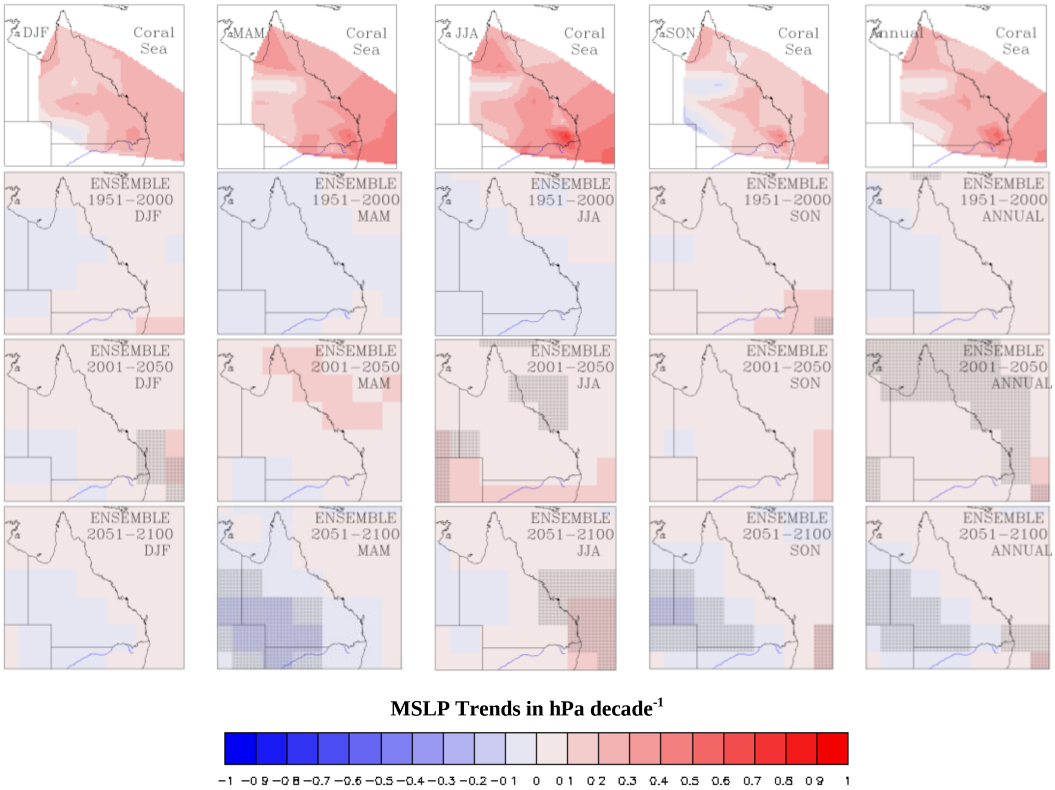

Figure 3.10 Seasonal and annual decadal MSLP trends (hPa decade^{-1}) for the multi–model ensemble over the NEA region and the periods 1951–2000, 2001–2050 and 2051–2100. BoM observations (top row) shown for comparison. Colour shading as in Figure 3.7 and grey shading represents regions where all models agree on the sign of the MSLP trend.

For 1951–2000, DJF shows small decreases in MSLP over western and northwestern parts of Queensland and small increases over southeastern regions and the Coral Sea, similar to the BoM observations. In MAM and JJA, nearly all of Queensland and parts of the Coral Sea are covered by small decreases in MSLP, which is opposite to the BoM observations. In SON, nearly all of Queensland is covered by a small increase in the MSLP, with a small decrease in the MSLP over the Mount Isa region, similar to the BoM observations. The multi–model ensemble mean of the annual decadal MSLP shows small increases over all of the Coral Sea and eastern Queensland and small decreases over western regions, which is similar to the BoM observations. There is almost no grey shading in the 1951–2000 ensembles, indicating the models do not all agree on the sign of the MSLP change. The MSLP trends in the models are generally weaker than the BoM observations.

For 2001–2050, DJF shows most of the NEA region is covered by small increases in the MSLP (except southwestern parts of Queensland), an increase in area compared to 1951–2000 and all models agree on this MSLP trend over the southeast corner of Queensland. In MAM and JJA, the ensembles show nearly the entire NEA region is covered by small increase in the MSLP, nearly a complete reversal to the 1951–2000 period. Two small regions over the northeast tropical coast and the far southwest part of Queensland now show all models agree on the increasing MSLP. In SON, the ensemble is very similar to 1951–2000, with increasing MSLP over nearly the entire NEA region. The multi–model ensemble mean for the annual decadal MSLP shows the entire NEA region has increasing MSLP, compared to 1951–2000. There are also large shaded areas adjacent to the east coast and the Cape York Peninsula, where all models agree on the sign of the MSLP trend.

For 2051–2100, there are significant changes in the MSLP trends, compared to 2001–2050. In DJF, there is a larger region of inland NEA that shows decreasing MSLP compared to 2001–2050, although coastal regions and the Coral Sea maintain increasing MSLP. In MAM, most of inland NEA is covered by decreasing MSLP and the models all agree on this change over a larger region, compared to 2001–2050. In JJA, most of the NEA region is covered by increasing MSLP except the far western parts of Queensland. Over SE QLD and the Coral Sea, all models agree on the increasing MSLP. In SON, a large area of inland NEA is covered by decreasing MSLP, similar to MAM, with all models agreeing on this trend over a large area.

Coastal regions of Queensland and the Coral Sea show an increase in MSLP, similar to 2001–2050. The multi–model ensemble mean for the annual decadal MSLP shows decreases in MSLP over inland regions of NEA and increases in MSLP over coastal regions and the Coral Sea, a change from the increasing MSLP over inland regions shown in 2001–2050.

It would have been possible to have completed a correlation analysis between modelled rainfall and the MSLP in the GCMs used above. However, it has already been shown that the GCMs did not replicate the late 20th century rainfall trends very well (section 2.5) and only a few models showed a significant correlation to the 20th century rainfall (section 2.4). However, this may become an area of active research for model evaluation in the future and is briefly discussed in section 7.4.

3.6.5 Summary

From this analysis, the five models selected for the 1951–2000 period do not replicate the changes seen in seasonal MSLP from BoM observations very well, with 10 plots showing decreasing MSLP over most of NEA, 6 plots show increasing MSLP (similar to BoM observations) and the remaining four plots, ‘mixed’ trends with increasing and decreasing MSLP. The MPI-ECHAM5 model shows three seasons with increasing MSLP (closest to observations) followed by CGCM3.1-T47 model with two seasons. Both these models show the strongest increases in MSLP occur over southeast regions of Queensland, similar to observations. The MPI-ECHAM5 and CGCM3.1-T47 models show increases in the annual decadal MSLP over most of the NEA region, also similar to observations. Decadal MSLP trends for the period 2001–2050 show increasing MSLP for most seasons and regions, whilst for 2051–2100, shows increasing MSLP over coastal areas and the Coral Sea and decreasing MSLP over inland areas. The models which show increasing MSLP generally have the strongest rainfall declines, described in Chapter Two. In Chapter Four, an analysis of MSLP changes using data from NCEP and GCMs over the Australian region investigates the links of the increasing MSLP over Queensland to changes in the strength of the subtropical ridge and the SAM.

3.7 DISCUSSION

The main results from this chapter using MSLP trends from the BoM observations, show there has been a persistent increase in MSLP over most of the NEA region during the second half of the 20th century and the beginning of the 21st century, with the largest increases in the MSLP occurring in the austral autumn and winter. The increase in MSLP varies from near zero along parts of the Northern Territory and Queensland border to ~2.5 hPa at Norfolk and Lord Howe Islands. In the SE QLD region, the largest increases in MSLP have occurred at Toowoomba (1.91 hPa) and other stations nearby such as Coffs Harbour, Brisbane Aero and Gaynah P.O (~1.5–1.75 hPa). The largest increases in the MSLP are over coastal regions of Queensland, SE QLD and the Tasman Sea in the austral autumn and winter. The seasons and proximity to the subtropical ridge indicates this is more likely to be the prime factor controlling the MSLP changes than the Australian monsoon trough. Although low frequency modulations occur in the ENSO, with decadal and multi–decadal variability (Allan et al. 1996), the influence of ENSO on Australian climate waxes and wanes over periods of decades and is dependent on factors such as the Inter-

Decadal Pacific Oscillation and sea surface temperatures (Power et al. 1999). SE QLD is more subject to the breakdown of the correlation between the SOI and rainfall than in any other part of Australia (Murphy and Ribbe 2004) and therefore long–term changes in MSLP in this region are unlikely to be attributed to ENSO. Nicholls (2009) also showed the rainfall declines over southern Australia are unlikely to be related to ENSO or the IOD using seas surface temperatures from the NINO3 index and the western pole of the IOD respectively.

A correlation analyses between rainfall and MSLP indicates that up to 42% of the rainfall variance (typically 10–20%) can be attributed to the changes in MSLP in this region, higher over SE QLD and the Tasman Sea, where the rainfall declines are also some of the highest. The correlation values are highest in the austral summer, autumn and spring and lowest in the austral winter according to the number of stations which are statistically significant at the 5% level. The positive correlation between the MSLP and rainfall in austral spring over northeast NSW is an interesting paradox and may represent atmospheric blocking in the Tasman Sea, which is more frequent in El Niño years (Renwick 1998) (Figure 3.6d), producing more rainfall.

The MSLP in the Australian region is highest in austral winter when the subtropical ridge is at its lowest latitude, and lowest in austral summer, as the subtropical ridge migrates southward and the monsoon migrates over northern Australia (Sturman and Tapper 1996; Drosdowsky 2005). This study using the BoM observations confirms this interpretation, with higher MSLP in the austral winter and lowest values in the austral summer (not shown). A recent study conducted on the latitude of the subtropical ridge by Drosdowsky (2005) concluded that there was no evidence of a poleward shift in the subtropical ridge during the second half 20th century. If this is indeed the case, then the increasing MSLP over NEA points to a widening northward of the subtropical ridge into the tropics over the NEA region during the second half of the 20th century. Larsen (2008) identified an intensification of the subtropical ridge in winter over Australia using HadSLP2r gridded MSLP data set during the 20th century. A strengthening of the subtropical high pressure belt over the Australian region was noted by Ansell et al (2000). If the increasing MSLP were related to ENSO, then a see saw of in the sea level pressure should occur centred on the tropics and subtropics (Trenberth and Caron 2000), not an increase in MSLP over a long time period, with the maximum increases over SE QLD and the Tasman Sea.

An analysis of MSLP trends from five IPCC–AR4 models over the NEA region, identified in Chapter Two, shows there is considerable variation in the MSLP trends between models and seasons, however two models do show similar MSLP trends to BoM observations over the Queensland region in 1951–2000. The MSLP changes in the 21st century projections show increases in the MSLP over central and southern Queensland and the Coral Sea during 2001–2050, with inland Queensland showing a change to lower MSLP during 2051–2100, most likely due to higher temperatures associated with global warming and thermal heating of the continent.

In the following chapter, an analysis using five IPCC–AR4 models and NCEP reanalysis MSLP data investigates the link between the increasing MSLP trends over SE QLD and the NEA region to global MSLP changes over the Australian region and the Southern Hemisphere during the 20th century. The increasing MSLP in the Queensland region is compared to the changes in the MSLP associated with the subtropical ridge in the mid–latitudes of Australia and the Southern Hemisphere and to the changes in the SAM. The MSLP trends from 21st century projections from the five IPCC–AR4 models will also be examined in a more global context.

CHAPTER 4 : DECADAL MSLP TRENDS OVER AUSTRALIA AND THE SOUTHERN HEMISPHERE

4.1 INTRODUCTION

In this chapter, the decadal MSLP trends shown in Chapter Three over Queensland and the NEA region are examined in context with much larger MSLP trends over the Australian region (100ºE–180ºE, 10ºN–50ºS) and the Southern Hemisphere (20ºS–90º). This chapter investigates the MSLP trends in five IPCC–AR4 models and data from the National Centers of Environmental Prediction (NCEP) over the Australian region and Southern Hemisphere, and possible links to climate change. There has been a number of papers indicating the teleconnections between the positive phase of the Southern Annular Mode (SAM) and changes in rainfall or MSLP over the Australian region (Karoly 2003; Cai and Cowan 2006; Gillett et al. 2006; Hendon et al. 2007; Meneghini et al. 2007) and other regions in the Southern Hemisphere (Gillett et al. 2006; Ummenhofer and England 2007). However, none have directly linked the increasing MSLP trends to changes in the subtropical ridge and the positive phase of SAM to the rainfall changes over NEA and SE QLD.

Data and methodology are described in section 4.2. Results of the MSLP analysis from five IPCC–AR4 models and NCEP data over the Australian region and Southern Hemisphere for 1951–2000, 2001–2050 and 2051–2100 periods are shown in section 4.3 and 4.4 respectively. A correlation analysis between the seasonal and annual MSLP from the NEA region and the SAM index is shown in section 4.5. A correlation analysis between the seasonal and annual MSLP from the Queensland region and Norfolk Island investigates the links to the subtropical ridge in section 4.6. A discussion on the results is presented in section 4.7.

4.2 DATA AND METHODOLOGY

4.2.1 IPCC–AR4 Data

In this study, five IPCC–AR4 models selected in Chapter Two are used to produce the decadal MSLP trends over the Australian region (100ºE–180ºE, 10ºN–50ºS) and the Southern Hemisphere (20ºS–90º). Five models are used for both the 20th century decadal MSLP trends and 21st century projections. Further details on these models can be found in Chapters Two and Three (section 3.2.2). A multi–model ensemble mean is provided using the four models from the A2 scenario.

4.2.2 NCEP Data

This study uses monthly MSLP data from the National Centers of Environmental Prediction (NCEP) and the National Center of Atmospheric Research (NCAR) with a resolution of ~2.5º x ~2.5º and covers the period from 1951–2007. This NCEP/NCAR reanalysis data is used to compare decadal MSLP trends to the five IPCC–AR4 models.

4.2.3 SAM Index

The observational based Southern Hemisphere Annular Mode Index was selected for a correlation analysis between the MSLP trends from the NEA region to the MSLP trends in the SAM. This SAM index represents Southern Hemisphere high–latitude atmospheric circulation variability developed by combining MSLP observations from six stations at 40ºS and 65ºS from around the South Pole (Marshall 2003). Although slightly modified by Marshall (2003), the numerical definition of the SAM is:

$$SAM = P^*_{40^oS} - P^*_{65^oS}$$

where $P^*_{40^oS}$ and $P^*_{65^oS}$ are the normalised monthly zonal MSLP at 40ºS and 65ºS respectively. This means when MSLP is higher (lower) at 65ºS than 40ºS, a negative (positive) phase or polarity is established in the SAM index. A fill description of the methodology and comparisons with NCEP data and other MSLP datasets can be found in Marshall (2003). This SAM index is available online at: http://www.antarctica.ac.uk/met/gjma/sam.html.

As the data for the SAM index is currently only available from 1957, the time series of the MSLP from some stations has been adjusted accordingly, with some small changes to the level of significance values, compared to Table 3.4. The annual and seasonal SAM index values used in the correlation analysis are shown in Appendix Two.

4.3 DECADAL MEAN SEA LEVEL PRESSURE TRENDS OVER THE AUSTRALIAN REGION

4.3.1 Period 1951–2000

The seasonal and annual decadal MSLP trends from the NCEP observations and five IPCC–AR4 models over the Australia region (100ºE–180ºE, 10ºN–50ºS) and 1951–2000 are shown in Figure 4.1. Observations from the NCEP data (top row) show the following. In DJF, increases in MSLP cover nearly all of Australia and most of the tropics and mid–latitudes and is strongest over SE QLD and east of New Zealand. Small decreases in MSLP occur over the Southern Ocean. In MAM, the increase in the MSLP over the Australian region is strongest than in any other season. Increases in MSLP occur over all of the tropics and mid–latitudes, with the largest increases over southeast Australia and New Zealand. Small decreases in MSLP occur over the Southern Ocean, similar to DJF. In JJA, increases in MSLP are similar to DJF and cover the tropics and mid–latitudes, although weaker than in MAM. Decreases in the MSLP occur over the Southern Ocean southwest of Australia and is stronger than in other seasons. The MSLP trends from the BoM observations in Chapter Three (section 3.3.4) are similar in size to the IPCC–AR4 models for both MAM and JJA. In SON, increases in the MSLP cover nearly all the Australian region, with the largest increases over eastern Australia.

The annual decadal MSLP trends from the NCEP observations (Figure 4.1 top row, right figure) shows small to moderate increases in MSLP cover nearly all the tropics and the mid–latitudes, with the strongest increases over eastern Australia and the

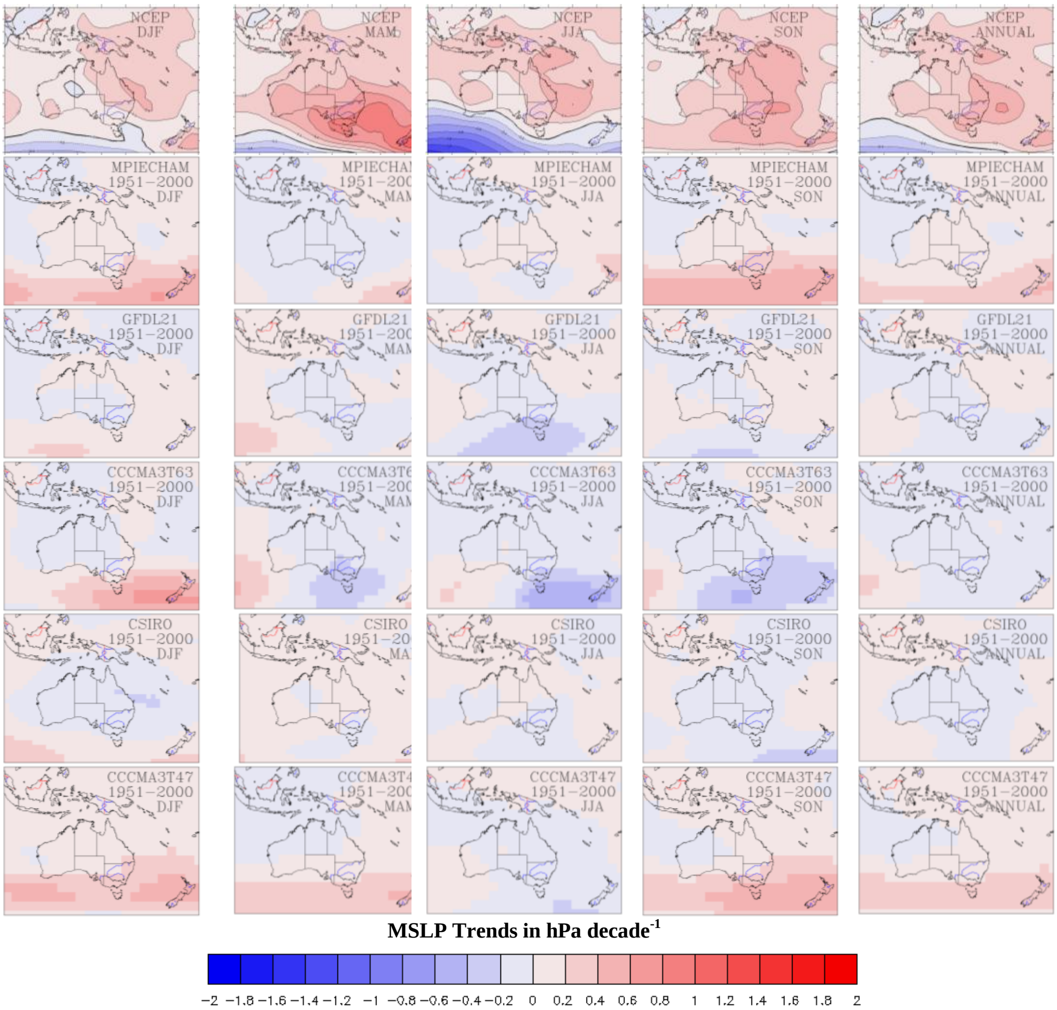

Figure 4.1 Seasonal and annual decadal MSLP trends (hPa decade^{-1}) from NCEP data (top row) and five IPCC–AR4 models (bottom rows) for the Australian region and the period 1951–2000. Regions shaded in red show increasing MSLP and blue decreasing MSLP.

Tasman Sea. Small decreases in the MSLP occur over the Southern Ocean south of Australia.

The five IPCC–AR4 models show the following seasonal decadal MSLP trends (Figure 4.1–lower rows). In DJF, the MPI-ECHAM5 and CGCM3.1-T47 models show small increases in the MSLP over Australia and larger increases in latitudes south and east of Australia. The GFDL-CM2.1 and CGCM3.1-T63 models show small decreases in MSLP over much of inland Australia and small to moderate increases in MSLP over the Southern Ocean, similar to the MPI-ECHAM5, and CGCM3.1-T47 models. In the CSIRO-MK3 model, small increases in MSLP occur over the Southern Ocean and small decreases over all of mainland Australia and the Tasman Sea. In MAM, the three models MPI-ECHAM5, GFDL-CM2.1 and CGCM3.1-T63 show a small decrease in the MSLP over Australia and oceans to the south or southeast. The CSIRO-MK3 and CGCM3.1-T47 models show a small increase in the MSLP over some parts of Australia and to the south or west over the oceans. In JJA, the GFDL-CM2.1, CGCM3.1-T63 and CGCM3.1-T47 models show small decreases in MSLP over much of Australia and latitudes south or southeast of the continent. The MPI-ECHAM5 and CSIRO-MK3 models show 'mixed' results, with increasing or decreasing MSLP over different regions. In SON, the MPI-ECHAM5 and CGCM3.1-T47 models show increases in the MSLP over most of Australia, with the stronger increases south and east of the continent. In contrast, the CGCM3.1-T63 and CSIRO-MK3 models show small to moderate decreases in MSLP over Australia and the oceans to the south and east of the continent. The GFDL-CM2.1 model shows 'mixed' results.

The annual decadal MSLP trends show small to moderate increases in MSLP over southern Australia and the Southern Ocean in the MPI-ECHAM5 and CGCM3.1-T47 models, with decreases in MSLP over northwestern Australia and the Indian Ocean. The GFDL-CM2.1, CGCM3.1-T63 and CSIRO-MK3 models show small decreases in the MSLP over Australia and the oceans to the south and southeast. The MPI-ECHAM5 and CGCM3.1-T47 models are most similar to the BoM observations (described in detail in section 3.3.4).

In summary, two models produce similar annual decadal MSLP trends over the Australian region compared to the NCEP reanalysis data, but generally produce increases in MSLP further south into the Southern Ocean. They are the same models that produced the closest MSLP trends to the BoM observations over the NEA region (section 3.6.1).

4.3.2 Period 2001–2050

The seasonal and annual decadal MSLP trends from the five IPCC–AR4 models over the Australia region and 2001–2050 are shown in Figure 4.2. In DJF, the GFDL-CM2.1, and CGCM3.1-T47 models show small increases in the MSLP over much of Australia (excepting some western areas) and the surrounding ocean. The CGCM3.1-T63 model shows a small to moderate decrease in the MSLP over most of Australia and the Southern Ocean, with small increases over the Coral Sea. The MPI-ECHAM5 and CSIRO-MK3 models show small increases and decreases in the MSLP over the northwest and south of Australia respectively. In MAM, the CGCM3.1-T63 and CGCM3.1-T47 models show small to moderate decreases in the MSLP over Australia and similar latitudes and small to moderate increases over the Southern Ocean. The GFDL-CM2.1 model shows mostly small increases in the MSLP over Australia and decreases over the Southern Ocean. The MPI-ECHAM5 and CSIRO-MK3 models show small increases in the MSLP over northern Australia and the Indian Ocean. In JJA, the GFDL-CM2.1 and CSIRO-MK3 models show moderate to strong increases in the MSLP over Australia and the oceans southwest of Western Australia. In contrast, the CGCM3.1-T63 model shows a small to moderate decreases in the MSLP over much of Australia and regions to the south and west.

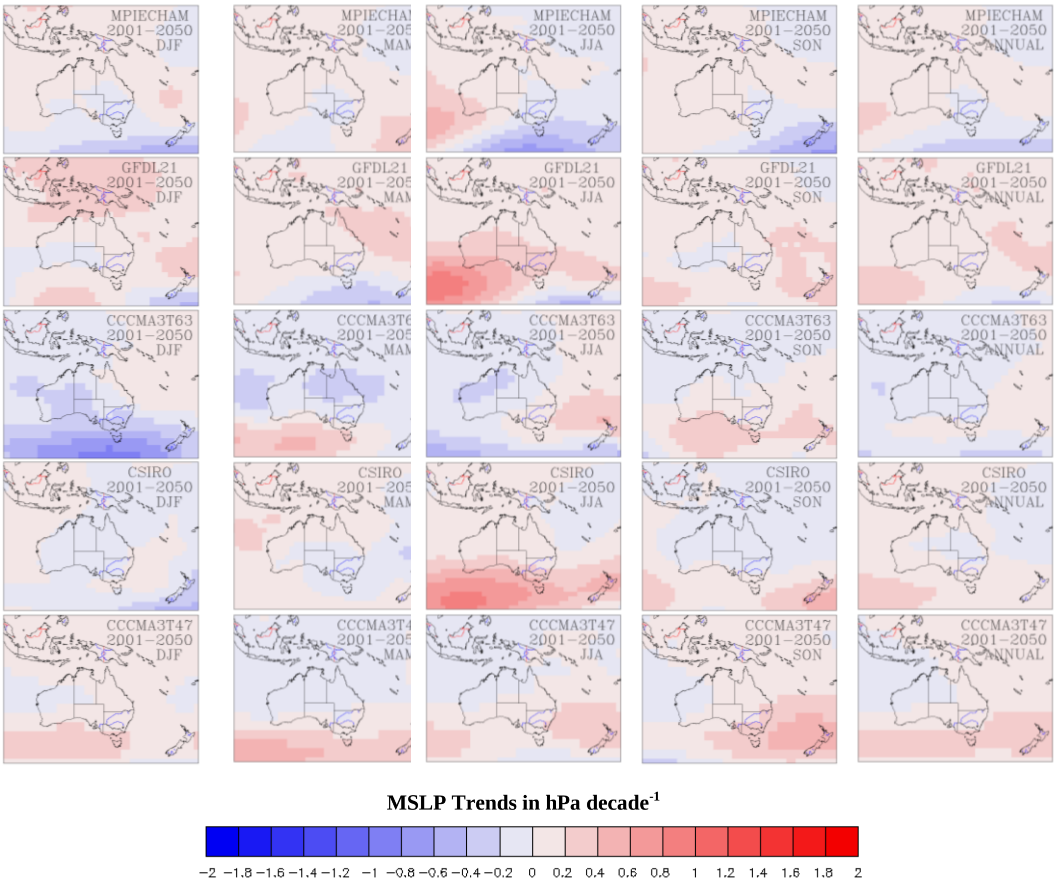

Figure 4.2 Seasonal and annual decadal MSLP trends (hPa decade^{-1}) for the Australian region from five IPCC–AR4 models and the period 2001–2050. Colour shading as in Figure 4.1.

The MPI-ECHAM5 and CGCM3.1-T47 models show increases in the MSLP over western and southern Australia respectively. In SON, the GFDL-CM2.1, CGCM3.1-T63 and CGCM3.1-T47 models show small to moderate increases in the MSLP over most of Australia, the Southern Ocean and the Tasman Sea. The MPI-ECHAM5 model shows small increases in the MSLP over most of Australia and small decreases around New Zealand. The CSIRO-MK3 model shows small decreases in the MSLP over most of Australia and small increases over the Southern Ocean.

The annual decadal MSLP trends show small to moderate increases in the MSLP over southern Australia and the Southern Ocean in the CSIRO-MK3 and CGCM3.1-

T47 models. The MPI-ECHAM5 model shows small to moderate decreases in the MSLP over the Southern Ocean south of Australia and increases over most of Australia. The GFDL-CM2.1 and CGCM3.1-T63 models show small to moderate increases and decreases in the MSLP over the Australian region respectively.

In summary, four models show increasing annual decadal MSLP over most of Australia and the mid–latitudes, compared to two models in 1951–2000.

4.3.3 Period 2051–2100

The seasonal and annual decadal MSLP trends from the five IPCC–AR4 models over the Australia region and 2051–2100 are shown in Figure 4.3. In DJF, the CSIRO-MK3 model shows small to moderate increases in the MSLP over nearly the entire Australian region. The MPI-ECHAM5 and GFDL-CM2.1 models have similar MSLP trends, with small to moderate increases in the MSLP over most of the oceans adjacent to Australia but with small decreases over some regions of Australia. The CGCM3.1-T63 and CGCM3.1-T47 models show small to moderate decreases in the MSLP over most of Australia and increases over the Southern Ocean. In MAM, the MPI-ECHAM5, GFDL-CM2.1 and CGCM3.1-T63 models show similar MSLP trends to DJF. The CGCM3.1-T47 model shows small decreases in the MSLP over most of Australia and similar latitudes. The CSIRO-MK3 model shows small decreases in the MSLP over Australia and small to moderate increases over the surrounding oceans. In JJA, the MPI-ECHAM5 and GFDL-CM2.1 models have similar MSLP trends, with small increases in the MSLP over oceans east and west of Australia, small decreases over Australia and moderate decreases over the Southern

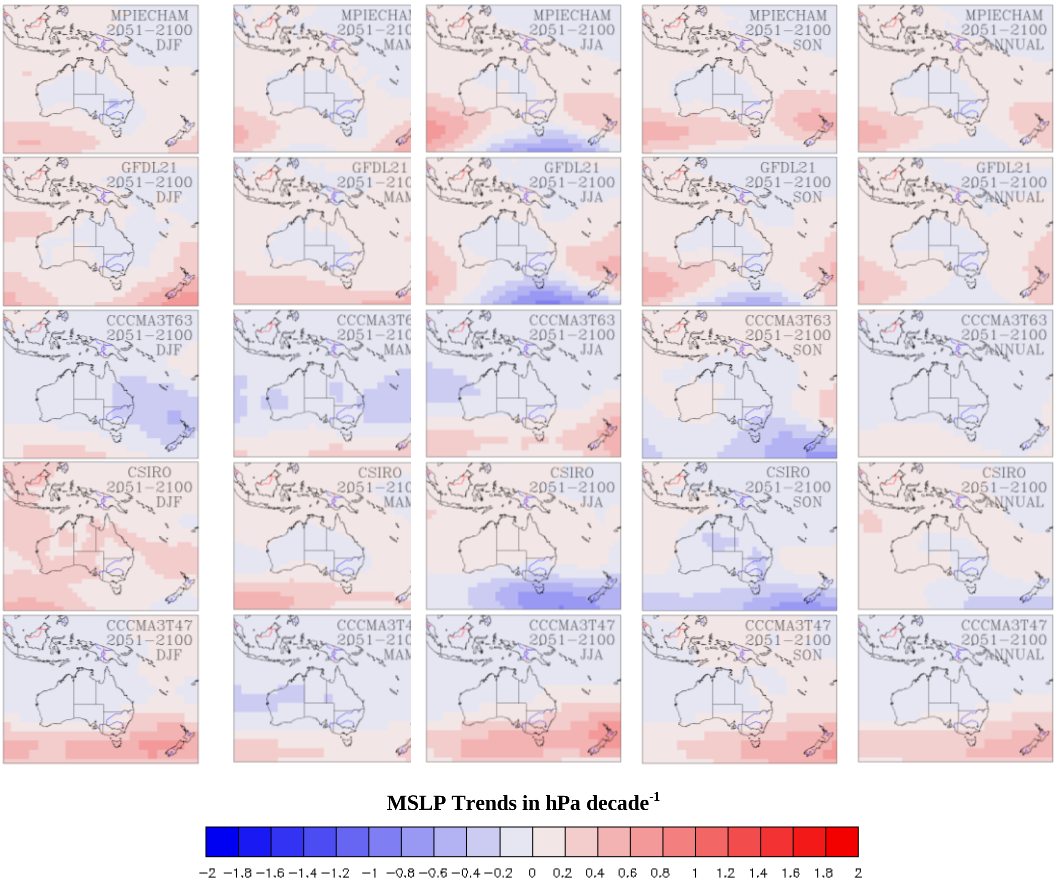

Figure 4.3 Seasonal and annual decadal MSLP trends (hPa decade^{-1}) for the Australian region from five IPCC–AR4 models and the period 2051–2100. Colour shading as in Figure 4.1.

Ocean. The CGCM3.1-T63 and CGCM3.1-T47 models also have similar MSLP trends, with small to moderate increases in the MSLP over southern Australia and the Southern Ocean and a small decrease over most of Australia and the tropics. The CSIRO-MK3 model shows small increases in the MSLP over Australia and moderate decreases south of Tasmania over the Southern Ocean. In SON, the MPI-ECHAM5 and GFDL-CM2.1 models have similar MSLP trends to JJA. The CGCM3.1-T63 and CSIRO-MK3 models show small to moderate decreases in the MSLP over most of Australia and the Southern Ocean. The CGCM3.1-T47 model shows similar MSLP trends to JJA.

The annual decadal MSLP trends show small to moderate increases in the MSLP over the oceans southwest and southeast of Australia in the MPI-ECHAM5 and GFDL-CM2.1 models, with small decreases over mainland Australia. The CGCM3.1-T47 model shows moderate increases in the MSLP over all the Southern Ocean and small decreases over the northern half of Australia. The CGCM3.1-T63 model shows small decreases in the MSLP over all of Australia, the tropics and mid–latitudes. The CSIRO-MK3 model shows small increases in the MSLP over all oceans around Australia except near New Zealand, where small to moderate decreases in the MSLP occur.

In summary, three models show increasing annual decadal MSLP over the mid–latitudes, compared to four models in 2001–2050 and four models show decreasing MSLP over inland Australia, compared to one model in 2001–2050.

4.3.4 Ensemble Means

Multi–model ensemble means of the seasonal and annual decadal MSLP trends over the Australian region and the periods 1951–2000, 2001–2050 and 2051–2100 are shown in Figure 4.4. The four models used are the MPI-ECHAM5, GFDL-CM2.1, CSIRO-MK3 and CGCM3.1-T47 from the A2 scenario. Grey shading indicates all four models agree on the sign of the MSLP trend. NCEP reanalysis data from the Australia region for 1951–2000 is shown for comparison (top row).

In 1951–2000, DJF shows increasing MSLP over large areas of eastern and southern Australia and the Tasman Sea, similar to the NCEP data. However, increasing MSLP

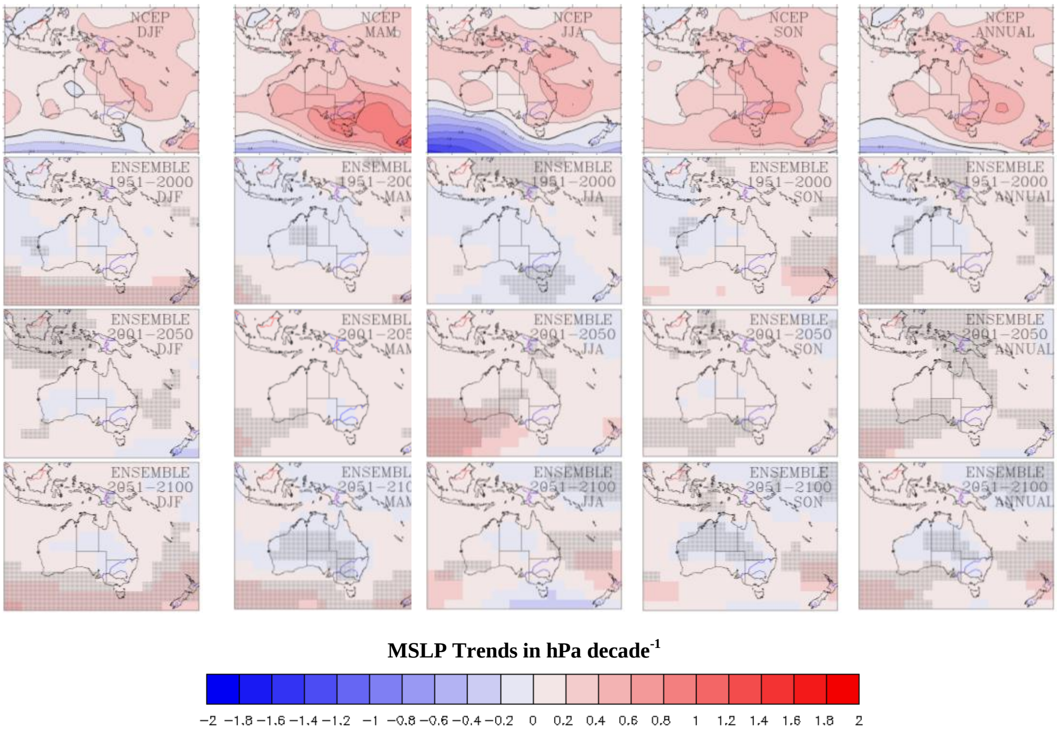

Figure 4.4 Seasonal and annual decadal MSLP trends (hPa decade^{-1}) from 1951–2000 from NCEP data (top row) and multi–model ensemble (bottom rows) over the Australian region and the periods 1951–2000, 2001–2050 and 2051–2100. Colour shading as for Figure 4.1 and grey shading represents regions where all models agree on the sign of the MSLP trend.

over the Southern Ocean (~50ºS) are opposite to NCEP observations. Over northwest Australia and the eastern Indian Ocean, a small decrease in the MSLP occurs in the ensemble, opposite to the NCEP data. In MAM, the increase of the MSLP over the Southern Ocean is lower than shown in the NCEP data. Most of central and northern Australia shows a small decrease in the MSLP, with all models agreeing on this trend southeast of Broome, opposite to the NCEP data. Over eastern Australia and the Tasman Sea, the NCEP data shows much larger increases in the MSLP. In JJA, much of Australia and the oceans south and northwest of the continent show decreases in the MSLP in the ensemble, with small increases over the Coral Sea and the area southwest of Western Australia. However, NCEP observations show an increase in the MSLP over the tropics and mid–latitudes and decreases over the Southern Ocean.

As discussed in section 3.6.1, MSLP trends in MAM and JJA from the models are generally not consistent with the BoM observations over the Queensland region. In SON, increasing MSLP covers much of southern and eastern Australia and the Southern Ocean and Tasman Sea. Northwestern Australia shows a small decrease in the MSLP as well as the adjacent Indian Ocean. The annual decadal MSLP trends are similar to SON, with the western half of the continent showing decreasing MSLP and eastern and southern Australia, higher MSLP.

In 2001–2050, DJF shows increasing decadal MSLP over nearly all the Australian region, with all models in agreement over very large area of Indonesia and most of the north Tasman Sea. A small area over the interior of Australia and near the South Island of New Zealand show small decreases in the MSLP. In MAM, nearly all the Australian region shows small increases in the MSLP, with all models in agreement over the region southwest of Western Australia. Only a small area over western and central NSW shows a small decrease in the MSLP. In JJA, nearly all of the Australian region shows a small increase in the MSLP (similar to MAM), with stronger increases over the southwest coastal region of Western Australia and the southeast Indian Ocean, where all models agree on this trend. In SON, the MSLP trends are similar to MAM, with small increases in the MSLP over most of the Australia region. The annual decadal MSLP trend shows similar spatial trends to the four seasons, with small increases in MSLP over nearly the entire Australian region, strongest southwest of Western Australia, where all models agree on the trend.

In 2051–2100, DJF shows increasing decadal MSLP over nearly all the Australian region, with the largest increases southwest, south and southeast of Australia over the

Southern Ocean and New Zealand, where all models agree on the trend. Small regions over inland Australia including the Northern Territory and Queensland show small decreases in the MSLP. In MAM, much of Australia is covered by a small decrease in the MSLP, with all models agreeing on this downward trend over more than half of Australia. A small decrease in the MSLP also occurs at low latitudes north and east of Papua New Guinea. Moderate increases in the MSLP occur over the Southern Ocean, similar to DJF. In JJA, increases in the MSLP cover much of the mid–latitudes, especially southwest of Western Australia and east of NSW and Queensland, where all models agree on this trend. The Northern Territory and north and east of Papua New Guinea show a small decrease in the MSLP, with moderate decreases over Tasmania and the seas further south. In SON, much of coastal Australia and surrounding oceans show a small increase in the MSLP, especially north of New Zealand. Inland parts of Australia and the oceans north and east of Papua New Guinea show a small decrease in the MSLP. The annual decadal MSLP trend shows similar trends to the four seasons, with small increases in the MSLP over the oceans around Australia, especially southwest of Western Australia and east of NSW and Queensland, where all the models agree on the trend. Small decreases in the MSLP occur over inland Australia and the region north and east of Papua New Guinea, where all models agree on the trend over much of the region.

4.3.5 Summary

An analysis of the five IPCC–AR4 models over the Australian region for 1951–2000 shows three models simulate decreases in the annual decadal MSLP and two models increasing or decreasing annual decadal MSLP over Australia. All the models simulate increasing MSLP over the regions southwest of Western Australia and over or east of New Zealand. The seasonal decadal MSLP trends from the five models show about ten plots simulate mostly decreasing MSLP, six plots ‘mixed’ trends and four plots increasing MSLP over Australia. Only two models realistically simulate the MSLP trends shown by the NCEP data over the Australian region. The NCEP reanalysis data shows much stronger MSLP trends in MAM than from the BoM observations (Chapter Three–section 3.3.4) over Queensland and the Tasman Sea, however the annual MSLP trends are quite similar.

An analysis of the decadal MSLP projections for 2001–2050 show three models simulate ‘mixed’ trends in the annual decadal MSLP trends and one model increasing or decreasing MSLP over Australia. Three models show increasing MSLP over much of the oceans around Australia, especially over mid or high latitudes and southwest of Western Australia. The seasonal decadal MSLP trends from the five models show about ten plots simulate ‘mixed’ trends in the MSLP and five plots increasing or decreasing MSLP over Australia.

An analysis of the decadal MSLP projections for 2051–2100 shows four models simulate decreasing annual decadal MSLP and one model ‘mixed’ trends over inland Australia. Three models show strong increases in the MSLP over the oceans, similar to 2001–2050, east and west or south of Australia. The seasonal decadal MSLP trends from the five models show ten plots simulate decreasing MSLP, eight plots ‘mixed’ trends and two plots increasing MSLP over Australia.

The multi–model ensemble mean for the annual decadal MSLP trend for 1951–2000 shows nearly all of oceans and coastal areas around Australia show increases in the MSLP, except over the northwest region of Australia, where small decreases in the MSLP occur. The multi–model ensemble for the annual decadal MSLP trend for 2001–2050 shows nearly the entire Australian region is dominated by increasing MSLP and this upward trend continues for 2051–2100, except that inland parts of the Australian continent shows a change to decreasing MSLP (albeit weaker), most likely due to rising temperatures offsetting the regional increase in MSLP.

4.4 DECADAL MEAN SEA LEVEL PRESSURE TRENDS OVER THE SOUTHERN HEMISPHERE

4.4.1 Period 1951–2000

Contoured seasonal and annual decadal MSLP trends from the NCEP reanalysis data (top row) and the five IPCC–AR4 models (lower rows) over the Southern Hemisphere (20ºS–90ºS) and 1951–2000 are shown in Figure 4.5. Observations from the NCEP data have a larger range in the MSLP trends (-5 to +5) than in the IPCC–AR4 models, due to large MSLP changes over the South Pole. This is further discussed in section 4.5. NCEP observations show all seasons are dominated by a moderate to strong decrease in the MSLP over the South Polar Region (~40º–90ºS), especially in the MAM and JJA. Two very small areas show small increases in the MSLP over the South Pole in SON and DJF. The low to mid–latitudes (~20º–40ºS) show a small increase in the MSLP, especially over the Indian Ocean. The annual decadal MSLP trend shows a strong decrease in the MSLP centred over the South

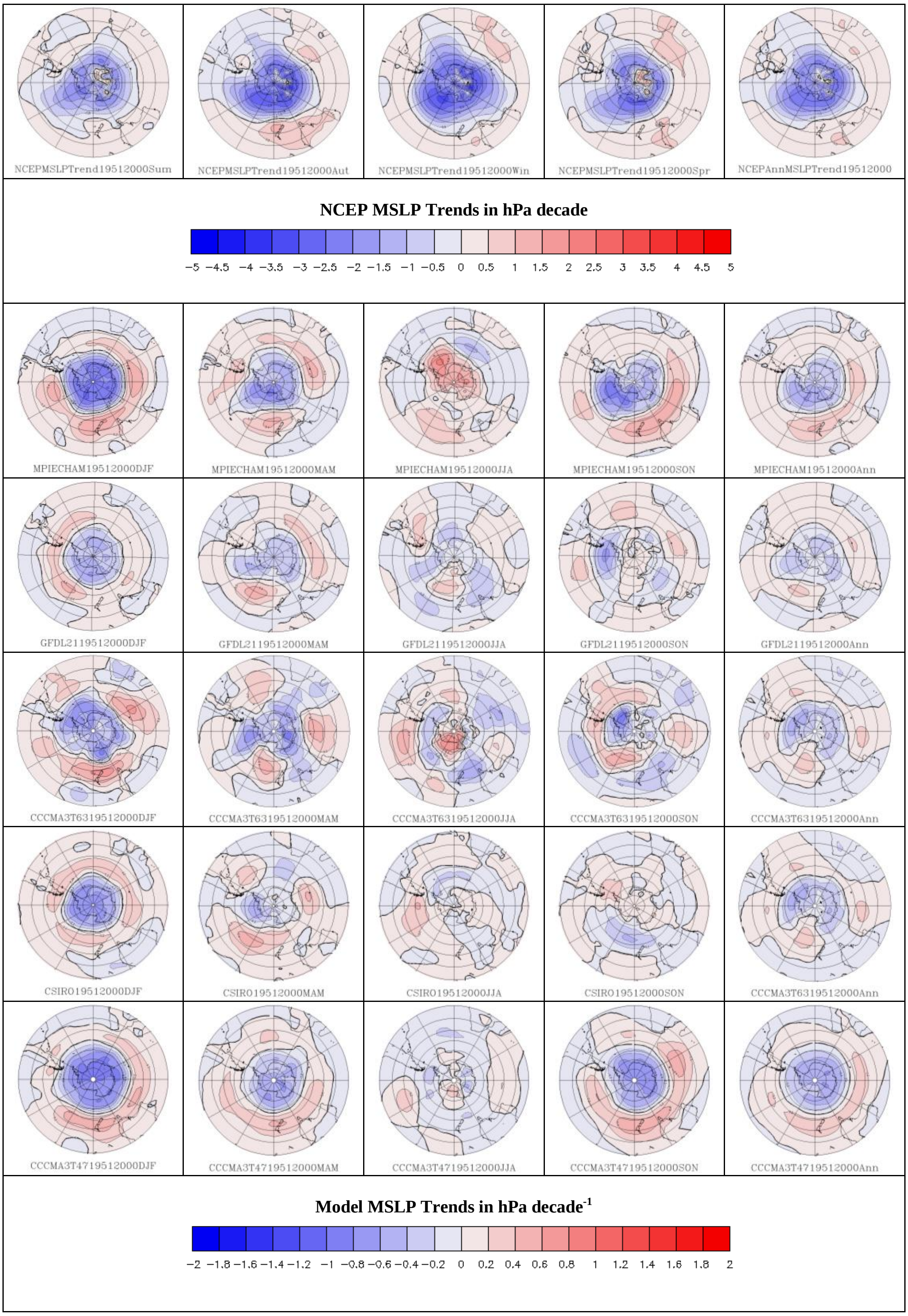

Figure 4.5 Contoured seasonal and annual decadal MSLP trends (hPa decade^{-1}) from NCEP data (top row) and five IPCC–AR4 models (bottom rows) over the Southern Hemisphere and the period 1951–2000. Regions shaded in red show increasing MSLP and blue decreasing MSLP. Note the larger range (-5 to +5) of MSLP trends from the NCEP data.

Pole (~50º–90ºS) and a small increase in the MSLP over the mid–latitudes (~20º–50ºS) including Australia.

In DJF, all five models show a moderate to strong annular decrease in the decadal MSLP over the South Polar Region (~60º–90ºS) and an increase in the MSLP over the mid–latitudes (~40º–60ºS), strongest in the MPI-ECHAM5 and CGCM3.1-T63 models. Increasing MSLP over the mid–latitudes forms two or three distinct zones, with the highest increase in the MSLP over the ocean basins, especially in the MPI-ECHAM5 and CGCM3.1-T63 models. In MAM, the decrease in the MSLP over the South Polar Region has decreased in all models and has become less annular. The increase in the MSLP over the mid–latitudes is only continuous around the globe in the CGCM3.1-T47 model, with the other models showing distinct bands of increasing MSLP in the Indian, Pacific or Atlantic Oceans. In JJA, a small increase in the MSLP occurs in the MPI-ECHAM5, CGCM3.1-T63 and CGCM3.1-T47 models over the South Polar Region. This is in contrast to the decrease in the MSLP in DJF and MAM. The increase in the MSLP over the mid–latitudes is discontinuous in all models and weaker than DJF or MAM. In SON, the decrease in the MSLP over the South Polar Region has been re-established in MPI-ECHAM5, CGCM3.1-T63 and CGCM3.1-T47 models, with increases in the MSLP in the mid–latitudes in four models. All seasons show a smaller decrease in the MSLP over a smaller region over the South Polar Region, compared to the NCEP reanalysis data. The increasing MSLP in the mid–latitudes is generally narrower in the models, forming distinct bands than in the NCEP data, which shows more broad and diffuse increases in the MSLP over the mid–latitudes.

The annual decadal MSLP trends show a generally annular decrease in the MSLP over the South Polar Region (50º–90ºS) in all models, which is smaller than in the NCEP data. An increase in the MSLP in the mid–latitudes is continuous around the South Polar Region in the MPI-ECHAM5 and CGCM3.1-T47 models but discontinuous in the other models. Overall, the MPI-ECHAM5 and CGCM3.1-T47 models simulate the annual MSLP trends closest to the NCEP observations.

In summary, five IPCC–AR4 models simulate the seasonal decadal MSLP trends closest to the NCEP observations in DJF and MAM and less well in JJA and SON. The annual MSLP trends in all the models over the South Polar Region are similar to the MSLP trends from the NCEP observations, but are weaker. These results are discussed in section 4.5. The increase in the MSLP in the mid–latitudes in the models is generally more narrow than the NCEP observations, with some tropical regions (~<30ºS) showing small decreases in MSLP. No models simulate the decrease in MSLP over the South Polar Region in all seasons. The CGCM3.1-T47 model shows changes in the MSLP closest to the NCEP observations.

4.4.2 Period 2001–2050

The seasonal and annual decadal MSLP trends from the five IPCC–AR4 models over the Southern Hemisphere and 2001–2050 are shown in Figure 4.6. In DJF, three models (GFDL-CM2.1, CGCM3.1-T63 and CSIRO-MK3) show increasing MSLP over the South Polar Region (opposite to the trend in 1951–2000) and two models a decrease. In the mid–latitudes, decreasing MSLP occurs in two models (CGCM3.1-T63 and CSIRO-MK3), increasing MSLP in the CGCM3.1-T47 model and 'mixed'

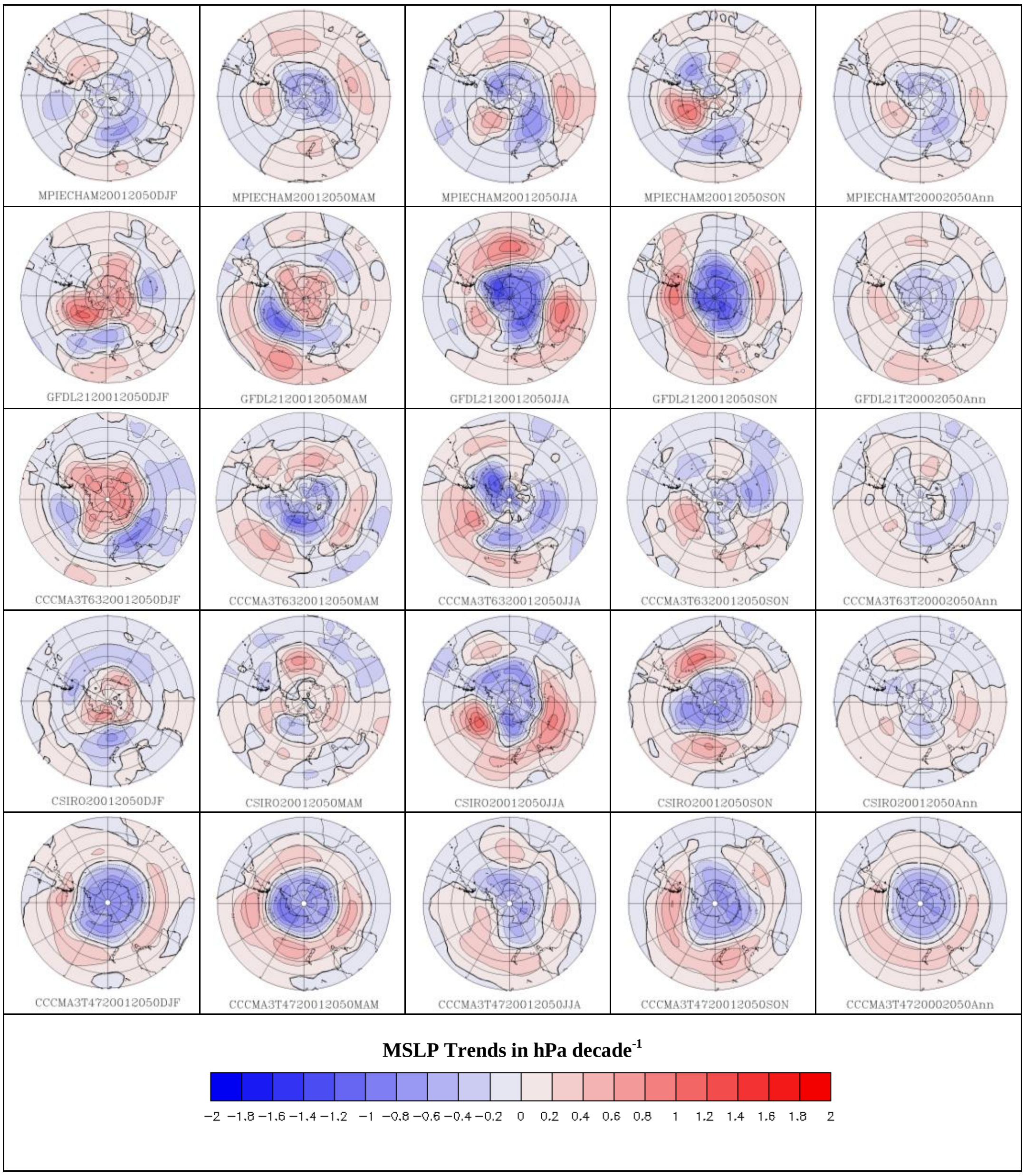

Figure 4.6 Contoured seasonal and annual decadal MSLP trends (hPa decade^{-1}) from five IPCC–AR4 models over the Southern Hemisphere and the period 2001–2050. Colour shading as in Figure 4.5.

changes, with increases and decreases in the MSLP in the MPI-ECHAM5 and GFDL-CM2.1 models. In MAM, three models (MPI-ECHAM5, CGCM3.1-T63 and CGCM3.1-T47) show a decrease in the MSLP over the South Polar Region (similar to 1951–2000) and the other two models, a small increase. In the mid–latitudes, the increasing MSLP is almost continuous around the globe in three models (CGCM3.1-T63, CGCM3.1-T47 and CSIRO-MK3) and forms a number of discontinuous bands in the other models, similar to 1951–2000. In JJA, all models show a decrease in the MSLP over the South Polar Region, especially in the GFDL-CM2.1 model. The mid–latitudes show several bands of increasing MSLP, similar to MAM over the Indian, Atlantic and Pacific Ocean in four models. In the CGCM3.1-T63 model, most of the Indian Ocean shows a small decrease in the MSLP, with the Pacific Ocean an increase. In SON, three models (GFDL-CM2.1, CSIRO-MK3 and CGCM3.1-T47) show decreasing MSLP over the South Polar Region and two models ‘mixed’ trends. The mid–latitudes show increases in the MSLP, similar to JJA, forming a semi–continuous circular band around the South Polar Region in three models. The MPI-ECHAM5 and CGCM3.1-T63 models show ‘mixed’ trends in the mid–latitudes with increasing MSLP over the Australia region.

The annual decadal MSLP trends show a small decrease in the MSLP over the South Pole and parts of the South Polar Region (50º–90ºS) and is generally less circular than 1951–2000 (except in the CGCM3.1-T47 model). Increasing MSLP over the mid–latitudes encompasses the South Polar Region in two models (GFDL-CM2.1 and CGCM3.1-T47) and is discontinuous in the other models, similar to 1951–2000. Only the CGCM3.1-T47 model maintains a decrease in the MSLP over the South Polar Region and an increase in the mid–latitudes in all seasons.

In summary, the five IPCC–AR4 models continue to show a decrease in the annual decadal MSLP over the South Polar Region and generally an increase in the MSLP over the mid–latitudes, similar to 1951–2000. Only the CGCM3.1-T47 model shows decreases in the MSLP over the South Polar Region in all seasons.

4.4.3 Period 2051–2100

The seasonal and annual decadal MSLP trends from the five IPCC–AR4 models over the Southern Hemisphere (20ºS–90ºS) and 2051–2100 are shown in Figure 4.7. In DJF, three models (MPI-ECHAM5, GFDL-CM2.1 and CGCM3.1-T47) show a

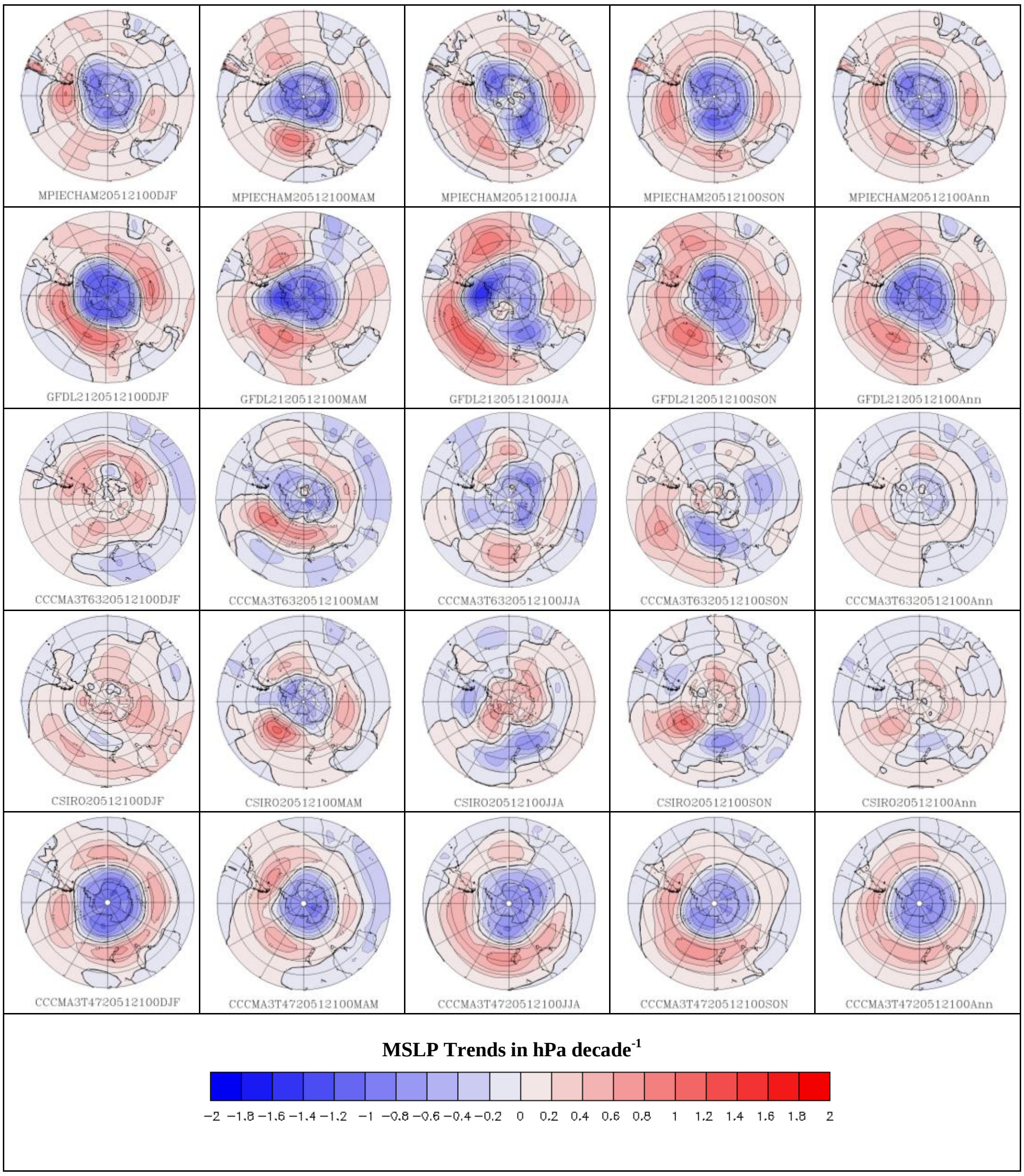

Figure 4.7 Contoured seasonal and annual decadal MSLP trends (hPa decade^{-1}) from five IPCC–AR4 models over the Southern Hemisphere and the period 2051–2100. Colour shading as in Figure 4.5.

moderate to strong annular decrease in the MSLP over the South Polar Region, a reversal in the GFDL-CM2.1 model, compared to 2001–2050. Two models (CGCM3.1-T63 and CSIRO-MK3) show a broad, less concentric increase in the MSLP over the South Polar Region. In the mid–latitudes (40ºS–60ºS), increasing MSLP occurs in all of the models, especially in the GFDL-CM2.1 model. The increase in the MSLP in the mid–latitudes is continuous and well defined around the South Polar Region in three models (GFDL-CM2.1, CGCM3.1-T63 and CGCM3.1-T47). In MAM, three models (MPI- ECHAM5, GFDL-CM2.1 and CGCM3.1-T47) show similar MSLP trends to DJF, with the CGCM3.1-T63 and CSIRO-MK3 models, a change to decreasing MSLP over the South Polar Region. In the mid–latitudes (~40ºS–60ºS), increasing MSLP occurs in all of the models and is generally stronger than DJF, with two or three zones of highest increasing MSLP trends over the southern ocean basins. In JJA, most the models show similar MSLP trends to MAM, except the CSIRO-MK3 model, which shows a reversal to increasing MSLP over the South Polar Region and generally decreasing MSLP over the mid–latitudes. In SON, most of the models show MSLP trends similar to JJA, except the CGCM3.1-T63 model, which shows ‘mixed’ trends of MSLP over the South Polar Region and a change to decreasing MSLP over the longitudes in the Indian Ocean.

The annual decadal MSLP trends shows a moderate to strong decrease in the MSLP over the South Polar Region and moderate to strong increase in the mid–latitudes (~20ºS–60ºS) in three models (MPI-ECHAM5, GFDL-CM2.1 and CGCM3.1-T47). A smaller decrease in the MSLP over the South Polar Region occurs in the CGCM3.1-T63 model and a small non–circular increase in the MSLP in the CSIRO-MK3 model.

In summary, the five IPCC–AR4 models become more aligned to decreases in the decadal MSLP over the South Polar Region, with three models showing decreases in the MSLP over the South Polar Region and increases in the mid–latitudes in all seasons, compared to one model in 2001–2050.

4.4.4 Ensemble Means

Multi–model ensemble means of the seasonal and annual decadal MSLP trends over the Southern Hemisphere and the periods 1951–2000, 2001–2050 and 2051–2100 are shown in Figure 4.8. The four models used are the MPI-ECHAM5, GFDL-CM2.1, CSIRO-MK3 and CGCM3.1-T47 from the A2 scenario. No shading has been included, as shown in section 4.3.4, so that the clarity of each image remains and the main MSLP trends are evident. NCEP data for the period 1951–2000 is shown for comparison (top row).

For 1951–2000, the DJF, MAM and SON seasons show small to moderate decreases in the decadal MSLP over the South Polar Region, weaker and smaller in area than in the NCEP observations. The same seasons also show increasing MSLP in the mid–latitudes similar to the NCEP observations, but over a smaller region (~30ºS–60ºS in the models versus 20ºS–50ºS from the NCEP data). Between ~20ºS–30ºS, the models show decreases in the MSLP, which is much smaller or absent in the NCEP observations. In JJA, the multi–mean ensemble shows the largest difference to the NCEP observations, with distinct decreases in the MSLP over the South Polar Region in the NCEP data absent in the ensemble, which shows small MSLP increases. The annual MSLP trend shows a small decrease in the MSLP over the

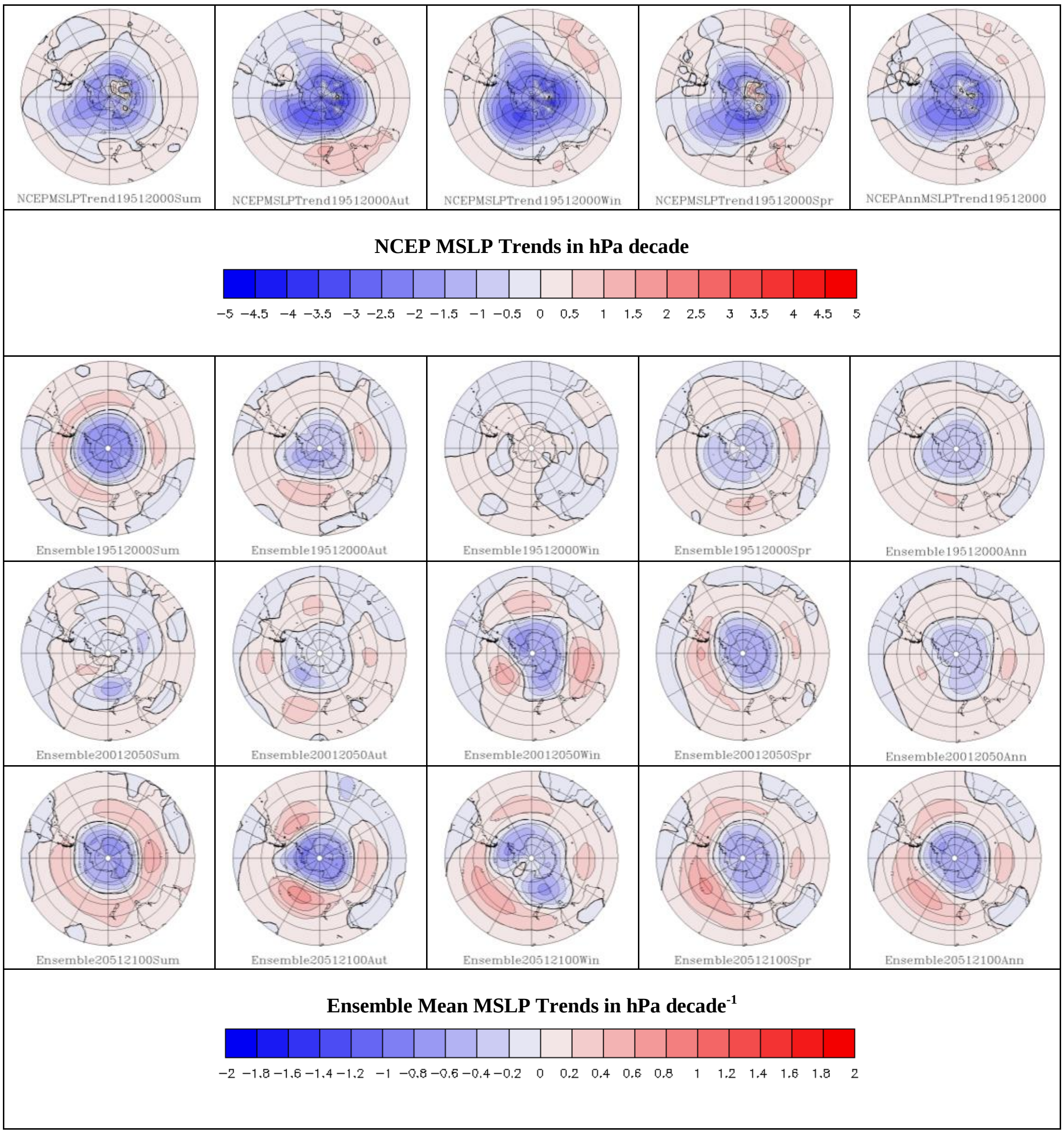

Figure 4.8 The seasonal and annual decadal MSLP trends (hPa decade^{-1}) from 1951–2000 for NCEP data (top row) and multi–model ensembles (bottom rows) over the Southern Hemisphere and the periods 1951–2000, 2001–2050 and 2051–2100. Colour shading as for in Figure 4.5. Note larger range of MSLP values from the NCEP data.

South Polar Region, smaller in size and weaker than the NCEP observations. Increasing MSLP in the mid–latitudes has about the same magnitude as the NCEP observations but does not extend as far equatorward. The small decreasing MSLP from ~20ºS–30ºS in the ensemble over the Indian Ocean does not occur in the NCEP observations.

For 2001–2050, DJF shows a small decrease in the decadal MSLP over most of the South Polar Region and small increases over the mid–latitudes in the Pacific and Indian Oceans, much weaker than the MSLP changes in the models from 1951–2000. In MAM, JJA, SON and the annual trend, the plots show small to moderate decreases in the MSLP over the South Polar Region and an increase in the MSLP over most of the mid–latitudes. A small decrease in the MSLP over low latitudes (~20ºS–30ºS) occurs over the eastern Pacific and Atlantic Oceans in all of the seasons.

For 2051–2100, all seasons and the annual trend show a small to moderate decrease in the decadal MSLP over the South Polar Region, much stronger than DJF and MAM in 2001–2050, and a small to moderate increase in the MSLP over the mid–latitudes. The small decrease in the MSLP at low latitudes (~20ºS–30ºS) is smaller in area than in 2001–2050, but still persists over the eastern Pacific Ocean.

4.4.5 Summary

The seasonal decadal MSLP trends for the Southern Hemisphere for 1951–2000 shows all models simulate decreasing MSLP over the South Polar Region in DJF and MAM, similar to the NCEP data, although not as strong and over a smaller region. The increase in the MSLP in the models in the mid–latitudes (associated with the subtropical ridge) occurs at higher latitudes (~40º–60ºS) than in the NCEP data (~20º–40ºS). In JJA, none of the models simulate the MSLP trends over the Southern Hemisphere similar to the NCEP data. In SON, three models show decreasing MSLP over the South Polar Region and the increasing MSLP over the mid–latitudes (and the subtropical ridge), similar to the NCEP observations. The annual decadal MSLP trend shows all models simulate a near circular decrease in the MSLP over the South Polar region, similar to the NCEP observations , although much weaker and over a smaller region. The MPI-ECHAM5 and CGCM3.1-T47 models simulate MSLP changes closest to observations shown by the NCEP data.

The seasonal decadal MSLP trends for the Southern Hemisphere for 2001–2050 show a number of differences compared to the 1951–2000 period. In DJF, three models simulate increasing MSLP over the South Polar Region, compared to five for the 1951–2000 period and two decreasing MSLP. In MAM, two models simulate increasing MSLP over the South Polar Region and three decreasing MSLP. In JJA, all models simulate decreasing MSLP over the South Polar Region and four models in SON. The annual decadal MSLP trend shows all models simulate decreases in the MSLP over the South Polar Region, although not as circular as for 1951–2000 and slighter weaker. Small increases in the MSLP in the mid–latitudes (and the subtropical ridge) are similar to the models from the 1951–2000 period.

The seasonal decadal MSLP trends for the Southern Hemisphere for 2051–2100 show three models simulate decreasing MSLP over the South Polar Region and two increases. All models show an increase in the MSLP over the mid–latitudes associated with the subtropical ridge. In MAM, all models show a decrease in the MSLP over the South Polar Region and an increase in the MSLP over the mid–latitudes (~40º–60ºS). In JJA, four models show a decrease in the MSLP over the South Polar Region and one model an increase. In SON, three models show a decrease in the MSLP over the South Polar Region, one model a small increase and the other ‘mixed’ results. An increase in the MSLP in the mid–latitudes occurs in three or four models for JJA and SON. The annual decadal MSLP trend shows three models have a moderate to strong decrease in the MSLP over the South Polar Region, one model a small decrease and the other model a small increase. All models show an increase in the annual decadal MSLP over the mid–latitudes associated with the subtropical ridge. Three models show the same MSLP trends over the South Polar Region and the mid–latitudes in all seasons, compared to one for 2001–2050 and none for 1951–2000.

Multi–model ensemble means of the seasonal and annual decadal MSLP trends for the 1951–2000 show similar changes to the NCEP observations for DJF, MAM, SON and the annual trend. The JJA ensemble mean is the most different from the NCEP observations, with a small increase in the MSLP over the South Polar Region and a small increase in the MSLP over the mid–latitudes. For 2001–2050, the MSLP trends for MAM, SON and the annual trend are essentially similar to 1951–2000, except for DJF and JJA, which show a reversal of the MSLP trend at the South Polar Region and in the mid–latitudes. For 2051–2100, all seasons and the ensemble mean show continuing decreasing MSLP over the South Polar Region and increasing MSLP over the mid–latitudes associated with the subtropical ridge. Small decreases in the MSLP occur at low latitudes over Australia, Africa and South America.

In this analysis, the projected decadal MSLP trends over the Southern Hemisphere for the 21st century are similar to the 20th century, with decreases in MSLP over the South Polar Region and increases over the mid–latitudes. Although only four models were used for the multi–model ensemble, the overall results are the very similar to a multi–model ensemble using all 18 models of the A2 scenario from the IPCC–AR4 report (not shown). This shows the decreases in the MSLP over the South Polar Region and the increases in the mid–latitudes (and the subtropical ridge) especially over the oceans around Australia, are very robust and unlikely to change in the 21st century.

4.5 CORRELATION BETWEEN THE SAM AND MSLP OVER THE NEA REGION

As discussed in sections 4.1, 4.3 and 4.4, the changes in the MSLP over the NEA region are likely to be related to changes in the subtropical ridge (with increasing MSLP in the mid–latitudes) and also to the positive polarity of SAM, with decreasing MSLP over the South Polar Region. As discussed in section 4.2.3, the definition of the SAM index means positive (negative) values represent increasing (decreasing) MSLP in the mid–latitudes and decreasing (increasing) MSLP in the high–latitudes. Therefore positive correlation values indicate increases in the MSLP from stations over the NEA region are related to increases in the MSLP in the mid–latitudes and decreases over the high–latitudes and the South Polar Region. To investigate these links, a correlation analysis between the SAM and the MSLP from twenty five stations over the NEA region is shown below. A time series of the annual SAM index and an ensemble mean of the annual MSLP from fourteen stations over the NEA region highlights some of the trends and similarities between the regions.

The results of the correlation analysis between the seasonal and annual SAM index and MSLP from twenty five stations from the NEA region are shown in Table 4.1. In

Table 4.1 The Seasonal and Annual Correlation between the SAM and the MSLP over the NEA region from ~1957–2008**.**

	Location	Period	Years	Level of Significance at 5% Level	DJF (Summer)	MAM (Autumn)	JJA (Winter)	SON (Spring)	Annual
1	Charleville	1957-2007	51	0.27	0.17	0.03	0.36	0.14	0.20
2	Roma	1957-2007	49	0.27	0.24	0.13	0.34	0.21	0.42
3	Toowoomba	1974-2007	34	0.35	0.21	0.07	**0.41**	0.08	0.43
4	Brisbane Aero	1957-2007	50	0.27	0.26	0.12	0.39	0.20	0.43
5	Longreach	1970-2007	38	0.33	0.28	0.03	0.28	0.04	0.32
6	Rockhampton	1957-2007	51	0.27	0.21	0.03	0.34	0.15	0.40
7	Mount Isa	1967-2007	40	0.30	0.26	-0.08	0.27	0.02	0.10
8	Townsville	1957-2007	51	0.27	**0.32**	-0.03	0.37	0.03	0.34
9	Mackay PO	1960-2007	46	0.29	0.22	-0.02	0.32	0.04	0.34
10	Weipa	1959-2007	37	0.33	0.16	0.05	0.22	0.06	0.23
11	Cairns	1957-2007	51	0.27	**0.29**	-0.10	0.33	0.07	0.25
12	Bourke	1957-2007	49	0.27	0.27	0.18	**0.43**	0.23	**0.46**
13	Moree	1965-2007	43	0.30	0.21	0.17	0.34	0.26	0.43
14	Coffs Harbour	1957-2007	51	0.27	0.17	0.17	**0.46**	**0.29**	**0.46**
15	Lord Howe Island	1957-2007	49	0.27	0.19	0.18	**0.44**	0.14	**0.46**
16	Norfolk Island	1957-2007	50	0.27	0.24	0.18	0.39	0.09	0.44
17	Willis island	1957-2007	48	0.29	0.28	-0.06	0.37	0.02	0.24
18	Georgetown	1957-2007	48	0.29	0.22	-0.06	0.39	-0.02	-0.02
19	Gaynah PO	1957-2007	50	0.27	**0.29**	0.05	0.35	0.22	0.43
20	Burketown	1957-2007	39	0.33	0.29	0.08	**0.44**	-0.09	0.26
21	Boulia	1957-2007	43	0.30	0.15	0.02	0.36	0.10	0.17
22	Clermont	1970-2008	38	0.33	0.18	0.11	0.30	0.21	0.38
23	Hughenden	1965-2008	41	0.30	0.18	-0.16	0.29	0.12	0.15
24	Birdsville	1957-2008	51	0.27	0.15	0.17	0.39	-0.03	0.30
25	Thargomindah	1957-2008	50	0.27	0.00	-0.03	0.26	0.07	0.16
	Overall Average				**0.22**	**0.09**	**0.35**	**0.12**	**0.31**
	Average R^2 value				**0.09**	**N/A**	**0.14**	**0.08**	**0.17**

Notes: **1**.Overall Average values (bottom row) are absolute values rounded to three significant figures.

2. The 'Years' column stands for the number of exact years used in calculating the correlation value.

3. Significant correlation values which are discussed in the text are highlighted in bold.

4. The level of significance (p=0.05) is for a two–tailed test.

5. R^2 is calculated only from stations with correlation values which exceed the statistically significant 5% level.

the DJF, only three stations, Townville (0.32), Cairns (0.29) and Gaynah PO (0.29) have significant correlation values above the statistically significant level of 5%. Overall, the twenty five stations have an average correlation value of 0.22. In MAM, no stations have correlation values above the statistically significant level of 5%. This indicates there does not appear to be any direct relationship between the SAM and MSLP over the NEA region in the austral autumn. The average correlation value from all stations is 0.09. In JJA, nineteen stations have correlation values above the statistically significant level of 5%, with Coffs Harbour (0.46), Lord Howe Island and Burketown both 0.44, Bourke (0.43) and Toowoomba (0.41) above 0.40. This indicates nineteen stations show a change in the MSLP related to the increase in MSLP in the mid–latitudes (and lower MSLP at higher latitudes) and shows the SAM is playing a role in the MSLP changes in austral winter over the NEA region. The average correlation value from all the stations is 0.35, which is much higher than the other seasons. In SON, only one station (Coffs Harbour 0.29) has a correlation value above the statistically significant level of 5%. An average correlation value for all the stations is 0.12 and indicates the SAM does not appear to be playing a significant role in the MSLP changes over the NEA region. The average r^2 value for the austral summer, winter and spring are low and range from 0.14 to 0.08 for stations with significant correlation values at the 5% level.

The annual correlation between the SAM index and the MSLP from over the NEA region shows fourteen stations have a correlation value above the statistically significant level of 5%, with the highest correlation values at Bourke, Coffs Harbour and Lord Howe Island (0.46). A total of ten stations have correlation values above 0.40, indicating increases in the annual MSLP are related to the SAM. The ten stations are located in SE QLD, adjacent to the east coast from Brisbane to Townsville, northern NSW and at Birdsville. The overall average correlation value from the twenty five stations is 0.31, slightly lower than the overall value of 0.35 for austral winter. The average r^2 value is 0.17 for the fourteen stations with significant correlation values above the 5% level.

A time series of the annual SAM index and the annual MSLP from fourteen stations (MSLP ensemble) across the NEA region (stations with correlation values above the 5% level–Table 4.1) is shown in Figure 4.9. The SAM index shows considerable variability from year to year, with a range generally between ~2–4 hPa. A long–term increase in the SAM index from negative values to positive values is shown by the

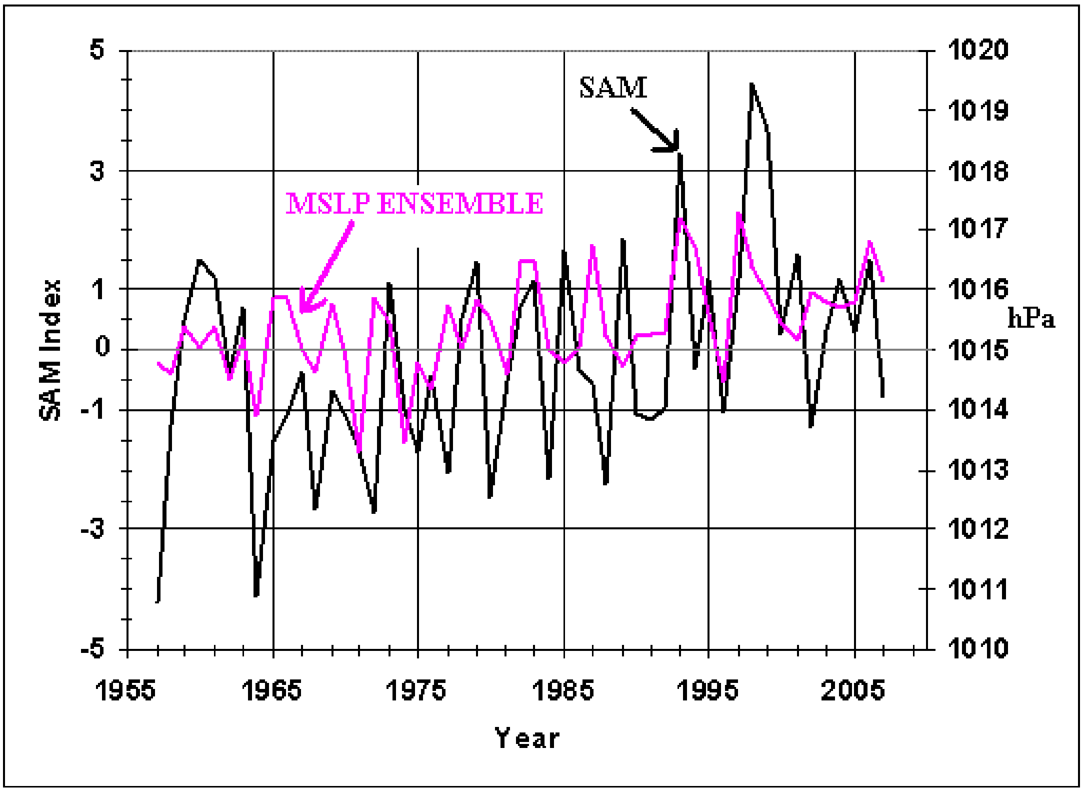

Figure 4.9 Time series of the annual SAM mode index (black) and the MSLP ensemble from 14 stations (purple) over the NEA region for 1957–2007.

time series. The MSLP ensemble has lower year to year variability (~1–2 hPa) and many of the peaks and troughs are in phase with the SAM index. The MSLP ensemble also shows an increase in the MSLP over the 50 year period from ~1015 hPa to ~1016 hPa, similar to the increase in MSLP discussed in Chapter Three (sections 3.3 and 3.4). Corresponding peaks between the SAM index and the MSLP ensemble occurred in 1963, 1965/66, 1969, 1982/1983, 1993 and 2006 and troughs in 1962, 1964, 1968 and 1996 respectively. Several other periods (1971/72, 1980/81 and 1997/98) show the MSLP ensemble from the NEA region leads or lags the SAM index peak or trough by one year. From ~1984 to 1990, the change in the SAM index and the MSLP ensemble are distinctly opposite to one another. The correlation between the SAM index and the fourteen stations shown by the MSLP ensemble in Figure 4.9 for the entire period (1957–2007) is 0.44, indicating ~19% of the variance in the MSLP can be explained by changes in the SAM index at these stations.

In summary, the austral winter shows the strongest correlation between the SAM index and the increase in the MSLP over the NEA region, however the correlation values are lower and most below the level of significant of 5% in the austral summer, autumn and spring. The annual correlation between the SAM index and the increase in the MSLP over the NEA region is statistically significant at ten stations, with similar correlation values to the austral winter. The strength of the significant correlation values in the austral winter and the annual period are similar to the correlation values between the MSLP and rainfall (Chapter Three–section 3.5), although the correlation values between rainfall and MSLP are strongest in the austral autumn.

4.6 CORRELATION BETWEEN THE MSLP AT NORFOLK ISLAND AND THE QUEENSLAND REGION

As shown in section 4.5, the strongest correlation between the SAM and MSLP over the NEA region occurs in the austral winter and the annual period. However, some of the strongest MSLP increases and rainfall declines occur in austral summer and autumn. To investigate the increase in MSLP across the NEA region and links to the subtropical ridge, a correlation analysis between the MSLP at Norfolk Island and the twenty four stations used in Chapter 3 and section 4.5 (above) is shown below. Norfolk Island is the most distant station from the Australian mainland used in this study and the increase in MSLP should be least affected by the seasonal heating experienced over the Australian continent during the austral spring, summer and autumn. Norfolk Island is located at a latitude of 29ºS, similar to other stations from southern Queensland and northern NSW and has some of the largest increases in MSLP in all seasons from the NEA region (Table 3.3). The increase in the MSLP at Norfolk Island is very likely to represent changes in the subtropical ridge over the east Australian and southwestern South Pacific Ocean regions, which is located close to the largest increases in the MSLP identified from the NCEP reanalysis data from 1951–2000 (Figure 4.1). Therefore, if the correlation values are high and positive, this would indicate the increases in MSLP over the Queensland region are in phase with the increase in MSLP at Norfolk Island. The similarity in the MSLP between stations has already been described earlier in Chapter 3 (section 3.4). This correlation analysis uses the same time intervals used in section 4.5 and the SAM, so comparisons between the correlation values from the different analyses can be made. A time series between the annual MSLP at Norfolk Island and an ensemble mean from all stations from over the Queensland region is provided to show the similarities and trends in the MSLP between the regions.

A summary of the correlation values between the seasonal and annual MSLP from Norfolk Island and the other twenty four stations from the Queensland region are shown in Table 4.2. In the DJF, only one station (Thargomindah with -0.14) does not show a significant correlation (at the 5% level) to the MSLP changes at Norfolk Island. The lowest correlation values occur at Boulia (0.57) and Georgetown and Birdsville with 0.59. The highest correlation values occur at Lord Howe Island (0.82), Toowoomba (0.80), Longreach (0.78) and Brisbane Aero (0.77). The average correlation value for all the stations is 0.68 (r^2=0.49), which is well above the average correlation value with the SAM of 0.22 (Table 4.1). In MAM, all stations have correlation values above the 5% level of significance, with the largest values at Lord Howe Island (0.90), Brisbane Aero (0.75), Toowoomba (0.74) and Coffs Harbour (0.72). The lowest correlation values occur at Thargomindah (0.28) and Willis Island and Cairns with 0.30. The average correlation value for all the stations is 0.54 (r^2=0.29) and this is the lowest of all the seasons, although much higher than the correlation value of 0.09 between the SAM and MSLP (Table 4.1). In JJA, only one station (Thargomindah with 0.23) has a correlation value below the 5% level of significance. The lowest correlation values occur at Georgetown (0.49) and Willis Island and Cairns with 0.61. The highest correlation values occur at Lord Howe Island (0.94), Toowoomba (0.91), Brisbane Aero (0.89) and Coffs Harbour (0.88). The average correlation value for all the stations is 0.74 (r^2=0.57), which is the highest for all the seasons and well above the average correlation value with the SAM of 0.35 (Table 4.1). In SON, two stations have negative correlations

Table 4.2 The Seasonal and Annual Correlation between MSLP at Norfolk Island and the Queensland region from 1957–2008**.**

	Location	**Period**	**Years**	**Level of Significance at 5% Level**	**DJF (Summer)**	**MAM (Autumn)**	**JJA (Winter)**	**SON (Spring)**	**Annual**
1	Charleville	1957-2007	51	0.27	0.73	0.59	0.81	0.70	0.78
2	Roma	1957-2007	49	0.27	0.74	0.67	0.82	0.73	0.87
3	Toowoomba	1974-2007	34	0.35	**0.80**	**0.74**	**0.91**	**0.85**	**0.90**
4	Brisbane Aero	1957-2007	50	0.27	**0.77**	**0.75**	**0.89**	**0.87**	**0.89**
5	Longreach	1970-2007	38	0.33	**0.78**	0.40	0.73	0.68	0.86
6	Rockhampton	1957-2007	51	0.27	0.74	0.60	0.84	0.83	0.84
7	Mount Isa	1967-2007	40	0.30	0.67	0.41	0.65	0.54	0.66
8	Townsville	1957-2007	51	0.27	0.71	0.49	0.77	0.75	0.83
9	Mackay PO	1960-2007	46	0.29	0.66	0.58	0.80	0.78	0.82
10	Weipa	1959-2007	37	0.33	0.62	0.63	0.65	0.54	0.80
11	Cairns	1957-2007	51	0.27	0.64	**0.30**	**0.61**	0.64	0.61
12	Bourke	1957-2007	49	0.27	0.63	0.53	0.81	0.72	0.83
13	Moree	1965-2007	43	0.30	0.76	0.69	0.85	0.80	0.88
14	Coffs Harbour	1957-2007	51	0.27	0.67	**0.72**	**0.88**	0.83	0.88
15	Lord Howe Island	1957-2007	49	0.27	**0.82**	**0.90**	**0.94**	**0.94**	**0.95**
16	Willis island	1957-2007	48	0.29	0.70	**0.30**	**0.61**	0.58	0.67
17	Georgetown	1957-2007	48	0.29	0.59	0.50	**0.49**	**0.53**	**0.56**
18	Gaynah PO	1957-2007	50	0.27	0.76	0.62	0.88	**0.88**	0.88
19	Burketown	1957-2007	39	0.33	0.70	0.46	0.66	**-0.27**	0.75
20	Boulia	1957-2007	43	0.30	0.57	0.40	0.73	0.54	**0.56**
21	Clermont	1970-2008	38	0.33	0.72	0.56	0.80	0.77	0.81
22	Hughenden	1965-2008	41	0.30	0.75	0.42	0.63	0.64	0.72
23	Birdsville	1957-2008	51	0.27	0.59	0.42	0.65	**0.44**	0.58
24	Thargomindah	1957-2008	50	0.27	**-0.14**	**0.28**	**0.23**	**-0.24**	**0.53**
	Overall Average				**0.68**	**0.54**	**0.74**	**0.67**	**0.77**
	Average R^2 value				**0.49**	**0.29**	**0.57**	**0.50**	**0.59**

Notes: **1**.Overall Average values (bottom row) are from absolute values rounded to three significant figures.

2. The ‘Years’ column stands for the number of exact years used in calculating the correlation value.

3. Significant correlation values which are discussed in the text are highlighted in bold.

4. The level of significance (p=0.05) is for a two–tailed test.

5. R^2 is calculated only from stations with correlation values which exceed the statistically significant 5% level.

(Thargomindah and Burketown with -0.24 and -0.27 respectively), but are below the 5% level of significance. Other lower correlation values occur at Birdsville (0.44) and Georgetown (0.53). The highest correlation values occur at Lord Howe Island (0.94), Gaynah PO (0.88), Brisbane Aero (0.87) and Toowoomba (0.85). The average correlation value for all the stations is 0.67 (r^2=0.50), which is well above the average correlation value between the SAM and MSLP of 0.12 (Table 4.1).

The annual correlation values from all the stations are above the 5% level of significance. The highest correlation values occur at Lord Howe Island (0.95), Toowoomba (0.90) and Brisbane Aero (0.89). Fourteen stations have correlation values above 0.80. These very high correlation values indicate the increases and decreases in the MSLP from these stations are very highly correlated and synchronous in the time series. The lowest correlation values occur at Thargomindah (0.53) and at Boulia and Georgetown with 0.56. The average annual correlation value is 0.77 and this is slightly higher than the highest seasonal average value in the austral winter of 0.74. The average r^2 value of 0.59 occurs across all the stations and the r^2 value is much higher at some stations, such as at Lord Howe Island with 0.90.

A time series of the annual MSLP at Norfolk Island and the annual MSLP from twenty four stations (MSLP ensemble), which all have correlation values above the 5% level of significance, is shown in Figure 4.9. The MSLP at Norfolk Island shows considerable variability from year to year, with a range generally between ~1–3 hPa and increases from ~1015 hPa to ~1017 hPa over the period of the time series. The yearly range in the MSLP from the MSLP ensemble is similar to Norfolk Island and many of the peaks and troughs in the time series are very similar. The start and end

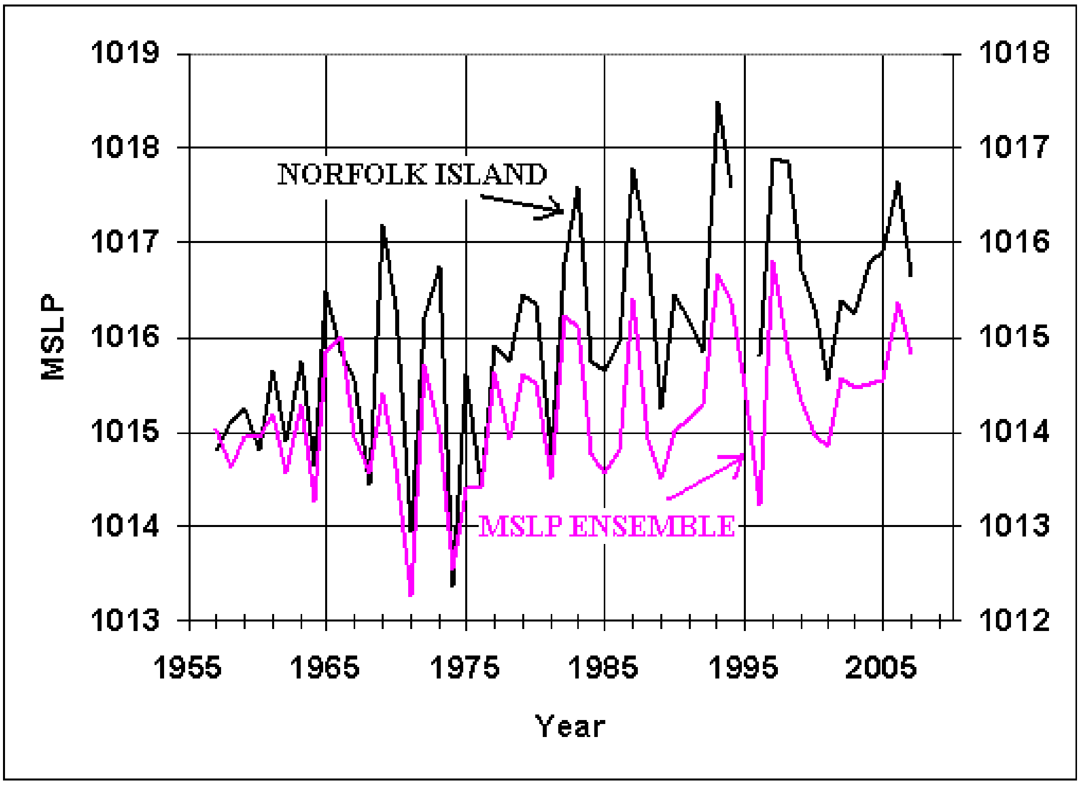

Figure 4.10 Time series of the annual MSLP at Norfolk Island (black) and the MSLP ensemble from 24 stations (purple) over the Queensland region for 1957–2007. Note there is one year of data missing from Norfolk Island in 1995.

of each time series for Norfolk Island and the MSLP ensemble is 1015 hPa and 1014 hPa and 1017hPa and 1015 hPa respectively. The time series diverge by ~1 hPa and this is consistent with the decadal MSLP changes discussed in Chapter Three (Section 3.3), which showed the fastest increases in MSLP occurred at Norfolk and Lord Howe Islands and Toowoomba, with lower increases over the rest of the Queensland region. The correlation value between the MSLP at Norfolk Island and the MSLP ensemble from the twenty four stations is high with a value of 0.85, indicating changes in the MSLP at Norfolk Island are similar to the changes in the MSLP over much of the Queensland region. An average r^2 value of 0.72 indicates 72% of the MSLP variance across the Queensland region can be explained by the change in the MSLP at Norfolk Island.

In summary, the changes in the MSLP over much of the Queensland region are very similar to the changes in the MSLP observed from Norfolk Island from 1957–2007. The annual period has an average correlation value of 0.77, followed by austral winter (0.74), summer (0.68), spring (0.67) and autumn (0.54). The austral winter has the strongest correlation with the MSLP at Norfolk Island and is also the season with the largest increases in the MSLP over the Queensland region. It also shows the strongest correlation to the SAM (Table 4.1). The changes in the MSLP at Norfolk Island are most likely to represent changes in the strength, width or latitude of the subtropical ridge (or combinations of these factors) in the eastern Australian and southwestern Pacific Ocean region during the 1957–2007 period.

4.7 DISCUSSION

In this chapter, the decadal MSLP trends from the NCEP reanalysis data and five IPCC–AR4 models were examined over the Australian region and the Southern Hemisphere for 1951–2100. The NCEP data shows all seasons have a strong decrease in the MSLP over the South Polar Region. However, the MSLP trend in the NCEP reanalysis data is higher than actual MSLP changes and the SAM index has been recently improved by using station observations from nearby stations (Marshall 2003). Hence, the MSLP changes over the South Polar Region are likely to be lower than shown in the NCEP observations. Marshall (2003) indicates the strongest MSLP changes have occurred in austral summer and are lowest in the austral winter, which is more in line with the results from the five IPCC–AR4 models (Figure 4.5) and the multi–model ensemble (Figure 4.8) shown here. This seasonality of the SAM is similar to results found by Cai and Cowan (2007) from an ensemble mean using 21

IPCC–AR4 models. They also show ozone–depletion forcing produces a more realistic SAM trend when compared to NCEP data corrected by station–based observations. Although two of the models used in this study do not include ozone (section 2.6), they still produce many of the important aspects of 20th century climate over the Southern Hemisphere and the NEA region.

The correlation analysis between the SAM index and the MSLP from over the NEA region (section 4.5) shows a significant correlation in the austral winter and the annual period. Although this study did not show a strong correlation between the SAM and the MSLP in the austral summer, autumn and spring, it is possible that an index incorporating only the MSLP over the South Polar Region, may have provided more definitive results, similar to the index used in the study by Nicholls (2009).

A correlation analysis between the MSLP at Norfolk Island and the stations from the Queensland region (section 4.6) shows a strong correlation between the increase in the MSLP at Norfolk Island and the rest of the Queensland region in all seasons, strongest in the austral winter. The changes in MSLP at Norfolk Island are likely to be a very good proxy for the changes in the subtropical ridge in the eastern Australian and southwestern Pacific Ocean regions and hence, most of the increases in the MSLP observed over the NEA region are most likely caused by changes in the subtropical ridge.

Although the increases in the MSLP in the austral summer and autumn did not correlate well with the changes in the SAM index, this could be explained by several factors. The SAM index is the normalised zonal MSLP difference between the MSLP at 40ºS and 65ºS and the changes in the SAM index in the austral summer and autumn may not be typical of the MSLP changes in the Australian region. In austral spring, summer and autumn, the subtropical ridge axis is generally further south than 40ºS and usually south of the Australian continent and over the central or south Tasman Sea. Seasonal heating and the formation of continental lows over the Australian continent, drive the subtropical ridge further south, more than other regions in the South Hemisphere. Hence, the changes in the subtropical ridge may not be well represented by the SAM mode index in the Australian region for the warmer months in the austral spring, summer and autumn. Nicholls (2009) showed 70% of the rainfall decline over southern Australia could be attributed to the increase in the MSLP related to the SAM. Although the major rainfall declines over the Queensland region are in the austral summer and autumn, this study shows the increases in the MSLP are just as significant as in the austral winter, and therefore rainfall declines of this magnitude could also be expected due to the SAM and the links to the subtropical ridge.

Another possible contributing factor to the increase in the MSLP over the NEA region maybe the changes in the year to year variability of the Hadley circulation and the descending region (the subtropical ridge) over the Australian region. Changes in the subtropical ridge have been identified by a number of authors (Drosdowsky 2005; Larsen 2008; Seidel et al. 2008; Nicholls 2009), with expansion of the Hadley circulation by 2º–4.5º into the mid–latitudes during 1979–2005 (Hu and Fu 2007; Lu et al. 2007). It is likely that changes in the Hadley circulation linked to convection in the tropics are unlikely to be homogenous across different longitudes, especially in the Australian region, where the seasonal hearting of the Australian continent and the convection with the equatorial tropics and monsoon interact to form a unique atmospheric circulation pattern, which may differ from the classic Hadley circulation described by many authors.

This chapter has shown the increasing MSLP over the Queensland and NEA region are part of a much larger changes in the atmospheric circulation over the Southern Hemisphere which have occurred during the late 20th century and are likely to continue well into the 21st century. The NCEP observations show the major MSLP changes over the Southern Hemisphere have been decreases in the MSLP over the South Polar Region and increases over the mid–latitudes (and the subtropical ridge), and are directly related to the positive polarity in the SAM. SAM is the dominant mode of atmospheric variability in the Southern Hemisphere (Marshall 2003; Cai and Cowan 2007) and numerous studies now show the main driver of the changes in the SAM are ozone depletion (Karoly 2003; Cai 2006; Crook et al. 2008) and increasing greenhouse gases (Cai and Cowan 2006, 2007). Hence, if the SAM, via these anthropogenic factors, are driving the MSLP changes over much of the Southern Hemisphere including increases in the MSLP over southern Australia (Gillett et al. 2006; Hendon et al. 2007) and changes in southern Australian rainfall (Hendon et al. 2007; Meneghini et al. 2007), then it is likely the SAM is also contributing to the rainfall decline at least in austral winter over much of NEA and SE QLD, by increasing the MSLP associated with the subtropical ridge and producing more subsidence in these regions. Despite the SAM having its strongest signal in austral summer, its impact on southwestern Western Australian rainfall with an austral winter maximum, has been shown to be very significant, even in seasons when it is weakest (Cai and Cowan 2006).

Although ENSO and the Indian Ocean Dipole (the IOD – which represents a coupled ocean-atmosphere mode of variability in the tropical Indian Ocean) are important drivers of climate variability in Australia, it is unlikely they are the primary cause of extreme conditions over southeastern Australia since 1995 (Ummenhofer et al. 2009). Further, Nicholls (2009) suggests the rainfall decline over southern Australia (>30ºS) from 1958–2007 is due to key changes in the subtropical ridge (which dominates over the Australian latitudes) and the SAM, and is less likely due to changes in the behaviour of ENSO and the IOD. Murphy and Ribbe (2004) indicate that the Indian Ocean sea surface temperatures have a limited impact on SE QLD rainfall. Four La Niña events have occurred post 1995, which usually produce above average rainfall (Wang and Hendon 2007) but have failed to prevent the rainfall decline across eastern Australia and SE QLD. ENSO and warm events are usually associated with drought over NEA, however this relationship has been seen to weaken over the Queensland region since the late 1970s (Cai et al. 2001). Therefore another primary cause is needed to account for the long–term rainfall decline (post 1950) across most of NEA and SE QLD. As shown in this chapter and Chapter Three, increasing MSLP across most of NEA and SE QLD has continued unabated, interrupted briefly by small decreases in MSLP during ENSO cold events. It seems likely that SAM has been underpinning the slow rise in MSLP in the low to mid–latitudes (broadening and strengthening the subtropical ridge) across most of NEA, especially SE QLD, contributing to some or most of the rainfall decline in this region, a factor which has yet not been attributed in any other study. The Hadley circulation has also been observed to be changing its characteristics in recent decades (Kobayashi and Maeda 2006; Lu et al. 2007; Seidel et al. 2008). Much of NEA and SE QLD lies beneath the descending arm of the Hadley circulation (Hesse et al.

2004; Seidel et al. 2008) and the degree this is contributing to the suppression of rainfall through upper level convergence and subsidence is currently uncertain, but it is unlikely to be the main cause of the increasing MSLP in the region. The Hadley circulation is intimately linked to the intertropical convergence zone (Hu et al. 2007) and hence changes in the hydrological cycle associated with global warming will also impact directly on the future Hadley circulation in the SE QLD region.

This analysis, as well as other studies (Yin 2005; Arblaster and Meehl 2006; Waugh et al. 2009), indicates the positive phase of the SAM is likely to continue well into the 21st century, driven by rising greenhouses gases, leading to further increases in the MSLP over the mid–latitudes and the subtropical ridge. The expansion of the Hadley cell under global warming is likely to exacerbate the dry conditions in the mid–latitudes and subtropical dry zones (Previdi and Liepert 2007). To further add to the decline in rainfall over the NEA region, the decrease in MSLP over the eastern Pacific (section 4.4.2 and 4.4.3) and the concomitant increase in westerly winds in multi–model ensembles over the equatorial region north and east of Papua New Guinea, indicate more warm phases of ENSO and “El Niño–like” conditions are likely during the 21st century. Increasing “El Niño–like” conditions have also been observed in other 21st century projections (Meehl et al. 2006) and in recent observations (Vecchi et al. 2006; Power and Smith 2007).

The multi–station ensemble (Figure 3.4) does show the long–term changes in the MSLP are now equal to or greater than the MSLP interannual variability associated with ENSO and other factors, and is now likely to be exacerbating the drought conditions in Queensland and other parts of eastern Australia. This study shows that the likely influence of the SAM extends well beyond the southern regions of Australia into the Queensland region. Interactions and teleconnections between the tropical ENSO and extratropical SAM are just starting to be recognised (L'Heureux and Thompson 2006; Previdi and Liepert 2007; Shi 2008). Recently, rainfall extremes in New Zealand have attributed to dominantly two atmospheric modes of variability: SAM and ENSO, which show a latitudinal gradation in influence of the respective phenomena (Ummenhofer and England 2007). Such a gradient is likely to exist over the eastern Australian region with the impacts of SAM extending further northwards than previously recognised, especially in the austral winter.

Although the increasing MSLP over most of NEA and Queensland during the second half of the 20th century are lower than in some other regions in the subtropics and mid–latitudes, it is likely they represent major changes in the global circulation related to the SAM and changes in the subtropical ridge. These increases in the MSLP are likely to be reducing the number or type of rain producing synoptic events and/or the intensity of rainfall associated with these features in the NEA region. Hence, changes to particular synoptic features may hold the key to the lower rainfall in this region. The SAM has already been shown to have reduced the number of storm tracks over southern Australian and rain producing systems (Cai and Cowan 2006; Gillett et al. 2006; Hope et al. 2006). One synoptic event which has reduced in number over the SE QLD region over the last few decades are tropical cyclones, which are important contributors to rainfall (Lough 1993). A small decline in the numbers of tropical cyclones in the Coral Sea was noted by Kuleshov et al. (2008) and landfall numbers by Dare and Davidson (2004). Tropical cyclones are highly sensitive to changes in the MSLP, the Southern Oscillation Index (Broadbridge and

Hanstrum 1998), wind shear (Nyberg et al. 2007), sea surface temperatures (Saunders and Lea 2008) and other factors. However, since tropical cyclones are relatively rare in the SE QLD region, they cannot account for all the long–term rainfall decline, including the austral winter when they are absent. Changes in the frequency and activity of cloud bands, easterly coast troughs and east coast lows are examples of important synoptic systems which maybe important in explaining the some of the rainfall decline. Further studies on these synoptic events will be required to substantiate if these factors (or others) are directly related to the rainfall decline over SE QLD and other regions of NEA.

In the next chapter, an analysis of the land cover changes over the SE QLD region during the second half of the 20^{th} century are investigated using a regional GCM from the Commonwealth Scientific and Industrial Research Organisation (CSIRO). This chapter will consider local factors which may have contributed to the rainfall decline over much of Queensland since the 1970s.

CHAPTER 5 : LAND COVER AND RAINFALL CHANGES OVER SOUTHEAST QUEENSLAND

5.1 INTRODUCTION

The relationship between global land cover and climate has been well documented in recent years (Gibbard et al. 2005; Werth and Avissar 2005; Liu et al. 2006), with land surface schemes now an important component of climate models (Pitman 2003) and simulating future climate (Zhao and Pitman 2002; Feddema et al. 2005; Davin et al. 2007; Notaro et al. 2007). Recent changes to the land cover and climate from many regions, such as the Sahel (Taylor et al. 2002; Los et al. 2006), the Amazon and Congo Basins (Hoffmann et al. 2003) and North America (Wang et al. 2006a; Wang et al. 2006b), indicates the regional climate is sensitive to changes in the land cover. This 'climate sensitivity' to land cover changes (LCC) occurs on many scales, from microclimates and the modifying of the growing–season of crops (Mahmood et al. 2004), to regional scales and atmosphere–land surface interactions, such as soil moisture and climate variability over Australia (Timbal et al. 2002) and global changes, such as the monsoon and soil moisture feedbacks (Douville et al. 2001; Douville 2002). The total global LCC due to human development is estimated to range from one–third to one–half of the planets surface (Pielke 2005) and these changes are likely to continue well into the future. Therefore, it is likely that humans have already significantly modified the world's climate due to LCC in many regions, irrespective of other factors, such as increasing greenhouse gases and ozone depletion.

Changes in the climate and weather have been recently dramatically represented during the European heatwave in 2003 which killed over 35,000 people when temperatures measured over cropped land were much higher (up to 15.4ºC) than over forested lands (Zaitchik et al. 2006). Land use and LCC modify the near–surface atmospheric conditions (Mahmood et al. 2004), with anthropogenic factors such as desertification, reforestation and deforestation, urbanisation and major river, lake and dam engineering having all played a role (McGuffie and Henderson-Sellers 2005). Land–atmospheric feedbacks include soil–moisture capacities, surface roughness, temperature, evaporation, albedo, latent heat and sensible heat fluxes, the evaporation–precipitation relationship (often referred to as the recycling ratio) and other factors. The importance of global LCC in simulating future climates and climate change has been describe by Feddema et al. (2005) and concludes that the inclusion of land–cover forcing (anthropogenic impacts) improves the quality of regional climate assessments in the IPCC scenarios. Recent analysis of the hydrological cycle in Amazonia from modelling of complete deforestation of the region produces a less vigorous hydrological cycle (Cassiano et al. 2007). Strong climate–biosphere feedbacks have also been well demonstrated in semi arid and arid regions (Lotsch et al. 2003; Kanae et al. 2006).

In Australia, LCC and climate in the southwest of Western Australia have been well studied in the last decade or so (Timbal et al. 2002; Pitman et al. 2004; Timbal 2004; Timbal and Arblaster 2006; Timbal et al. 2006), where a rapid decline in rainfall during the second half of the 20^{th} century has occurred (Smith et al. 2000; Smith 2004; Li, Y. et al. 2005). Such LCC have been recently described as enhancing the drying of southwestern Western Australia, where vegetation cover and land clearing has affected modelled rainfall (Pitman et al. 2004; Timbal and Arblaster 2006). Energy fluxes and cumulus cloudiness have been studied from two contrasting land covers (agricultural versus native perennial vegetation). The higher latent heat fluxes over native perennial vegetation have led to enhanced cumulus development in the austral summer (Ray et al. 2003). Using high–resolution mesoscale modelling to simulate temperature and rainfall, up to 50% of the observed warming in southwestern Western Australia was identified from LCC (Pitman et al. 2004).

In Queensland, LCC have been described from a number of regions. An important factor controlling the catchment–scale water balance is the seasonal variation of climate, which is highly sensitive to soil moisture capacity (Potter et al. 2005). Studies in the Comet region of central Queensland on catchment hydrology in a natural forest cover dominated by Brigalow (*Acacia harpophylla*), indicate land clearing has generated in increase in runoff by around 40% (Siriwardena et al. 2005). Runoff and river flows are a major factor in determining the size of the prawn catch in the Gulf of Carpentaria, where increased rainfall from monsoonal rains increases the size of the banana prawn fishery (Catchpole and Auliciems 1999). Leaf canopy has major impacts on evaporation and the contribution to runoff and the surface hydrology. Water balance studies in the tropical rainforests in northern Queensland show up to 30% of the rainfall is intercepted by forest canopy and lost to evaporation (Wallace and McJannet 2006). In a varying environment, vegetation plays an active role in determining the observed vegetation–rainfall distributions (Zeng et al. 2002).

These studies from Australia and overseas, show the strong links between land cover and climate and this chapter is designed to investigate some of the 20th century changes in the land cover over the SE QLD region, where recent rainfall declines have placed unprecedented strains on water resources (Chapter Two). In this study, rainfall changes related to the albedo and vegetation in a regional climate model are investigated. The conformal–cubic atmospheric model (CCAM), the Dean–Graetz vegetation scheme, the 'Natural' and 'Present' land cover over the SE QLD region and the set of experiments proposed using the CCAM model are described in section 5.2. Results from the CCAM experiments are described in section 5.3 and a discussion is provided in section 5.4.

5.2 DATA AND METHODOLOGY

5.2.1 Conformal–Cubic Atmospheric Model (CCAM)

This study has selected the conformal–cubic atmospheric model (CCAM) to investigate regional LCC over SE QLD from a number of other models for several reasons. The model has been used for over 10 years at the Commonwealth Scientific and Industrial Research Organisation (CSIRO) at Aspendale (Melbourne), Australia and has been used for eight day forecasting over parts of Australia since 1997. It currently provides this service at www.csiro.au/services/pps69.htpp. A very high resolution CCAM model (~1 km) has been recently used by the Swiss syndicate's 'Alinghi' sailing team at the Americas Cup in Valencia (Spain) and was pivotal in their victory in 2003 against Team New Zealand in the Hauraki Gulf in Auckland (http://www.csiro.au/files/mediarelease/mr2003/Alinghi.htm). The CCAM model has been used in a number of studies in Australia, such as the Fitzroy and Rockhampton Basins (McGregor et al. 2006), the Murray–Darling Basin and eastern Australia, and overseas in Fiji (Lal et al. 2007), the East Asian and Australian monsoon (McGregor and Nguyen 2003) and other tropical simulations (McGregor et al. 2008). Regional climate modelling with a resolution up to 8 km has been able to simulate many aspects of 20th century rainfall and temperature climatology.

The CCAM model includes a comprehensive set of physical parameterizations similar to those of the CSIRO–MK3 GCMs (McGregor et al. 2008) and is formulated on a quasi–uniform grid, which can be readily moved and centred over a particular region and downscaled for regional modelling analysis to high resolutions (< 10 km). There are 18 vertical levels in the atmosphere that can be used to simulate climate for both 20th and 21st century climate. The high resolution model and adaptive grid enables many important boundary layer processes to be investigated and means for example, the effects of topography, land cover and vegetation, urban development and soil moisture profiles can be analysed in far greater detail that would other wise be possible in low resolution (~2º or about 222 km) GCMs.

There are ~150 named variables in the CCAM model output produced from standard fields, boundary conditions or derived fields, most of which are standard in many GCMs. Some of the standard variables (including boundary conditions) are: meridional and zonal winds, latent and sensible heat fluxes, surface pressure, temperature (maximum and minimum), albedo, land height, vegetation type, surface roughness, potential evaporation, sea surface temperature and relative humidity. There are six soil moisture and temperature levels and one field for soil type with

~12 divisions. The derived fields are calculated from one or more variables in the model and some of these include the total cloud fraction, low, middle and high cloud fractions, frozen and liquid water, precipitation including convective precipitation, water mixing ratio, average cloud base and cloud top, divergence, surface pressure tendency, wetness fractions in six soil layers, runoff, geopotential height and various short and long wave parameters at the surface and top of the atmosphere. In addition, there are various output fields which are calculated at three hourly intervals including the zonal and meridional winds, screen temperature, relative humidity and precipitation. The main output fields used in this study are precipitation, minimum and maximum temperature, albedo, vegetation type and land surface height.

The area for the regional modelling selected for this research covers the SE QLD region and extends from 23.5ºS to 32ºS and 145ºE to 154ºE (~800 x 800 km) on a grid spacing of 19 km using a C48 grid (Figure 5.1). Although this may cause some spurious 'edge effects', with the eastern boundary of the grid capturing only part of the East Australian Current, the main focus of the study is on albedo and vegetation changes on land.

5.2.2 Land Cover Scheme

The CCAM model has two land cover scheme alternatives: the 12 vegetation types of the Simple Biosphere Model (SiB) (Sellers et al. 1986) or the 31 Dean–Graetz's vegetation types (AUSLIG 1990). This study has selected the Dean–Graetz's vegetation scheme because it has a larger range of Australian vegetation types and was designed in Australia (Table 5.1). Each vegetation type has the following

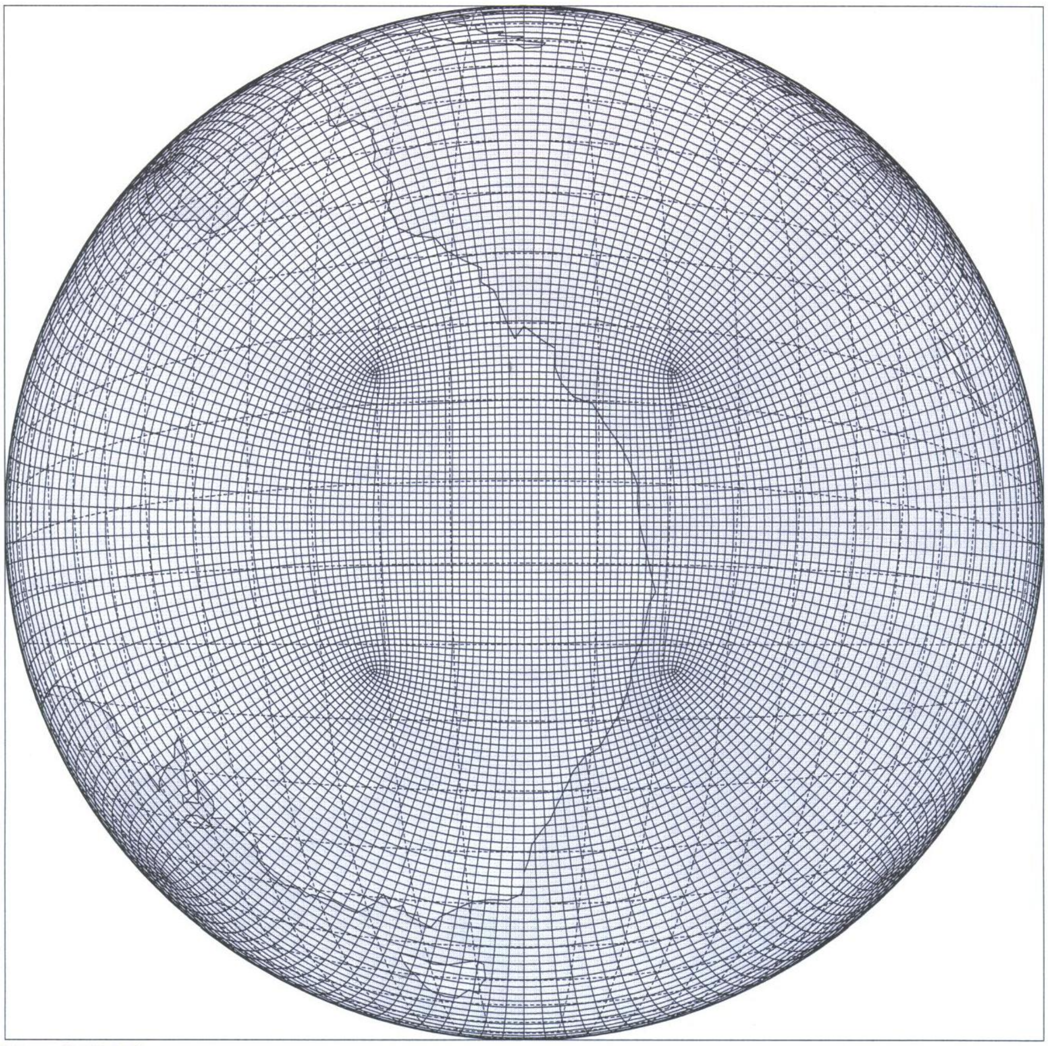

Figure 5.1 Conformal–cubic atmospheric model grid (C48) centred over SE QLD region. The grid has a 19 sq km resolution and the four vertices enclose the region from about Longreach in the northwest, to the area east of Rockhampton, south to east of Port Macquarie and then west to Cobar and includes the Brisbane region.

attributes in the model: height of vegetation cover (HC:CM), percentage of foliage cover (PFC) and the vegetation leaf area index (VEGLAI). Although in the CCAM model the land cover representation is essentially static, the vegetation type or albedo values can be altered to desired values, prior to compiling the model. The different vegetation types influence changes in the stomatal resistance, surface roughness, surface hydrology and surface albedo (Kowalczyk et al. 1991). Therefore, changes in the vegetation and albedo values should produce corresponding changes in the

Table 5.1 List of the 31 land cover types in the Dean–Graetz vegetation scheme.

Name	Code	HC:CM	PFC:%	VEGLAI
Ocean	0	0	0	0
Tall dense forest	1	4200	100	4.8
Tall mid-dense forest	2	3650	85	6.3
Dense forest	3	2500	85	5.0
Mid-dense forest	4	1700	50	3.75
Sparse forest (woodland)	5	1200	20	2.78
Very sparse forest (woodland)	6	1000	5	2.5
Low dense forest	7	900	85	3.9
Low mid–dense forest	8	700	50	2.77
Low sparse forest (woodland)	9	550	20	2.04
Tall mid-dense shrublands (scrub)	10	300	50	2.6
Tall sparse shrubland	11	250	20	1.69
Tall very sparse shrubland	12	200	5	1.9
Low mid-dense shrubland	13	100	50	1.37
Low sparse shrubland	14	60	20	1.5
Low very sparse shrubland	15	50	5	1.21
Sparse hummock grassland	16	50	20	1.58
Very sparse hummock grassland	17	45	5	1.41
Dense tussock grassland	18	75	85	2.3
Mid-dense tussock grassland	19	60	50	1.2
Sparse tussock grassland	20	45	20	1.71
Very sparse tussock grassland	21	40	5	1.21
Dense pasture/herbfield (perennial)	22	60	85	2.3
Dense pasture/herbfield (seasonal)	23	60	85	2.3
Mid-dense pasture/herbfield (perennial)	24	45	50	1.2
Mid-dense pasture/herbfield (seasonal)	25	45	50	1.2
Sparse herbfield	26	35	20	1.87
Very sparse herbfield	27	30	5	1.0
Littoral (coastal fringe)	28	250	50	3.0
Permanent lake	29	0	0	0
Ephemeral lake	30	0	0	0
Urban	31	0	0	0

Notes: **1**. The ‘code’ number is the same number used in CCAM by CSIRO;
2. The ‘HC:CM’ abbreviation is the ‘height of cover’ in centimetres;
3. The ‘PFC:%’ abbreviation is the ‘percentage foliage cover’ over the surface and
4. The ‘VEGLAI’ abbreviation is the ‘vegetation leaf area index.’

modelled climate (including rainfall and temperature) output from the CCAM model over short or long time periods, which can be readily analysed on seasonal or annual time scales. The Dean–Graetz's vegetation scheme was developed in Australia in the

1990s by Dean–Graetz from the CSIRO and many other co–workers (AUSLIG 1990). It is the probably the most comprehensive compilation of land cover and vegetation types completed in Australia. A summary of the Dean–Graetz vegetation scheme and the land cover types used in the CCAM model are shown in Table 5.1.

The Dean–Graetz vegetation scheme currently has two main vegetation descriptions available over Australia. A land cover known as the ‘Natural Vegetation’ scheme, describing the floristic types when European settlement began around ~1788, and the ‘Present Vegetation’ scheme, which represents the more recent land cover in the mid–1980s (AUSLIG 1990). The ‘Natural Vegetation’ and ‘Present Vegetation’ schemes over the SE QLD region are shown in Figures 5.2 and 5.3 respectively.

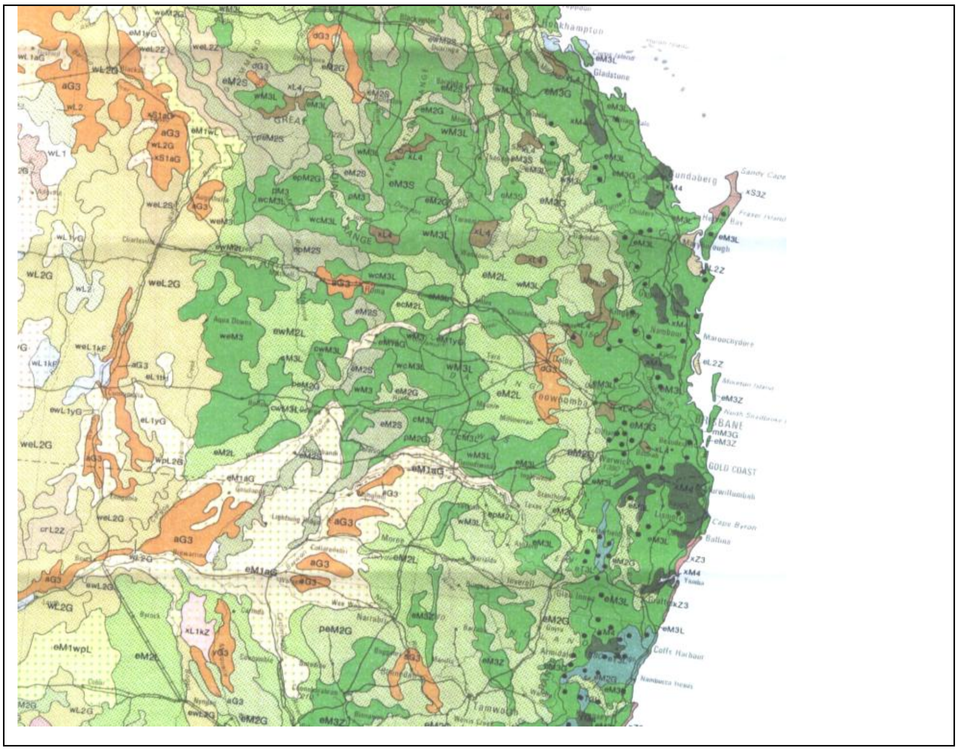

Figure 5.2 The ‘Natural Vegetation’ land cover over the SE QLD region at ~1788, approximately when European settlement began, with forests shown in shades of green and herbaceous plants and grasslands in shades of yellow and brown. The shades of light and medium blue stand for littoral complex and tall vegetation (>30 m in height) respectively.

The ‘Natural Vegetation’ land cover scheme representing the land cover for ~1788, shows much of the eastern half of the SE QLD region, east of ~150º, is covered by medium to tall trees and west of ~150º, dominated by low to medium trees or herbaceous plants and grasslands (Figure 5.2). It is however, not currently available to be incorporated directly into the CCAM model. In the ‘Present Vegetation’ scheme, which represents the land cover in the mid–1980s, much of the medium to tall vegetation east of ~150º has been removed and replaced by grasslands or low trees, and west of ~150º, is now dominated by low trees, herbaceous plants, grasslands and agriculture. The white area with red triangles in the eastern and central region of the map (Table 5.1–code=28, littoral) is an error and has been

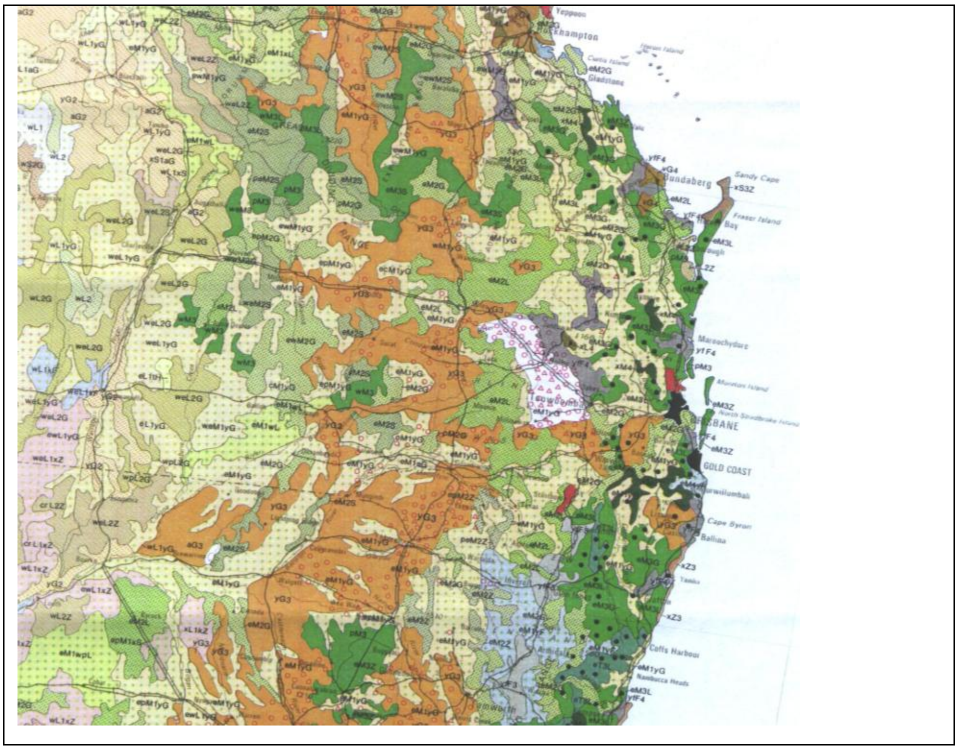

Figure 5.3 The ‘Present Vegetation’ land cover over the SE QLD region based on the mid–1980s showing extensive clearing of the forest cover and replacement by herbaceous plants and grasslands in shades of brown and grey respectively. The shades of light and medium blue stand for littoral complex and tall vegetation (>30 m in height) respectively.

changed to code 24 (mid– dense pasture; perennial) in this study. This small region was changed with an ‘nspecial’ code adjustment in one of the scripts prior to running the downscaled experiments over SE QLD.

5.2.3 CCAM Modelling over Southeast Queensland

The region selected for the high resolution regional modelling for this research, covers the SE QLD region and northern NSW (Figure 5.1). It extends from near Longreach (23.5ºS, 145ºE), southward to near Cobar (32ºS, 145ºE), eastward to near Port Macquarie (32ºS, 154ºE) and northward to near the area east of Rockhampton (23.5º, 145ºE), covering a region of ~800 x 800 km on a grid spacing of 19 km. This region centred on SE QLD, has had large areas cleared of the native vegetation and has experienced significant rainfall reductions during the second half of the 20th century (Chapters One and Two). It also has the largest population and population growth in Queensland, with growing water demands on limited water resources.

The time interval from 1971–2000 was selected to examine land cover changes in the CCAM model over SE QLD based on the following rationale. The NCEP reanalysis data is of higher quality, as described by Marshall (2003) from ~1970, and hence the ‘nudging’ of the regional model will be more accurately constrained by global climate. It is also the period when much of the land clearing and LCC occurred in Queensland and SE QLD for extensive agricultural development. It also represents a period of extreme decadal variability in Australian and Queensland rainfall, with one of the wettest decades occurring in the 1970s, followed by the severe 1982–83 drought and the long, persistent droughts in the early 1990s, providing interesting contrasts and challenges for the CCAM model. This study using the CCAM model is motivated by the continued rainfall declines over the SE QLD region. Although a number of aspects in the CCAM model relating to land cover and LCC could have been investigated, such as the soil moisture, soil types, surface roughness and leaf area index, this was beyond the scope of this study, and only an analysis on the albedo and vegetation has been completed here.

A total of six simulations (or experiments) (MR1–MR6) were completed, with one simulation over the Australia region and five downscaled simulations over the SE QLD region during the period 1971–2000 (Table 5.2). However, due to spurious rainfall values obtained from the two vegetation simulations, no results are shown from these two experiments (MR5–MR6). The first simulation (MR1) assimilates the NCEP data from over the Australian region into a 60 km resolution run. Sea surface temperatures and weak “global” wind nudging from above 500 hPa are incorporated into the model and the Australian land cover is represented by a coarse Dean–Graetz's ‘Present Vegetation’ scheme. In the second simulation (MR2), a downscaled version of CCAM using a 19 km resolution is produced over SE QLD (Figure 5.1) using a finer (19km) ‘Present Vegetation’ scheme. In this simulation, the ‘Present Vegetation’ scheme is composed of heavily fragmented land cover and albedo values (Figure 5.3). The two simulations (MR3–MR4) are identical to MR2, but have new albedo values assigned east and west of 152ºE (Table 5.2). Hence, any changes in the rainfall and temperature should be solely due to the changes made to the albedo values. All simulations include two years of spin up (1969–1970) and the daily model outputs (~1Gb) are averaged into monthly files (~13 Mb) for subsequent rainfall, maximum and minimum temperature analyses. All results from the

Table 5.2 Land cover simulations using CCAM over the SE QLD region for the period 1971–2000.

Model Run Number	Type of Simulation	Resolution (km)	Vegetation Status over SE QLD (West)/East)		Albedo SE QLD (West)/East)		Longitude Bisector	Motivation
MR1	**NCEP**	**60**	**Present Vegetation** (mid 1980s)		N/A		N/A	NCEP data assimilation
MR2	**Control**	**19**	**Present Vegetation** (mid 1980s)		**Set by Present Vegetation**		N/A	Baseline to examine rainfall and temperature changes
MR3	**Albedo**	**19**	**Present Vegetation** (mid 1980s)		0.12	0.06	152ºE	Land cover same as Model No.2.
MR4	**Albedo**	**19**	**Present Vegetation** (mid 1980s)		0.40	0.06	152ºE	Land cover same as Model No.2.
MR5	**Vegetation**	**19**	Mid-dense forest (Code 4)	Tall mid-dense forest (Code 2)	No change		152ºE	Land cover similar to 'Natural Vegetation' land cover ~1788.
MR6	**Vegetation**	**19**	Pastoral (Code 24)	Tall mid-dense forest (Code 2)	No change		152ºE	Land cover similar to 'Present Vegetation' land cover ~1788.

Note 1. For the Vegetation and albedo over SE QLD, the west and east sectors are separated by the longitude 152ºE. Results from MR5 and MR6 are not shown.

simulations are compared to the BoM observations for the same period. The time step used in each of the model runs for the six models (MR1–MR6) is 12 minutes.

The albedo values used in the CCAM model are altered using an 'nspecial'code which is written into the model script and compiled prior to running the model. In MR3 and MR4, the albedo values were altered east and west of the arbitrary north–south line (152ºE). The average albedo from the Dean–Graetz's vegetation types west of 152ºE, varies from 0.20–0.30 and east of about the 152ºE, varies from 0.12–0.13 in the 'Present Vegetation' scheme. Hence, the taller and thicker forested areas (darker) have a lower albedo and the lower forests and mid–dense pastoral (lighter) have a higher albedo. In MR3, the albedo was changed to 0.12 and 0.06 west and east of the north–south line at 152ºE, respectively. This reduces the contrast and lowers the albedo compared to MR2. In MR4, the albedo is changed to 0.40 west of the north–south line at 152ºE, a much higher value than 0.12 in MR3. This provides a large contrast in the albedo values east and west of the north–south line at 152ºE, compared to both the MR2 and MR3 runs. The high albedo (0.40) is analogous to the highest albedo values (~0.40) recorded over the central parts of Australia from a global dataset compilation used in France (Masson et al. 2003). Although the albedo has been changed into rigid block values east and west of 152ºE, the vegetation types remain fragmented, the same as in MR2. A similar methodology was applied to the vegetation simulations; however, as the results were inconclusive, no detail description of these is given here.

Annual rainfall across the region varies from over 1000mm east of the Great Divide, to about 500 mm and less in the Charleville region further west. Further climate data is available in Chapter One. The rainfall isohyets for the SE QLD region trend mostly north–south, parallel to the coast, with only minor deviations due to local changes in topography and other factors. Much of the rainfall in the SE QLD region is developed in a moist easterly flow with a summer maximum in rainfall, and using an arbitrary a north–south arbitrary boundary (152ºE) for the changes in the land cover or albedo is similar to the 'natural architecture' in the region, such as the Great Dividing Range, which controls the natural forest boundaries and catchments.

5.3 RESULTS

5.3.1 CCAM 60 km Model (MR1)

The results of the annual maximum and minimum temperature (ºC) and rainfall (mm year^{-1}) from the 60 km CCAM model simulation (MR1) and the BoM observations (0.25º grid) over Australia and the period 1971–2000 are shown in Figure 5.4 (a–f).

The contoured annual maximum temperatures (Figure 5.4a) over Australia are very similar to the BoM observations (Figure 5.4b), with similar regional patterns and spacing of the contour intervals. The highest annual maximum temperatures in the CCAM model occurs near Broome and Kununurra (>35ºC), compared to ~34ºC near Port Hedland and Kununurra in the BoM observations. The lowest annual maximum temperatures in the CCAM model occur over the southeast of the continent (Alpine areas) and Tasmania, with a temperature of ~17ºC and ~14ºC respectively. The lowest annual maximum temperatures from the BoM observations are in the same regions, with a temperature of ~16ºC and ~13ºC respectively.

The contoured annual minimum temperatures (Figure 5.4c) over Australia are also similar to the BoM observations (Figure 5.4d), with comparable regional patterns in the contour intervals. The highest annual minimum temperature in the CCAM model occurs over northern and coastal areas of Australia from about Port Hedland to Cooktown (~22–23ºC). In the BoM observations, the highest annual minimum temperatures are more limited in extent to the northern and coastal areas of the Northern Territory and the northern half of the Cape York Peninsula. The lowest annual minimum temperatures in the CCAM model occur over southeast parts of Australia and Tasmania (similar to the lowest maximum temperatures) with temperatures of ~6–8ºC, similar to the BoM observations.

The contoured annual rainfall over Australia (Figure 5.4e) is also similar to the rainfall distribution shown in the BoM observations (Figure 5.4f), with comparable regional patterns in the contours. The highest annual rainfall (>600 mm $year^{-1}$) in the CCAM model occurs over southwestern Western Australia, the Kimberley, the

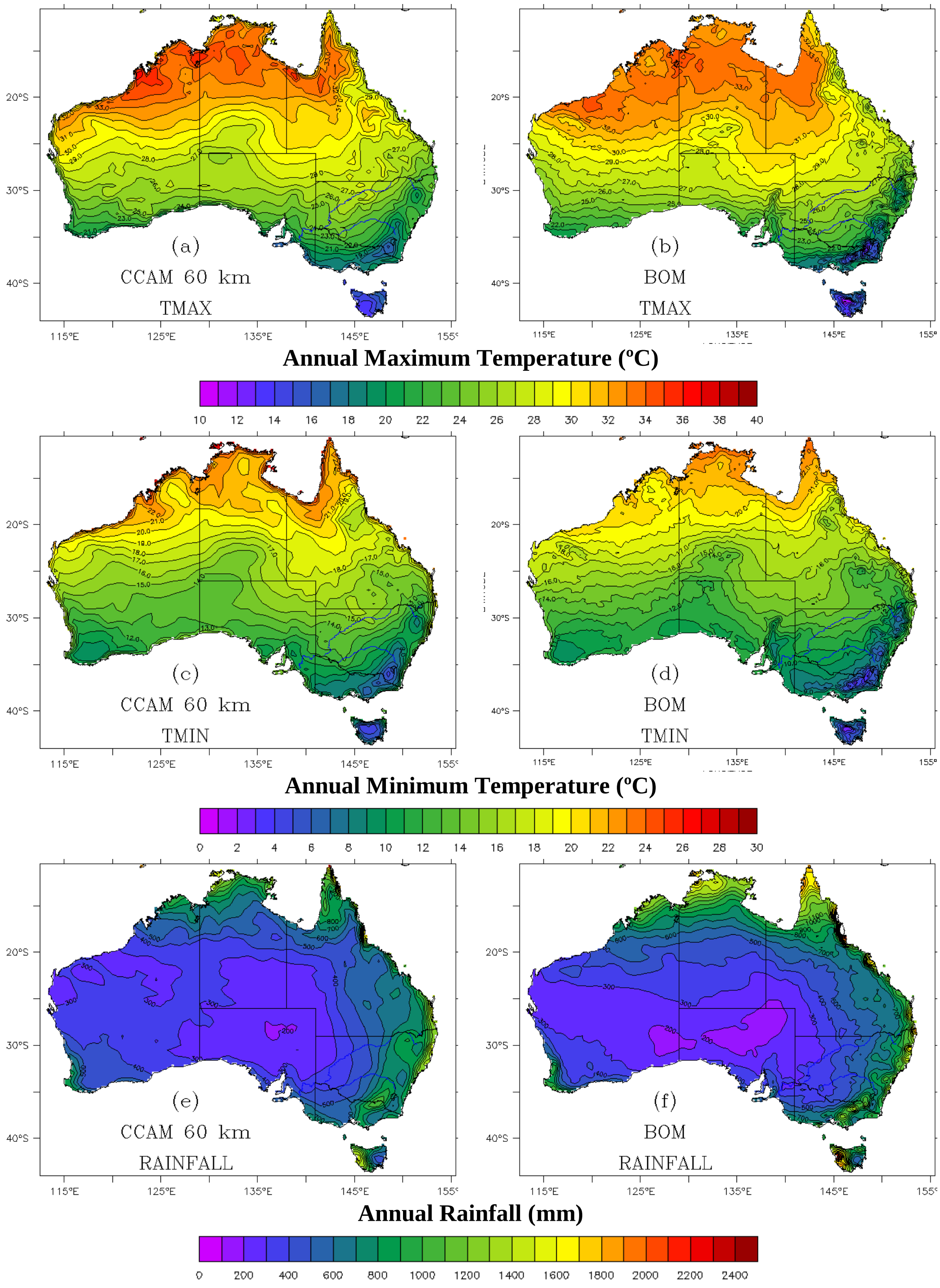

Figure 5.4 (a–f) Contoured annual maximum and minimum temperatures (ºC) and rainfall (mm year^{-1}) from the 60 km CCAM model simulation **MR1** (a,c,e) and the BoM observations (b,d,f) over Australia and the period 1971–2000. Temperature and rainfall contours are in intervals of 1ºC and 100 mm respectively.

Arnhem Land regions, the Cape York Peninsula and the east coast of Queensland, NSW, Victoria and Tasmania, similar to the BoM observations. However, the tropical regions inland from the Cairns region and southwest and west of Burketown show significantly lower rainfall (>200 mm year^{-1}) than the BoM observations. The lowest annual rainfall (<200 mm year^{-1}) in the CCAM model occurs over central Australia, near Oodnadatta and covers a much smaller region than in the BOM observations. Generally the CCAM model has slightly underestimated the rainfall in higher rainfall regions, such as coastal and tropical areas, and slightly overestimated rainfall in the drier regions of inland Australia, which is similar to many of the IPCC–AR4 models discussed in Chapter Two (section 2.3.1).

5.3.2 CCAM 19 km Model (MR2) using the 'Present Vegetation' Scheme

Results from the annual maximum and minimum temperature (ºC), rainfall (mm year^{-1}) and differences (CCAM simulation minus the BoM observations) from the 19 km CCAM model simulation (MR2) using the Dean–Graetz's 'Present Vegetation' scheme over SE QLD and the period 1971–2000, are shown in Figure 5.5 (a–i). The BoM observations are gridded at a spacing of ~28 km (Figure 5.5 (b, e, h)) compared to the CCAM model of 19 km, hence there is more detail shown in the CCAM plots.

The contoured annual maximum temperatures (Figure 5.5a) over the SE QLD region are similar to the BoM observations (Figure 5.5b), with the warmest temperatures over the northern and northwest regions and the coolest temperatures over eastern and southeast regions. The highest maximum temperatures in the CCAM model are ~27–28ºC versus ~28–29ºC from the BoM observations over northwestern regions. The lowest maximum temperatures in the CCAM model are 17–18ºC versus ~19–20ºC from the BoM observations over the Northern Tablelands of NSW. The differences between the maximum temperatures in the CCAM model and the BoM observations are shown in Figure 5.5c. This shows the model simulates slightly lower maximum temperatures (~1–2ºC in blue) than the BoM observations over most of the region, except for slightly higher maximum temperatures (0.5–1.0ºC in red) over small areas far northern parts, the southwest and the coastal plains of NSW.

The contoured annual minimum temperatures (Figure 5.5d) over the SE QLD region are very similar to the BoM observations (Figure 5.5e), with the warmest minimum temperatures over northern and western regions and coastal areas and the coldest minimum temperatures over southeast regions, especially over the high altitude areas of the Northern Tablelands of NSW. The highest minimum temperatures in the model are similar to the BoM observations of ~15–16ºC over northwestern, northern and northeast coastal regions. The lowest maximum temperatures are also similar to the BoM observations, ranging from 7–8ºC over the Northern Tablelands of NSW. The differences between the minimum temperatures in the CCAM model and the BoM observations are shown in Figure 5.5f. This shows the model simulates slightly higher minimum temperatures (0.5–1.5ºC) over most of the region compared to the BoM observations. Small negative anomalies around the Brisbane and coastal areas north to Hervey Bay, indicate slightly lower minimum temperatures in the model.

The contoured annual rainfall from the CCAM model and the BoM observations are shown in Figure 5.5g and Figure 5.5h respectively. The rainfall patterns are generally very similar between the model and the BoM observations, with the highest rainfall occurring along the coastal regions and lowest rainfall over western inland areas. The 1000 mm contour line in the CCAM model and the BoM observations is generally

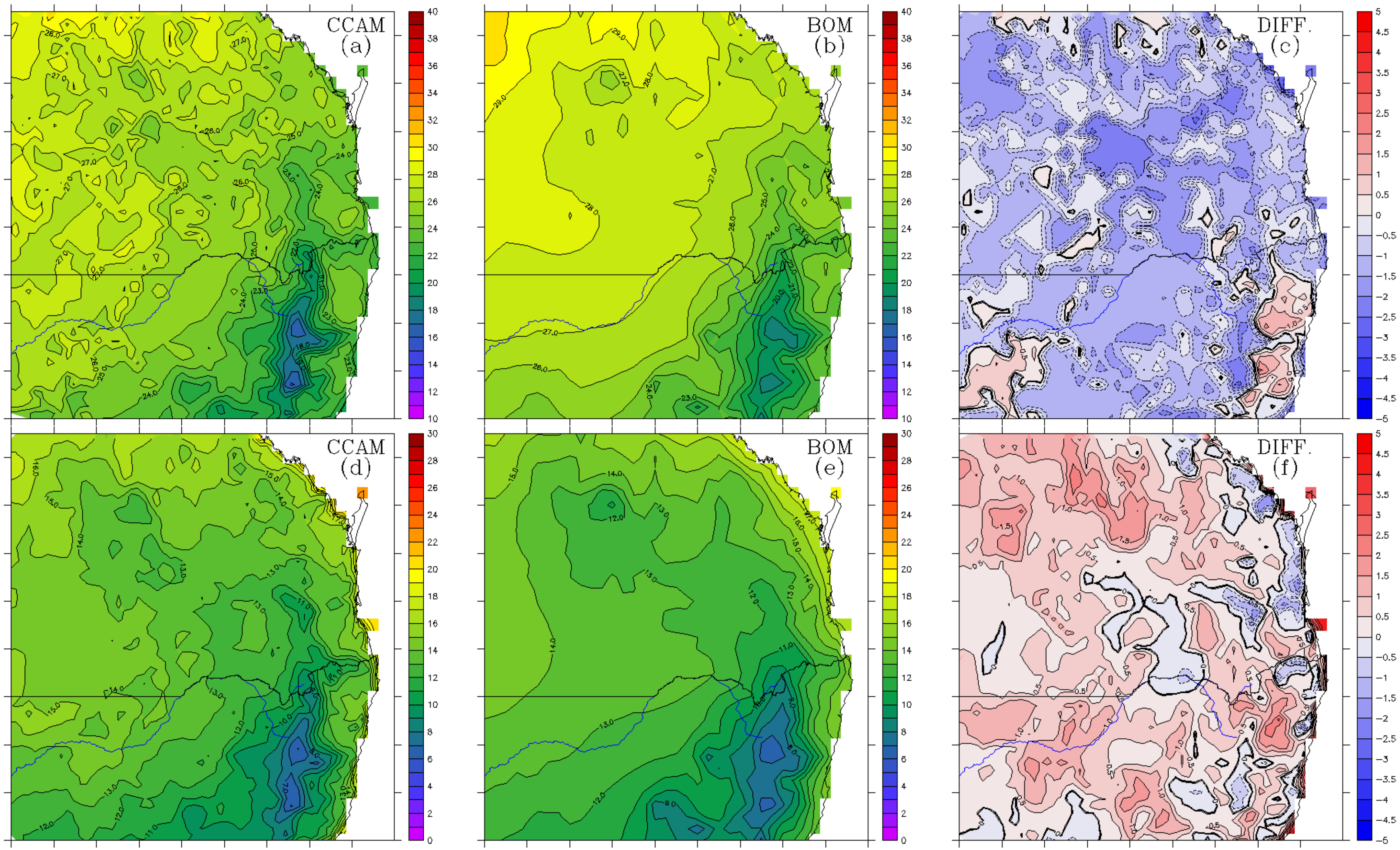
CCAM
(a)
BOM
(b)
DIFF.
(c)
CCAM
(d)
BOM
(e)
DIFF.
(f)

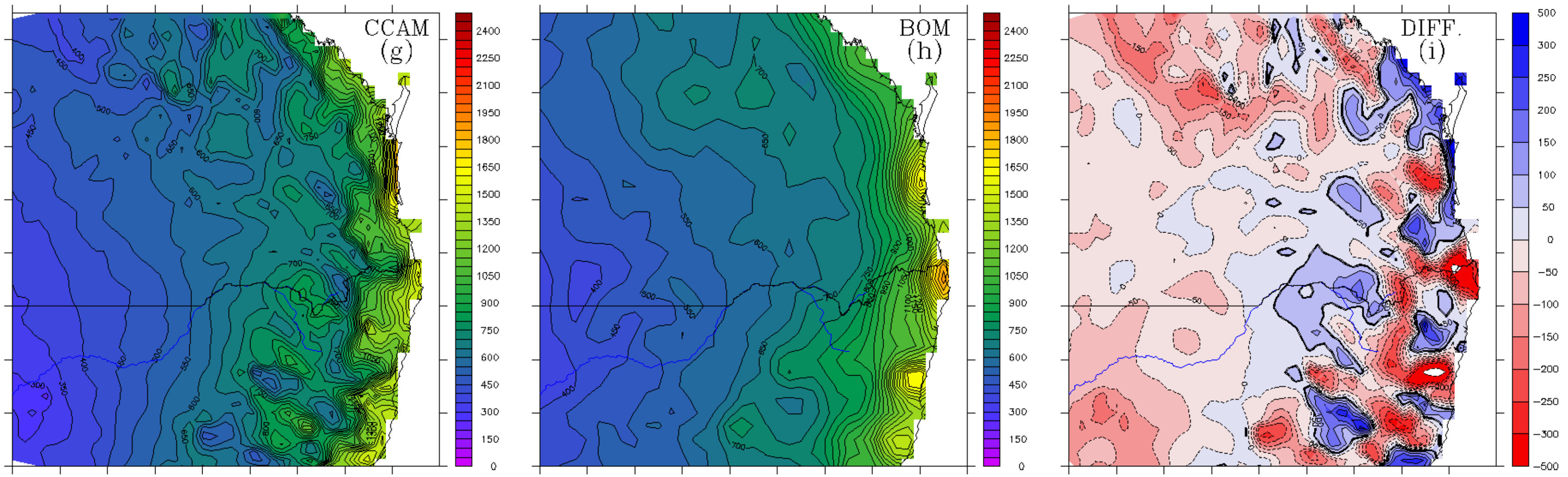

Figure 5.5 (a–f (previous page) and g–i (above)) Contoured annual maximum and minimum temperatures (ºC) and rainfall (mm year^{-1}) from the 19 km CCAM model simulation **MR2** (a,d,g), the BoM observations (b,e,h) and Differences (c,f,i) over SE QLD and the period 1971–2000. Temperature and rainfall contours are in intervals of 1ºC and 100 mm respectively. Difference contours intervals are 0.5ºC and 50 mm for temperature and rainfall respectively.

located about 100 km inland, although in the CCAM model, its is much more irregular, compared to the BoM observations, where it forms an almost parallel line to the east coast. The highest rainfall in the CCAM model is over 1500 mm over the Sunshine Coast, north of Brisbane and over ~1200 mm along the rest of the coast. In the BoM observations, the highest rainfall is just south of the Gold Coast with over 1800 mm. Three of the four major zones with the highest rainfall on the east coast also occur in the model, albeit with lower rainfall values. The high rainfall zone near Coffs Harbour is not well simulated in the CCAM model. The lowest rainfall is ~300 mm over the far southwest area near Bourke in the CCAM model and ~400 mm from the BoM observations. Isohyets generally trend north–south west of about 150ºE in the model and west of 152ºE in observations. The differences between the annual rainfall in the CCAM model and the BoM observations are shown in Figure 5.5i. Over most inland regions, west of ~150ºE, the model slightly underestimates rainfall (0–50 mm), with higher values (50–100 mm) over the southwest and northern inland regions. Over coastal regions, the rainfall anomalies are 'mixed', with either too much or too little rainfall. For example, the model simulates too much rainfall over the Hervey Bay region and too little rainfall over the Gold Coast region. The model simulates slightly higher rainfall (0–100 mm) over the region west of Toowoomba and the area south towards Moree.

In summary, the control run (MR2) used the 'Present Vegetation' scheme which produced slightly cooler maximum temperatures and slightly warmer minimum temperatures compared to the BoM observations. Rainfall over inland areas was generally lower than in the BoM observations but over coastal regions, produced much more variable rainfall, with higher or lower values.

5.3.3 Albedo Changes in the 19 km Models (MR3–MR4)

5.3.3.1 MR3 Model

Results from the annual maximum and minimum temperature (ºC), rainfall (mm year^{-1}) and differences for the period 1971–2000 over the SE QLD region are shown in Figure 5.6 (a–i) for MR3. The albedo in MR3 has been changed to 0.12 and 0.06 west and east of 152ºE respectively. The BoM observations are shown in the central plots in Figure 5.6 (b, e, h).

The contoured annual maximum temperatures (Figure 5.6a) over the SE QLD region are similar to the BoM observations (Figure 5.6b), with the warmest temperatures in the CCAM model over the northern and northwest regions (~26–28ºC) and the coolest temperatures (~17–18ºC) located over Northern Tablelands of NSW. The differences in the annual maximum temperatures between the CCAM model and the BoM observations are shown in Figure 5.6c. This shows slightly cooler maximum temperatures (-0.5–1.5ºC) over most of the region, with a few small areas with slightly warmer temperatures (0.5–1.5ºC) than in the BoM observations. This is similar to the control run MR2 and Figure 5.5c.

The contoured annual minimum temperatures (Figure 5.6d) over the SE QLD region are similar to the BoM observations (Figure 5.6e), with the warmest minimum temperatures (~14–16ºC) over northern and western regions and coastal areas and the coolest minimum temperatures (~7–8ºC) over southeast regions, especially over the high altitude areas of the Northern Tablelands of NSW. The differences between the

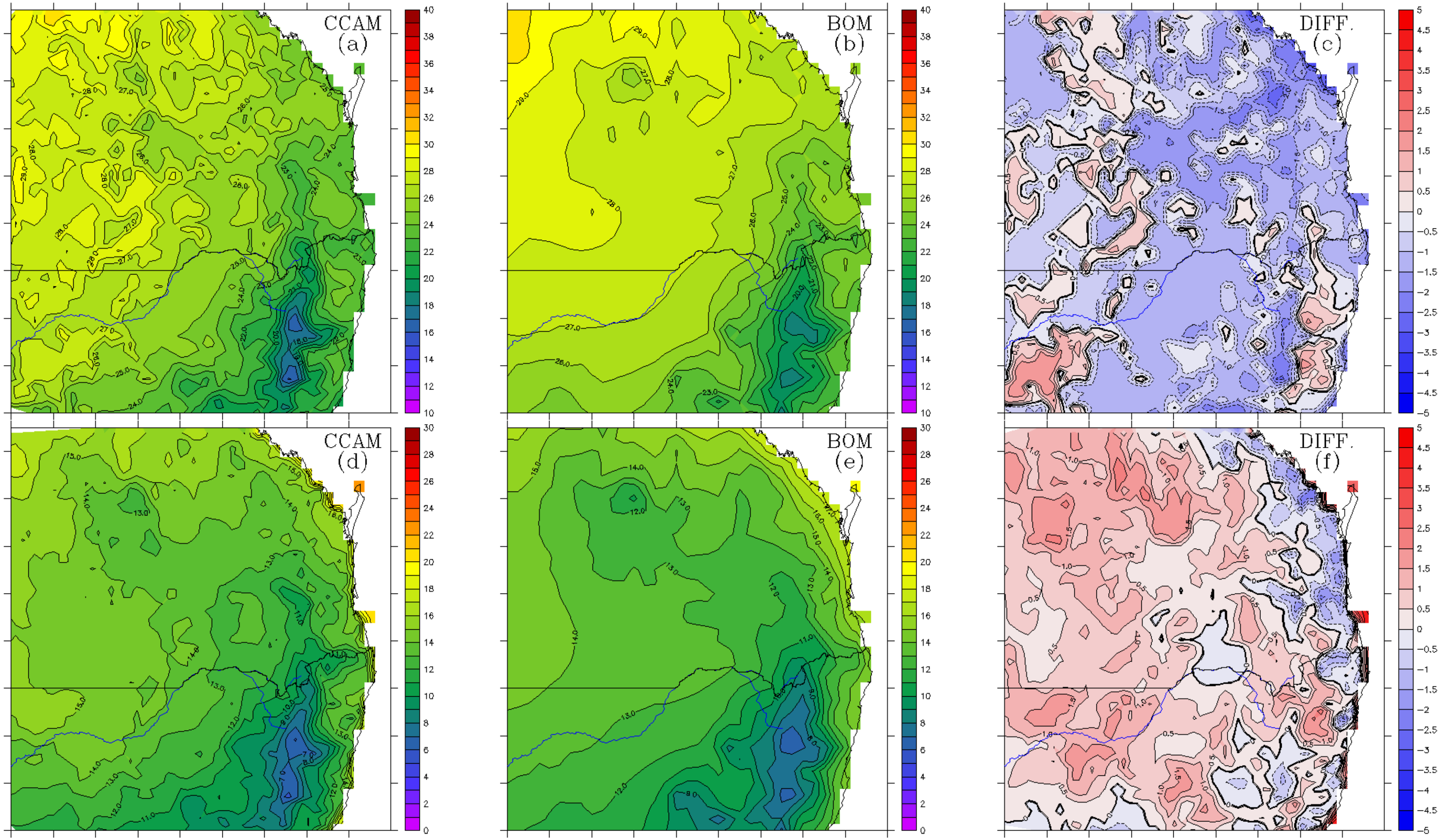
CCAM
(a)
BOM
(b)
DIFF.
(c)
CCAM
(d)
BOM
(e)
DIFF.
(f)

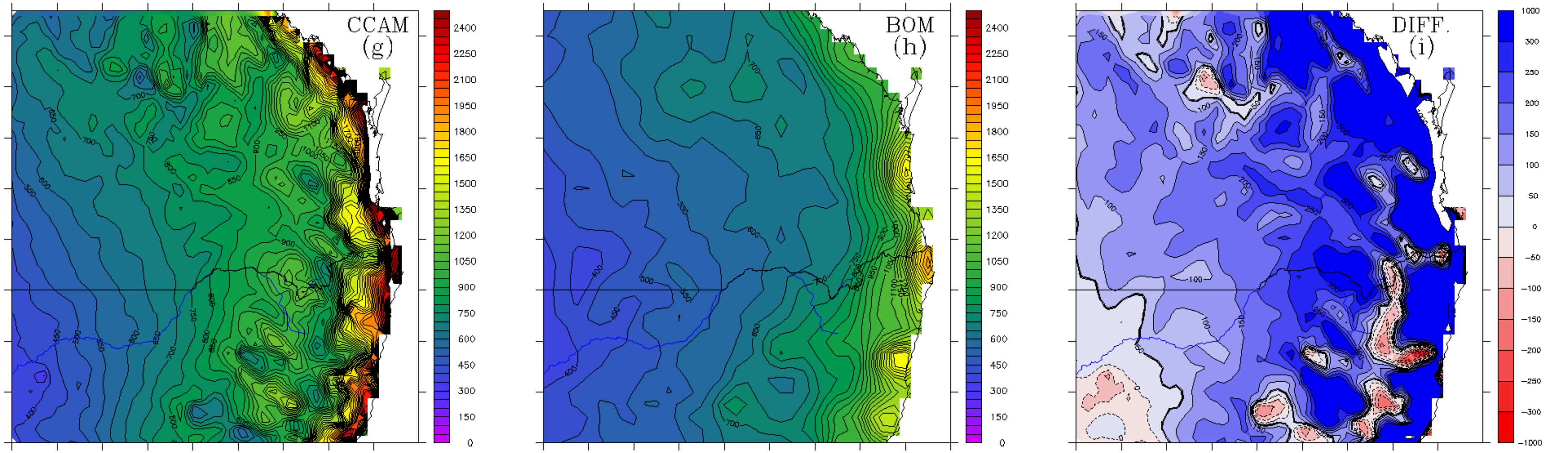

Figure 5.6 (a–f (previous page) and g–i (above)) Contoured annual maximum and minimum temperatures (ºC) and rainfall (mm year^{-1}) from the 19 km CCAM model simulation **MR3** (a,d,g), the BoM observations (b,e,h) and Differences (c,f,i) over SE QLD and the period 1971–2000. Temperature and rainfall contours are in intervals of 1ºC and 100 mm respectively. Difference contours intervals are 0.5ºC and 50 mm for temperature and rainfall respectively.

minimum temperatures in the CCAM model and the BoM observations are shown in Figure 5.6f. This shows the model simulates slightly higher minimum temperature (~0.5–1.5ºC) over most of the region. Negative anomalies occur along most of the coast, especially north of about Brisbane area and coastal areas north to Hervey Bay, indicating slightly lower minimum temperatures (~0.5–1.0ºC) in the model. This is also similar to MR2 and Figure 5.5f.

The contoured annual rainfall for the CCAM model and the BoM observations are shown in Figure 5.6g and Figure 5.6h respectively. The annual rainfall patterns are generally very similar between the model and the BoM observations; however there is considerably higher rainfall along the coastal region, compared to MR2 (Figure 5.5g). The highest rainfall in the model is over 2400 mm along the coast (higher than BoM observations) and the lowest rainfall over western inland areas of ~400 mm (similar to the BoM observations). The differences between the annual rainfall in the CCAM model and the BoM observations are shown in Figure 5.6i. Over most of the inland areas, higher rainfall covers most of the region, with increases generally between 100–300 mm, increasing towards the coast. Only in the far southwest corner does the CCAM model produce lower rainfall than the BoM observations. Along the coastal region, much higher rainfall is simulated over most of the region, with increases of 300–1000 mm, and even higher values closer to the coast.

In summary, the MR3 model using a lower albedo east and west of 152ºE produced higher rainfall over most of the region west of ~152ºE and much higher rainfall east of ~152ºE. The higher rainfall is associated with lower maximum temperatures and slightly warmer minimum temperatures.

5.3.3.2 MR4 Model

Results from the annual maximum and minimum temperature (ºC), rainfall (mm year^{-1}) and differences for the period 1971–2000 over the SE QLD region are shown in Figure 5.7 (a–i) for MR4. The albedo in MR4 has been changed to 0.40 west of 152ºE, and remains the same as in the MR3 model with an albedo of 0.06 east of 152ºE. The BoM observations are shown in the central plots in Figure 5.7 (b, e, h).

The contoured annual maximum temperatures (Figure 5.7a) over the SE QLD region are similar to the BoM observations (Figure 5.7b), with the warmest temperatures in the CCAM model over the northern and northwest regions (~24–26ºC) and the coolest temperatures (~15–17ºC) located over the Northern Tablelands of NSW. The differences between the annual maximum temperatures in the CCAM model and the BoM observations are shown in Figure 5.7c. This shows the clear demarcation of the boundary where the albedo was changed at 152ºE, with much colder maximum temperatures (-3.0 to -4.5ºC) west of 152ºE, slightly cooler maximum temperatures (-0.5 to -1.5ºC) east of 152ºE over north coastal regions and slightly warmer temperatures (0.5–1.5ºC) over a small area in the southern coastal region.

The contoured annual minimum temperatures (Figure 5.7d) over the SE QLD region are similar in distribution, but cooler than the BoM observations (Figure 5.7e), with the warmest minimum temperatures (~12–14ºC) over northern and western regions and coastal areas and the coolest minimum temperatures (~6–8ºC) over southeast regions of NSW. The differences between the minimum temperatures in the CCAM model and the BoM observations are shown in Figure 5.7f. This shows the model

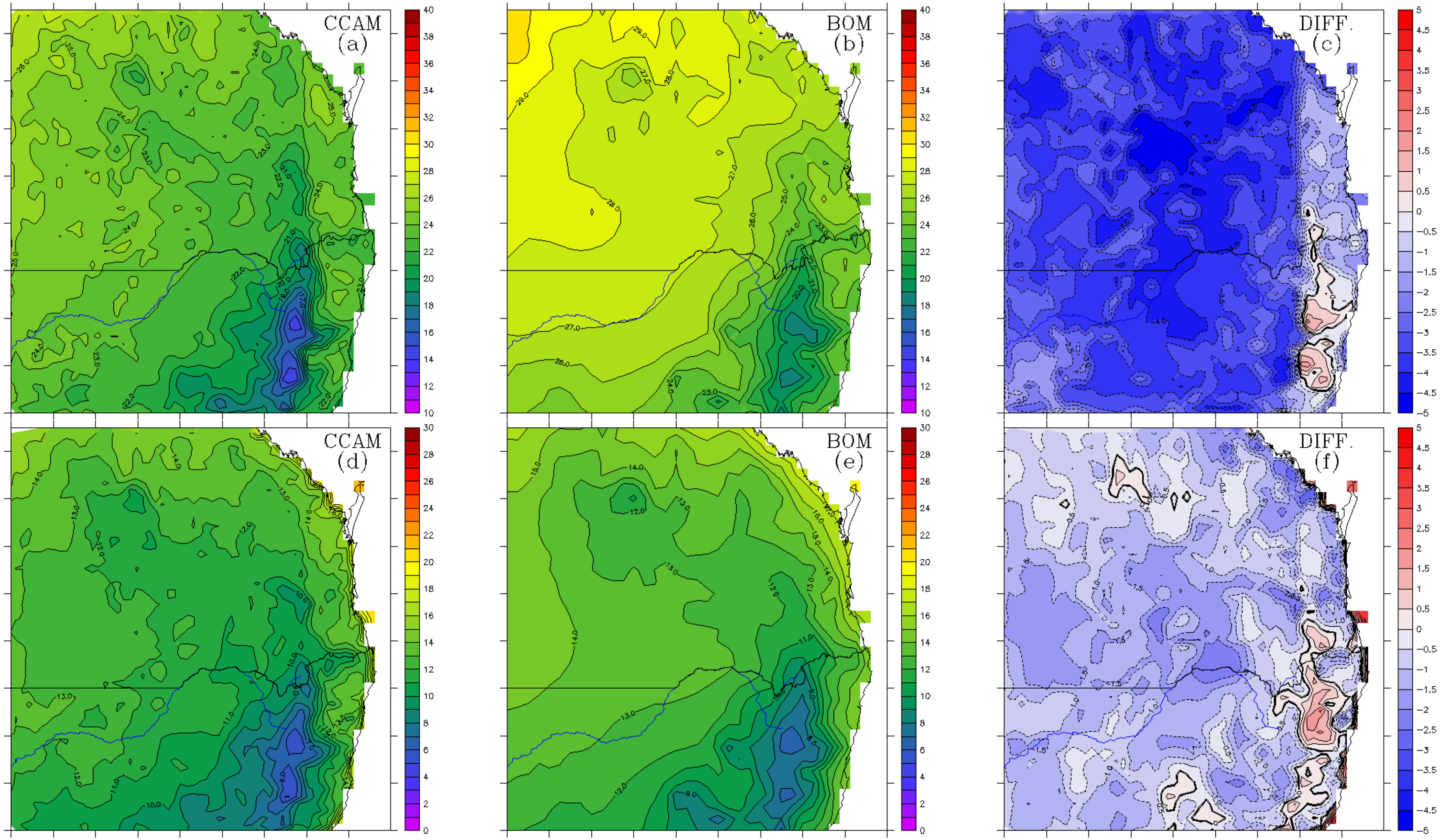

CCAM
(a)
BOM
(b)
DIFF.
(c)
CCAM
(d)
BOM
(e)
DIFF.
(f)

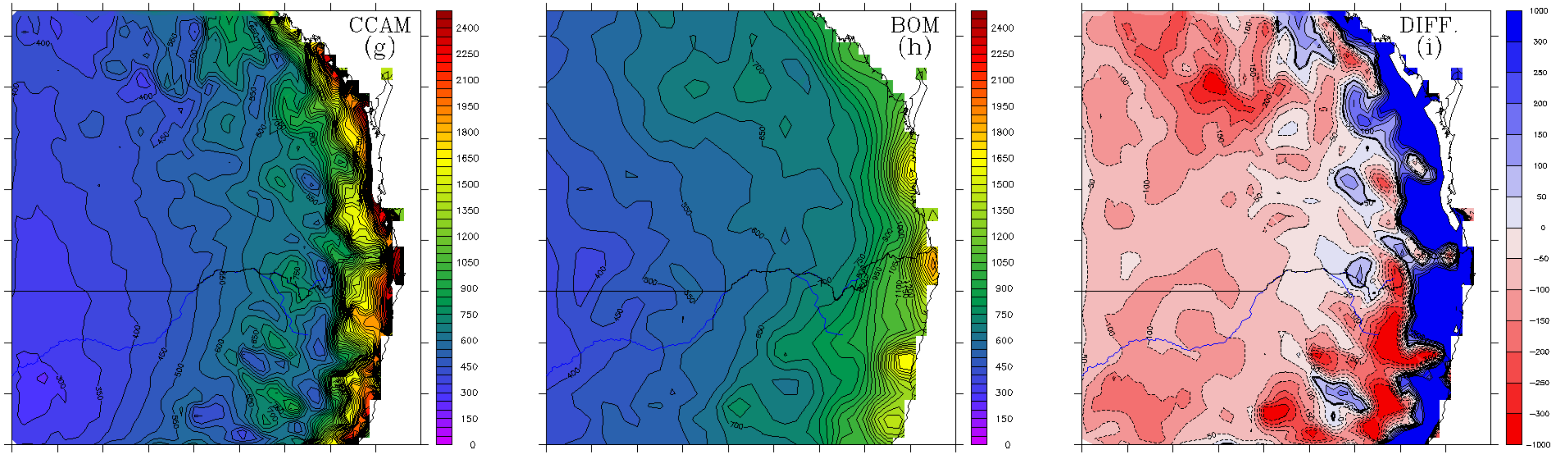

Figure 5.7 (a-i) Contoured annual maximum and minimum temperatures (ºC) and rainfall (mm year^{-1}) over SE QLD and the period 1971–2000 from the 19 km CCAM model simulation **MR4** (a,d,g), the BoM observations (b,e,h) and Differences (c,f,i). Temperature and rainfall contours are in intervals of 1ºC and 100 mm respectively. Difference contours intervals are 0.5ºC and 50 mm for temperature and rainfall respectively.

simulates lower minimum temperatures (-0.5 to -1.5ºC) over most of the region, except for a few small areas in the southeast corner by the coast. This is a major change from results in the MR3 model (Figure 5.6f), where minimum temperatures were generally warmer than the BoM observations.

The contoured annual rainfall for the CCAM model and the BoM observations are shown in Figure 5.7g and Figure 5.7h respectively. The annual rainfall patterns are similar with north–south trending isohyets. However, there is considerably higher rainfall along the coastal region (>2400 mm) in the CCAM model, compared to the BoM observations. The lowest rainfall in the model occurs over western inland areas of ~300–350 mm, which is lower than the BoM observations (~400–450 mm). The differences between the annual rainfall in the CCAM model and the BoM observations are shown in Figure 5.7i. Over most of the inland region, much lower rainfall (~50–200 mm) occurs in the CCAM model compared to the BoM observations, with even larger reductions over the Carnarvon Ranges (up to 300 mm). Closer to the coast, a sharp increase in rainfall occurs, producing much higher rainfall (>250 mm) than in the BoM observations.

In summary, the MR4 model using a much higher albedo west of 152ºE, produced much lower rainfall over most of the inland region, except near the coast and east of ~152ºE. The higher rainfall is associated with much lower maximum temperatures and slightly cooler minimum temperatures.

5.3.4 Rainfall and Land Surface Height

Results from the CCAM simulations and the BoM observations show the rainfall and temperature are closely aligned to the land surface height (Figure 5.8). The higher rainfall totals occur along and over the Great Dividing Range (elevation generally

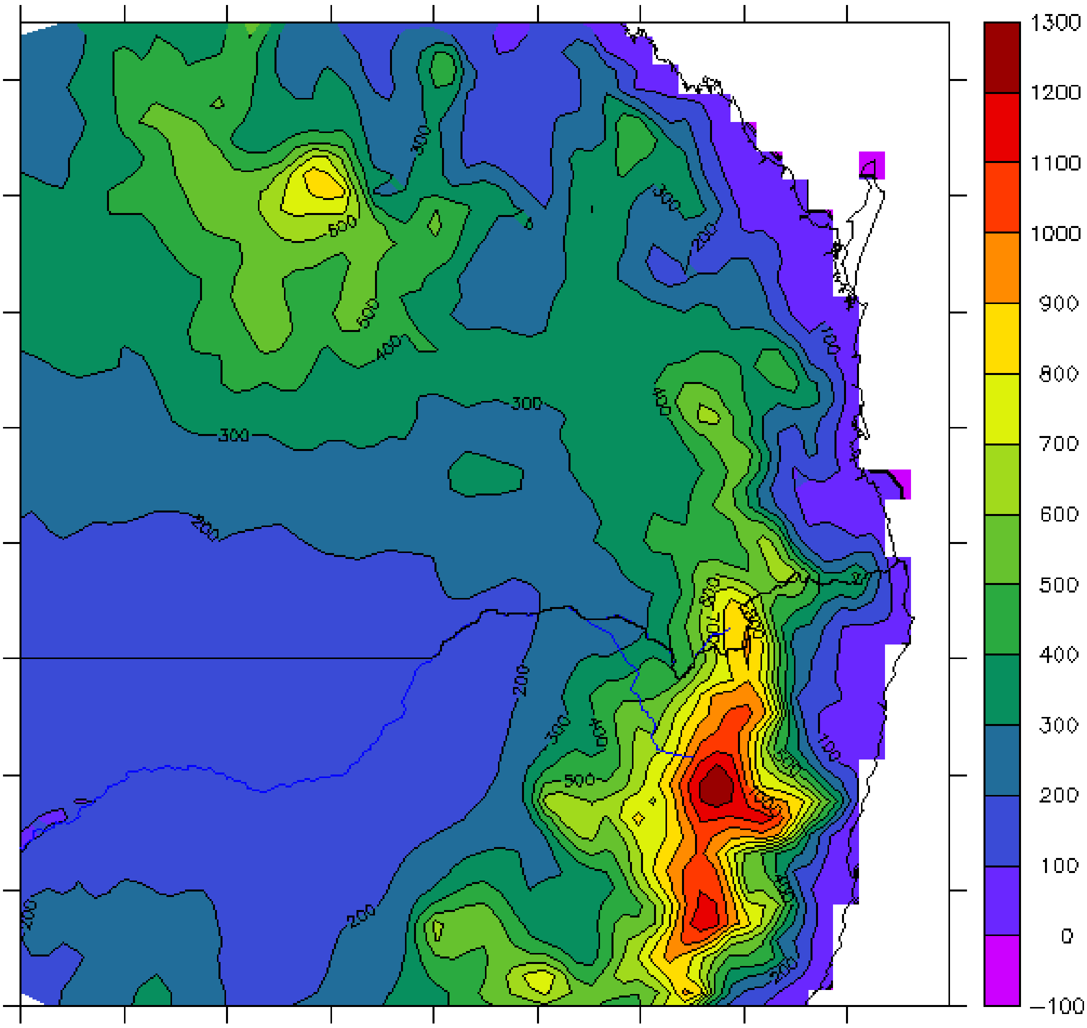

Figure 5.8 Map of the surface height (m) in the CCAM model contoured at 100m intervals. The Great Dividing Range is highlighted by the light green yellow, orange and red shades over eastern parts SE QLD and northern NSW. The yellow shades located over the northern region of SE QLD represent the Carnarvon Ranges.

between 400–1200 m), such as in the Northern Tablelands in northern NSW and the coastal ranges in SE QLD, and also have the lowest minimum and maximum temperatures. Over the western and southwestern regions, the elevation is generally between 100–400m, forming wide gently sloping plains, with more uniform rainfall shown in both the BoM observations and the CCAM simulations.

As shown by this set of experiments, rainfall in regional climate simulations is also sensitive to land surface height and this was also demonstrated in Chapter Two, where most GCMs underestimated the coastal rainfall in the Queensland region.

5.4 DISCUSSION

In the initial CCAM control run (MR2) over the SE QLD region, the 'Present Vegetation' scheme produced maximum and minimum temperature and rainfall simulations more similar to the BoM observations (as expected) than the experimental models MR3 or MR4. The MR2 model shows CCAM is producing slightly lower maximum temperatures and slightly warmer minimum temperatures than in the BoM observations. The similarities of the spatial rainfall patterns between the BoM observations and the MR2 model, such as the higher coastal rainfall with large localised differences and the lower rainfall inland with a smaller range of rainfall across the region, indicates the main components of the regional atmospheric circulation have been well simulated in the model. The higher coastal rainfall indicates onshore winds and orographic rainfall are produced in the CCAM model, as well as the rainfall shadow west of the coastal Great Dividing Ranges. Some of the small differences in the rainfall and temperature could be related due to the coarse resolution of the 'Present Vegetation' land cover in the CCAM model. The resolution of the vegetation shown in Figure 5.3 is in much greater detail than in the CCAM model and shows the close association of the vegetation types with relief and soils. Dynamical LCC schemes are currently being developed in new GCMs, which will be able to simulate year by year changes in the vegetation cover over a region, far closer to the actual changes seen in the landscape produced by agriculture, grazing and other human activities.

In the simulations using different regional albedo values, the change to a lower albedo east and west of 152ºE in MR3, produced much higher rainfall over nearly all of SE QLD, especially along the coast. However, there are similarities between MR2 and MR3, with the maximum and minimum temperatures lower and higher respectively in both simulations, indicating the changes made to the albedo, although small, maintained the spatial distribution and range of temperatures in the model. The lower maximum temperatures are likely to be caused by more cloud cover and rainfall. The higher minimum temperatures are most likely caused by more cloud cover and rainfall, reducing night time radiation loss.

In the MR4 simulation, the large contrast in the albedo between the eastern and western zones along the approximate location of the Great Diving Range, provided strong changes to both rainfall and temperature. The higher albedo west of the Great Dividing Ranges reduced maximum temperatures by about 3–4.5ºC and overnight minimum temperatures were also reduced significantly by 1–1.5ºC. The higher albedo has led to much cooler maximum temperatures, presumably by reflecting incoming short wave radiation away from the surface during the day. The cooler maximum temperatures and lower rainfall are most likely to have produced lower minimum temperatures due to less cloud cover and higher amounts of radiation loss at night. The higher albedo and the colder temperatures may have caused lower rainfall over the inland regions, with a 10–30% reduction in rainfall, presumably due to less convection and more subsidence in the model. In contrast, the coastal regions, which maintained the same albedo value from MR3, had only small changes in the maximum and minimum temperature, but much higher rainfall (50–100% increase or more). This is more difficult to explain by simple changes to atmospheric circulation, such as an increase or decrease in the onshore winds. Although not fully investigated in this study, detailed cloud cover, surface energy balances and regional circulation changes could be avenues for future research on regional climate and rainfall in regional climate models.

Although the vegetation experiments (MR5 and MR6) were unsuccessful as they produced far more rainfall in the simulations than had been expected, this provides an opportunity for more research to be conducted over SE QLD and other parts of Australia, where rainfall changes are impacting on the availability of water resources. If the 'Present Vegetation' scheme produces rainfall closer to the BoM observations than the 'Natural Vegetation' scheme, this would indicate the high sensitivity of the CCAM model to different vegetation types and the importance of the land cover to rainfall changes. However, due to the strong land cover fragmentation in the control run (MR2), it is not immediately apparent whether the vegetation or albedo (or both together) are having the strongest impact on the boundary layer processes and the spatial distribution of rainfall in this region. In a recent study completed by McAlpine et al (2007) using the CSIRO-MK3 model with pre–European and present day land cover characteristics over Australia, they showed a small warming was evident over eastern Australia, with a small decrease in rainfall over southeast

Australia, indicating that LCC were potentially an important contributing factor to the changes in regional climate during the 20th century. These results are similar to this study and shows further research is needed to estimate the strength of the rainfall change with different land cover and albedo values.

The LCC affecting regional climate are becoming an increasing important field of study due to climate change, environmental factors, water resource management, fire control and other socio–economic factors. LCC such as irrigation, mask the effects of warming caused by increasing greenhouse gases (Kueppers et al. 2007), whilst others such as the urban heat island amplify, the warming signal. In recent land cover research and climate modelling in the Amazon Basin, climate change and rainfall has been studied between two different crops: pasture land and soybean croplands. Results indicate that the very high albedo of the soybean crop causes larger decreases in precipitation than for pasture land (Costa et al. 2007). This is similar to the results shown here using the MR4 model over SE QLD, with a higher albedo value reducing the rainfall over pastoral and crop regions, west of the Great Dividing Ranges. Climate change detection using a global land surface vegetation scheme has been studied in a number of GCMs, indicating an anthropogenic warming trend is detectable in six of seven global regions during the past half century (Hongyan et al. 2007). Some GCMs indicate higher rainfall occurs over evergreen and summergreen vegetated regions in tropical and subtropical areas (Alessandri et al. 2007). The seasonal aspects of the rainfall and temperature associated with changes in the albedo and vegetation were not investigated in this study and this would be another potential avenue for more detailed research. Ultimately, a better understanding of the regional vegetation land cover and boundary layer processes which influence climate, will provide a better basis for management of landscapes in a more sustainable, environmental and economically viable way and assist with the regional land planning schemes, similar to those already being discussed for urban areas such as Melbourne (Coutts et al. 2007).

In the next chapter, a palaeoenvironmental study on lake sediments from a small lake in SE QLD, west of the Great Dividing Range will be used to establish a Holocene palaeoclimate record, where few records have been developed previously. This will enable the current climate and climate change already observed over Queensland and the SE QLD region to be placed into a longer perspective.

CHAPTER 6 : A HOLOCENE PALAEOENVIRONMENTAL RECORD FROM LAKE BROADWATER, SOUTHEAST QUEENSLAND

6.1 INTRODUCTION

Palaeoenvironmental records can provide a wealth of information on the past environmental history of a region including the palaeoclimatic and palaeohydrological conditions, long before the observation record was developed. This provides an opportunity to explore climate and climate change over a much longer period, so that the climate changes experienced today can be viewed in context with much longer records. The current declining rainfall trend over NEA and SE QLD may partly be a continuum of a much longer cycle of ENSO variability that started ~5 kyr B.P. with an abrupt increase in magnitude ~3 kyr B.P (Gagan et al. 2004). In this study, initially it was hoped that a comparative study between 20th century rainfall from the BoM records and sedimentation characteristics at Lake Broadwater could be determined, similar to other studies such as Kalugin et al (2005) and Cameron et al. (2002). This would have enabled a very high resolution record with decadal scale rainfall variability to be established and extended back several centuries beyond the observational record, similar to the high resolutions completed on corals (De'ath et al. 2009) and tree rings (Fowler et al. 2008). However, due the much older age of the sediments found in this study, such a detailed analysis could not be completed. This chapter explores the environmental changes from a small lake located in the Darling Downs region in SE QLD over a longer time period than current observation records, from the mid–Holocene to the present.

A number of palaeoenvironmental records from lake sediments have been constructed from a number of locations in Queensland including Fraser Island (Longmore 1997; Donders et al. 2006), North Stradbroke Island (McGowan et al. 2008; Petherick et al. 2008), Whitsunday Island (Genever et al. 2003), the Atherton Tableland (Kershaw 1970, 1971, 1975, 1983, 1994) and the Cape York Peninsula (Luly et al. 2006) using palynology, geochemical analysis and stratigraphy. However, there is a paucity of similar such palaeoenvironmental reconstructions from inland Australia (Kershaw 1995; Harle et al. 2005; Lynch et al. 2007), with none from the Condamine River catchment in the upper reaches of the Murray–Darling Basin in Queensland (Figure 6.1).

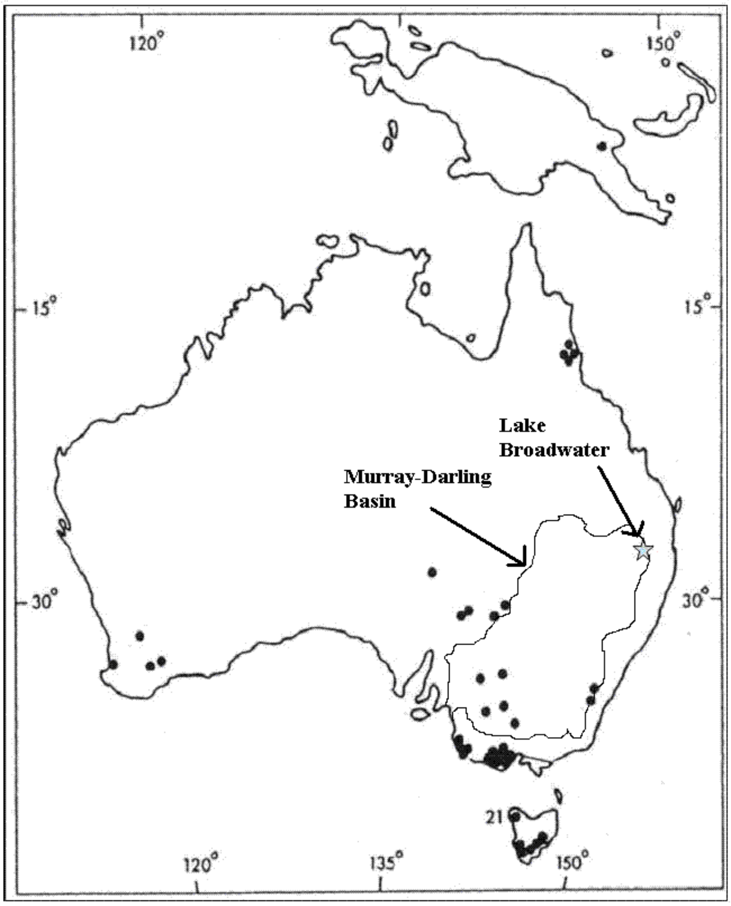

Figure 6.1 Locations of Australian lake sediments and palaeo–records. Modified after Harle et al (2005). The location of Lake Broadwater in the upper Murray–Darling Basin is shown as a star in SE QLD.

Lacustrine sediments provide some of the best archives for palaeoclimatic information in terrestrial settings (Last and Smol 2001) and continuously record regional climatic and environmental information (Chen et al. 2005). Fluctuations in the grain size of lake sediments record subtle changes in the hydrological conditions associated with regional climate and environmental change and have been used successfully to correlate across different regions (Håkanson and Jansson 1983). Grain size analysis has been used recently from a number of lakes including Lake Baikal (Kashiwaya et al. 2001), Dali Lake (Xiao et al. 2008) and from Yallalie, Australia (Dodson and Lu 2005), to establish palaeoenvironmental conditions and climate.

To develop a palaeoenvironmental history and a palaeoclimate record for SE QLD, a number of locations in the Darling Downs were assessed and Lake Broadwater was immediately recognised as a possible site for such a reconstruction. In this study, the analysis of lake sediments from Lake Broadwater provides an insight into the sedimentation history and palaeoenvironmental conditions that prevailed during the Holocene in the Upper Condamine River region. The palaeoenvironmental conditions enable the major changes in the palaeohydrological conditions during sedimentation to be identified and hence an interpretation of the regional palaeoclimate to be established. The Lake Broadwater regional setting is described in section 6.2, the methodology in section 6.3, detailed results in section 6.4 and a discussion and interpretation of the results with comparisons to other palaeoenvironmental records from eastern Australia and elsewhere in section 6.5.

6.2 LAKE BROADWATER REGIONAL SETTING

6.2.1 Site Selection

The Lake Broadwater Conservation Park is located 30 kilometres southwest of Dalby, in the Darling Downs region of SE QLD and in the Condamine River catchment in the upper reaches of the Murray–Darling Basin (Figure 6.2). The park covers over 1220 hectares of natural bushland, with the lake occupying about 350 hectares. Over 450 species of plants and 220 species of bird have been identified in the park (EPA 2006). Lake Broadwater Conservation Park is the only naturally occurring water body of this type in the Darling Downs region and is listed in the Australian Directory of Nationally Important Wetlands. Lake Broadwater was selected as it offered the best opportunity to obtain a sediment core from mostly

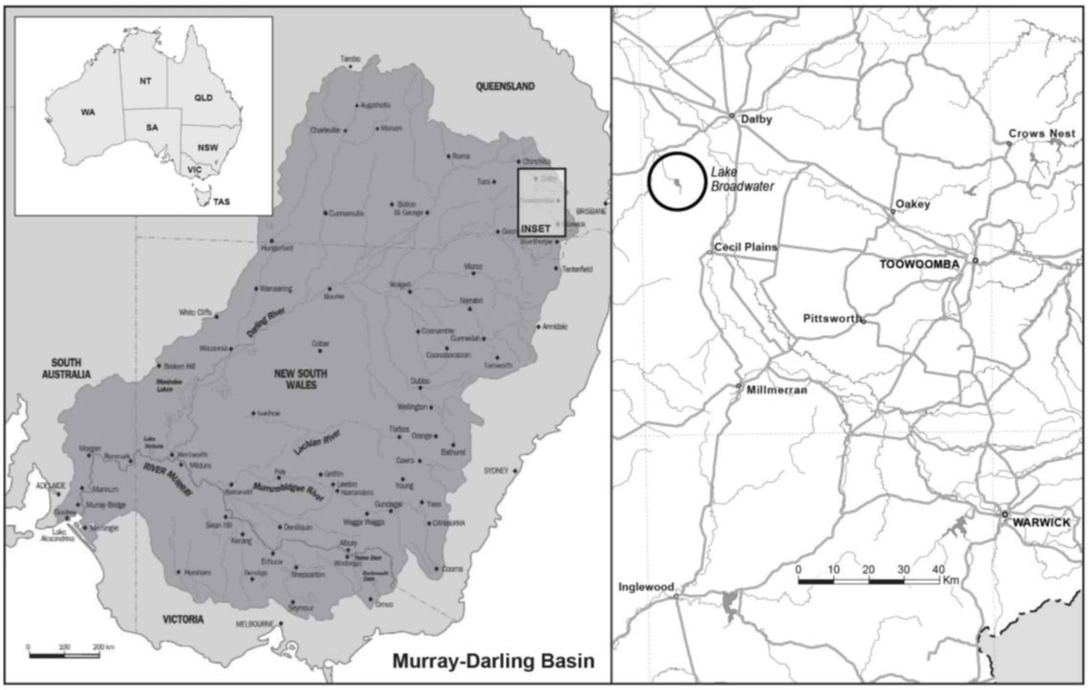

Figure 6.2 Location map of Lake Broadwater (left) in Queensland, Australia and the catchment area of the Murray–Darling Basin (dark grey). Detailed location map of Lake Broadwater and surrounding area in SE QLD (right) and the Condamine River. Compiled by USQ Graphics.

undisturbed lake sediments in a region where intensive agriculture and grazing has been developed over a wide area.

Lake Broadwater is a mature, shallow eutrophic lake that has had a relatively stable Holocene making it ideal for developing a palaeoenvironmental history of the region. When the lake is full, it is about four metres deep and water flows out from the northern corner of the lake into an area called the 'overflow' leading into Wilkie Creek and the Condamine River. The origins of the lake are still a 'mystery' although the most likely explanation is that it once formed part of the Condamine River flood plain and was carved out during periods of higher rainfall and river flows (Scott 1988). A panoramic view of the lake is shown in Figure 6.3.

Figure 6.3 Panoramic view looking east from the main recreation area at Lake Broadwater, taken on the 20th October 2006. There is no water in the lake and the green vegetation marks the lowest area in the lake where the core was collected.

6.2.2 Geology

Lake Broadwater is located on the margins of the northwest trending Surat and Moreton Basins, which formed during the Late Jurassic to Early Triassic epoch (Figure 6.4a) and is characterized by extensive sedimentary fluviatile deposits up to 2

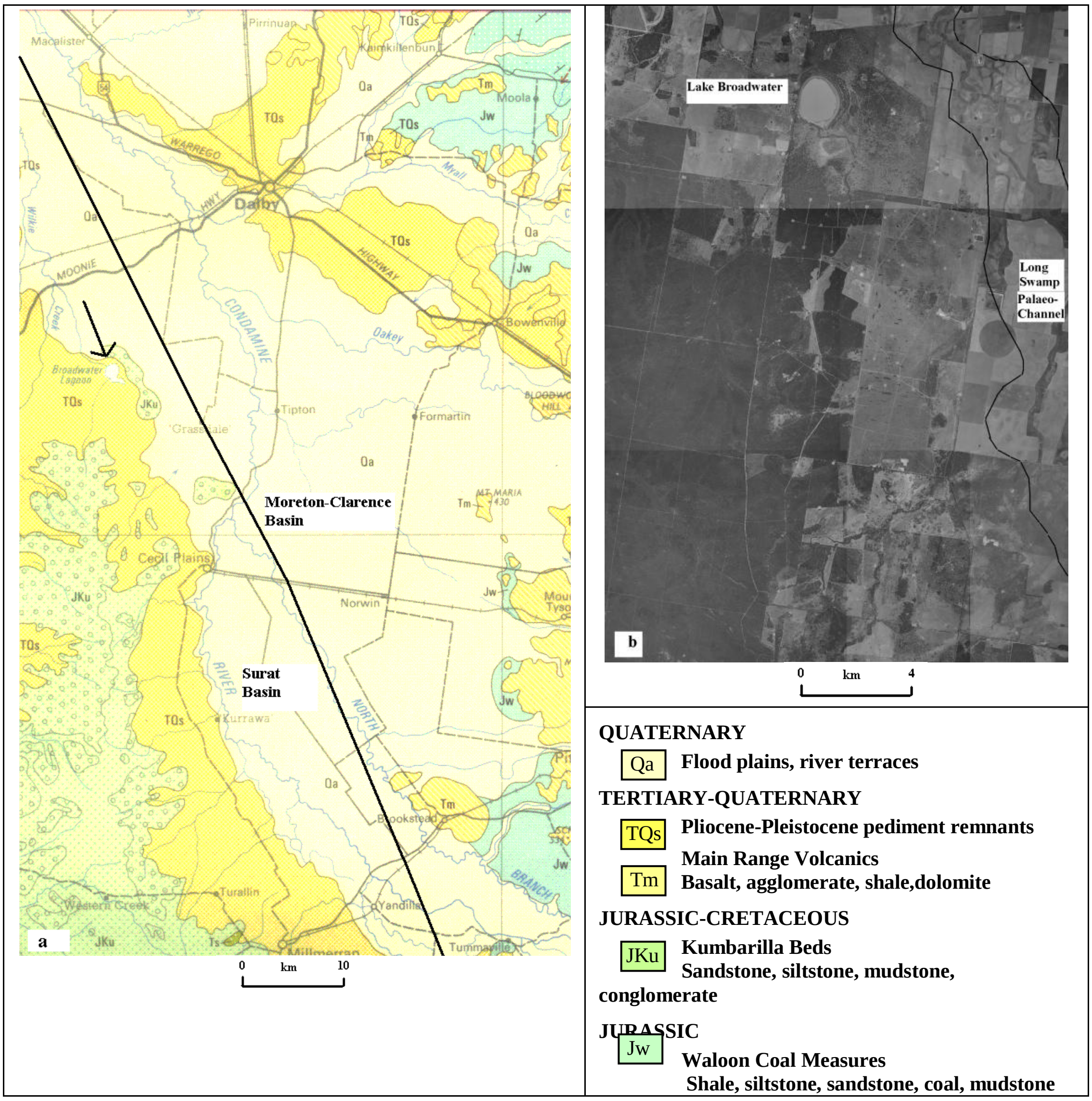

Figure 6.4 (a) The geology of the Lake Broadwater region and the location of the lake (arrowed). **(b)** Long Swamp palaeochannel east of Lake Broadwater from serial photograph mosaic.

km thick of coarse quartzose to sub–labile sand and silt ending with labile sands, silts, muds and coal (Day et al. 1983).

During the Tertiary, following uplift and planation, much of the region was exposed to widespread lateritisation and deep weathering profiles developed over the sedimentary basins. In the Moreton basin, basaltic volcanic activity developed in the mid–Tertiary and was widespread, with extensive eruptions forming the Main Range

Volcanics (Willey 2003), east of Lake Broadwater in the Toowoomba region. During the Quaternary, rapid and frequent changes in the world's climate were dominated by glacial and interglacial episodes with extensive ice sheets developed in the Northern Hemisphere. This resulted in the Murray–Murrumbidgee–Darling river system developing a variety of types of palaeochannels, reflecting changing flow discharges and sediment loads (Williams et al. 1998). Extensive alluvial deposits cover a wide area adjacent and east of Lake Broadwater, associated with the floodplain sedimentation and earlier palaeochannels (such as Long Swamp) of the Condamine River (Figure 6.4b). These alluvial deposits overlie much of the Moreton–Clarence Basin geology and form the extensive fertile plains that are intensely farmed around the lake today.

At Lake Broadwater, the local geology consists of extensive flat plains of sandy clay soil (alluvium) covering much of the area around the lake. There are a number of small outcrops of sandstone from the Kumbarilla beds (Mid Jurassic to early Cretaceous) north and east of the lake and further to the south within the catchment area. The Kumbarilla beds are composed of sandstone, siltstones and mudstone with some conglomerate (Mond 1973; Exon 1976).

6.2.3 Climate and Hydrology

The climate of the Lake Broadwater Conservation Park and the Darling Downs region can be classified as subtropical with an austral summer rainfall maximum (Colls and Whitaker 1993; Sturman and Tapper 1996) and weak summer seasonality (Hesse et al. 2004). Like the arid zone of central Australia, the Lake Broadwater region lies under the descending arm of the Southern Hemisphere Hadley cell and the subtropical ridge for much of the year (Hesse et al. 2004). As discussed in Chapters One and Two, other important synoptic features include east coast troughs, east coast lows and upper troughs are important in delivering rains to the region, which usually occurs from November to March (see Figure 1.3 (a–d)). There is a gradual decline in rainfall from east to west across the region due to the prevailing moist easterly winds. Lake Broadwater is located ~200 km inland from the east coast in the lee of the Great Dividing Range, and easterly winds from the Coral Sea become drier, producing a lower mean annual rainfall of ~600–700 mm. Mean maximum temperatures in the region vary from ~33ºC in austral summer to ~20ºC in austral winter. Mean minimum temperatures vary from ~20ºC in austral summer to ~5ºC in austral winter, with widespread frosts (~10–20 per year) occurring in the winter months. Thunderstorms are common in the austral spring, summer and early autumn months with an average of 5–7 days per month, although this can vary greatly from year to year. Severe storms are also common at this time, with rain, hail and strong winds. The relative humidity is significantly lower than Toowoomba and is very similar to Dalby, located to the north (Figures 6.2 and 6.4a). In the austral summer, winds are generally warm easterly, but westerly winds can be very hot blowing from the interior. In contrast, in the austral winter, westerly or southwesterly winds can be very cold. The trees directly around Lake Broadwater slow wind velocities over the lake, reducing evaporation. There is an increase in sunshine hours from east to west across the Darling Downs region, with ~3000 hours recorded per annum at Dalby (Scott 1988).

The Darling Downs region has considerable rainfall variability, similar to other regions of Australia such as Brisbane, the Northern Tablelands of New South Wales (NSW) and the border region of NSW and northern Victoria (Nicholls et al. 1997). BoM observations indicate the highest annual rainfall was in 1983 (~1055 mm) and the lowest annual rainfall in 1919 (~314 mm). In recent years since the early 1980s, there has been a gradual decline in the annual rainfall, consistent with the rainfall declines seen over much of eastern Australia and Queensland (Murphy and Ribbe 2004) and was discussed previously in detail in Chapters One and Two. The annual rainfall at Lake Broadwater during the last nine years (2000–2008) is now ~574 mm (a 20% decline compared to nearby Dalby which had an average rainfall of 720 mm during 1961–1990). This compares with an annual rainfall of ~950 mm at Toowoomba prior to 2000, but is now much lower at ~650 mm (a 32% decline)(BoM 2008).

Lake Broadwater is a shallow ephemeral lake which has undergone major water level fluctuations in recent times. Based on local reports, Lake Broadwater has dried out during the 20th century on at least six occasions: 1935–1939, 1966, 1969, 1987 and 1992 and more recently in 2002, 2006 and April 2008. These periods usually coincide with low annual rainfall of below ~600 mm in two or more consecutive years and also with El Niño events (Figure 3.4).

6.2.4 Soils

Six land resource areas and soils types (in brackets) have been distinguished in the Lake Broadwater area (Scott 1988; Harris et al. 1999). The soils derived from the

Condamine River (Condamine–1a soil type) and recent alluvial deposits (including Long Swamp) are composed of black and grey, medium to heavy cracking clays with minor coarse sand forming the broad plains adjacent to the river east and southeast of Lake Broadwater. They generally exhibit a unimodal grain size distribution. Soils located to the northwest of Lake Broadwater (Tara gilgai–5b) are composed of brown to grey cracking heavy clays that form gilgai micro–relief. They exhibit a strong bimodal grain size distribution of fine sands and clay. Soils derived from the gentle plains over sandstone bedrock around Lake Broadwater, mainly to the west and south, consist of bleached sands and loams over brown and grey clays (Downfall–9a). These form the dominant soil type directly around Lake Broadwater and are currently being deposited around the margins of the lake. They also have a strong bimodal grain size distribution of fine sands and clay. The low rises and undulating plains northeast of the lake and covering a wide area to the south, are comprised of bleached sands to loams over mottled, grey or yellow clays (Weranga–12a). On top of the low rises, plateaus and sandstone hills are shallow gravelly sands to loams over mottled grey or yellow clays (Drome–12b).

6.2.5 Vegetation

Remnant vegetation at Lake Broadwater is closely associated with the different soil and regolith (Scott 1988; Harris et al. 1999). On the alluvial plains, Poplar box (*Eucalyptus populnea*), Queensland blue gum (*E. tereticornis*) open woodland or grasslands dominate. On the gilgai soils, brigalow (*Acacia harpophylla*), belah forest (*Casuarinas cristata*) and wilga (*Geijera parviflora*) species are common. Poplar box (*E. populnea*) and gum topped box (*E. moluccana*) open woodland are characteristic of vegetation on the gentle plains over sandstone. On the rises and plateaus with soil types 12a and 12b, the vegetation is dominated by combinations of narrow leaved ironbark (*E. crebra*), white cypress pine (*Callitris glaucophylla*), bull oak (A. *luehmannii*), rusty gum (*Angophora floribunda*) and poplar box (*E. populnea*) in open forest. Recent low water levels have led to terrestrial vegetation covering most of the lake surface to a height of 1.5 m with the herb *Polygonaceae persicaria*.

6.3 METHODOLOGY

6.3.1 Introduction

A 1.7 m core was obtained from a carefully selected site (with minimal disturbance) in the middle of the dry lake bed in March 2007. Although this analysis was conducted on a single core, three other cores collected from the same area within a few months, show similar stratigraphy and grain size changes to the core used for this analysis. A number of other palaeoenvironment records have been established using single cores from lakes in eastern Australia (Longmore 1997; Harle et al. 2002; Genever et al. 2003; Black et al. 2006; Petherick et al. 2008) and elsewhere (Augustinus et al. 2005; Shichi et al. 2006; Wünnemann et al. 2006; Xiao et al. 2008) Detailed stratigraphy, multi–element geochemistry and grain size analysis of the core samples were used to identify significant trends and changes in the palaeoenvironmental conditions in the lake during sedimentation with lead (^{210}Pb) and carbon (^{14}C) dating used to establish the chronology.

Mapping of the Lake Broadwater catchment area was undertaken to classify the soils and geological units into regolith types. This mapping would provide details on the spatial distribution of regolith–landform types and how these may have influenced sedimentation into the lake.

6.3.2 Core Analysis from Lake Broadwater

6.3.2.1 Laboratory Analysis

Lake samples were collected from Lake Broadwater (detailed field sampling procedures are described in Appendix Three) and returned to the University of Southern Queensland (USQ). Bulk densities of the lake samples were measured using procedures described by Lal (2002). The cores and core catchers were cut in half to expose the core, wrapped in cellophane and stored in a cool fridge (~4ºC) to reduce oxidation. During initial analysis, the core was divided into 1 cm intervals, logged similar to that of Troels–Smith (Kershaw 1997), photographed and magnetic susceptibility (KT–9 Kappameter in mT) readings taken every 10 cm. The magnetic susceptibility of lake sediments is a technique used in studies elsewhere of Holocene sediments (Anderson and Rippey 1988; Ojala and Saarinen 2002; Whittaker et al. 2008) for identifying changes in catchment erosion (Anderson and Rippey 1988; Rühland et al. 2006).

A range of other analyses were performed on the core samples. It was tested for the presence of carbonate using 10% HCl. Twenty samples were collected for grain size analyses and twenty larger samples (~50–100 g) selected at 5 cm or 10 cm intervals to calculate moisture percentage. After drying, the larger samples were split into three identical–sized samples for ^{210}Pb dating, organic, carbonate and silicate percentage determination by weight loss on ignition (LOI) and multi–element geochemistry by ICPAES and CNS analyser. Samples for ^{210}Pb dating, grain size analyses, multi–element geochemistry and later ^{14}C radiocarbon dating were sent to the Australian Nuclear Science and Technology Organisation (ANSTO) at Lucas Heights, Sydney for analysis.

6.3.2.2 Grain Size Analysis

A total of twenty samples were taken every 5–10 cm from the core for grain size analysis. At the Faculty of Engineering at USQ, samples were dispersed in a solution of deionised water using an ultrasonic probe (Branson Digital Sonifer) and aliquots from this solution sent to ANSTO for analysis using a Malvern Mastersizer (2.19) and laser diffraction. The laser diffraction method provides more detail on grain sizes than traditional sieving or sedimentation methods (Buurman et al. 1997) and techniques using the results from the laser diffraction are improving (Konert and Vandenberghe 2008). Grain size analysis can provide important information to sediment provenance (Blott et al. 2004) and changes in grain size infer changes in the palaeo–hydrology (Sperazza et al. 2004). Duplicate pairs of the same sample were analysed with some samples re–run at a later stage to confirm results. Grain size categories determined by the laser diffraction include: sand fractions >63 µm, silt fractions from 2–63 µm and clay fractions <2 µm from a total of 64 samples. Grain size analysis was completed in conjunction with the ^{210}Pb dating for normalising the results, as changes in grain size can affect the absorption of unsupported ^{210}Pb.

Particle size analysis was completed using the ANSTO method ENV-l-007-001 (laser diffraction). The Malvern Mastersizer measures particle size diameters in the range of 0.05–880 μm and calculates average and medium grain sizes including the clay, silt and sand percentages (by volume). Textural descriptions of the lake sediments from grain size data is based on descriptions by Shephard (1954) and particle size subdivisions used are from the Wentworth size classes (Berkman 1995). Grain size distributions were calculated for selected intervals identified by the geological logging.

6.3.2.3 Conventional Lead (^{210}Pb) Dating

Lead (^{210}Pb) is a natural radioisotope with a half life of 22.26 years and has been used extensively for dating of recent sediments on a time scale of 100–200 years in many sedimentary environments (Oldfield and Appleby 1984). The ^{210}Pb and Radium-226 (^{226}Ra) isotopes accumulate in the lake sediments from a number of sources including transport from the catchment region to the lake, atmospheric fallout, indirect atmospheric fallout and radon decay in the water column. The source of ^{210}Pb from the eroded material is known as the ‘supported’ activity and the excess from atmospheric fallout, indirect atmospheric fallout and radon decay in the water column is known as the ‘unsupported’ ^{210}Pb, with the principal source from direct atmospheric fallout. It is the ‘unsupported’ ^{210}Pb that is used as it decays exponentially with time in accordance to its half life. The ‘supported’ ^{210}Pb activity is estimated from assay of the ^{226}Ra. The calculation of the Polonium-210 (^{210}Po) and ^{226}Ra activity in the samples enables sedimentation rates to be estimated. A detailed description on ^{210}Pb models for lake sediments is given by Oldfield and Appleby (1984).

Lead (^{210}Pb) dating was completed on the top section (~80 cm) of the core as it was considered these sediments should lie within the time scale of 100–200 years. Ten lake samples were selected from the following depths: 0–1 cm, 2–3 cm, 3–4, 5–6 cm, 10–11 cm, 15–16 cm, 21–21 cm, 40–41 cm, 60–61 cm and 80–81 cm. A description of the ^{210}Pb dating technique completed at ANSTO can be found in Appendix Four.

6.3.2.4 Geochemistry

Organic, carbonate and siliciclastic material percentages were derived by LOI in the Ecology Lab at USQ, similar to the techniques described in Heiri et al (2001). Nineteen core samples were submitted to ANSTO and the Institute for Environmental Research for multi–element geochemistry using the ICPAES for the standard elements Fe, Mn, Al, Ba, Ca, Mg, Sr, Na, K, Cu, Pb and Zn and a CNS analyser (Leco CNS2000) for C, N and S percentages, with results reported in mg/kg or percentages. Further analysis was conducted at the ALS Chemex laboratories in Brisbane using ICP–MS (ME-MS42 method) for Pb and Cd values. Details of the analytical techniques can be found in Appendix Five.

6.3.2.5 Carbon (^{14}C) Dating

After the results from the ^{210}Pb dating were obtained, radiocarbon (^{14}C) dating was completed on six samples selected at regular intervals throughout the core. Samples were analysed using Accelerator Mass Spectrometry (AMS) at ANSTO using the 10MV tandem accelerator ANTARES (Australian National Tandem Research Accelerator). Details on the methodology used at ANSTO and calculations of the conventional radiocarbon ages can be found in Fink et al (2004) and Stuiver and Polach (1977), respectively, whilst applications of radiocarbon dating can be found in Walker (2005). After the standard pre–treatment method for lake samples, there was insufficient carbon or free charcoal (<0.025%) in all six samples to allow standard radiocarbon dating. An alternative method for radiocarbon dating using the humic acid fraction in the samples was attempted and proved successful. Samples were chemically processed using a single acid step only (Taylor et al. 2005).

6.3.3 Regolith Mapping

A regolith map was constructed of the catchment and surrounding area of Lake Broadwater, to determine the major regolith units and identify the major sources of recent sedimentation into the lake. Regolith formation and landform evolution control geochemical dispersion (Smith 1996) and therefore the geochemistry of the sedimentation into the lake. Mapping of floodplains with potential hillslope/channel coupling enables external sources of sediment to be identified (Hooke 2003) whilst a variety of surface deposits and soils may not have formed under the same conditions that exist today (Pain and Oilier 1995).

The base map of the Lake Broadwater area was completed from aerial photographs (Dalby 9143 – 1:40,000; 2006) and the topographic map (sheet 9143 – 1:100,000; 1973). Regolith subdivisions were determined using a combination of aerial photos, orthophoto maps (Ducklo, Tipton and Broadwater Gully 1:25,000), regional geology map (Moreton Geology – 1:500,000; 1980), local geology (Dalby – 1:250,000) and field mapping. A similar classification of regolith types was developed for exploration activities in Western Australia (Anand et al. 1993) and in this study, have used a modified scheme after Sanders and Croker (1997). To assist in the interpretation of the surface regolith mapping, a number of drill hole logs were obtained from the groundwater database at the Department of Natural Resources and Water (Queensland) as well as exploration reports, providing some subsurface geological information.

6.4 RESULTS

6.4.1 Core Analyses from Lake Broadwater

6.4.1.1 Core Logging

The Lake Broadwater sediments are massive with no distinctive bedding or layering identified in any part of the core. The composition of the lake sediments (lithology), bulk density (g/cm^3), magnetic susceptibility (mT), recovery and moisture % and grain size parameters are shown in Figures 6.5 (a–g)and 6.6 (a–g).

The surface sample (0–1 cm) was composed of dry, brown (occasionally medium grey), fine to medium sands and minor silt with varying amounts of organic material

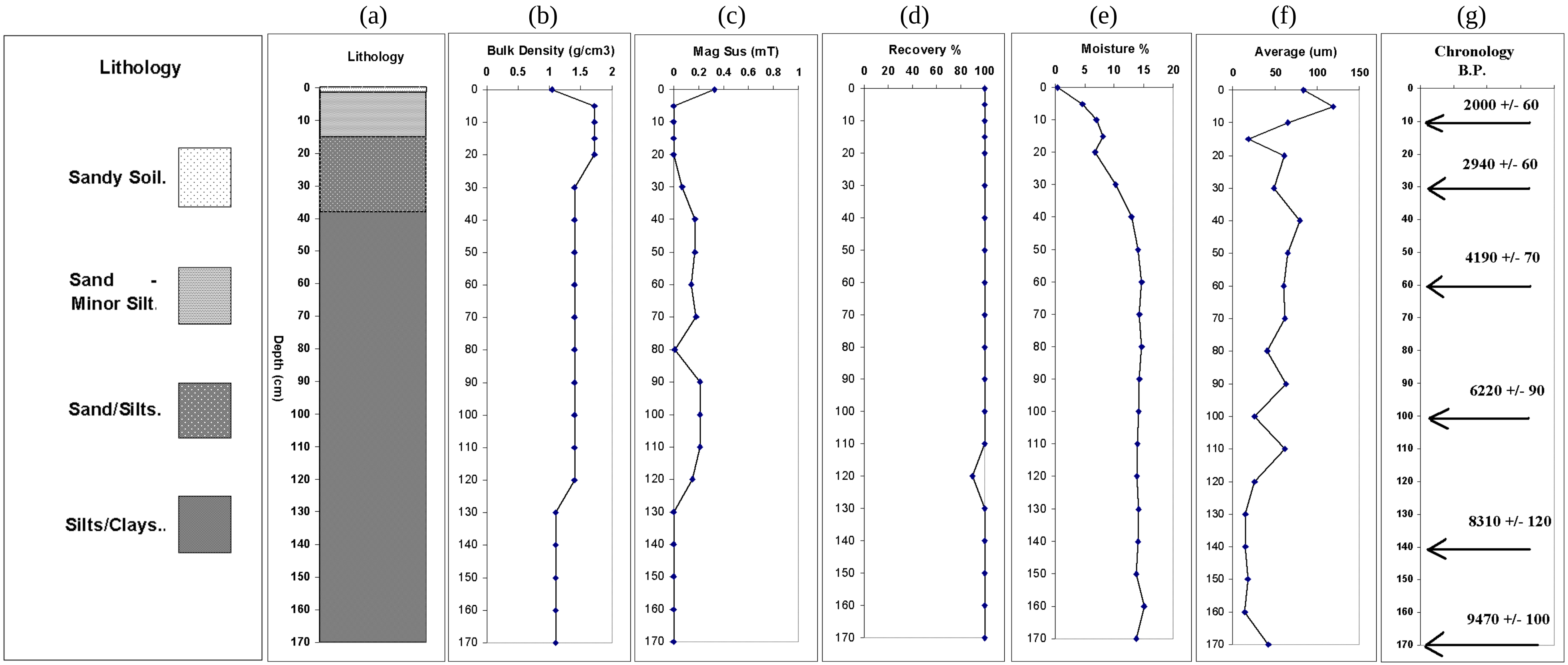

Figure 6.5 (a–g) Lake sediment variation in lithology, bulk density (g/cm^3), magnetic susceptibility (mT), recovery %, moisture %, average grain size (µm) and radiocarbon (^{14}C) chronology from Lake Broadwater, SE QLD.

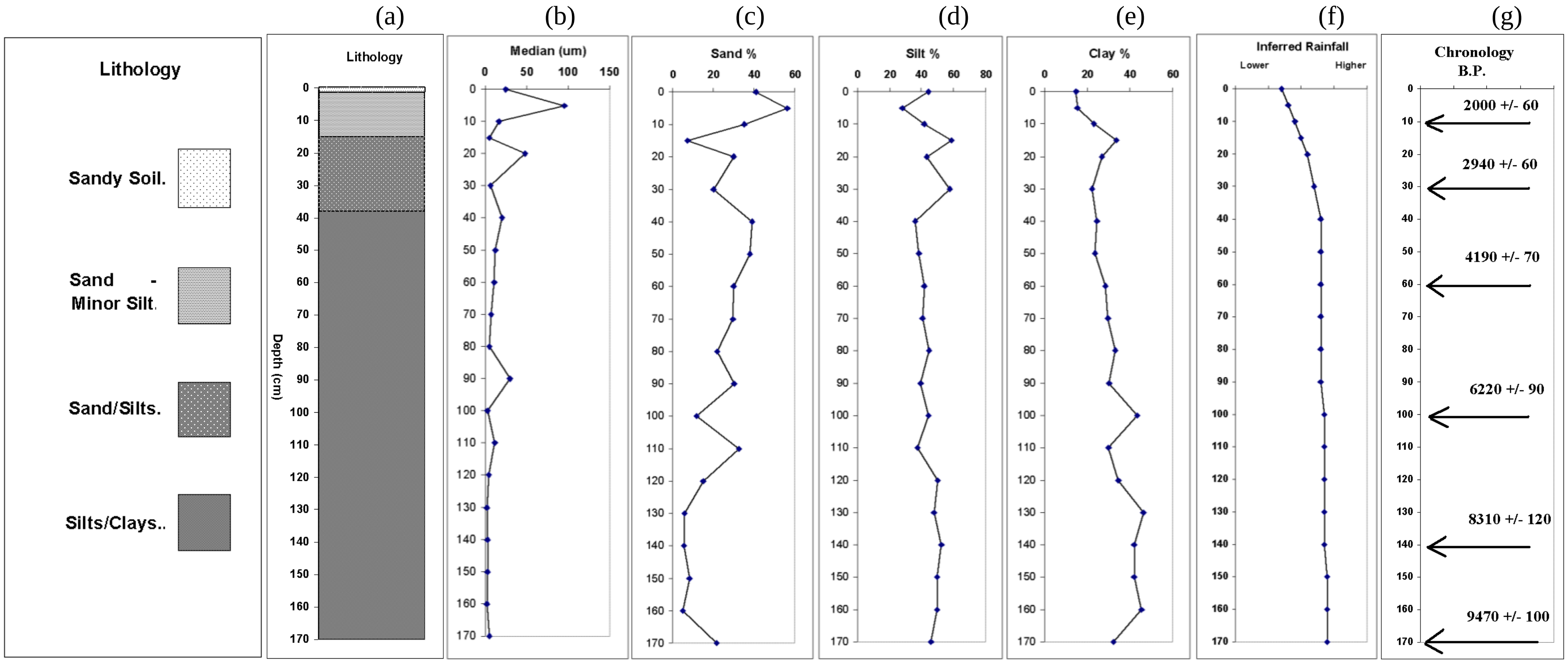

Figure 6.6 (a–g) Lake sediment variation in lithology, grain size parameters (µm), inferred rainfall changes and radiocarbon (^{14}C) chronology from Lake Broadwater, SE QLD.

(small leaf material). Small amounts of anhedral quartz grains were identified in the sample. The lake sediments collected from the interval 1–21 cm consisted of light brown (minor dark greys), coherent, fine grained sands and minor silts. Small desiccation cracks (<1 mm) and hairline roots with yellow–orange goethite staining indicates recent oxidation in this part of the core. There is a gradual decrease in the grain size from the surface, with dominantly fine sands above 15 cm and fine sands and minor silts in the interval from 15–21 cm.

The sediment texture from 21–121 cm is composed of fine sands, silts and clays. From 21–38 cm, the sediments are composed of moist, medium brown to dark grey, fine grained sands and silts with weak goethite staining. Below 38 cm, the sediments consisted of medium brown to dark grey, very fine grained silts and clays, with moderate and patchy pervasive goethite staining to 67 cm. Below 67 cm, mostly weak pervasive goethite occurs to 121 cm. Similar to the interval of 1–21 cm, there is a gradual decrease in grain size from 21–38 cm. The lake sediments from 121–171 cm consist of moist, medium brown to dark grey, very fine grained silts and clays (puggy clays) with no significant goethite staining. The changes in sand size identified at 15 cm and 38 cm are gradational. A summary of the lithology is shown in Figures 6.5(a) and 6.6(a).

Bulk density varied from 1.04 g/cm^3 for the unconsolidated sandy sediments at the surface, to 1.72 g/cm^3 at 1–21 cm. From 21–121cm, the average bulk density was 1.40 g/cm^3 and from 121–171 cm, 1.10 g/cm^3 (Figure 6.5b). Magnetic susceptibility of the lake sediments was generally low (< 0.4 mT) with the highest reading recorded from the surface sample (0.33 mT). Only very low magnetic susceptibility values of between 0.14–0.21 mT were detected in the rest of the core (Figure 6.5c). There was minimal core loss (<5%) between the three sections of core and hence the core recovery percentage was high (Figure 6.5d). Some compression of the lake sediments did occur in the intervals from 121–171 cm. The test for carbonates (using HCl 10%) did not show any visible reaction. Moisture content (%) varied from <1 % for the surface sample, increasing to >5% from 10 cm, >10 % from 30 cm and below 50 cm had a moisture content of ~14–15% (Figure 6.5e).

In summary, the lake sediments are composed of fine sands with minor silts between 0–15 cm, grading into fine sands and silts between 15–38 cm. Below 38 cm, the sediments are composed of silts and clays with small amounts of fine sand. The inferred rainfall trend based on the grain size is shown in Figure 6.6f.

6.4.1.2 Grain Size Analysis

Particle size analysis (ranging from 0.05–880 μm diameter) revealed a fining trend from the surface to the base of the core. From 0–30 cm, the average grain size in the core was quite variable (~20–100 μm), from 30–120 cm, it decreased to 10–20μm and below 120 cm it was less than 5 μm (Figures 6.5f and 6.6b). This was mirrored by sand, silt and clay percentages, clearly showing increasing sand towards the surface. The sand percentage varied from ~20% near the base of the core increasing to ~30% at ~100 cm and ~40–60% near the surface (Figure 6.6c). The silt component remained fairly consistent throughout the profile averaging ~40% but was more variable near the surface (Figure 6.6d). The clay percentage increased with depth, which averaged from ~20% near the surface to ~40% at the base (Figure 6.6e).

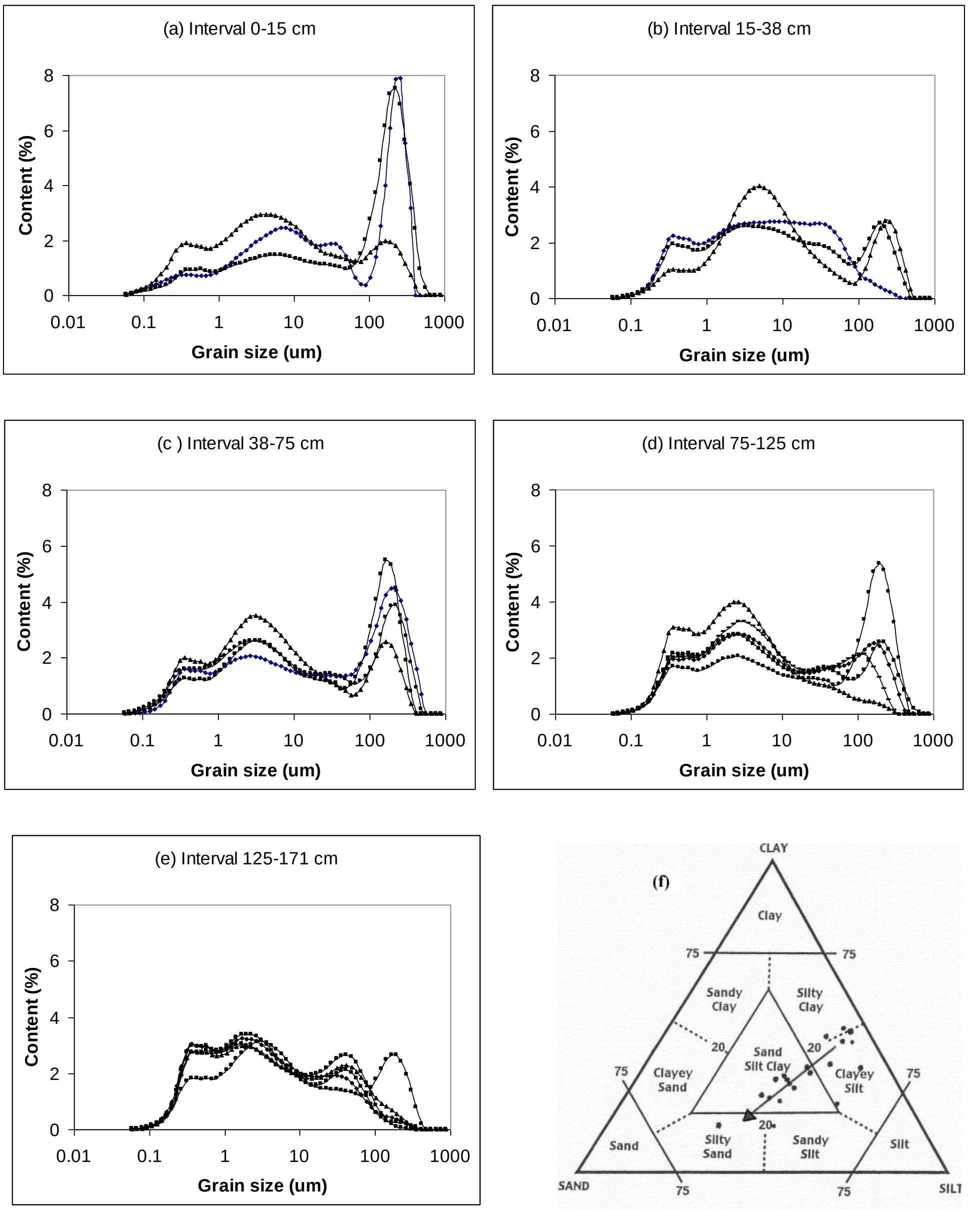

Figure 6.7 (a–f) Grain size characteristics for selected intervals from Lake Broadwater (a) 0–15 cm; (b) 15–38 cm, (c) 38–75 cm, (d) 75–125 cm, (e) 125–171 cm and (f) Ternary diagram of textural groups with arrow indicating grain size trend towards the surface.

Grain size distributions from five selected intervals in the core are shown in Figure 6.7, highlighting that the lake sediments are characterised by a poorly sorted, dominantly bimodal population of fine sands and silts/clays above 125 cm (Figure 6.7a–d) and a moderately sorted, mostly unimodal population of silts/clays below ~125 cm (Figure 6.7e). The samples above 125 cm show two peaks in grain size at

~3–5 μm (clay) and ~200 μm (fine sand). Below 125 cm, the peak in the clays is much broader (0.3–10 μm) and the peak at ~200 μm, generally much weaker. The ternary diagram for clastic dominated sediments (Figure 6.7f) reveals clayey silt or silty clay at the base of the core grades into sand/silt/clay at ~75 cm and silty sand at ~15 cm. The change in the grain size from the base of the core to the surface is indicated by the black arrow. Details of the grain size results from the Malvern Mastersizer and laser diffraction can be found in Appendix Six.

6.4.1.3 Multi–Element Geochemistry

The lithology and results of the bulk geochemistry analysis from the lake sediments are shown in Figures 6.8 (a–i), 6.9 (a–i) and 6.10 (a–h). All siliciclastic matter values were high throughout, with the lowest value in the surface sample of ~88%, increasing to 93–94% between 2–31 cm and decreasing to ~91% at 170–171 cm (Figure 6.8b). Carbonate matter values were low at 1–1.5% increasing to ~2% toward the base (Figure 6.8c). Organic matter values were highest in the surface sample (0–1 cm) at ~11%, decreasing to ~5–6% below 5 cm and increased slightly towards the base of the core (Figure 6.8d).

Multi–element geochemistry using ICPAES and ICP–MS analysed the concentrations of 13 elements from the sediments and results are shown in Figures 6.8–6.10. Both Fe and Mn values increased two or three times with depth compared to surface values (Figure 6.8e–f). Fe concentrations were relatively stable at 1–2% near the surface, increasing to ~4% at 150 cm. Mn concentrations were more variable with the surface sample at 74 ppm, decreasing to 52 ppm at 5–6 cm, increasing to 97

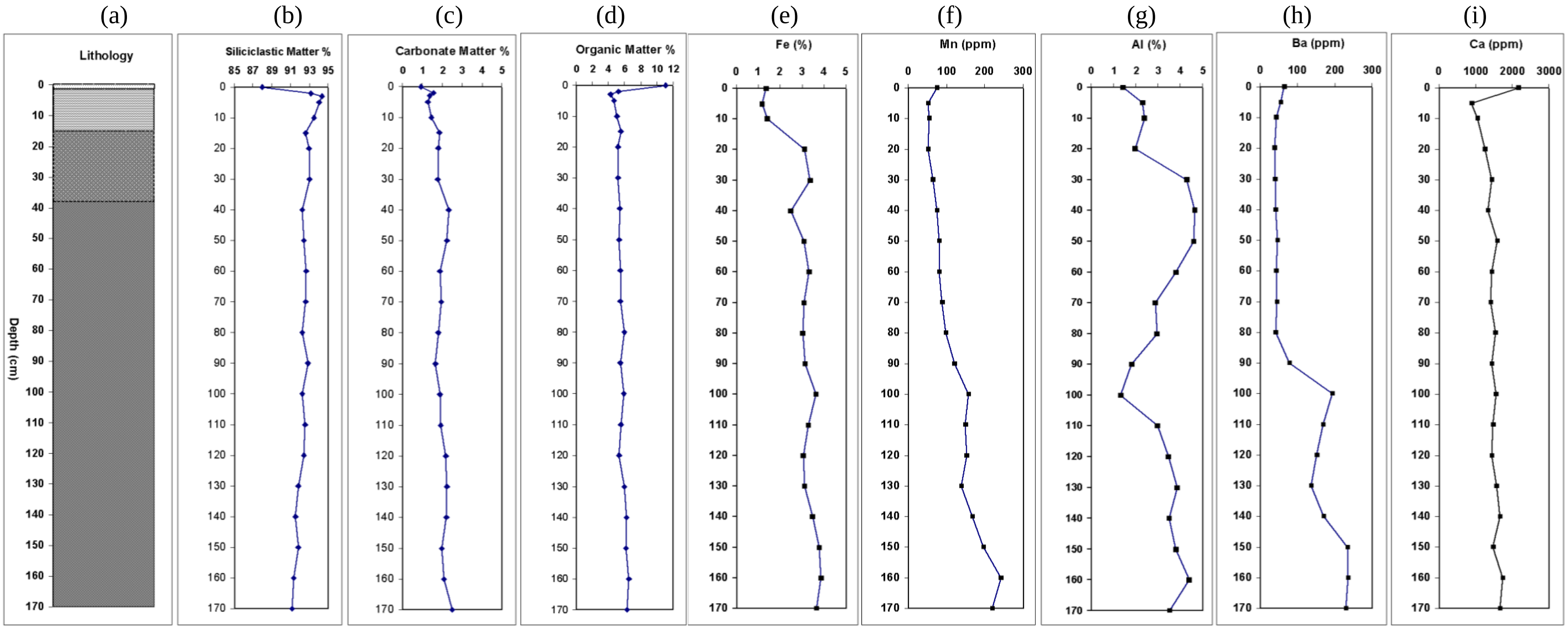

Figure 6.8 (a–i) Lake sediment variation in lithology and bulk and multi–element geochemistry from Lake Broadwater, SE QLD.

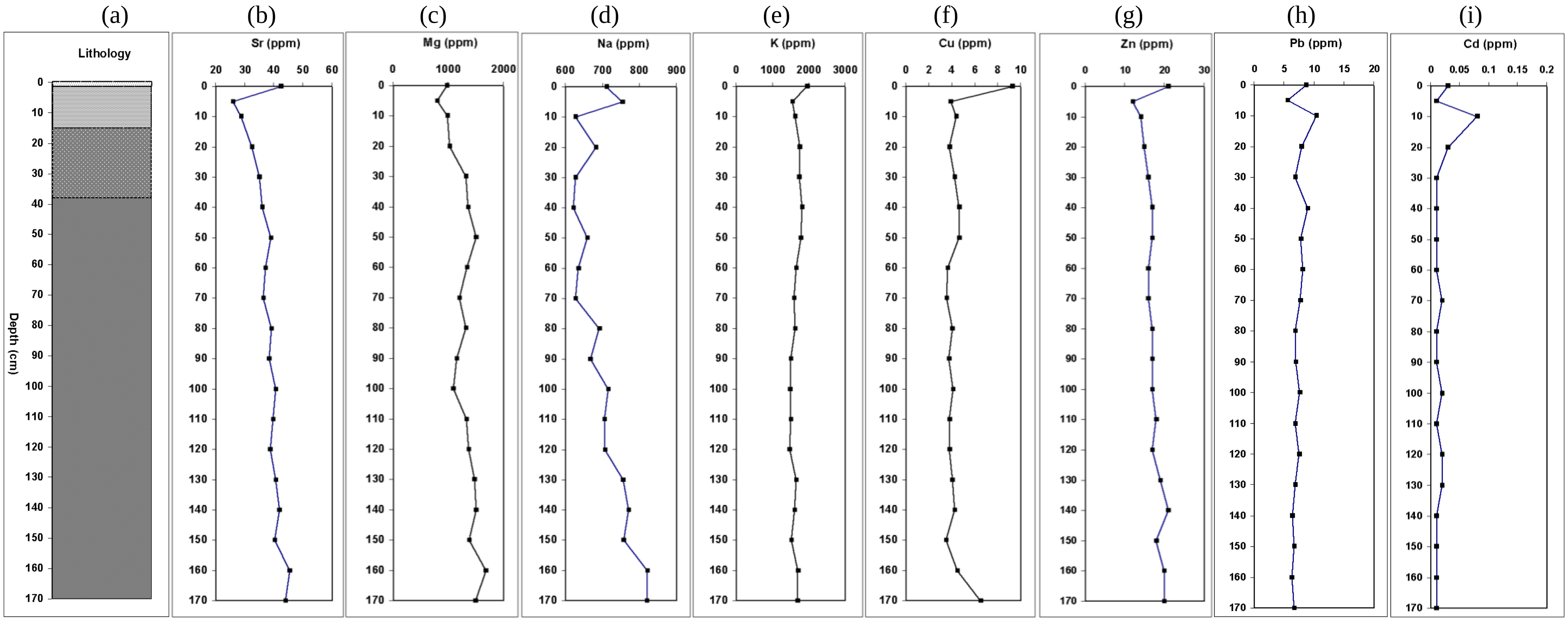

Figure 6.9 (a–i) Lake sediment variation in lithology and multi–element geochemistry from Lake Broadwater, SE QLD.

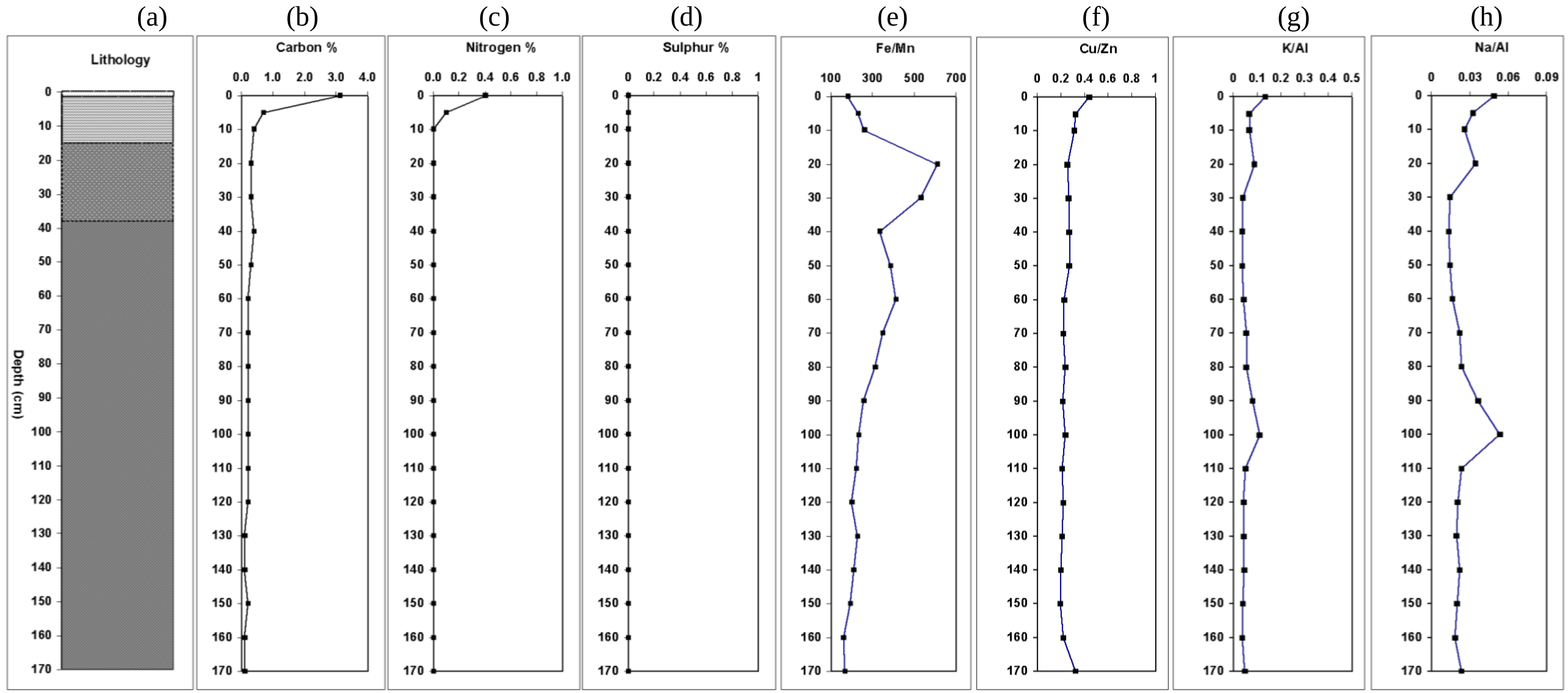

Figure 6.10 (a–h) Lake sediment variation in lithology and bulk and multi–element geochemistry ratios from Lake Broadwater, SE QLD

ppm at 80–81 cm and >200 ppm at 170–171 cm. The Al concentrations showed considerable variability with depth: low at 0–16 cm (1.5–2.5%), increasing at 40–51 cm (4–6%), decreasing at 90–101 cm (~1.5%) and increasing again from 120 cm (3.5–4.5%)(Figure 6.8g). The Ba concentrations remained nearly constant from the surface to 91 cm, averaging ~50 ppm and rising sharply to values >150 ppm from 90–101 cm and over 230 ppm from 150–171 cm (Figure 6.8h). The Ca trend from the surface to the end of the core is almost identical to the Sr trend. The Ca concentrations had a peak value at the surface of 2170 ppm, reducing to ~900 ppm at ~5cm, rising to ~1500 ppm in the rest of the core (Figure 6.8i). Sr concentrations are also highest in the surface sample with 53 ppm, reducing to ~30 ppm from 5–21 cm and than increasing slightly to 45 ppm at 170–171 cm (Figure 6.9b). Mg concentrations increase slightly down the profile with near surface samples at 0–11 cm averaging ~920 ppm, increasing to ~1500 ppm in the interval from 130–171 cm (Figure 6.9c). Na concentrations were more variable with the highest in the near surface interval (0–6 cm) averaging ~730 ppm, decreasing to ~640 ppm (10–71 cm) and increasing steadily to ~820 ppm (160–171 cm)(Figure 6.9d). K concentrations were quite stable, with a peak value of 1950 ppm at the surface and averaging ~1625 ppm with depth (Figure 6.9e). Cu concentrations decreased sharply from 9.28 ppm at the surface to 3.9 ppm at 5 cm and averaging ~4 ppm down the profile (Figure 6.9f). Zn concentrations showed a similar trend to Cu, with a peak value of 21 ppm at the surface, decreasing to ~13 ppm between 5–11 cm and increasing to 20 ppm at the base (Figure 6.9g). As Pb levels were below the detection limit (~30 ppm), samples were reanalysed using lower detection limits. The Pb values averaged ~7.4 ppm, ranging from 5.6–10.4 ppm, with a small peak at 10–11 cm, whilst a similar trend was found in the Cd values (Figure 6.9h). Cd values ranged from 0.01 to 0.08 ppm with a peak value at 10–11 cm (Figure 6.9i).

The CNS analyser was used to determine the C, N and S percentage values (Figure 6.10 b–d). The carbon concentration was highest in the surface sample at 3.1% decreasing rapidly to 0.7% at 5–6 cm before reaching ~0.1% at the base. N concentrations were only detectible in the surface sample with a value of 0.4%, while S concentrations were below the detection limit of 0.1% for all samples. Results from the geochemical analyses are shown in Appendix Five.

6.4.1.4 Lead (^{210}Pb) and Radiocarbon (^{14}C) Dating

A chronological framework is essential to any understanding of landscape development (Twidale and Campbell 1993). The eight samples from the Lake Broadwater core showed that the unsupported ^{210}Pb activity was highest (31.8 +/- 1.4 mBq/g) in the surface sample (0–1 cm) but there was very low unsupported ^{210}Pb activity (0.3 to 3.3 mBq/g) at depth (Figure 6.11). Two further samples analysed between 1–5 cm also showed very low unsupported ^{210}Pb activity (1.3–2.0 mBq/g). In order to determine the chronology of the sediment core, the activities of the unsupported ^{210}Pb should exhibit a gradual decay from the surface. Given that only the surface sample had significant unsupported ^{210}Pb, the sediment layers could not be dated using the ^{210}Pb dating method.

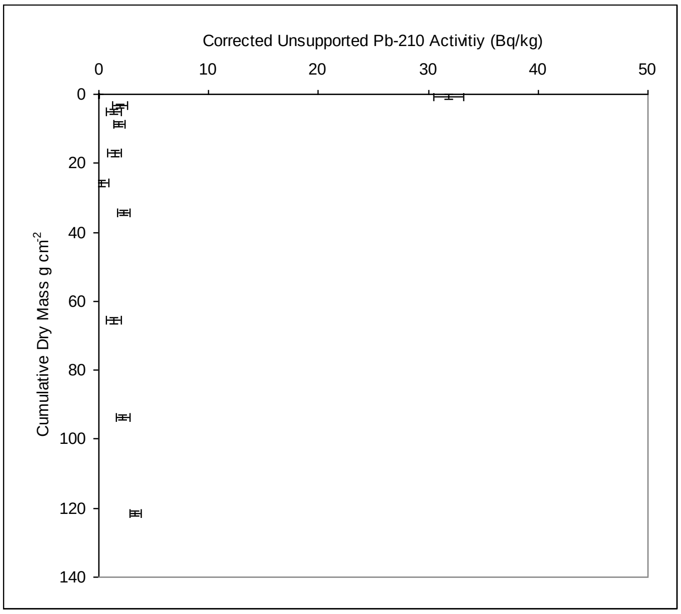

Figure 6.11 Unsupported lead (^{210}Pb) activity from lake sediments from Lake Broadwater. The only significant ^{210}Pb activity occurs in the top 0–1 cm. Analysis completed at Lucas Heights, Sydney.

Six lake samples from the core were submitted to ANSTO for radiocarbon (^{14}C) dating after the ^{210}Pb dating was unsuccessful. Table 6.1 presents results from the radiocarbon (^{14}C) dating on the humic acid fraction of the core. The sample at 10–11 cm had a conventional radiocarbon age of 2.00 +/-0.06 kyr B.P. (OZK333) whilst a maximum conventional radiocarbon age of 9.47 +/- 0.10 kyr B.P. (OZK338) was reported at 170–171 cm. The four remaining samples show the conventional radiocarbon ages steadily increased at ~1–2 kyr with increasing depth. This results in a fairly constant sedimentation rate averaging ~0.18 mm year^{-1} over the entire period (Figure 6.12). However, the interval from the surface to the first sample at 10–11 cm had a significantly slower sedimentation rate of ~0.05 mm year^{-1}, assuming the surface age represents zero years. A small graphic of the chronology is shown in Figures 6.5(g) and 6.6(g). Results of the radiocarbon (^{14}C) dating, ANSTO code numbers, percent Modern Carbon (pMC) and the $\delta(^{13}$C) per mil values reported from

ANSTO at Lucas Heights (Sydney) in March 2008 using the generous AINSE grant are shown in Appendix Four.

Table 6.1 Summary of the Radiocarbon (^{14}C) data from the Humic Acid Fraction from Lake Broadwater, Dalby, Queensland (March 2008).

Depth (cm)	**ANSTO code**	**$\delta\ ^{13}C$ %**	**% Modern Carbon**	**^{14}C age (yr B.P)**
10–11	OZK333	-18.8	77.96 ± 0.53	2000 ± 60
30–31	OZK334	-18.5	69.22 ± 0.50	2940 ± 60
60–61	OZK335	-18.9	59.37 ± 0.51	4190 ± 70
110–111	OZK336	-19.1	46.09 ± 0.47	6220 ± 90
140–141	OZK337	-21.9	35.53 ± 0.50	8310 ± 120
170–171	OZK338	-20.3	30.76 ± 0.35	9470 ± 100

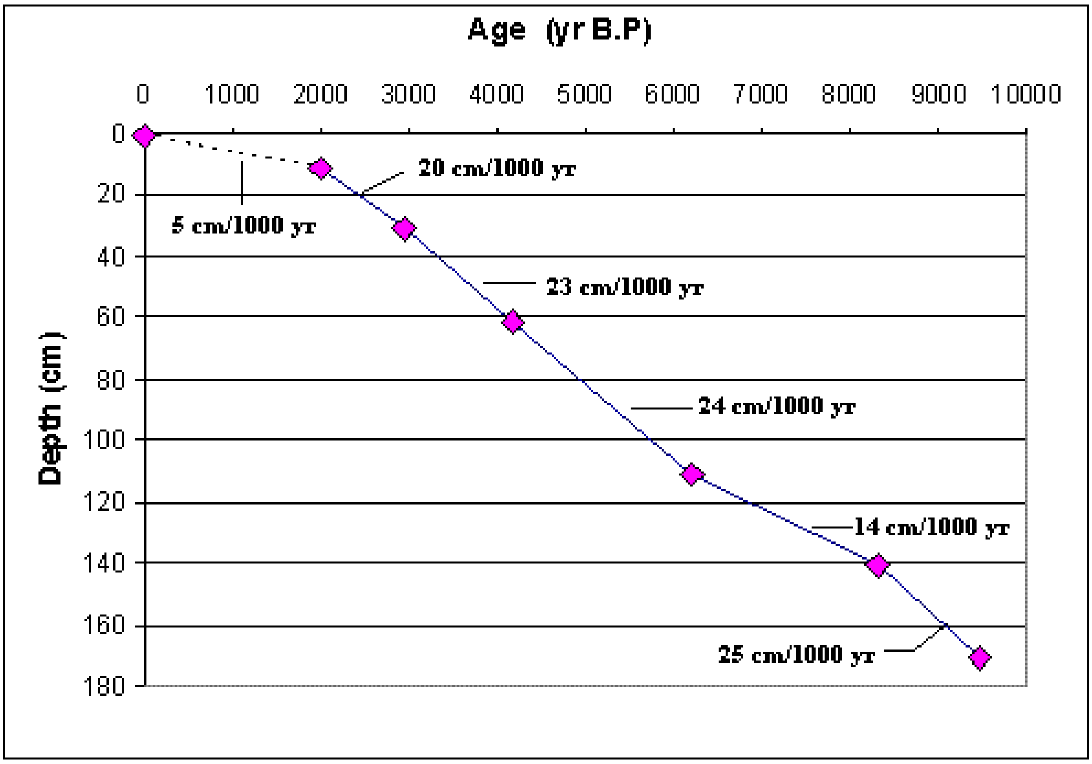

Figure 6.12 Age/depth curve for lake sediments from Lake Broadwater and the estimated sedimentation rates for each interval between the ^{14}C radiocarbon dates.

6.4.2 Regolith Mapping

6.4.2.1 Introduction

Mapping of the Lake Broadwater catchment and surrounding areas, identified two major regolith groups: depositional and erosional regimes (Figure 6.13). These formed during the Tertiary and have been modified by Quaternary and Holocene weathering processes. The depositional regime consists of four main units and covers ~75% of the region, whilst the erosional regime, which has been divided into three main regolith units, covers ~25% of the area (similar to Scott (1988) and Harris et al. (1999)). A detailed regolith map (~1:40,000) is shown in Map 1 (back cover or sleave pocket).

6.4.2.2 Surface Regolith Units

The most widespread depositional regolith unit is the alluvial sandy clay sediments (D_{SW}) which forms the broad sheet wash plains covering ~50% of the mapped area. These sediments surround Lake Broadwater on the west, south and east flanks. Lake Broadwater (D_{LB}) is distinct from all the other depositional units in the area as it is the only lake feature. Surrounding the lake on all sides is a low ridge (<10 m in height) of sandy lake deposits (D_{LL}) or sandy levees which formed during high water stands and by the entrapment of sand in the vegetation adjacent to the lake (Scott 1988). This sandy ridge is most prominent on aerial photographs. Further to the east and southeast, the area of rich agricultural land consisting of black and dark grey soil and clay alluvial deposits (D_{LS}) represents old palaeochannel deposits (Long Swamp) which previously joined the Condamine River further to the southeast.

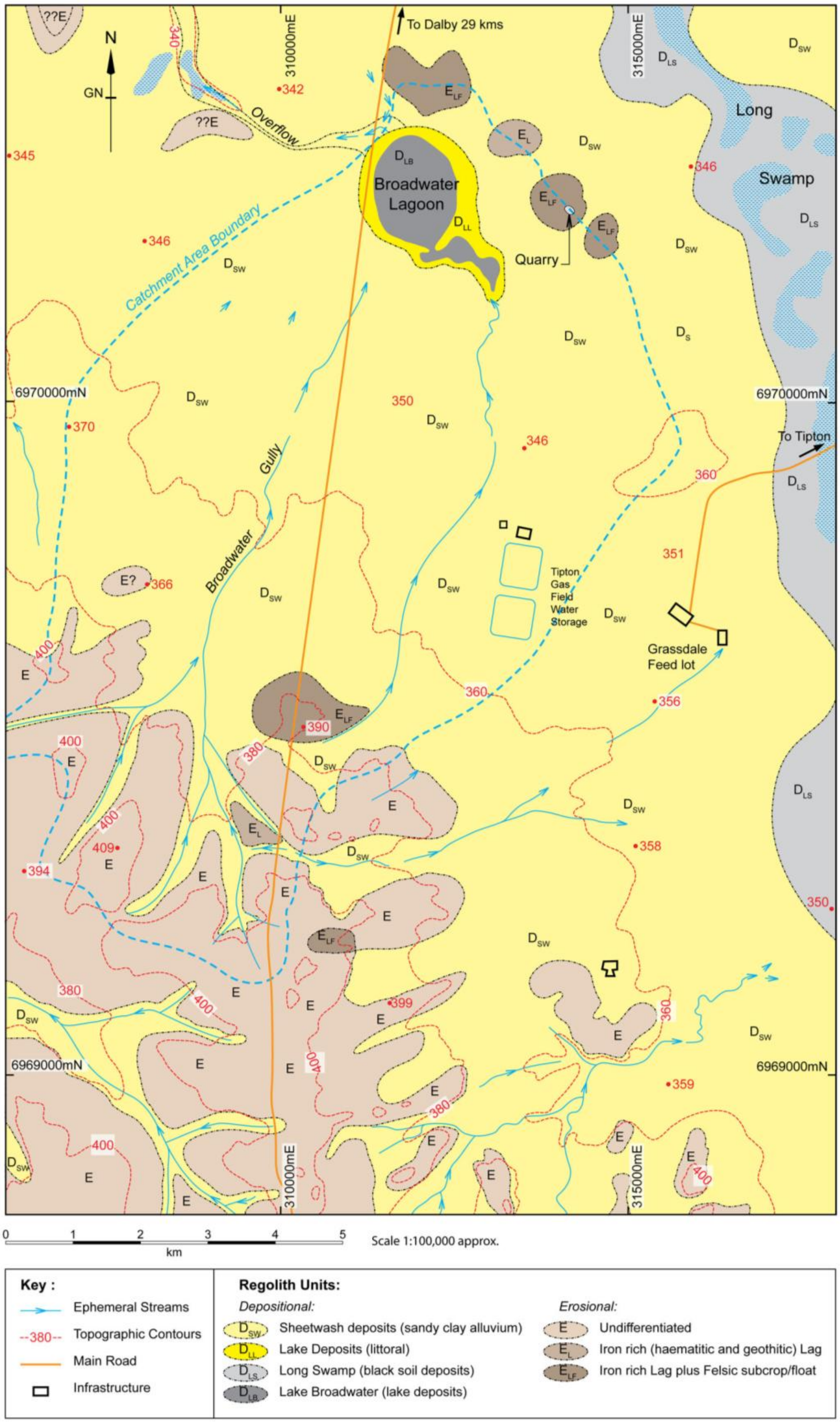

Figure 6.13 Regolith map of the Lake Broadwater area with regolith units, approximate rainfall catchment area and the Long Swamp palaeochannel. Digitised by USQ graphics.

The Long Swamp area currently drains to the northwest where it eventually joins Wilkie Creek and flows towards the Condamine River. Erosional units are exposed to the east, northeast and north of the lake and a wide area to the south on the low rises and hills. To the east of the lake, a small quarry has been excavated in the weathered felsic bedrock (sandstone). The sandstones in the quarry are generally strongly weathered and bleached with minor goethite staining on fractures. The bedrock is covered by a veneer of iron rich gravel (lag) with some felsic subcrop and float (E_{LF}). The other small rises (<10 m in height) in this area consist of E_{LF} or E_L (iron rich lag with mixed haematite and goethite). The region to the south of the lake on the low hills (<50 m in height) is composed of mostly undifferentiated iron rich lag and gravel deposits (E) with minor E_{LF} and E_L. Some outcrops of the weathered felsic bedrock occur with scattered float. This area to the south of Lake Broadwater is locally known as 'hard rock country', and is the main source for significant runoff during heavy rain into the lake.

6.4.2.3 Depth of Transported Cover

Data from geological logging from a number of drill holes completed for groundwater, oil and gas exploration around Lake Broadwater indicates a complex sequence of Tertiary transported alluvial sediments with alternating fine sands and clays up to 22 m deep. A layer of fine sand up to 4 m thick (forming the sandy levees around the lake) is underlain by brown clays and minor sand lenses. Thin basal fine white sand occurs in some drill holes overlying the Jurassic to Early Cretaceous weathered basement of sandstones. Although some uncertainty exists in the logs whether some of the sands or clays intercepted were weathered bedrock or part of the

Tertiary alluvial sequence, the depth of transported material suggests that the Lake Broadwater area was part of a much larger river system, probably linked to the Condamine River and the adjacent Long Swamp palaeochannel. Tertiary sediments on the alluvial plains of the Condamine River system are up to 100 m thick in the Dalby area and include the Pliocene Chinchilla Sand, Pleistocene stream and lake deposits and Quaternary stream deposits (Exon 1976).

6.5 DISCUSSION

Textural parameters provide important information on the provenance, mechanisms of transport, palaeoclimate and palaeohydrological conditions (Last and Smol 2001). Changes in the grain size from clastic dominated sediments from multiple provenances have been used to determine lake levels during the Holocene of Dali Lake in Inner Mongolia (Xiao et al. 2008). The Lake Broadwater core revealed an upward trend of coarsening grain sizes, from silts and clays to sands and minor silts, especially near ~38 cm and ~15 cm. Grain size analyses conducted by laser diffraction on the Lake Broadwater lacustrine sediments were consistent with grain sizes revealed in the core by logging, although they did not pick up the increase in sand sizes above about 38 cm and were more variable than logged in the core. They also show increasing average and median grain size towards the surface and a change from a unimodal to bimodal population distribution. A number of other studies using laser diffraction have shown grain sizes can be overestimated by a number of size classes (Syvitski 1991; McCave et al. 2006; Konert and Vandenberghe 2008). The sediments analyzed by the laser diffraction in this study may also have overestimated the grain sizes in some samples. Fluvial sediments are composed generally of two components, a saltation–dominated sand fraction and a silt and clay component held in continuous suspension and deposited on floodplains by overbank flooding (Blatt et al. 1980). The coarser sand fractions are more likely to be derived from local sources and the latter from more distal sources such as the Condamine River. However, a small contribution of aeolian sand into the lake is also possible.

Bulk density values are highly dependent on soil conditions during sampling (Sumner 2000). Consequently, the low moisture contents of the silts and clays may have partially contributed to the low bulk density values due to the low ground water table. The bulk densities of the core are quite variable, however values for the interval 1–21 cm are consistent with those from sandy loams and the lower bulk densities at the end of the core for silts and clays (Lal 2002).

The magnetic susceptibility of the core is generally very low partly due to insufficient quantities of sediment from the core to obtain an accurate measurement. The very low magnetic susceptibility measurements indicate the erosional Fe rich lags near the lake to the north and east and much further south, have not contributed significant amounts of material into the lake. Goethite staining indicates recent oxidation of the Fe in the lake sediments. However, a local source of weak magnetite/maghemite generated in the lake sediments in situ by magnetotactic bacteria cannot be discounted (Oldfield 2007).

The geochemistry of the lake samples represents the broad mineral composition of the lake sediments. The increasing percentage of siliciclastic material and decreasing clay percentage toward the surface of the core represents increasing sand and decreasing clay components, respectively. The relatively low Al values (2%) in the top 20 cm of core indicates lower clay values with more sand; whereas higher Al values (3–4%) lower in the profile, indicate a higher percentage of clay minerals. The positive correlation between Fe and Mn values and the abrupt change in the Fe/Mn ratio (Figure 6.10e) between 10–40 cm may reflect changes in the redox conditions during sedimentation (Wersin et al. 1991), or the recent oxidation indicated by goethite staining as the lake surface dried. The drying of the lake surface may also have concentrated the Ca, Sr, K and Na values in the surface sample. Increasing Na values with depth indicates increasing groundwater salinity with depth and this is confirmed by the water testing from boreholes (Na and Cl values >1000 ppm) adjacent to the lake. The very low or below detection limit of many samples with C% and N% levels prevented the C/N ratios being determined and hence the sources of organic matter being identified (Meyers 1994; Last and Smol 2001).

The high Cu and Zn levels in the surface sample (0–1 cm) may represent an anthropogenic signal in the lake sediments. The Cu/Zn ratio is highest at the surface and base of the core (Figure 6.10f). A weaker peak occurs in the Pb and Cd values and the strong peak of these two elements at 10–11 cm is unexplained. Trends in the K/Al and Na/Al ratios (Figure 6.10g–h) can distinguish whether the heavy metals are anthropogenic or derived from the catchment area (Augustinus et al. 2005; Tylmann 2005). A small peak in these ratios at the surface confirms an anthropogenic source is likely. However, the cause of the peak in the K/Al and Na/Al ratios at 100–101 cm is not known. Local anthropogenic sources may account for these heavy metals from agricultural activities in parts of the catchment and/or recreational boating on the lake during higher water levels. Recent anthropogenic activities have explained anomalous heavy metals values recorded from other lakes (Lottermoser et al. 1993; Augustinus et al. 2005; Chirinos et al. 2005; Tylmann 2005) with high Cu and Zn values attributed to nearby industrial activity at Lake Illawarra (Payne et al. 1996). High Cu values have also been reported from atmospheric fallout (Plessow et al. 2001).

The regolith mapping of the catchment area around Lake Broadwater identified a major source for some of the sands being deposited around and into the lake. The erosional units covering much of the catchment area south of Lake Broadwater contain exposed weathered felsic outcrop/subcrop of sandstones and other siliceous sediments. Sands eroded from these sources have been dispersed onto the plains adjacent to these hills, whilst the iron rich lag has remained mostly restricted adjacent to the low hills. The proximity, size and drainage patterns of Lake Broadwater and the Long Swamp palaeochannel indicate they most likely evolved from the same fluvial–alluvial system that formed the Condamine River basin to the east and southeast (Figures 6.4 and Figure 6.13). The present catchment area of Lake Broadwater is dominated by the low hills and rises (<50 m high) south of the lake and it is now isolated from the Long Swamp palaeochannel by a low rise (<10 m high) of sandy alluvium.

Sedimentation in Lake Broadwater appears to have been continuous and mostly undisturbed for the entire period of deposition of ~10,000 years. Radiocarbon (^{14}C) dating of Lake Broadwater sediments shows a relatively uniform rate of sedimentation dating back to the early Holocene (Figure 6.12). Constant sedimentation from 9.47 ± 0.10 kyr B.P. to 2.00 ± 0.60 kyr B.P. suggests that the lake has undergone minimal change during the Holocene, whilst establishing a unique and complex biodiversity of flora and fauna around the lake (Scott 1988). The fine grained nature of the sediments may have limited the movement of the humic acids in the profile, although this cannot be discounted (Tuniz 2001) and some caution on the precise age of the lake sediments is required (Oswald et al. 2005; Blaauw et al. 2007). Bioturbation may have mixed sediments locally, however the constant sedimentation rates would suggest this has had a minimal impact (Olsson 1991). Extrapolation of the sedimentation rates between radiocarbon (^{14}C) ages indicates significant palaeoenvironmental changes have occurred at ~3.2 kyr B.P (38 cm) and ~2.2 kyr B.P (15 cm), leading to increases in grain sizes.

The changes in grain size indicate some variation in the sedimentary source feeding into Lake Broadwater. Increasing grain size and lower lake levels have been attributed to lower rainfall in an arid zone of China (Wünnemann et al. 2006) and grain size distributions (silt–size percentages and median grain size) reflecting inwashing and variations in precipitation rates, have been recorded from a small lake in Inner Mongolia (Jin et al. 2006). There may also be a small contribution from Australian aeolian dust that has been deposited into the lake (McTainsh and Lynch 1996; McTainsh and Strong 2007), especially above ~10 cm, where the estimated sedimentation rate is much lower. Aeolian–fluvial interactions have been shown to be important drivers of sedimentation characteristics in the Cooper Creek over a much longer time scales, and in regions where significant rainfall changes have occurred in the past (Maroulis et al. 2007). However, no significant aeolian deposits are known in the Lake Broadwater region.

Although river patterns and their associated deposits are complex (Twidale 2004), the following synthesis accounts for the sedimentation characteristics identified at Lake Broadwater during the Holocene. The lake sediments show a decrease in the percentage of clays and an increase in the percentage of sand, especially at about 38 cm (~3.2 kyr B.P.) and 15 cm (~2.2 kyr B.P.) and a slow change from a dominantly unimodal to bimodal grain size distribution during the ~10 kyrs of sedimentation. This may indicate the provenance of the sediments has evolved from a distal to a proximal source. The main source of the silts and clays in Lake Broadwater below ~38 cm are likely to be the Condamine River and the Long Swamp palaeochannel, being deposited/infilled from suspension/overbank flows. Sediments associated with the Condamine floodplain also have a dominantly unimodal silt and clay dominated grain size (Harris et al. 1999). Lake Broadwater was probably connected to the Long Swamp palaeochannel from the southeast (Figure 6.13) via a channel which has now been covered by sandy sediments. A change to lower rainfall with less dense vegetation would have initiated more local sediment to become transported in and around the lake (via traction and saltation), with less flooding and floodplain sedimentation from the Condamine River reaching Lake Broadwater. Hence a change from wetter conditions, higher lake levels and fine grained sedimentation up to ~3.2 kyr B.P. gradually changed to drier conditions, with lower lake levels and coarser grained sedimentation from ~3.2 kyr B.P., with further rainfall decreases at ~2.2 kyr B.P. is envisaged. Constant sedimentation rates indicate the locally derived sediments made up the balance of input into the lake, while sediments from Long Swamp palaeochannel were slowly reduced. It is possible that lower sedimentation rates from ~10 cm (~2.0 kyr B.P.) represents the final cessation of sediment input from the Long Swamp palaeochannel and this would have led to greater fluctuations in lake levels, with marginal sediments and sands washing into the lake more frequently. Alternatively, the eastward migration of the Condamine River to its present location may have also reduced muddy overbank and flood plain deposits in the Long Swamp and Lake Broadwater area, eventually forming the present drainage and landscape. A combination of these factors may contribute to the overall sedimentation characteristics found at Lake Broadwater.

Although the core from Lake Broadwater covers a period of ~10 kyr B.P., the evolution of the Lake Broadwater and the Long Swamp palaeochannel related to the Condamine River are likely to be much older, forming during glacial times (Williams et al. 1998) or earlier, similar to other long–lived alluvial systems in Australia (Page and Nanson 2006; Nanson et al. 2008). The sedimentation characteristics of the Condamine River are similar to other regions in the Murray–Darling Basin, where transport of high sediments loads and low channel slopes leads to the dominance of aggradation processes and river avulsion (Page et al. 2003; Page and Nanson 2006).

The results from this study indicate a change from a higher to lower rainfall regime and more arid conditions at ~3.2 kyr B.P. This is consistent with other Holocene changes identified from a number of lakes and proxy records from eastern Australia (Kershaw 1995; Gagan et al. 2004; Harle et al. 2005; Donders et al. 2007). Modern fluvial activity started at 5–9 kyr B.P. on the Murray River system (Ogden et al. 2001) and pollen analysis from lakes in the lower section of the Darling River, downstream from the Condamine River and Lake Broadwater, indicates late Holocene aridity from ~4.0 kyr B.P. (Cupper 2005). A mid–late Holocene arid phase at ~4.7–3.4 kyr B.P. has been identified from nearby North Stradbroke Island, where dust deposition peaks are second only to those seen during the last glacial maximum (McGowan et al. 2008; Petherick et al. 2008). A decline in rainfall from Fraser Island from ~4 kyr B.P. was interpreted from palynological records (Longmore 1997) and more recently at ~3 kyr B.P. (Donders et al. 2006). Three periods reflecting major changes in ENSO have occurred during the post glacial transition and the Holocene. The three intervals being from 17–9 kyr B.P., 9–5 kyr B.P. and 5 kyr B.P. to the present have been identified from charcoal abundances, determined from 10 lake and wetland records adjacent to the Indo–Pacific Warm Pool (Gagan et al. 2004). Higher charcoal abundances in the intervals from 17–9 kyr B.P. and 5 kyr B.P. to the present reflect higher precipitation variability and lower charcoal abundances in the interval from 9–5 kyr B.P., with lower rainfall variability. Further, terrestrial records indicate a marked increase in the ENSO activity ~3 kyr ago (Gagan et al. 2004). The results from this study show a marked change in the nature of sedimentation at ~3.2 kyr B.P. and 2.2 kyr B.P. This is consistent with the evolution of the ENSO periodicities described by Gagan et al (2004) and indicates ENSO may have been an important factor in determining rainfall variability in the SE QLD region for much of the mid–late Holocene.

In the future, a simulation of the Holocene climate over the SE QLD region using a regional climate model, such as the CCAM model used in Chapter Five would provide a longer term record of climate variability and climate change in the region. This would have allowed a broad comparison to be made between the regional modelling and palaeo analysis completed from Lake Broadwater and also with other palaeoclimate records from SE QLD and adjacent regions. Pollen analysis from the sediments at Lake Broadwater would also be another source of palaeoenvironmental information which would supplement the data collected and establish a detailed record of flora and vegetation changes in the catchment during the Holocene. Other potential sources for proxy records exist in the region, such as tree rings (red cedars in the Springbrook, Lamington and Border Ranges National Parks) and sediments from permanent or semi–permanent wetlands such as Lake Clarendon Yallamundi lagoon and the Pelican lagoons (nature reserves in Charlies Creek north of Chinchilla). Early instrumental records from the 19th century from Sydney and the Dutch East Indies (Indonesia) may also shed light on some of the large scale atmospheric circulation changes over Queensland and eastern Australia at this time.

In summary, a combination of data from stratigraphy, grain size, geochemistry and regolith mapping combined with radiocarbon (^{14}C) dating has enabled a detailed Holocene palaeoenvironmental record to be established for Lake Broadwater. Sediment accumulation rates of 15–25 cm/kyr in the lake are remarkably consistent for most of the profile, except from ~10 cm to the surface, where the accumulation rate is lower. The relatively stable grain size from ~9 kyr B.P. (171 cm) to ~3.2 kyr B.P. (38 cm) indicates a relatively stable palaeoclimate regime, with higher rainfall and sedimentation at Lake Broadwater derived from fluvial sources such as the floodplains of the Condamine River. An increase in grain size at ~38 cm (~3.2 kyr B.P.) points to a change in the palaeoenvironmental conditions with lower regional rainfall, reduced deposition of fines by less frequent flood waters from the Condamine River and more localised rainfall/runoff and reworking of localised sediments. This pattern of Lake Broadwater sedimentary processes, especially since ~2.2 kyr B.P., appears to have continued through to the present day. The sedimentary changes revealed in the core between ~3.2–2.2 kyr B.P. most likely reflect a significant decrease in rainfall with the onset of stronger El Niño conditions resulting in vegetation changes, with eucalypt expansion and rainforest decline in this region, which has been recorded elsewhere in eastern Australia at this time (Kershaw 1995; Genever et al. 2003; Cupper 2005). The onset of modern Holocene ENSO periodicities at ~5 kyr B.P. with an abrupt increase in ENSO magnitude ~3 kyr B.P. is consistent with the results described from this study (Gagan et al. 2004).

CHAPTER 7 : CONCLUSIONS

7.1 IPCC–AR4 MODELS AND RAINFALL PROJECTIONS

In this study, a number of methodologies using data from the BoM, NCEP reanalysis, the SAM index and 21 IPCC–AR4 GCMs have been used to analyse the rainfall decline over NEA and SE QLD during the 20th and beginning of the 21st century. An analysis of the rainfall trends shows significant rainfall declines of 20–30% have already occurred over large regions of central and southern Queensland in the austral summer and autumn since ~1951. This study has identified the subtropical ridge and the SAM as the key drivers of the MSLP changes in the NEA region and the MSLP increases are likely to be responsible for some or most of the rainfall decline that has occurred during the second half of the 20th century and the start of the 21st century. Some key findings from this study include:

- Rainfall declines over much of Queensland have now reached 20–30% and higher (40–50%) in coastal regions between Mackay and Townsville during the period from 1951–2007;
- All seasons show an increase in the MSLP over NEA, which is strongest in coastal and the SE QLD region in the austral autumn and winter;
- The changes in the MSLP and rainfall are negatively correlated, with higher MSLP leads to lower rainfall over most of NEA, with the highest correlations and number of stations in the austral summer, autumn and spring over coastal regions;

- The increasing MSLP over much of NEA and SE QLD has been caused by the strengthening and expansion of the subtropical ridge into the tropics;
- The increasing MSLP associated with the subtropical ridge appears to be directly linked (correlated) to the positive polarity of the SAM in at least the austral winter and for the annual period in Queensland;
- The increase in the MSLP over ~50 years over the SE QLD region is now equal to or greater than the interannual variability exerted by ENSO and ;
- As the subtropical ridge is an integral part of the Hadley circulation, the changes in the subtropical ridge in the Queensland region indicate likely changes have also occurred in the atmospheric circulation dynamics of the Hadley circulation.

Although other factors, such as the changes in the land cover maybe contributing to the rainfall decline over SE QLD, the coherent trend in the SAM and increases in the MSLP have been shown to contribute to the major rainfall declines over southern Australia during the second half of the 20th century (Nicholls 2009). As the changes in the SAM are related to anthropogenic activities, such as ozone depletion and the rising levels of greenhouse gases, some of the rainfall declines across NEA and SE QLD are likely the result of climate change and not solely from natural variability. Anthropogenic activities are now believed to be the main causes of the rainfall decline in southern and southwestern Western Australia, so this should be of no surprise for SE QLD region and other regions in Queensland.

By using a number of GCMs from the IPCC–AR4 and the A2 emission scenario, 21st century projections point to further rainfall declines over most of NEA and SE QLD.

Key points shown by these models and the multi–model ensemble mean for the 21st century include:

- The rainfall declines that have occurred in the second half of the 20th century and the start of the 21st century are likely to continue and intensify, especially in the second half of the 21st century over southern and SE QLD and dominate all seasons;
- Rainfall projections from multi–model ensembles indicate rainfall declines between 2–6% by 2031–2051 and 6–12% by 2081–2100 over much of the Queensland region, except the far north of the Cape York Peninsula, which shows small rainfall increases;
- Increases in the MSLP in the mid–latitudes, coastal regions of Queensland and the Coral Sea will continue due to the positive phase of SAM, especially in the second half of the 21st century and
- The broadening and strengthening of the subtropical ridge identified from observations during the second half of the 20th century and the start of the 21st century is likely to continue due to the influence of the SAM, with changes in the Hadley circulation likely to further reinforce the lower rainfall regime over southern and SE QLD.

The decline in rainfall since 2000 over most regions in Queensland (except the Cape York Peninsula and the Mount Isa area) including SE QLD, such as at Toowoomba, have already reached 10–20%, higher (30–40%) in southwestern Queensland and the Mackay region, compared to the 1961–1990 mean rainfall. It is not possible currently to predict with certainty whether the rainfall declines during the start of the 21st century are likely to be exceeded during the rest of the century. Further research, as well as more detailed studies using higher resolution models, will be required to improve the confidence in future rainfall projections.

The likely continuation of rainfall declines over the SE QLD region and many other areas of southern and central Queensland will have major consequences on the population, especially agricultural activities and the regional flora and fauna. Lower rainfall will produce a non–linear response to runoff, similar to other regions in the Murray–Darling Basin and southwestern Western Australia, with less water available for harvesting, irrigation, potable water supplies and environmental flows. This will have direct impacts on many water users, including more stringent water restrictions on water uses, higher costs and longer periods with lower water allocations due to longer droughts. Less noticeable impacts will be on groundwater resources (such as the Great Artesian Basin), where recharge events will have lower volumes with longer time intervals between recharge events. Although most human activities can adapt and mitigate against these changes (Bouma et al. 1996; Pittock 2003; BoM 2004), the impacts on forests, bushlands and pasture will be large (McKeon et al. 2004), with increased stresses due to longer droughts, more frequent severe fire seasons and longer periods of higher temperatures and heat stress. Costs to the rural and farming communities are likely to be substantial, with significant economic losses expected (BoM 2004). The sooner the change to a more sustainable future is initiated within the community and government, the less severe the impacts and adaption costs are likely to be due to climate change in Queensland and throughout Australia (Tate 2004; Government 2005).

7.2 ATTRIBUTIONS OF RAINFALL CHANGES OVER QUEENSLAND

In this study, the rainfall declines and increases in the MSLP that have occurred over much of NEA during the 20th and the early part of the 21st century are likely to continue well into the 21st century, especially over coastal regions and the Coral Sea. The MSLP changes are part of much larger changes in the Southern Hemisphere atmospheric circulation, with increases in the MSLP over the mid–latitudes related to the subtropical ridge and decreases in MSLP over the South Polar Region related to the continued positive phase of the SAM. The increase in the MSLP associated with the location and strength of the subtropical ridge in the mid–latitudes of eastern Australian may play an increasing role in the climate and rainfall dynamics over southern Queensland and other parts of Australia. IPCC–AR4 GCMs show these circulation changes are projected to continue well into the 21st century, with rising greenhouses gases becoming the main driver of the SAM after ozone levels have potentially recovered. The changes in the tropical and Hadley circulations may also contribute to the increasing MSLP associated with the subtropical ridge. However, the relative proportion of increasing MSLP that can be directly attributed to the Hadley circulation is unclear, and further research is required in this area to identify its significance for SE QLD and other mid–latitude regions in Australia.

7.3 PALAEOCLIMATE RECONSTRUCTION

The palaeoclimate reconstruction completed at Lake Broadwater indicates the upper regions of the Murray–Darling Basin region have experienced a natural change to drier conditions and a lower rainfall regime over the past few thousand years. This suggests that the flora and fauna may have already begun to adapt to lower rainfall and natural climate change over the past few millennia. These results are consistent with other Holocene palaeoclimate records developed in eastern Australia from other lake sediments and proxy records, indicating the approximate onset of modern day ENSO variability started ~3.2 kyr B.P. The rainfall declines which have occurred since ~1950, and have intensified over the last ten years or so, are likely to have placed further stress on the regions biodiversity. Further projected decreases in rainfall expected in the 21st century, with the likelihood of more frequent droughts, may exceed those seen during the last few thousand years during the late Holocene.

Further potential exists at the Lake Broadwater Conservation Park for palynology studies and coring below 1.71 m on the lake sediments, to identify impacts and changes to the local flora during the Holocene and potentially extend the record into the late Pleistocene, past the last glacial maximum (~15,000 B.P.). This would facilitate comparisons to much longer palaeoclimate records established at other sites, such as at Fraser Island and the Atherton Tablelands.

7.4 FUTURE DIRECTIONS

As the long–term water deficits continue over much of southern Queensland and much of eastern Australia (including the Murray–Darling Basin), there has been no comprehensive study on the type of synoptic features that have led to the rainfall decline over southern and SE QLD in the austral summer and autumn seasons. It is a high priority to identify which type of synoptic features, including the frequency and intensity, have contributed to the rainfall decline and have been affected by the regional increase in the MSLP. Once some of these synoptic features have been identified, GCMs can be examined to see how well they are simulated in both the 20^{th} and 21^{st} century simulations, and used to validate and increase the confidence in future climate projections. In the austral spring season, small increases in rainfall were identified over most of NEA during 1951–2000, with increasing MSLP. What has been the cause of this rainfall increase? Has it been caused by an increase in austral spring thunderstorm activity, such as observed in November 2008 over SE QLD? Are these rainfall trends likely to continue into the 21^{st} century or will they weaken as the positive phase of SAM continues, with further increases in the MSLP? It is unlikely the rainfall response to the increase in the MSLP over the Queensland regions is linear and hence further increases in MSLP may led to greater rainfall decreases than estimated in this study. Global warming will also increase the water holding capacity of the atmosphere producing higher intensity rainfall events, which may temporarily offset some of the rainfall declines, such as those experienced during La Niña years.

Model evaluation is becoming an increasingly important field of climate research where GCMs are tested to simulate the 20th century aspects of climate on numerous time scales, including the ability to reproduce the general circulation patterns and synoptic features of regional climate. Correlation analysis between modelled rainfall and the MSLP from GCMs would assist in model evaluation and help improve the confidence of future 21st century projections in a wider spectrum of climate elements.

On a more global scale, does the increasing MSLP over much of Queensland and the mid–latitudes represent changes from the SAM or is there also a significant contribution from the weakening of the Walker circulation and changes in the Hadley circulation? Conservation of mass suggests the SAM is the main driver of the global MSLP changes. What are the likely changes in the mid–latitudes MSLP, with increases in the tropical hydrological cycle? Will this lead to further changes in the location, strength and persistence of the subtropical ridge? Although the subtropical ridge and the SAM are likely to be contributing to most of the MSLP rise over SE QLD, the increased in convection associated with the Australian summer monsoon may also be suppressing convection and rainfall over SE QLD (and nearby regions) as it nears northern parts of Australia early in the austral summer, by increasing the upper level subsidence via the Hadley circulation. Increased rainfall was noted over parts of the Cape York Peninsula in some projections in this study, consistent with an increase in the hydrological cycle expected under global warming. It's proximity over northern Australia during the rest of the wet season may effectively suppress some of the austral summer and autumn rainfall over southern and SE QLD. These avenues of research will help provide more answers to the rainfall declines over SE QLD and other parts of Australia.

The land cover analysis discussed in Chapter Five using CCAM looked a number of experiments using changes in the albedo and vegetation cover and how these may affect regional climate in the SE QLD region. Although our analysis does show the albedo affected rainfall in this region, with higher albedo leading to lower rainfall over pastoral and agricultural regions west of the Great Dividing Range, further research is needed in areas such as the atmospheric circulation changes, surface energy balances, surface roughness, leaf area index, soil types and soil moisture. This will assist in the understanding of the changes in the atmosphere circulation dynamics and how this links to changes in the climate elements such as rainfall, temperature and humidity across the region. Cross sections and flux calculations in GCMs can identify changes in convergence or divergence, vertical motion, moisture fluxes and velocity potential and hence identify some of the synoptic features that are likely to be affected or suppressed under the new environmental conditions associated with global warming. Although in this study, the cloud cover changes were not directly analysed from the CCAM model, improved microphysics parameterisations included in many models means this could be explored further, especially with 21st century projections, with changes in the global climate expected with increasing amounts of global warming.

Further palaeoclimate records need to be developed to confirm some of the rainfall trends identified in this study over mid–late Holocene from similar sites in the Darling Downs or surrounding regions. Many small lakes exist in the region, especially along the Condamine River, where a number of small lakes have been separated from the main river flow over the last few millennia. At Lake Broadwater, a much longer palaeoclimate record could be developed from the deep sediment profile that exists in the lake. This would provide potentially hundreds of thousands of years of a palaeoenvironmental record and of palaeoclimatic conditions in the region and be extremely useful for correlating with longer palaeo-records from elsewhere in Australia and Asia. The simulation of a long climate record (~10,000 years) using a regional climate model (such as the CCAM model) over the SE QLD region during the Holocene, would establish a modelled climate record with climate variability, allowing direct comparisons to be made to some of the palaeoclimate records in the region and potentially identify other changes in rainfall that have yet to be identified from existing palaeoenvironmental studies.

REFERENCES

Ahrens, CD 2003, *Meteorology Today: An Introduction to Weather, Climate and the Environment*, Seventh edn, Thomson Brooks/Cole.

Alessandri, A, Gualdi, S, Polcher, J & Navarra, A 2007, 'Effects of Land Surface-Vegetation on the Boreal Summer Surface Climate of a GCM', *Journal of Climate*, vol. 20, no. 2, pp. 255-78.

Alexander, LA, Hope, P, Collins, D, Trewin, B, Lynch, A & Nicholls, N 2007, 'Trends in Australia's climate means and extremes: a global context.', *Australian Meteorological Magazine*, vol. 56, no. March, pp. 1-18.

Alexander, LV & Arblaster, JM 2009, 'Assessing trends in observed and modelled climate extremes over Australia in relation to future projections', *International Journal of Climatology*, vol. 29, no. 3, pp. 417-35.

Allan, R, Lindesay, J & Parker, D 1996, *El Niño Southern Oscillation and Climate Variability*, CSIRO Publishing.

Allan, RJ & Haylock, MR 1993, 'Circulation Features Associated with the Winter Rainfall Decrease in Southwestern Australia', *Journal of Climate*, vol. 6, no. 7, pp. 1356-67.

Anand, RR, Churchward, HMC, Smith, RE, Smith, K, Gozzard, JR, Craig, MA & Munday, TJ 1993, *Classification and Atlas of Regolith-Landform Mapping Units - Exploration Perspectives for the Yilgarn Craton*, CSIRO/AMIRA Project P240A, Restricted Report 440R.

Anderson, NJ & Rippey, B 1988, 'Diagenesis of magnetic minerals in the recent sediments of a eutrophic lake', *Limnology and Oceanography*, vol. 33, no. 6, part 2, pp. 1476-92.

Ansell, TJ, Reason, CJC, Smith, IN & Keay, K 2000, 'Evidence for decadal variability in southern Australian rainfall and relationships with regional pressure and sea surface temperature', *International Journal of Climatology*, vol. 20, no. 10, pp. 1113-29.

Arblaster, JM & Meehl, GA 2006, 'Contributions of External Forcings to Southern Annular Mode Trends', *Journal of Climate*, vol. 19, no. 12, pp. 2896-905.

Archer, CL & Caldeira, K 2008, 'Historical trends in the jet streams.', *Geophysical Research Letters*, vol. 35, pp. L08803, doi:10.1029/2008GL033614.

Ashok, K, Guan, Z & Yamagata, T 2003, 'Influence of the Indian Ocean Dipole on the Australian winter rainfall', *Geophysical Research Letters*, vol. 30, no. 15.

Augustinus, P, Reid, M, Andersson, S, Deng, Y & Horrocks, M 2005, 'Biological and Geochemical Record of Anthropogenic Impacts in Recent Sediments from Lake Pupuke, Auckland City, New Zealand', *Journal of Paleolimnology*, vol. 35, pp. 789-805.

AUSLIG 1990, *Atlas of Australian Resources - Vegetation* Third Series.

Berkman, DA 1995, *Field Geologists' Manual*, Third Revised Edition edn, vol. Monograph Series 9, The Australian Institute of Mining and Metallurgy, Melbourne.

Blaauw, M, Christen, JA, Mauquoy, D, Plicht, Jvd & Bennett, KD 2007, 'Testing the timing of radiocarbon-dated events between proxy archives', *Holocene*, vol. 17, no. 2, pp. 283-8.

Black, MP, Mooney, SD & Martin, HA 2006, 'A >43,000-year vegetation and fire history from Lake Baraba, New South Wales, Australia', *Quaternary Science Reviews*, vol. 25, no. 21-22, pp. 3003-16.

Blatt, H, Middleton, G & Murray, R 1980, *Origin of Sedimentary Rocks*, Prentice-Hall International, New Jersey.

Blott, SJ, Croft, DJ, Pye, K, Saye, SE & Wilson, HE 2004, 'Particle size analysis by laser diffraction', *Geological Society, London, Special Publications*, vol. 232, pp. 63-73.

BoM 2004, *Drought, Dust and Deluge - A Century of Climate Extremes in Australia*, Australian Government -Bureau of Meteorology.

---- 2008, 'Rainfall datasets from Bureau of Meteorology website http://www.bom.gov.au/climate/data/weather-data.shtml'.

Bouma, WJ, Pearman, GI & Manning, MR 1996, *Greenhouse: Coping with Climate Change*, CSIRO Publishing.

Brand, S, Dethloff, K & Handorf, D 2008, 'Tropospheric circulation sensitivity to an interactive stratospheric ozone.', *Geophysical Research Letters*, vol. 35, pp. L05809, doi:10.1029/2007GL032312.

Broadbridge, LW & Hanstrum, BN 1998, 'The relationship between tropical cyclones near Western Australia and the Southern Oscillation Index', *Australian Meteorological Magazine*, vol. 47, pp. 183-9.

Brutsaert, W 2006, 'Indications of increasing land surface evaporation during the second half of the 20th century.', *Geophysical Research Letters*, vol. 33, pp. L20403, doi:10.1029/2006GL027532.

Buurman, P, Pape, T & Muggler, CC 1997, 'Laser Grain-Size Determination in Soil Genetic Studies 1. Practical Problems. ', *Soil Science*, vol. 162, no. 3, pp. 211-8.

Cai, W 2006, 'Antarctic ozone depletion causes an intensification of the Southern Ocean super-gyre circulation', *Geophysical Research Letters*, vol. 33, pp. L03712, doi:10.1029/2005GL024911.

Cai, W & Cowan, T 2006, 'SAM and regional rainfall in IPCC AR4 models: Can anthropogenic forcing account for southwest Western Australian winter rainfall reduction?', *Geophysical Research Letters*, vol. 33, pp. L24708, doi:10.1029/2006GL028037.

---- 2007, 'Trends in Southern Hemisphere Circulation in IPCC AR4 Models over 1950-99: Ozone Depletion versus Greenhouse Forcing', *Journal of Climate*, vol. 20, no. 4, pp. 681-93.

---- 2008a, 'Dynamics of late autumn rainfall reduction over southeastern Australia', *Geophysical Research Letters*, vol. 35, pp. L09708, doi:10.1029/2008GL033727. .

---- 2008b, 'Evidence of impacts from rising temperature on inflows to the Murray-Darling Basin.', *Geophysical Research Letters*, vol. 35, pp. L07701, doi:10.1029/2008GL033390.

Cai, W, Whetton, PH & Pittock, AB 2001, 'Fluctuations of the relationship between ENSO and northeast Australian rainfall', *Climate Dynamics*, vol. 17, no. 5-6, pp. 421-32.

Cai, W, Shi, G, Cowan, T, Bi, D & Ribbe, J 2005, 'The response of the Southern Annular Mode, the East Australian Current, and the southern mid-latitude ocean circulation to global warming.', *Geophysical Research Letters*, vol. 32, pp. L23706, doi:10.1029/2005GL024701.

Cai, W, Cowan, T, Dix, M, Rotstayn, L, Ribbe, J, Shi, G & Wijffels, S 2007, 'Anthropogenic aerosol forcing and the structure of temperature trends in the southern Indian Ocean.', *Geophysical Research Letters*, vol. 34, pp. L14611, doi:10.1029/2007GL030380.

Cai, WJ 2004, 'Multidecadal variability of rainfall in an Australian region and its linkage with the southern annular mode.', paper presented to Western Pacific Geophysics Meeting Supplement, Honolulu, Hawaii.

Cameron, NG, Schnell, OA, Rautio, ML, Lami, A, Livingstone, DM, Appleby, PG, Dearing, JA & N.L.Rose 2002, 'High-resolution analyses of recent sediments from a Norwegian mountain lake and comparison with instrumental records of climate', *Journal of Paleolimnology*, vol. 28, pp. 79–93.

Cassiano, DA, Charles, JV, George, CH, José, AM, Dingman, SL & Barry, DK 2007, 'The effects of deforestation on the hydrological cycle in Amazonia: a review on scale and resolution', *International Journal of Climatology*, vol. 27, no. 5, pp. 633-47.

Catchpole, A & Auliciems, A 1999, 'Southern Oscillation and the Northern Australian prawn catch', *International Journal of Biometeorology*, vol. 43, no. 3, pp. 110-2.

Charles, SP, Bari, MA, Kitsiosb, A & Batesa, BC 2007, 'Effect of GCM bias on downscaled precipitation and runoff projections for the Serpentine catchment, Western Australia', *International Journal of Climatology*, vol. 27, pp. 1673–90.

Chen, J, Wan, G, Zhang, DD, Chen, Z, Xu, J, Xiao, T & Huang, R 2005, 'The ‘Little Ice Age’ recorded by sediment chemistry in Lake Erhai, southwest China', *Holocene*, vol. 15, no. 6, pp. 925-31.

Chirinos, LR, Urrutia, R, Fagel, N, Bertrand, S, Gamboa, N, Araneda, A & Zaror, C 2005, 'Chemical Profiles in Lake Sediments in Laguna Chica De San Pedro (Bio-Bio Region, Chile)', *Journal of the Chilean Chemical Society* vol. 50, no. 4, pp. 697-710.

Christensen, JH, Hewitson, B, Busuioc, A, Chen, A, Gao, X, Held, I, Jones, R, Kolli, RK, Kwon, WT, Laprise, R, Rueda, VM, Mearns, L, Menéndez, CG, Räisänen, J, Rinke, A, Sarr, A & Whetton, P (eds) 2007, *Regional Climate Projections. In: Climate Change 2007: The Physical Science Basis. Contribution of Working Group I to the Fourth Assessment Report of the Intergovernmental Panel on Climate Change*, Cambridge University Press, Cambridge, United Kingdom and New York, NY, USA.

Clement, AC 2006, 'The Role of the Ocean in the Seasonal Cycle of the Hadley Circulation.', *Journal of Atmospheric Science*, vol. 63, no. 12, pp. 3351-65.

Colls, K & Whitaker, R 1993, *The Australian Weather Book*, Second edn, National Book Distributors.

Cook, GD & Heerdegen, RG 2001, 'Spatial variation in the duration of the rainy season in monsoonal Australia.', *International Journal of Climatology*, vol. 21, no. 14, pp. 1723-32.

Costa, MH, Yanagi, SNM, Souza, PJOP, Ribeiro, A & Rocha, EJP 2007, 'Climate change in Amazonia caused by soybean cropland expansion, as compared to caused by pastureland expansion', *Geophysical Research Letters*, vol. 34, pp. L07706, doi:10.1029/2007GL029271.

Coutts, AM, Beringer, J & Tapper, NJ 2007, 'Impact of Increasing Urban Density on Local Climate: Spatial and Temporal Variations in the Surface Energy Balance in Melbourne, Australia', *Journal of Applied Meteorology and Climatology*, vol. 46, no. 4, pp. 477–93.

Crook, JA, Gillett, NP & Keeley, SPE 2008, 'Sensitivity of Southern Hemisphere climate to zonal asymmetry in ozone.', *Geophysical Research Letters*, vol. 35, pp. L07806, doi:10.1029/2007GL032698.

CSIRO & Meteorology, Bo 2007, *Climate change in Australia. technical report 148pp*.

Cupper, ML 2005, 'Last glacial to Holocene evolution of semi-arid rangelands in southeastern Australia', *Holocene*, vol. 15, no. 4, pp. 541-53.

Dai, A 2006, 'Precipitation Characteristics in Eighteen Coupled Climate Models.', *Journal of Climate*, vol. 19, no. 18, pp. 4605-30.

Dare, RA & Davidson, NE 2004, 'Characteristics of Tropical Cyclones in the Australian Region', *Monthly Weather Review*, vol. 132, no. 12, pp. 3049–65.

Davin, EL, Noblet-Ducoudré, Nd & Friedlingstein, P 2007, 'Impact of land cover change on surface climate: Relevance of the radiative forcing concept', *Geophysical Research Letters*, vol. 34, pp. L13702, doi:10.1029/2007GL029678.

Day, RW, W.G.Whitaker, Murray, CG, Wilson, IH & Grimes, KG 1983, *Queensland Geology A companion volume to the 1:2,500,000 scale geological map (1975)*, Publication 383.

De'ath, G, Lough, JM & Fabricius, KE 2009, 'Declining Coral Calcification on the Great Barrier Reef', *Science*, vol. 323, no. 5910, pp. 116-9.

Dodson, JR & Lu, H 2005, 'Salinity episodes and their reversal in the late Pliocene of south-western Australia', *Palaeogeography, Palaeoclimatology, Palaeoecology*, vol. 228, pp. 296-304.

Donders, TH, Wagner, F & Visscher, H 2006, 'Late Pleistocene and Holocene subtropical vegetation dynamics recorded in perched lake deposits on Fraser Island, Queensland, Australia', *Palaeogeography, Palaeoclimatology, Palaeoecology*, vol. 241, no. 3-4, pp. 417-39.

Donders, TH, Haberle, SG, Hope, G, Wagner, F & Visscher, H 2007, 'Pollen evidence for the transition of the Eastern Australian climate system from the post-glacial to the present-day ENSO mode', *Quaternary Science Reviews*, vol. 26, no. 11-12, pp. 1621-37.

Douville, H 2002, 'Influence of Soil Moisture on the Asian and African Monsoons. Part II: Interannual Variability', *Journal of Climate*, vol. 15, no. 7, pp. 701-20.

Douville, H, Chauvin, F & Broqua, H 2001, 'Influence of Soil Moisture on the Asian and African Monsoons. Part I: Mean Monsoon and Daily Precipitation', *Journal of Climate*, vol. 14, no. 11, pp. 2381-403.

Douville, H, Mélia, DS & Tyteca, S 2006, 'On the tropical origin of uncertainties in the global land precipitation response to global warming.', *Climate Dynamics*, vol. 26, no. 4, pp. 367-85.

Dowdy, S, Wearden, S & Chilko, D 2004, *Statistics for Research*, Third edn, Wiley.

Drosdowsky, W 2002, 'SST phases and Australian rainfall.', *Australian Meteorological Magazine*, vol. 51, no. 1, pp. 1-12.

---- 2005, 'The latitude of the subtropical ridge over eastern Australia: The L index revisited', *International Journal of Climatology*, vol. 25, no. 10, pp. 1291-9.

England, MH, Ummenhofer, CC & Santoso, A 2006, 'Interannual Rainfall Extremes over Southwest Western Australia Linked to Indian Ocean Climate Variability.', *Journal of Climate*, vol. 19, no. 10, pp. 1948-69.

EPA 2006, *Darling Downs and Granite Belt - Travellers Guide and Map*, Queensland Government - Queensland Parks and Wildlife Service.

Evans, JL & Allan, RJ 1992, 'El Niño/Southern Oscillation Modification to the Structure of the Monsoon and Tropical Cyclone Activity in the Australian Region.', *International Journal of Climatology*, vol. 12, pp. 611-23.

Exon, NF 1976, *Geology of the Surat Basin in Queensland*, Australian Govt. Pub. Service, Canberra.

Feddema, JJ, Oleson, KW, Bonan, GB, Mearns, LO, Buja, LE, Meehl, GA & Washington, WM 2005, 'The Importance of Land-Cover Change in Simulating Future Climates', *Science*, vol. 310, no. 5754, pp. 1674-8.

Fink, D, Hotchkis, M, Hua, Q, Jacobsen, G, Smith, AM, Zoppi, U, Child, D, Mifsud, C, Gaast, Hvd, Williams, A & Williams, M 2004, 'The ANTARES AMS facility at ANSTO', *Nuclear Instruments and Methods in Physics Research Section B: Beam Interactions with Materials and Atoms* vol. 223-224, pp. 109-15.

Fowler, AM, Boswijk, G, Gergis, J & Lorrey, A 2008, 'ENSO history recorded in Agathis australis (kauri) tree rings. Part A: kauri's potential as an ENSO proxy', *International Journal of Climatology*, vol. 28, no. 1, pp. 1-20.

Gagan, MK, Hendy, EJ, Haberle, SG & Hantoro, WS 2004, 'Post-glacial evolution of the Indo-Pacific Warm Pool and El Niño-Southern Oscillation', *Quaternary International*, vol. 118-119, pp. 127-43.

Gallant, AJE, Hennessy, KJ & Risbey, J 2007, 'Trends in rainfall indices for six Australian regions: 1910-2005.', *Australian Meteorological Magazine*, vol. 56, pp. 223-39.

Genever, M, Grindrod, J & Barker, B 2003, 'Holocene palynolology of Whitehaven Swamp, Whitsunday island, Queensland, and implications for the regional archaeological record', *Palaeogeography, Palaeoclimatology, Palaeoecology*, vol. 201, pp. 141-56.

Gibbard, S, Caldeira, K, Bala, G, Phillips, TJ & Wickett, M 2005, 'Climate effects of global land cover change', *Geophysical Research Letters*, vol. 32.

Gillett, NP, Kell, TD & Jones, PD 2006, 'Regional climate impacts of the Southern Annular Mode', *Geophysical Research Letters*, vol. 33, pp. L23704, doi:10.1029/2006GL027721.

Gnanadesikan, A & Stouffer, RJ 2006, 'Diagnosing atmosphere-ocean general circulation model errors relevant to the terrestrial biosphere using the Köppen climate classification', *Geophysical Research Letters*, vol. 33, pp. L22701, doi:10.1029/2006GL028098.

Government, Q 2005, *South East Queensland Regional Plan 2005-2026*, Queensland State Government.

Håkanson, L & Jansson, M 1983, *Principles of lake sedimentology*, Springer, Berlin.

Hall, WB, McKeon, GM, Carter, JO, Day, KA, Howden, SM, Scanlan, JC, Johnston, PW & Burrows, WH 1998, 'Climate Change in Queensland'sGrazing Lands: 11. An Assessment of the Impact on Animal Production from Native Pastures', *Rangelands Journal*, vol. 20, no. 2, pp. 177-205.

Harle, K, Etheridge, D, Whetton, P, Jones, R, Hennessy, KJ, Goodwin, I, Brooke, B, Ommen, Tv, Barbetti, M, Barrows, T, Chappell, J, De Deckker, P, Fink, D, Gagan, M, Haberle, S, Heijnis, H, Henderson-Sellers, A, Hesse, P, Hope, G, Kershaw, P & Nicholls, N 2005, *Building a future on knowledge from the past: what palaeo-science can reveal about climate change and its potential impacts in Australia*, CSIRO, Australia, June 2005.

Harle, KJ, Heijnis, H, Chisari, R, Kershaw, AP, Zoppi, U & Jacobsen, G 2002, 'A chronology for the long pollen record from Lake Wangoom, western Victoria (Australia) as derived from uranium/thorium disequilibrium dating', *Journal of Quaternary Science*, vol. 17, no. 7, pp. 707-20.

Harris, PS, Biggs, AJW & Coutts, AJ 1999, *Central Darling Downs Land Management Manual - Field Manual.*, Department of Natural Resources.

Hartmann, DL 1994, *Global Physical Climatology*, vol. 56, International Geophysics Series, Academic Press.

Heiri, O, Lotter, AF & Lemcke, G 2001, 'Loss on ignition as a method for estimating organic and carbonate content in sediments: reproducibility and comparability of results', *Journal of Paleolimnology*, vol. 25, no. 1 DOI 10.1023/A:1008119611481 pp. 101-10

Hendon, HH, Thompson, DWJ & Wheeler, MC 2007, 'Australian Rainfall and Surface Temperature Variations Associated with the Southern Hemisphere Annular Mode.', *Journal of Climate*, vol. 20, no. 11, pp. 2452-67.

Hennessy, KJ, Suppiah, R & Page, CM 1999, 'Australian rainfall changes, 1910-1995.', *Australian Meteorological Magazine*, vol. 48, no. 1, pp. 1-13.

Hesse, PP, Magee, JW & Kaars, Svd 2004, 'Late Quaternary climates of the Australian arid zone:a review', *Quaternary International*, vol. 118–119, pp. 87–102.

Hoffmann, WA, Schroeder, W & Jackson, RB 2003, 'Regional feedbacks among fire, climate, and tropical deforestation', *Journal of Geophysical Research*, vol. 108, no. (D23), pp. 4721, doi:10.1029/2003JD003494.

Hongyan, D, Nathan, PG, Andrew, JW & Francis, WZ 2007, 'Climate Change detection over different land surface vegetation classes', *International Journal of Climatology*, vol. 27, no. 2, pp. 211-20.

Hooke, J 2003, 'Coarse sediment connectivity in river channel systems: a conceptual framework and methodology', *Geomorphology*, vol. 56, pp. 79-94.

Hope, PK 2006, 'Projected future changes in synoptic systems influencing southwest Western Australia.', *Climate Dynamics*, vol. 26, pp. 765-80.

Hope, PK, Drosdowsky, W & Nicholls, N 2006, 'Shifts in the synoptic systems influencing southwest Western Australia.', *Climate Dynamics*, vol. 26, pp. 751-64.

Hu, Y & Fu, Q 2007, 'Observed poleward expansion of the Hadley circulation since 1979', *Atmospheric Chemistry and Physics*, vol. 7, pp. 5229-36.

Hu, Y, Li, D & Liu, J 2007, 'Abrupt seasonal variation of the ITCZ and the Hadley circulation', *Geophysical Research Letters*, vol. 34, pp. L18814, doi:10.1029/2007GL030950.

IPCC 2000, *IPCC Special Report Emission Scenarios - Summary for Policymakers. A Special Report of IPCC Working Group III*.

---- 2007, *Summary for Policymakers. In: Climate Change 2007: The Physical Science Basis. Contribution of Working Group I to the Fourth Assessment Report of the Intergovernmental Panel on Climate Change.*, Cambridge, United Kingdom and New York, NY, USA.

Jin, Z, Li, F, Cao, J, Wang, S & Yu, J 2006, 'Geochemistry of Daihai Lake sediments, Inner Mongolia, north China: Implications for provenance, sedimentary sorting, and catchment weathering', *Geomorphology*, vol. 80, pp. 147-63.

Jones, DA & Beard, G 1998, 'Verification of Australian monthly district rainfall totals using high resolution gridded analyses', *Australian Meteorological Magazine*, vol. 47, no. 1, pp. 41-54.

Kalugin, I, Selegei, V, Goldberg, E & Seret, G 2005, 'Rhythmic fine-grained sediment deposition in Lake Teletskoye, Altai, Siberia, in relation to regional climate change', *Quaternary International*, vol. 136, pp. 5–13.

Kanae, S, Hirabayashi, Y, Yamada, T & Oki, T 2006, 'Influence of “Realistic” Land Surface Wetness on Predictability of Seasonal Precipitation in Boreal Summer', *Journal of Climate*, vol. 19, no. 8, pp. 1450-60.

Karoly, DJ 2003, 'Ozone and Climate Change', *Science*, vol. 302, pp. 236-7.

Karoly, DJ & Braganza, K 2005, 'Attribution of Recent Temperature Changes in the Australian Region.', *Journal of Climate*, vol. 18, no. 3, pp. 457-64.

Kashiwaya, K, Ochiai, S, Sakai, H & Kawai, T 2001, 'Orbit-related long-term climate cycles revealed in a 12-Myr continental record from Lake Baikal', *Nature*, vol. 410, pp. 71-4.

Kershaw, AP 1997, 'A modification of the Troels-Smith system of sediment description and portrayal', *Quaternary Australasia*, vol. 15, no. 2, pp. 63-8.

Kershaw, P 1970, 'A pollen diagram from Lake Euramoo, north-east Australia.', *New Phytologist*, vol. 69, pp. 785-805.

---- 1971, 'A pollen diagram from Quincan Crater, north-east Australia.', *New Phytologist*, vol. 70, pp. 669-81.

---- 1975, 'Stratigraphy and pollen analysis of Bromfield swamp, north-eastern Queensland, Australia.', *New Phytologist*, vol. 75, pp. 173-91.

---- 1983, 'A Holocene pollen diagram from Lynch's Crater, north-eastern Queensland, Australia', *New Phytologist*, vol. 94, pp. 669-82.

---- 1994, 'Pleistocene vegetation of the humid tropics of northeastern Queensland, Australia.', *Palaeogeography, Palaeoclimatology, Palaeoecology*, vol. 109, pp. 399-412.

---- 1995, *"Environmental change in Greater Australia." In: Transistions: Pleistocene to Holocene in Australia and Papua New Guinea.*, vol. 69, Antiquity.

Kobayashi, C & Maeda, S 2006, 'Phase shift of the seasonal cycle in the Hadley Circulation in recent decades.', *Geophysical Research Letters*, vol. 33, pp. L22703, doi:10.1029/2006GL027682.

Konert, M & Vandenberghe, J 2008, 'Comparison of laser grain size analysis with pipette and sieve analysis: a solution for the underestimation of the clay fraction ', *Sedimentology*, vol. 44, no. 3, pp. 523-35.

Kowalczyk, EA, Garratt, JR & Krummel, PB 1991, *A Soil-Canopy scheme for Use in a Numerical Model of the Atmosphere - 1D Stand - Alone model.*, Technical Paper No. 23, CSIRO Australia.

Kueppers, LM, Snyder, MA & Sloan, LC 2007, 'Irrigation cooling effect: Regional climate forcing by land-use change', *Geophysical Research Letters*, vol. 34, pp. L03703, doi:10.1029/2006GL028679.

Kuleshov, Y, Qi, L, Fawcett, R & Jones, D 2008, 'On tropical cyclone activity in the Southern Hemisphere: Trends and the ENSO connection.', *Geophysical Research Letters*, vol. 35 pp. L14S08, doi:10.1029/2007GL032983.

L'Heureux, ML & Thompson, DWJ 2006, 'Observed Relationships between the El Niño-Southern Oscillation and the Extratropical Zonal-Mean Circulation', *Journal of Climate*, vol. 19, no. 2, pp. 276-87.

Lal, M, McGregor, JL & Nguyen, KC 2007, 'Very high-resolution climate simulation over Fiji using a global variable-resolution model', *Climate Dynamics*, vol. 30, no. 2-3, pp. 293-305.

Lal, R (ed.) 2002, *Encyclopedia of Soil Science*, Marcel Dekker.

Larsen, SH 2008, 'Australian winter anticyclonicity, 1850-2006', *Journal of Geophysical Research*, vol. 113, pp. D06105,doi:10.1029/2007JD008873.

Last, WM & Smol, JP (eds) 2001, *Tracking Environmental Change Using Lake Sediments Volume 2: Physical and Geochemical Methods*, vol. 2, Developments in Paleoenvironmental Research, Kluwer Academic Publishers.

Lavery, BM, Joung, G & Nicholls, N 1997, 'An extended high-quality historical rainfall dataset for Australia.', *Australian Meteorological Magazine*, vol. 46, no. 1, pp. 27-38.

Li, F, Chambers, LE & Nicholls, N 2005, 'Relationships between rainfall in the southwest of Western Australia and near-global patterns of sea surface temperature and mean sea level pressure variability.', *Australian Meteorological Magazine*, vol. 54, no. 1, pp. 23-33.

Li, Y, Cai, W & Campbell, EP 2005, 'Statistical Modelling of Extreme Rainfall in Southwest Western Australia.', *Journal of Climate*, vol. 18, no. 6, pp. 852-63.

Lin, J-L 2007, 'Interdecadal variability of ENSO in 21 IPCC AR4 coupled GCMs', *Geophysical Research Letters*, vol. 34, pp. L12702, doi:10.1029/2006GL028937.

Liu, Z, Notaro, M, Kutzbach, J & Liu, N 2006, 'Assessing Global Vegetation-Climate Feedbacks from Observations', *Journal of Climate*, vol. 19, no. 5, pp. 787-814.

Longmore, ME 1997, 'Quaternary Palynological records from Perched Lake Sediments, Fraser Island, Queensland, Australia: Forest History and Climatic Control', *Australian Journal of Botany*, vol. 45, pp. 507-26.

Los, SO, Weedon, GP, North, PRJ, Kaduk, JD, Taylor, CM & Cox, PM 2006, 'An observation-based estimate of the strength of rainfall-vegetation interactions in the Sahel', *Geophysical Research Letters*, vol. 33, pp. L16402, doi:10.1029/2006GL027065.

Lotsch, A, Friedl, MA, Anderson, BT & Tucker, CJ 2003, 'Coupled vegetation-precipitation variability observed from satellite and climate records', *Geophysical Research Letters*, vol. 30, no. (14), pp. 1774, doi:10.029/2003GL017506.

Lottermoser, BG, Oberhãnsli, R, Zolitschka, B, Negendank, JFW, Schütz, U & Boenecke, J 1993, 'Environmental Geology and Geochemistry of Lake Sediments (Holzmaar, Eifel, Germany)', in JFW Negendank & B Zolitschka (eds), *Paleolimnology of European Maar Lakes*, Springer-Verlag, vol. 49, pp. 305-16.

Lough, JM 1991, 'Rainfall Variations in Queensland, Australia: 1891-1986.', *International Journal of Climatology*, vol. 11, pp. 745-68.

---- 1992, 'Variations of Sea-Surface Temperatures off North-Eastern Australia and Associations with Rainfall in Queensland 1956-1987', *International Journal of Climatology*, vol. 12, no. 8, pp. 765-82.

---- 1993, 'Variations of Some Seasonal Rainfall Characteristics in Queensland, Australia: 1921-1987', *International Journal of Climatology*, vol. 13, pp. 391-409.

Lu, J, Vecchi, GA & Reichler, T 2007, 'Expansion of the Hadley cell under global warming.', *Geophysics Research Letters*, vol. 34, pp. L06805, doi:10.1029/2006GL028443.

Luly, JG, Grindrod, JF & Penny, D 2006, 'Holocene palaeoenvironments and change at Three-Quarter Mile Lake, Silver Plains Station, Cape York Peninsula, Australia', *Holocene*, vol. 16, no. 8, pp. 1085-94.

Lynch, AH, Beringer, J, Kershaw, P, Marshall, A, Mooney, S, Tapper, N, Turney, C & Kaars, SVD 2007, 'Using the Paleorecord to Evaluate Climate and Fire Interactions in Australia', *Annual Review of Earth and Planetary Sciences*, vol. 35, no. (doi:10.1146/annurev.earth.35.092006.145055), pp. 215-39.

Mahmood, R, Hubbard, KG & Carlson, C 2004, 'Modification of growing-season surface temperature records in the northern great plains due to land-use transformation: verification of modelling results and implication for global climate change', *International Journal of Climatology*, vol. 24, no. 3, pp. 311-27.

Maroulis, JC, Nanson, GC, Price, DM & Pietsch, T 2007, 'Aeolian–fluvial interaction and climate change: source-bordering dune development over the past 100 ka on Cooper Creek, central Australia', *Quaternary Science Reviews*, vol. 26, pp. 386-404.

Marshall, GJ 2003, 'Trends in the Southern Annular Mode from Observations and Reanalyses', *Journal of Climate*, vol. 16, no. 24, pp. 4134-43.

Masson, V, Champeaux, J-L, Chauvin, F, Meriguet, C & Lacaze, R 2003, 'A Global Database of Land Surface Parameters at 1-km Resolution in Meteorological and Climate Models', *Journal of Climate*, vol. 16, no. 9, pp. 1261-82.

McAlpine, CA, Syktus, J, Deo, RC, Lawrence, PJ, McGowan, HA, Watterson, IG & Phinn, SR 2007, 'Modeling the impact of historical land cover change on Australia's regional climate', *Geophysical Research Letters*, vol. 34, pp. L22711, doi:10.1029/2007GL031524.

McCave, IN, Hall, IR & Bianchi, GG 2006, 'Laser vs. settling velocity differences in silt grainsize measurements: estimation of palaeocurrent vigour', *Sedimentology*, vol. 53, pp. 919-28.

McGowan, HA, Petherick, LM & Kamber, BS 2008, 'Aeolian sedimentation and climate variability during the late Quaternary in southeast Queensland, Australia', *Palaeogeography, Palaeoclimatology, Palaeoecology*, vol. 265 pp. 171–81.

McGregor, JL & Nguyen, K 2003, 'Simulations of the East Asian and Australian monsoons using a variable-resolution model.', paper presented to Proceedings of the 2nd Workshop on Regional Climate modelling for Monsoon System, Yokohama, March 2003.

McGregor, JL, Nguyen, KC & Kane, T 2006, *High-resolution climate-change projections for the Fitzroy Basin.*, CSIRO Marine and Atmospheric Research, Aspendale, Victoria, Research.

McGregor, JL, C.Nguyen, K & Katzfey, JJ 2008, *A variety of tropical climate simulations using CCAM*, The Centre for Australian Weather and Climate Research

McGuffie, K & Henderson-Sellers, A 2005, *A Climate Modelling Primer*, John Wiley and Sons, Ltd.

McKeon, G, Hall, W, Henry, B, Stone, G & Watson, I 2004, *Pasture Degradation and Recovery in Australia's Rangelands: Learning from History*.

McTainsh, G & Strong, C 2007, 'The role of aeolian dust in ecosystems', *Geomorphology*, vol. 89, no. 1-2, pp. 39-54.

McTainsh, GH & Lynch, AW 1996, 'Quantitative estimates of the effect of climate change on dust storm activity in Australia during the Last Glacial Maximum', *Geomorphology*, vol. 17, no. 1-3, pp. 263-71.

Meehl, GA, Washington, WM, Santer, BD, Collins, WD, Arblaster, JM, Aixue, H, Lawrence, DM, Haiyan, T, Buja, LE & Strand, WG 2006, 'Climate Change Projections for the Twenty-First Century and Climate Change Commitment in the CCSM3', *Journal of Climate*, vol. 19, no. 11, pp. 2597-616.

Meneghini, B, Simmonds, I & Smith, IN 2007, 'Association between Australian rainfall and the Southern Annular Mode.', *International Journal of Climatology*, vol. 27, no. 1, pp. 109-21.

Meyers, PA 1994, 'Preservation of elemental and isotopic source identification of sedimentary organic matter', *Chemical Geology*, vol. 114, pp. 289-302.

Moise, AF, Colman, RA & Zhang, H 2005, 'Coupled model simulations of current Australian surface climate and its changes under greenhouse warming: an analysis of 18 CMIP2 models.', *Australian Meteorological Magazine*, vol. 54, no. 4, pp. 291-307.

Mond, A 1973, *1:250,000 Geological Series -Explanatory Notes - Dalby, Queensland*, Canberra.

Murphy, FB & Ribbe, J 2004, 'Variability of Southeastern Queensland Rainfall and Climate Indices.', *International Journal of Climatology*, vol. 24, no. 6, pp. 703-21.

Murphy, JM, Sexton, DMH, Barnett, DN, Jones, GS, Webb, MJ, Collins, M & Stainforth, DA 2007, 'Quantification of modelling uncertainties in a large ensemble of climate change simulations.', *Nature*, vol. 430, pp. 768-72.

Nanson, GC, Price, DM, Jones, BG, Maroulis, JC, Coleman, M, Bowman, H, Cohen, TJ, Pietsch, TJ & Larsen, JR 2008, 'Alluvial evidence for major climate and flow regime changes during the middle and late Quaternary in eastern central Australia', *Geomorphology*, vol. 101, pp. 109-29.

Narisma, GT & Pitman, AJ 2006, 'Exploring the Sensitivity of the Australian Climate to Regional Land-Cover-Change Scenarios under Increasing CO_2 Concentrations and Warmer Temperatures.', *Earth Interactions*, vol. 10, pp. (7), doi:10.1175/EI154.1.

Narisma, GT, Foley, JA, Licker, R & Ramankutty, N 2007, 'Abrupt changes in rainfall during the twentieth century.', *Geophysical Research Letters*, vol. 34, pp. L06710, doi:10.1029/2006GL028628.

Narisma, GT, Pitman, AJ, Eastman, J, Watterson, IG, Pielke, R & Beltrán-Przekurat, A 2003, 'The role of biospheric feedbacks in the simulation of the impact of historical land cover change on the Australian January climate.', *Geophysical Research Letters*, vol. 30, pp. (22), 2168, doi:10.1029/2003GL018261, 2003.

Nicholls, N 2004, 'The Changing Nature of Australian Droughts.', *Climatic Change*, vol. 63, no. 3, pp. 323-36.

---- 2006, 'Detecting and attributing Australian climate change: a review.', *Australian Meteorological Magazine*, vol. 55, pp. 199-211.

---- 2009, 'Local and remote causes of the southern Australian autumn-winter rainfall decline, 1957-2007', *Climate Dynamics*, pp. Doi 10.1007/s00382-0090527-6.

Nicholls, N, Drosdowsky, W & Lavery, B 1997, 'Australian rainfall variability and change.', *Weather*, vol. 52, pp. 66-72.

Nicholls, N, Lavery, B, Frederiksen, C, Drosdowsky, W & Torok, S 1996, 'Recent apparent changes in relationships between the El Niño–Southern oscillation and Australian rainfall and temperature.', *Geophysical Research Letters*, vol. 23, no. 23, pp. 3357-60.

NLWRA 2001, *Australian Agriculture Assessment 2001. Volume 2*, National Land and Water Resources Audit.

Notaro, M, Vavrus, S & Liu, Z 2007, 'Global Vegetation and Climate Change due to Future Increases in CO2 as Projected by a Fully Coupled Model with Dynamic Vegetation', *Journal of Climate*, vol. 20, no. 1, pp. 70-90.

Nowak, H & Leighton, RM 1997, 'Relationships between east Australasian anticyclonicity, the Southern Oscillation and Australian rainfall.', *Australian Meteorological Magazine*, vol. 46, no. 4, pp. 267-76.

Nyberg, J, Malmgren, BA, Winter, A, Jury, MR, Kilbourne, KH & Quinn, TM 2007, 'Low Atlantic hurricane activity in the 1970s and 1980s compared to the last 270 years', *Nature*, vol. 447, no. 7145, pp. 698-701.

Ogden, R, Spooner, N, Reid, M & Head, J 2001, 'Sediment dates with implications for the age of the conversion from palaeochannel to modern fluvial activity on the Murray River and tributaries', *Quaternary International*, vol. 83-85, pp. 195-209.

Ojala, AEK & Saarinen, T 2002, 'Palaeosecular variation of the Earth's magnetic field during the last 10000 years based on the annually laminated sediment of Lake Nautäjarvi, central Finland ', *The Holocene*, vol. 12, no. 4, pp. 391-400.

Oki, T & Kanae, S 2006, 'Global Hydrological Cycles and World Water Resources.', *Science*, vol. 313, no. 25 August, pp. 1068-72.

Oldfield, F 2007, 'Sources of fine-grained magnetic minerals in sediments: a problem revisited', *Holocene*, vol. 17, no. 8, pp. 1265-71.

Oldfield, F & Appleby, PG 1984, 'Empirical testing of ^{210}Pb-dating models for lake sediments', in EY Haworth & WG Lung (eds), *In: Lake Sediments and Environmental History*, Leicester University Press, vol. 210, pp. Chapter 3; 93-124.

Olsson, IU 1991, 'Accuracy and precision in sediment chronology', *Hydrobiologia*, vol. 214, no. 1, pp. 25-34.

Oswald, WW, Anderson, PM, Brown, T, Brubaker, LB, Hu, FS, Lozhkin, AV, Tinner, W & Kaltenrieder, P 2005, 'Effects of sample mass and macrofossil type on radiocarbon dating of arctic and boreal lake sediments', *Holocene*, vol. 15, no. 5, pp. 758-67.

Page, KJ & Nanson, GC 2006, 'Stratigraphic architecture resulting from Late Quaternary evolution of the Riverine Plain, south-eastern Australia', *Sedimentology*, vol. 43, no. 6, pp. 927-45.

Page, KJ, Nanson, GC & Frazier, PS 2003, 'Floodplain Formation and Sediment Stratigraphy Resulting from Oblique Accretion on the Murrumbidgee River, Australia ', *Journal of Sedimentary Research*, vol. 73, no. 1, pp. 5-14.

Pain, CF & Oilier, CD 1995, 'Inversion of relief — a component of landscape evolution', *Geomorphology*, vol. 12, no. 2, pp. 151-65.

Payne, M, Chenhall, BE, Murrie, M & Jones, BG 1996, 'Spatial variation of sediment-bound zinc, lead, copper and rubidium in Lake Illawarra, a coastal logoon in eastern Australia', *Journal of Coastal Research*, vol. 13, no. 4, pp. 1181-91.

Perkins, SE, Pitman, AJ, Holbrook, NJ & McAneney, J 2007, 'Evaluation of the AR4 Climate Models and Simulated Daily Maximum Temperature, Minimum Temperature, and Precipitation over Australia Using Probability Density Functions.', *Journal of Climate*, vol. 20, no. 17, pp. 4356-76.

Petherick, LM, McGowan, HA & Kamber, BS 2008, 'Reconstructing transport pathways for late Quaternary dust from eastern Australia using the composition of trace elements of long traveled dusts', *Geomorphology*, vol. in press, p. 13 pp.

Pielke, RA 2005, 'Land Use and Climate Change', *Science*, vol. 310, no. 9 December, pp. 1625-6.

Pitman, AJ 2003, 'The evolution of, and revolution in, land surface schemes designed for climate models.', *International Journal of Climatology*, vol. 23, no. 5, pp. 479-510.

Pitman, AJ & Perkins, SE 2008, 'Regional projections of future seasonal and annual changes in rainfall and temperature over Australia based on skill-selected AR4 models.', *Earth Interactions*, vol. 12, no. 12, pp. 1-50.

Pitman, AJ, Narisma, GT, Sr., RAP & Holbrook, NJ 2004, 'Impact of land cover change on the climate of southwest Western Australia.', *Journal of Geophysical Research*, vol. 109, pp. D18109, doi:10.1029/2003JD004347.

Pittock, B 2003, *Climate Change: An Australian Guide to the Science and Potential Impacts.*, Australian Greenhouse Office.

Plessow, K, Acker, K, Heinrichs, H & Möller, D 2001, 'Time study of trace elements and major ions during two cloud events at the Mt. Brocken ', *Atmospheric Environment*, vol. 35, no. 2, pp. 367-78.

Potter, NJ, Zhang, L, Milly, PCD, McMahon, TA & Jakeman, AJ 2005, 'Effects of rainfall seasonality and soil moisture capacity on mean annual water balance for Australian catchments', *Water Resources Research*, vol. 41.

Power, S, Casey, T, Folland, C, Colman, A & Mehta, V 1999, 'Inter-decadal modulation of the impact of ENSO on Australia', *Climate Dynamics*, vol. 15, no. 5, pp. 319-24.

Power, SB & Smith, IN 2007, 'Weakening of the Walker Circulation and apparent dominance of El Niño both reach record levels, but has ENSO really changed?', *Geophysical Research Letters*, vol. 34, pp. L18702, doi:10.1029/2007GL030854.

Previdi, M & Liepert, BG 2007, 'Annular modes and Hadley cell expansion under global warming', *Geophysical Research Letters*, vol. 34, pp. L22701, doi:10.1029/2007GL031243.

Rakich, CS, Holbrook, NJ & Timbal, B 2008, 'A pressure gradient metric capturing planetary-scale influences on eastern Australian rainfall.', *Geophysical Research Letters*, vol. 35, pp. L08713, doi:10.1029/2007GL032970.

Ray, DK, Nair, US, Welch, RM, Han, Q, Zeng, J, Su, W, Kikuchi, T & Lyons, TJ 2003, 'Effects of land use in Southwest Australia: 1. Observations of cumulus cloudiness and energy fluxes', *Journal of Geophysical Research*, vol. 108, no. (D14), pp. 4414, doi:10.1029/2002JD002654.

Renwick, JA 1998, 'ENSO-Related Variability in the Frequency of South Pacific Blocking', *Monthly Weather Review*, vol. 126, no. 12, pp. 3117–23.

Rotstayn, LD, Keywood, MD, Forgan, BW, Gabric, AJ, Galbally, IE, Gras, JL, Luhar, AK, McTainsh, GH, Mitchell, RM & Young, SA 2008, 'Possible impacts of anthropogenic and natural aerosols on Australian climate: a review', *International Journal of Climatology*, vol. 29, no. 4, pp. 461–79.

Rühland, K, Phadtare, NR, Pant, RK, Sangode, SJ & Smol, JP 2006, 'Accelerated melting of Himalayan snow and ice triggers pronounced changes in a valley peatland from northern India', *Geophysical Research Letters*, vol. 33, pp. L15709, doi:10.1029/2006GL026704.

Ryan, B & Hope, P 2005, *Indian Ocean Climate Initiative Stage 2: Report of Phase 1 Activity.*, Available online at http://www.ioci.org.au/publications/pdf/2005202-IOCI%20reportvis2.pdf, Published by the Indian Ocean Climate Initiative.

Salzmanna, N, Freib, C, Vidaleb, P-L & Hoelzlea, M 2007, 'The application of Regional Climate Model output for the simulation of high-mountain permafrost scenarios.', *Global Planetary Change*, vol. 56, pp. 188-202.

Sanders, AJ & Croker, J 1997, 'Delineation of regolith boundaries using remotely sensed data and correlation with regolith geochemistry', paper presented to An International Conference on Crustal Evolution, Metallogeny and Exploration of the Yilgarn Craton - An Update, Kalgoorlie.

Saunders, MA & Lea, AS 2008, 'Large contribution of sea surface warming to recent increase in Atlantic hurricane activity', *Nature*, vol. 451, no. 7178, pp. 557-60.

Scott, G 1988, *Lake Broadwater: The Natural History of an Inland Lake and its Environs,* Darling Downs Institute Press.

Seidel, DJ, Fu, Q, Randel, WJ & Reichler, TJ 2008, 'Widening of the tropical belt in a changing climate', *Nature Geoscience*, vol. 1, pp. 21-4

Sellers, PJ, Mintz, Y, Sud, YC & Dalcher, A 1986, 'A Simple Biosphere Model (SiB) for Use within General Circulation Models', *Journal of Atmospheric Science*, vol. 43, no. 6, pp. 505-31.

Shaun, F & Jonathan, N 2007, 'Effect of ENSO on Queensland seasonal landfalling tropical cyclone activity.', *International Journal of Climatology*, vol. 27, no. 10, pp. 1327-34.

Shephard, FP 1954, 'Nomenclature based on sand-silt-clay ratios', *Journal of Sedimentary Petrology*, vol. 24, pp. 151-8.

Shi, G 2008, 'Variability and Change of the Indo-Pacific Climate System and their Impacts upon Australian Rainfall.', PHD thesis: University of Southern Queensland.

Shi, G, Ribbe, J, Cai, W & Cowan, T 2008, 'An interpretation of Australian rainfall projections.', *Geophysical Research Letters*, vol. 35, pp. L02702, doi:10.1029/2007GL032436.

Shichi, K, Kawamuro, K, Takahara, H, Hase, Y, Maki, T & Miyoshif, N 2006, 'Climate and vegetation changes around Lake Baikal during the last 350,000 years', *Palaeogeography, Palaeoclimatology, Palaeoecology*, vol. 248, no. 3-4, pp. 357-75.

Shukla, J, DelSole, T, Fennessy, M, Kinter, J & Paolino, D 2006, 'Climate model fidelity and projections of climate change.', *Geophysical Research Letters*, vol. 33, pp. L07702, doi:10.1029/2005GL025579.

Siriwardena, L, Finlayson, BL & McMahon, TA 2005, 'The impact of land use change on catchment hydrology in large catchments: The Comet River, Central Queensland, Australia.', *Journal of Hydrology*, vol. 326, no. 1-4, pp. 199-214.

Skinner, BJ, Porter, SC & Botkin, DB 1999, *The Blue Planet: An Introduction to Earth System Science*, Second edn, John Wiley & Sons, Inc.

Sloyan, BM & Kamenkovich, IV 2007, 'Simulation of Subantarctic Mode and Antarctic Intermediate Waters in Climate Models', *Journal of Climate*, vol. 20, no. 20, pp. 5061-80.

Smith, DM, Cusack, S, Colman, AW, Folland, CK, Harris, GR & Murphy, JM 2007, 'Improved Surface Temperature Prediction for the Coming Decade from a Global Climate Model.', *Science*, vol. 317, pp. 796-9.

Smith, I 2004, 'An assessment of recent trends in Australian rainfall.', *Australian Meteorological Magazine*, vol. 53, no. 3, pp. 163-73.

Smith, IN, McIntosh, P, Ansell, TJ, Reason, CJC & McInnes, K 2000, 'Southwest Western Australian winter rainfall and its association with Indian Ocean climate variability.', *International Journal of Climatology*, vol. 20, no. 15, pp. 1913-30.

Smith, RE 1996, 'Regolith research in support of mineral exploration in Australia ', *Journal of Geochemical Exploration*, vol. 57, no. 1-3, pp. 159-73.

Solomon, S 1999, 'Stratospheric Ozone Depletion: A Review of Concepts and History', *Reviews of Geophysics*, vol. 37, no. 3, pp. 275-316.

Sperazza, M, Moore, JN & Hendrix, MS 2004, 'High-Resolution Particle Size Analysis of Naturally Occurring Very Fine-Grained Sediment Through Laser Diffractometry', *Journal of Sedimentary Research*, vol. 74, no. 5, pp. 736-43.

Stainforth, DA, Aina, T, Christensen, C, Collins, M, Faull, N, Frame, DJ, Kettleborough, JA, Knight, S, Martin, A, Murphy, JM, Piani, C, Sexton, D, Smith, LA, Spicer, RA, Thorpe, AJ & Allen, MR 2005, 'Uncertainty in predictions of the climate response to rising levels of greenhouse gases', *Nature*, vol. 433, pp. 403-6.

Stone, RC 1989, 'Weather Types at Brisbane, Queensland: An example of the use of Principal Components and Cluster Analysis.', *International Journal of Climatology*, vol. 9, pp. 3-32.

Stone, RC & Auliciems, A 1992, 'SOI phase relationships with rainfall in eastern Australia.', *International Journal of Climatology*, vol. 12, no. 6, pp. 625-36.

Stone, RC, Hammer, GL & Marcussen, T 1996, 'Prediction of global rainfall probabilities using phases of the Southern Oscillation Index.', *Nature*, vol. 384, no. 21 November, pp. 252-5.

Stuiver, M & Polach, A 1977, 'Reporting of ^{14}C data', *Radiocarbon*, vol. 19, no. 3, pp. 355-63.

Sturman, AP & Tapper, NJ 1996, *The Weather and Climate of Australia and New Zealand*, First edn, Oxford University Press.

---- 2006, *The Weather and Climate of Australia and New Zealand.*, Second edn, Oxford University Press.

Sumner, ME (ed.) 2000, *Handbook of Soil Science*, CRC Press.

Sun, Y, Solomon, S, Aiguo, D & Portmann, RW 2006, 'How Often Does It Rain?', *Journal of Climate*, vol. 19, no. 6, pp. 916-34.

Sun, Y, Solomon, S, Dai, A & Portmann, RW 2007, 'How Often Will It Rain?', *Journal of Climate*, vol. 20, no. 19, pp. 4801-18.

Suppiah, R 2004, 'Trends in the southern oscillation phenomenon and Australian rainfall and changes in their relationship.', *International Journal of Climatology*, vol. 24, no. 3, pp. 269-90.

Suppiah, R & Hennessy, KJ 1996, 'Trends in the intensity and frequency of heavy rainfall in tropical Australia and links with Southern Oscillation.', *Australian Meteorological Magazine*, vol. 45, no. 1, pp. 1-17.

Suppiah, R, Hennessey, KJ, Whetton, PH, McInnes, K, I.Macadam, J.Bathols, Ricketts, J & Page, CM 2007, 'Australian climate change projections derived from simulations performed for the IPCC 4th Assessment Report.', *Australian Meteorological Magazine*, vol. 56, pp. 131-52.

Syvitski, JPM 1991, *Principles, Methods, and Applications of Particle Size Analysis*, Cambridge University Press, New York.

Tanaka, HL, Ishizaki, N & Kitoh, A 2004, 'Trend and interannual variability of Walker, monsoon and Hadley circulations defined by velocity potential in the upper troposphere.', *Tellus: Series A*, vol. 56, no. 3, pp. 250-69.

Tate, A 2004, *Solutions for a Sustainable Future*, Focus Publishing Pty Ltd.

Taylor, CM, Lambin, EF, Stephenne, N, Harding, RJ & Essery, RLH 2002, 'The Influence of Land Use Change on Climate in the Sahel', *Journal of Climate*, vol. 15, no. 24, pp. 3615-29.

Taylor, JE, Rasmussen, KL, Doudna, G, Plicht, Jvd & Egsgaard, H 2005, 'Qumran Textiles In The Palestine Exploration Fund, London: Radiocarbon Dating Results', *Palestine Exploration Quarterly*, vol. 137, no. 2, pp. 159–67.

Thompson, DWJ & Solomon, S 2002, 'Interpretation of recent Southern Hemisphere climate change.', *Science*, vol. 296, pp. 895-9.

Timbal, B 2004, 'Southwest Australia past and future rainfall trends', *Climate Research*, vol. 26, no. 3, pp. 233-49.

Timbal, B & Arblaster, JM 2006, 'Land cover change as an additional forcing to explain the rainfall decline in the south west of Australia', *Geophysical Research Letters*, vol. 33, pp. L07717, doi:10.1029/2005GL025361.

Timbal, B, Arblaster, JM & Power, S 2006, 'Attribution of the Late-Twentieth-Century Rainfall Decline in Southwest Australia.', *Journal of Climate*, vol. 19, no. 10, pp. 2046-62.

Timbal, B, Power, S, Colman, R, Viviand, J & Lirola, S 2002, 'Does Soil Moisture Influence Climate Variability and Predictability over Australia?', *Journal of Climate*, vol. 15, no. 10, pp. 12-30.

Trenberth, KE 1992, *Climate System Modelling.*, Cambridge University Press.

Trenberth, KE & Caron, JM 2000, 'The Southern Oscillation Revisited: Sea Level Pressures, Surface Temperatures, and Precipitation.', *Journal of Climate*, vol. 13, no. 24, pp. 4358-65.

Tuniz, C 2001, 'Accelerator mass spectrometry: ultra-sensitive analysis for global science', *Radiation Physics and Chemistry*, vol. 61, pp. 317–22.

Twidale, CR 2004, 'River patterns and their meaning', *Earth-Science Reviews*, vol. 67, pp. 159–218.

Twidale, CR & Campbell, EM 1993, *Australian Landforms: Structure, Processes and Time*, Gleneagles Publishing, Adelaide.

Tylmann, W 2005, 'Lithological and geochemical record of anthropogenic changes in recent sediments of a small and shallow lake (Lake Pusty Staw, northern Poland)', *Journal of Paleolimnology*, vol. 33, pp. 313-25.

Ummenhofer, CC & England, MH 2007, 'Interannual Extremes in New Zealand Precipitation Linked to Modes of Southern Hemisphere Climate Variability', *Journal of Climate*, vol. 20, no. 21, pp. 5418-40.

Ummenhofer, CC, England, MH, McIntosh, PC, Meyers, GA, Pook, MJ, Risbey, JS, Gupta, AS & Taschetto, AS 2009, 'What causes southeast Australia's worst droughts?', *Geophysical Research Letters*, vol. 36, no. , pp. L04706, doi:10.1029/2008GL036801.

Vecchi, GA, Soden, BJ, Wittenberg, AT, Held, IM, Leetmaa, A & Harrison, MJ 2006, 'Weakening of tropical Pacific atmospheric circulation due to anthropogenic forcing.', *Nature*, vol. 441, no. 4 may, pp. 73-6.

Vera, C, Silvestri, G, Liebmann, B & González, P 2006, 'Climate change scenarios for seasonal precipitation in South America from IPCC-AR4 models.', *Geophysical Research Letters*, vol. 33, pp. L13707, doi:10.1029/2006GL025759.

Verdon, DC & Franks, SW 2005, 'Indian Ocean sea surface temperature variability and winter rainfall: Eastern Australia.', *Water Resources Research*, vol. 41, pp. W09413, doi:10.1029/2004WR003845.

Verdon, DC, Wyatt, AM, Kiem, AS & Franks, SW 2004, 'Multidecadal variability of rainfall and streamflow: Eastern Australia.', *Water Resources Research*, vol. 40, pp. W10201, doi:10.1029/2004WR003234.

Walker, M 2005, *Quaternary Dating Methods*, John Wiley and Sons, Ltd.

Wallace, J & McJannet, D 2006, 'On interception modelling of a lowland coastal rainforest in northern Queensland, Australia', *Journal of Hydrology*, vol. 329, no. 3-4, pp. 477-88.

Wang, G & Hendon, HH 2007, 'Sensitivity of Australian Rainfall to Inter-El Niño variations', *Journal of Climate*, vol. 20, no. 16, pp. 4211-26.

Wang, W, Anderson, BT, Phillips, N, Kaufmann, RK, Potter, C & Field, M 2006a, 'Feedbacks of Vegetation on Summertime Climate Variability over the North American Grasslands. Part I: Statistical Analysis', *Earth Interactions*, vol. 10, pp. 1–27

Wang, W, Anderson, BT, Entekhabi, D, Parsons, RM, Huang, D, Kaufmann, RK, Potter, C & Myneni, RB 2006b, 'Feedbacks of Vegetation on Summertime Climate Variability over the North American Grasslands. Part II: A Coupled Stochastic Model', *Earth Interactions*, pp. 1–30

Waugh, DW, Oman, L, Kawa, SR, Stolarski, RS, Pawson, S, Douglass, AR, Newman, PA & Nielsen, JE 2009, 'Impacts of climate change on stratospheric ozone recovery', *Geophysical Research Letters*, vol. 36, pp. L03805, doi:10.1029/2008GL036223.

Wentz, FJ, Ricciardulli, L, Hilburn, K & Mears, C 2007, 'How Much More Rain Will Global Warming Bring?', *Science*, vol. 317, no. July 13, pp. 233-5.

Wersin, P, Höhener, P, Giovanoli, R & W.Stumm 1991, 'Early diagenetic influences on iron transformations in a freshwater lake sediment', *Chemical Geology*, vol. 90, pp. 233-52.

Werth, D & Avissar, R 2005, 'The local and global effects of African deforestation', *Geophysical Research Letters*, vol. 32, no. L12704, doi:10.1029/2005GL022969.

Wetherald, RT & Manabe, S 2002, 'Simulation of hydrologic changes associated with global warming.', *Journal of Geophysical Research*, vol. 107, pp. D19, 4379,doi:10.1029/2001JD001195.

Whetton, P, Macadam, I, Bathols, J & O'Grady, J 2007, 'Assessment of the use of current climate patterns to evaluate regional enhanced greenhouse response patterns of climate models.', *Geophysical Research Letters*, vol. 34, pp. L14701, doi:10.1029/2007GL030025.

Whetton, PH, McInnes, KL, Jones, RN, Hennessy, KJ, Suppiah, R, Page, CM, Bathols, J & Durack, PJ 2005, *Australian climate change projections for impact assessment and policy application: A review.* , CSIRO Marine and Atmospheric Research, Aspendale (Victoria).

Whittaker, TE, Hall, BL, Hendy, CH & Spaulding, SA 2008, 'Holocene depositional environments and surface-level changes at Lake Fryxell, Antarctica', *The Holocene*, vol. 8, no. 5, pp. 775–86.

Willey, EC 2003, 'Urban geology of the Toowoomba conurbation, SE Queensland, Australia', *Quaternary International*, vol. 103, pp. 57–74.

Williams, M, Dunkerley, D, De Deckker, P, Kershaw, P & Chappell, J 1998, *Quaternary Environments*, Second edn, Arnold - Oxford University Press.

Williams, PD, Guilyardi, E, Sutton, R, Gregory, J & Madec, G 2007, 'A new feedback on climate change from the hydrological cycle.', *Geophysical Research Letters*, vol. 34, pp. L08706, doi:10.1029/2007GL029275.

Wright, WJ 1997, 'Tropical-extratropical cloudbands and Australian rainfall: 1. climatology', *International Journal of Climatology*, vol. 17, no. 8, pp. 807-29.

Wünnemann, B, Mischke, S & Chen, F 2006, 'A Holocene sedimentary record from Bosten Lake, China', *Palaeogeography, Palaeoclimatology, Palaeoecology*, vol. 234, pp. 223-38.

Xiao, J, Chang, Z, Si, B, Qin, X, Itoh, S & Lomtatidze, Z 2008, 'Partitioning of the grain-size components of Dali Lake core sediments: evidence for lake-level changes during the Holocene', *Journal of Paleolimnology*, vol. 40, no. 4, DOI 10.1007/s10933-008-9274-7.

Yin, JH 2005, 'A consistent poleward shift of the storm tracks in simulations of 21st century climate', *Geophysical Research Letters*, vol. 32, pp. L18701, doi:10.1029/2005GL023684.

Zaitchik, BF, Macalady, AK, Bonneau, LR & Smith, RB 2006, 'Europe's 2003 heat wave: a satellite view of impacts and land–atmosphere feedbacks', *International Journal of Climatology*, vol. 26, no. 6, pp. 743-69.

Zeng, N, Hales, K & Neelin, JD 2002, 'Nonlinear Dynamics in a Coupled Vegetation-Atmosphere System and Implications for Desert-Forest Gradient', *Journal of Climate*, vol. 15, no. 23, pp. 3474-87.

Zhang, X & Walsh, JE 2006, 'Toward a Seasonally Ice-Covered Arctic Ocean: Scenarios from the IPCC AR4 Model Simulations', *Journal of Climate*, vol. 19, no. 9, pp. 1730-47.

Zhang, X, Zwiers, FW, Hegerl, GC, Lambert, FH, Gillett, NP, Solomon, S, Stott, PA & Nozawa, T 2007, 'Detection of human influence on twentieth-century precipitation trends.', *Nature*, vol. 448, no. 7152, pp. 461-5.

Zhao, M & Pitman, AJ 2002, 'The regional scale impact of land cover change simulated with a climate model', *International Journal of Climatology*, vol. 22, no. 3, pp. 271-90.

GLOSSARY OF ACRONYMS AND DEFINITIONS

Annual decadal rainfall trends: The decadal trend in annual rainfall

Annual decadal MSLP trends: The decadal trend in annual MSLP

A2 scenario: One the of highest emission scenarios used by the IPCC–AR4

A1B scenario: Emission scenario slightly lower than A2

AINSE: Australian Institute of Nuclear Science and Engineering

AMS: Accelerator Mass Spectrometry

ANSTO: Australian Nuclear Science and Technology Organisation

ANTARES: Australian National Tandem Research Accelerator

BoM: Bureau of Meteorology

CCAM: Conformal Cubic Atmospheric Model

CMIP3: Coupled Model Intercomparison Project Phase 3

CNS : Carbon, Nitrogen, Sulphur

CSIRO: Commonwealth Scientific and Industrial Research Organisation

DJF: December, January, February

Ensemble Mean: Combined results from two or more runs from the same model using the same initial conditions

ENSO: El Nino-Southern Oscillation

GCMs: Global Climate Models and Global Circulation Models

HCl: Hydrochloric Acid

ICPAES: Inductively Coupled Plasma Atomic Emission Spectrometry

IOD: Indian Ocean Dipole

IPCC–AR4: Intergovernmental Panel on Climate Change – Fourth Assessment

Report

JJA: June, July, August

LCC: Land Cover Changes

LOI: Loss on Ignition

MAM: March, April, May

MR1-MR6: Six experiments conducted over Australia and southeast Queensland using the CCAM model

MSLP: Mean Sea Level Pressure

NCAR: National Center of Atmospheric Research

NCEP: National Centers for Environmental Prediction (USA)

NEA: Northeast Australia

NSW: New South Wales

PCMDI: Program for Climate Model Diagnosis and Intercomparison Project

RMSE: Root Mean Square Error

SAM: Southern Annular Mode

Seasonal decadal rainfall trends: The decadal trend in seasonal rainfall

Seasonal decadal MSLP trends: The decadal trend in seasonal MSLP

SE QLD: Southeast Queensland

SiB: Simple Biosphere Model

SON: September, October, November

USQ: University of Southern Queensland

WCRP: World Climate Research Program

APPENDIX ONE

Monthly RMSE Values from 21 IPCC–AR4 Models

Over NEA and 1901–2000.

Table: Monthly RMSE values from 21 IPCC–AR4 models from over NEA and 1901–2000.

Model	Jan	Feb	Mar	Apr	May	Jun	Jul	Aug	Sep	Oct	Nov	Dec	Season Average	Rank
1. CGCM3.1-T47	47.51	22.72	13.88	9.184	8.84	9.673	9.558	11.71	9.972	8.535	18.72	36.86	**17.3**	**6**
2. CGCM3.1-T63	35.61	21.41	17.24	11.67	11.08	7.316	11.03	11.36	11.11	7.919	14.58	28.04	**15.7**	**3**
3. CNRM-CM3	54.3	54.35	43	39.12	18.57	7.887	6.465	5.56	4.951	7.202	32.09	50.93	**27**	**16**
4. CSIRO-MK3.0	34.66	48.22	25.4	13.3	10.3	11.04	9.405	5.669	4.481	8.581	10.88	20.9	**16.9**	**4**
5. GFDL-CM2.0	42.93	35.28	31.57	16.99	11.41	6.714	4.431	7.601	4.987	10.71	11.87	19.09	**17**	**5**
6. GFDL-CM2.1	28.53	34.5	15.99	9.453	12.22	7.995	4.804	3.776	4.58	7.735	12.16	21.89	**13.6**	**2**
7. GISS-AOM	58.13	56.73	41.47	12.79	11.41	7.949	5.651	4.336	5.353	13.42	22.63	34.85	**22.9**	**13**
8. GISS-ER	61.02	59.07	26.83	18.49	16.79	12.79	9.741	7.998	15	21.01	42.09	59.73	**29.2**	**19**
9. GISS-EH	92.78	91.08	63.02	61.04	40.66	23.46	17.95	21.85	28.6	43.73	76.62	103.3	**55.3**	**21**
10. IAP-FGOALS1.0	37.84	48.71	17.11	15.72	13.23	13.26	17.86	28.84	37.04	29.66	38.69	40.24	**28.2**	**17=**
11. INM-CM3.0	31.75	31.03	33.86	17.04	9.686	10.35	11.55	16.15	18.11	17.15	24.17	33.2	**21.2**	**11**
12. IPSL-CM4	80.57	71.85	56.54	19.19	11.75	9.347	5.966	5.971	8.434	17.88	29.49	51.01	**30.7**	**20**
13. MIROC3.2 (hires)	37.85	40.69	30.82	17.06	12.35	9.211	7.938	16.75	19.07	22.76	40.16	40.79	**24.6**	**15**
14.MIROC3.2(medres)	37.14	34.8	30.3	20.85	12.73	12.27	10.5	17.78	25.3	34.17	52.68	49.7	**28.2**	**17=**
15. MIUB-ECHO-G	51.45	40.28	21.32	7.729	5.879	4.482	6.079	5.066	8.018	15.21	43.77	52.84	**21.8**	**12**
16. MPI-ECHAM5	22.18	17.75	15.41	5.865	5.325	6.09	7.287	6.403	6.851	11.57	11.56	15.73	**11**	**1**
17. MRI-CGCM2.3.2a	41.4	31.08	30.31	13.02	7.867	8.154	8.814	8.53	9.918	14.94	14.19	28.86	**18.1**	**8**
18. NCAR-CCSM3.0	46.25	41.9	26.75	7.64	4.703	9.133	9.283	8.039	7.942	11.18	37.85	40.95	**21**	**10**
19. NCAR-PCM1	54.69	52.46	26.21	13.28	10.8	15.37	9.821	7.448	7.081	9.854	26.05	43.8	**23**	**14**
20. UKMO-HadCM3	37.97	25.41	16.18	9.832	5.503	6.803	7.045	15.61	17.26	12.97	28.37	54.57	**19.8**	**9**
21. UKMO-HadGEM	32.45	29.79	22.51	20.58	14.72	9.05	8.127	10.1	9.113	9.354	19.51	26.02	**17.6**	**7**
Average	**46.05**	**42.34**	**28.84**	**17.14**	**12.18**	**9.92**	**9.02**	**10.79**	**12.53**	**15.98**	**28.96**	**40.63**	**22.86**	

APPENDIX TWO

Annual and seasonal values of the SAM index used in the Correlation analysis with MSLP (downloaded from http://www.antarctica.ac.uk/met/gjma/sam.html website and links therein).

SAM data from 1957 to 2008.

ANN	AUT	WIN	SPR	SUM	
1957	−4.24	−2.52	−0.68	−3.55	−2.52
1958	−1.27	−2.97	−0.92	1.42	1.12
1959	0.47	−0.94	−1.22	3.20	0.31
1960	1.52	0.74	0.32	1.00	−0.08
1961	1.22	0.48	0.93	0.85	2.19
1962	−0.41	−0.02	−1.39	−1.36	2.64
1963	0.71	0.80	−1.44	0.42	−1.77
1964	−4.12	0.97	−6.62	−0.45	−3.55
1965	−1.52	−2.25	0.88	1.90	−1.65
1966	−1.11	−2.46	1.04	0.07	−3.25
1967	−0.38	0.27	2.35	0.06	−0.89
1968	−2.65	−3.00	1.01	−3.42	−3.13
1969	−0.69	−0.60	1.66	0.95	0.51
1970	−1.11	−1.65	0.36	−2.00	−0.48
1971	−1.69	−1.23	0.63	−2.48	−1.69
1972	−2.72	−2.24	−1.55	−0.55	−0.70
1973	1.12	−0.24	2.46	−1.70	2.44
1974	−1.01	1.62	−2.70	−0.58	−2.57
1975	−1.70	−2.35	−1.67	1.26	0.08
1976	−0.43	1.78	0.51	0.27	−4.50
1977	−2.04	−1.64	−2.21	1.77	−0.04
1978	0.49	−0.57	0.57	0.69	−0.01
1979	1.48	1.27	3.67	−0.44	−1.68
1980	−2.48	−2.23	−0.41	−2.65	0.90
1981	−0.55	−2.04	−1.68	−0.06	1.24
1982	0.69	2.65	1.54	−1.10	−2.06
1983	1.14	−1.03	1.18	2.24	−0.53
1984	−2.14	−0.51	−0.79	0.48	−3.04
1985	1.66	0.76	1.07	2.10	−0.28
1986	−0.33	−2.17	0.38	1.88	−1.14
1987	−0.58	−0.85	0.83	0.78	0.26
1988	−2.24	−1.05	−1.97	−3.70	1.50
1989	1.86	2.45	1.21	0.19	0.51
1990	−1.08	−3.18	−1.14	1.54	−0.06
1991	−1.17	0.31	−0.71	−1.56	−1.30
1992	−0.96	−1.51	−2.06	1.72	−0.34
1993	3.28	2.14	3.23	2.06	1.95
1994	−0.29	−0.62	−0.41	−2.31	2.56
1995	1.19	1.47	−3.16	1.80	0.91
1996	−1.04	1.55	−1.62	−2.20	1.31
1997	1.16	1.45	1.75	−1.81	0.74
1998	4.46	1.84	3.16	1.90	2.80
1999	3.67	2.08	0.30	2.70	4.22
2000	0.26	2.09	−0.40	−2.25	−1.52
2001	1.57	0.32	0.09	2.90	2.56
2002	−1.32	−2.14	−0.03	−4.09	0.34
2003	0.35	1.76	0.74	−0.78	−0.49
2004	1.17	0.67	2.32	0.29	0.33
2005	0.30	1.31	−0.25	0.58	−2.12
2006	1.51	1.73	0.54	0.81	1.63
2007	−0.77	−1.03	−2.03	−1.57	3.11
2008	2.02	−0.49	1.76	1.86	1.81
2009		−0.06			

APPENDIX THREE

Field Sampling Methodology.

A PVC pipe with a diameter of 130 mm (8 mm wall thickness) and an aluminium pipe with a diameter of 75 mm (1.5 mm wall thickness) were designed specifically for retrieving sediments from Lake Broadwater. The first unconsolidated lake sample (0–1cm) was scraped off the surface by hand and placed in small plastic vials. Lake samples from 1–21 cm were recovered by gently hammering a 20 cm length of aluminium pipe into the sediments. The sediments around the aluminium pipe were dug out until the aluminium pipe and core could be easily removed. This provided a small flat platform below the surface where the larger and longer PVC pipe (~1.4 m) could be placed to recover the next lake samples. The PVC pipe was hammered into the lake sediments as far as possible (121 cm below the surface) and pulled out using a kangaroo jack. Another length of longer aluminium pipe (~ 2.8 m) was placed into the hole left by the PVC and hammered into the sediments (171 cm below surface) as far as possible and also removed using a kangaroo jack. The water table was not intercepted at any stage

APPENDIX FOUR

^{210}Pb Dating Procedures at ANSTO and Radiocarbon (^{14}C) Dating Results from ANSTO.

At ANSTO, approximately 5.0 g of each sample was weighed into beakers with two tracers (^{209}Po and Ba-133) added, digested in HNO_3 and placed on a hot plate at 120ºC in a fume cupboard overnight. Hydrogen peroxide (H_20_2) acid was added to completely oxidise the samples. The samples and 6 M HCl were placed into a centrifuge to separated solid and supernatant constituents. The liquid supernatant was placed into a separation flask with diethyl ether to remove the iron from the liquid phase. The iron rich solution was decantered off and the remaining solution dried overnight on a hot plate. Small silver discs were placed into new solutions containing the fortified sample so that auto deposition of polonium could occur over a period of 4–6 hours. The silver discs where removed from the solution and ^{210}Po analysed by alpha spectrometry. The ^{226}Ra which is present in the remaining liquid is concentrated on a colloidal precipitate of barium sulphate on a membrane filter and assayed also via alpha spectrometry. This analysis was completed over five days and detailed methodologies used include: ENV-l-044-031 (sedimentation rate determination), ENV-l-044-006 (for bulk iron removal by ether extraction), ENV-l-044-023 (for polonium analysis), ENV-l-044-027 (for ^{226}Ra analysis) and ENV-l-044-001 (alpha spectrometry)

Australian Government

ansto
Nuclear-based science benefiting all Australians

REPORT ON AMS ANALYSIS
(AINSE Grant 07/103P; Run 298)

7 March 2008

Dr Martine Maron [Andrew Cotrill]
University of Southern Queensland
Toowoomba QLD 4350

Email: maron@usq.edu.au

RADIOCARBON RESULTS

	ANSTO code	Sample Type	Submitter ID	$\delta(^{13}C)$	percent Modern Carbon		Conventional Radiocarbon age	
				per mil	pMC	1σ error	yrs BP	1σ error
1	OZK333	Lake sediments	C1	-18.8	77.96	0.53	2000	60
2	OZK334	Lake sediments	C2	-18.5	69.22	0.50	2950	60
3	OZK335	Lake sediments	C3	-18.9	59.37	0.51	4190	70
4	OZK336	Lake sediments	C4	-19.1	46.09	0.47	6220	90
5	OZK337	Lake sediments	C5	-21.9	35.53	0.50	8310	120
6	OZK338	Lake sediments	C6	-20.3	30.76	0.35	9470	100

NB – Samples were chemically processed using a single acid step only instead of the normal AAA process. The results are for the humic acid fraction.

Note:

1. The $\delta(^{13}C)$ values quoted above relate solely to the graphite derived from the fraction that was used for the radiocarbon measurement. It is sometimes the case that the $\delta(^{13}C)$ of this fraction is not the same as that of the bulk material.
2. The ages quoted are radiocarbon ages, not calendar ages.
3. The ages have been rounded according to M. Stuiver and A. Polach (1977). The definition of percent Modern Carbon and Conventional Radiocarbon age can also be found in this publication.
4. Please use the ANSTO Code number in publications. The AMS facility should be referenced as Fink *et*

References:

D. Fink, M. Hotchkis, Q. Hua, G. Jacobsen, A. M. Smith, U. Zoppi, D. Child, C. Mifsud, H. van der Gaast, A. Williams and M. Williams (2004) The ANTARES AMS facility at ANSTO, NIM B 223-224, 109-115.

M. Stuiver and A. Polach (1977) Reporting of ^{14}C data, *Radiocarbon* 19(3), 355-363. Available on-line at: http://radiocarbon.library.arizona.edu/radiocarbon/GetFileServlet?file=file:///data1/pdf/Radiocarbon/Volume 19/Number3/azu_radiocarbon_v19_n3_355_363_v.pdf&type=application/pdf

AUSTRALIAN NUCLEAR SCIENCE AND TECHNOLOGY ORGANISATION

Issued by Andrew Jenkinson, ANSTO – Institute for Environmental Research, PMB 1, Menai NSW 2233 (AUSTRALIA)
Tel: +61-2-97173478; e-mail: avj@ansto.gov.au; http://www.ansto.gov.au/nugeo/ams/index.html

APPENDIX FIVE

Geochemistry Lab Analyses and Results.

Bulk Geochemistry completed at USQ:

Pre–weighed and dried samples of ~20 g were heated in a furnace oven (Model Labec) to 550ºC for 2 hours cooled in as desiccator and weighed using an HR–Series (200) Precision electric balance (± 0.001 g). Samples were reheated to 950ºC for 4 hours and reweighed with the weight changes representing organic and carbonate matter respectively. The remaining sample is composed of siliciclastic material.

Multi–Element Geochemistry:

Digestion and laboratory analysis was completed using ANSTO methods ENV-l-035-001 and ENV-l-035-027: ICPAES respectively.

Table 1. Geochemistry of lake sediments from Lake Broadwater, Dalby, Queensland..

Depth (cm)	OM (%)	CaCO3(%)	SM (%)	Corg (%)	Al (ppm)	Fe (ppm)	Mn (ppm)	Ba (ppm)	Ca (ppm)	Sr (ppm)
0-1.	11.091	0.92	87.989	3.1	14500	13600	74.4	63.7	2170	42.5
2-3.	5.259	1.58	93.161							
3-4.	4.273	1.36	94.367							
5-6.	4.697	1.27	94.033	0.7	23200	11900	51.8	54.7	899	25.9
10-11.	5.052	1.45	93.498	0.4	23900	14100	54.4	42.5	1050	28.7
15-16	5.553	1.85	92.597							
20-21.	5.196	1.81	92.994	0.3	19900	31200	51.3	37.9	1250	32.4
30-31.	5.182	1.77	93.048	0.3	43000	33700	63.4	39.9	1440	35.0
40-41.	5.431	2.33	92.239	0.4	46600	25000	74.8	41.3	1340	35.9
50-51.	5.323	2.24	92.437	0.3	46200	30900	80.0	45.5	1580	39.0
60-61.	5.447	1.9	92.653	0.2	38200	33200	80.8	43	1450	37.2
70-71.	5.479	1.94	92.581	0.2	28800	30800	88.1	45.1	1410	36.4
80-81.	5.955	1.81	92.235	0.2	29600	30300	97.4	41.9	1540	39.2
90-91.	5.495	1.65	92.855	0.2	18200	31300	121	77.8	1440	38.3
100-101.	5.884	1.88	92.236	0.2	13400	36500	157	193.1	1550	40.6
110-111.	5.561	1.92	92.519	0.2	29800	32900	149	168.4	1480	39.7
120-121.	5.356	2.19	92.454	0.2	34800	30500	152	151.6	1440	38.7
130-131.	5.931	2.24	91.829	0.1	38700	31200	138	136.8	1570	40.7
140-141.	6.264	2.2	91.536	0.1	35000	34900	168	169.3	1670	41.9
150-151.	6.191	1.98	91.829	0.2	38100	38000	197	234.4	1480	40.2
160-161.	6.532	2.1	91.368	0.1	44100	38800	242	235.5	1740	45.4
170-171.	6.339	2.49	91.171	0.1	35200	36700	220	230	1670	44.1

Depth (cm)	% C	% N	%S	Mg (ppm)	Na (ppm)	K (ppm)	Cu (ppm)	Pb (ppm)	Zn (ppm)
0-1.	3.1	0.4	<0.1	977	711	1950	9.28	<40	21
2-3.									
3-4.									
5-6.	0.7	<0.1	<0.1	798	754	1550	3.91	<40	12
10-11.	0.4	<0.1	<0.1	980	627	1630	4.38	<40	14
15-16									
20-21.	0.3	<0.1	<0.1	1030	682	1750	3.81	<40	15
30-31.	0.3	<0.1	<0.1	1320	627	1730	4.22	<30	16
40-41.	0.4	<0.1	<0.1	1360	621	1820	4.63	<40	17
50-51.	0.3	<0.1	<0.1	1500	659	1780	4.62	<40	17
60-61.	0.2	<0.1	<0.1	1340	635	1650	3.63	<50	16
70-71.	0.2	<0.1	<0.1	1200	628	1590	3.56	<40	16
80-81.	0.2	<0.1	<0.1	1320	691	1630	4.06	<40	17
90-91.	0.2	<0.1	<0.1	1150	667	1500	3.74	<50	17
100-101.	0.2	<0.1	<0.1	1090	715	1490	4.07	<40	17
110-111.	0.2	<0.1	<0.1	1330	705	1500	3.78	<50	18
120-121.	0.2	<0.1	<0.1	1370	706	1470	3.78	<50	17
130-131.	0.1	<0.1	<0.1	1470	756	1650	4.04	<40	19
140-141.	0.1	<0.1	<0.1	1500	771	1610	4.26	<30	21
150-151.	0.2	<0.1	<0.1	1380	757	1510	3.52	<40	18
160-161.	0.1	<0.1	<0.1	1680	821	1700	4.47	<40	20
170-171.	0.1	<0.1	<0.1	1490	819	1690	6.51	<30	20

Notes:
1/ OM is organic matter; SM is siliciclastic matter.
2/ OM, CaCO3 and SM % determined at USQ.
3/ All other geochemistry completed at ANSTO using an AINSE grant.
4/ Samples 2-3, 3-4, 15-16 were not assayed at ANSTO.

Table 2. Geochemistry of lake sediments from Lake Broadwater, Dalby, Queensland.

Depth (cm)	ME-MS42 Cd (ppm)	ME-MS42 Cu (ppm)	ME-MS42 Pb (ppm)
LOR	**0.01**	**0.2**	**0.2**
0-1	0.03	13.5	8.7
5-6	0.01	7.4	5.6
10-11	0.08	158.5	10.4
20-21	0.03	48.3	7.9
30-31	0.01	19.6	6.9
40-41	0.01	19.2	9.0
50-51	0.01	21.9	7.8
60-61	0.01	14.6	8.1
70-71	0.02	19.4	7.7
80-81	0.01	14.6	6.9
90-91	0.01	20.4	7.0
100-101	0.02	24.9	7.6
110-111	0.01	14.7	6.9
120-121	0.02	14.2	7.5
130-131	0.02	17.1	6.9
140-141	0.01	12.3	6.4
150-151	0.01	13.1	6.7
160-161	0.01	8.5	6.3
170-171	0.01	9.1	6.7

Notes: 1/ Analyses completed at ALS Chemex, Stafford, Brisbane, July 2008.
2/ Certificate of Analysis: BR08087079; Project 4745/100/603.
3/ Pulps used were identical to ANSTO.
4/ Samples 2–3, 3–4, 15–16 were not assayed at ALS.

APPENDIX SIX

Grain Size Analysis Results Using Laser Diffraction

(Malvern Mastersizer 2.19).